Georgia Water Resources Institute (GWRI) Research Supported by USGS Grants 104b/g

Science Report

Fiscal Year 2022 – 2023

Developed by

Aris P. Georgakakos
Director, Professor

Husayn El Sharif
Assistant Director, Research Scientist

Georgia Water Resources Institute
Georgia Institute of Technology

Sponsored by

The United States Geological Survey
Water Resources Research Act Program
(104b Base Grant & 104g National Competitive Grant)

National Institutes for Water Resources (NIWR)

October 2023

Georgia Water Resources Institute (GWRI)
Research Supported by USGS Grants 104b/g

Science Report

Developed by

Aris P. Georgakakos
Director, Professor

Husayn El Sharif
Assistant Director, Research Scientist

Georgia Water Resources Institute
Georgia Institute of Technology

Sponsored by

The United States Geological Survey
Water Resources Research Act Program
(104b Base Grant & 104g National Competitive Grant)

National Institutes for Water Resources (NIWR)

October 2023

Table of Contents

Project ID	2022GA00B
Project Type	Administration
Award Type	Base Grant (104b)
Project Title	GWRI Program Administration & Reseach Support
Project PI	Georgakakos, Aris
Academic Institution of PI	Georgia Institute of Technology
Congressional District of project	GA-5

TECHNICAL REPORT

GA202200B

What follows are extended abstracts published in the Proceedings of the 2023 Georgia Water Resources Conference. The research efforts in the following abstracts were supported by the FY 2022-2023 WRRA 104b base grant:

- **Historical Climate Trends in Georgia**
- **Assessment of Agricultural Yield and Irrigation Demand for the ACF River Basin**
- **Future Climate Trends in Georgia**

HISTORICAL CLIMATE TRENDS IN GEORGIA

Shivani Chougule, Husayn El Sharif, and Aris P. Georgakakos

REFERENCE: *Proceedings of the 2023 Georgia Water Resources Conference*, held March 30–31, 2023, at the University of Georgia.

Abstract. Climate variability and trends are important for Georgia's agriculture and the management of water resources. According to the EPA (US EPA, 2016), while Georgia has warmed less than most of the United States during the past century, over the next few decades the state is expected to become warmer and experience more severe floods and droughts. In this study, we assess the Georgia climate trends from 1980s to the present-day, using data from the Climatic Research Unit (CRU) gridded (~ 50x50 km) time series data (Harris *et al.,* 2020).

Assessments are performed for the monthly average minimum daily temperature (TMN), monthly average daily temperature (TMP), monthly average maximum daily temperature (TMX), monthly potential evapotranspiration (PET), monthly precipitation (PRE), and the difference between monthly precipitation and potential evapotranspiration (PRE - PET). This study focuses on state-wide climatic trends, and for this reason, all gridded variable data are first averaged over the entire state. Moreover, to identify trends at different time resolutions, the state-wide data are analyzed at monthly, annual, bi annual, and four-year time scales.

Figures 1, **2**, and **3** show that there has been a clear rising trend in state-wide average daily minimum, mean, and maximum temperatures over the last 10 to 15 years. Comparing the pre- and post-2010 historical periods, these temperature increases equal or exceed 1.5 ºC (or 2.7 ºF) for all three variables. Furthermore, the 1-, 2-, and 4-year rolling average sequences indicate that the interval (in years) during which each temperature variable *exceeds* a specific threshold has also been rising sharply. For example, prior to 2010, Georgia's 4-yr average maximum temperature *only slightly* exceeded 18 ºC (64.6 ºF) during 1990–1993 (3 yrs), 2001 (1 yr), and 2006–2007 (2 yrs). By contrast, post 2010, Georgia's 4-yr average maximum temperature has exceeded 18 ºC *continuously* for more than 12 years. The rising temperature trends are expected to have important implications for agriculture, hydrology, water resources management, human health, and other socio-economic sectors.

A similar rising trend is observed for potential evapotranspiration (PET), which denotes the maximum water amount abstracted from the land by the atmosphere **(Figure 4)**. All moving average sequences plotted in this figure show the increasing trend indicate an increase in the duration of higher potential evapotranspiration **(Figure 4)**. In particular, the 4-yr moving average plot shows that pre-2010, the average PET was approximately 108 mm/month (~ 4.25 in/month) and attained a maximum of 113.5 mm/month (4.47 in/month). Post-2010, however, the average PET has reached 113.5 mm/month (4.47 in/month), has continuously *exceeded* the pre-2010 average (of 108 mm/month), and has attained a new maximum of 117 mm/month (4.6 in/month). Depending on precipitation changes (see below), these PET trends may have adverse impacts for Georgia's agriculture, hydrology (surface and subsurface), and water resources management, as under a no-change precipitation scenario, they imply a growing water supply deficit.

The precipitation data are shown on **Figure 5**. Precipitation is more variable (over all time scales) than temperature and PET, and its trends are more difficult to ascertain. The plots indicate that heavy (maximum) precipitation appears to be increasing, but average precipitation appears to remain stable or increase slightly. Thus, a key question is whether the precipitation trends counteract those of the PET.

The plots of (PRE-PET) in **Figure 6** is a first attempt to glean an answer to this question. The plots in this figure show that in the last decade, the difference (PRE-PET) exhibits a pattern similar to that of the 1987-1997 historical period. They also show that the period 1997-2013 was unprecedented in deficit (PRE-PET < 0) persistence and severity. Thus, the data presented here do not yet suggest a *statistically* conclusive answer to the above question. If, however, the Georgia climate in the next 10 years repeats the 1997-2013 pattern, this would suggest a clear climatic shift toward extended and deep deficits.

We also note that part of the difficulty in reaching a conclusive answer to the previous question is that the quantity PRE-PET is not a suitable metric for assessing water cycle changes. Specifically, the previous analysis focuses on *average* values of PRE and PET and ignores their distinctly different variability over finer time scales. A conclusive answer may be obtained by explicitly incorporating the underlying hydrologic processes in the water cycle and assessing the shifts in soil moisture, streamflow, and surface and subsurface water storage. Such a hydrologic assessment is currently on-going for different hydrologic basins at the Georgia Water Resources Institute (GWRI).

Lastly, the assessment presented in this article pertains to climatic averages for the *entire* state. However, Georgia's climate exhibits noteworthy differences at least over three climatic regions, including the Blue Ridge Mountain region in the north, the Piedmont plateau in the middle, and the coastal region in the south **(Figure 7)**. Another on-going effort at GWRI is to assess the observed climatic shifts in each of these regions, quantify the most likely climatic projections, and assess their water resources implications for the state's economy and environment.

Acknowledgements. This study was sponsored by the Georgia Water Resources Institute at Georgia Tech.

References:

Harris, I., Osborn, T. J., Jones, P., & Lister, D. (2020). Version 4 of the CRU TS monthly high-resolution gridded multivariate climate dataset. Scientific Data, 7(1), 109. https://doi.org/10.1038/s41597-020-0453-3

U.S. Environmental Protection Agency (EPA). (2016). What Climate Change Means for Georgia. US EPA. https://19january2017snapshot.epa.gov/sites/production/files/2016-09/documents/climate-change ga.pdf

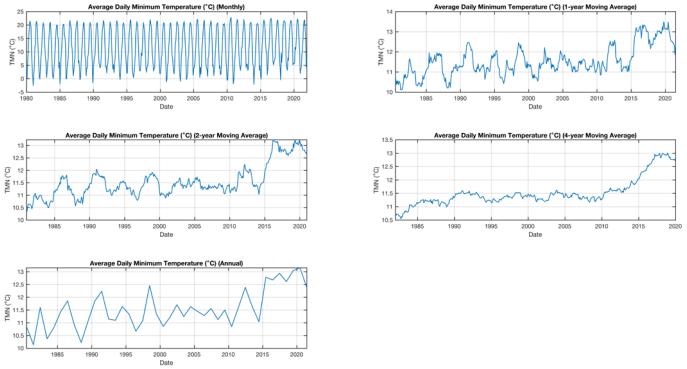

Figure 1. Average daily minimum temperature (TMN): Monthly, 1-year, 2-year, 4-year moving average sequences and annual series.

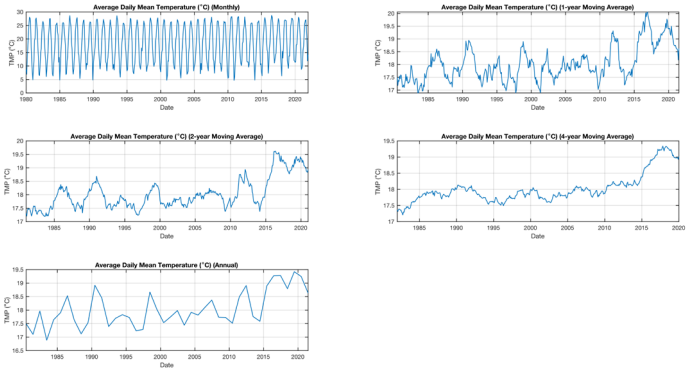

Figure 2. Average daily mean temperature (TMP): Monthly, 1-year, 2-year, 4-year moving average sequences and annual series.

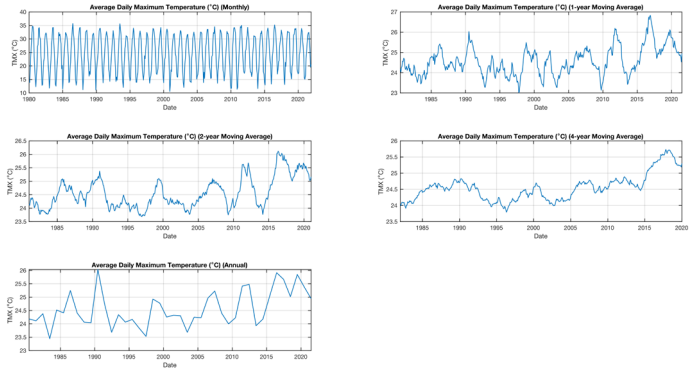

Figure 3. Average daily maximum temperature (TMX): Monthly, 1-year, 2-year, 4-year moving average sequences and annual series.

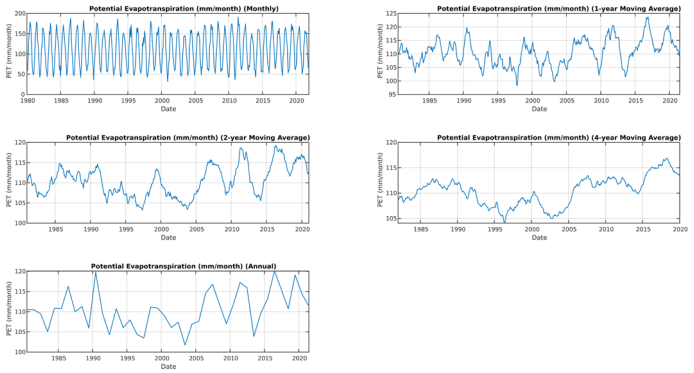

Figure 4. Potential Evapotranspiration (PET): Monthly, 1-year, 2-year, 4-year moving average sequences and annual series.

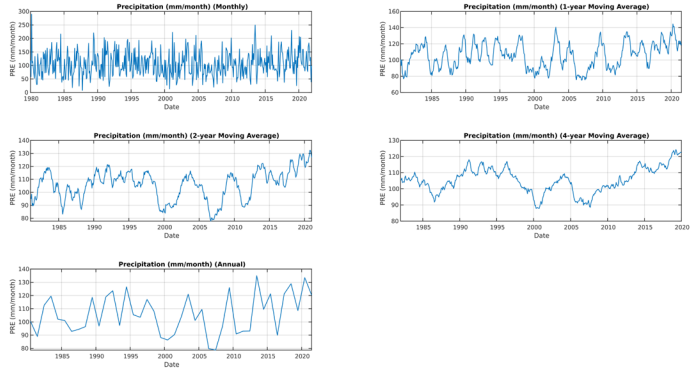

Figure 5. Precipitation (PRE): Monthly, 1-year, 2-year, 4-year moving average sequences and annual series.

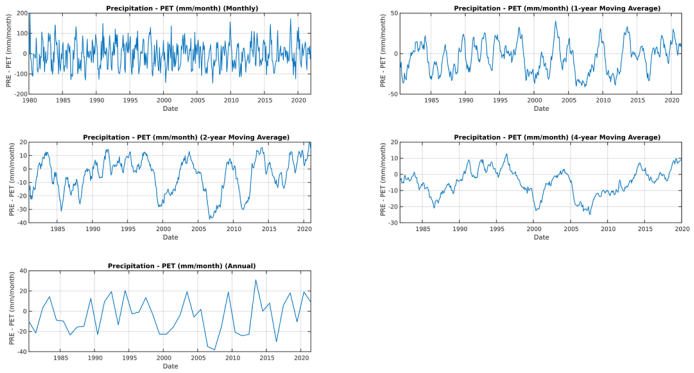

Figure 6. Difference between precipitation (PRE) and PET: Monthly, 1-year, 2-year, 4-year moving average sequences and annual series.

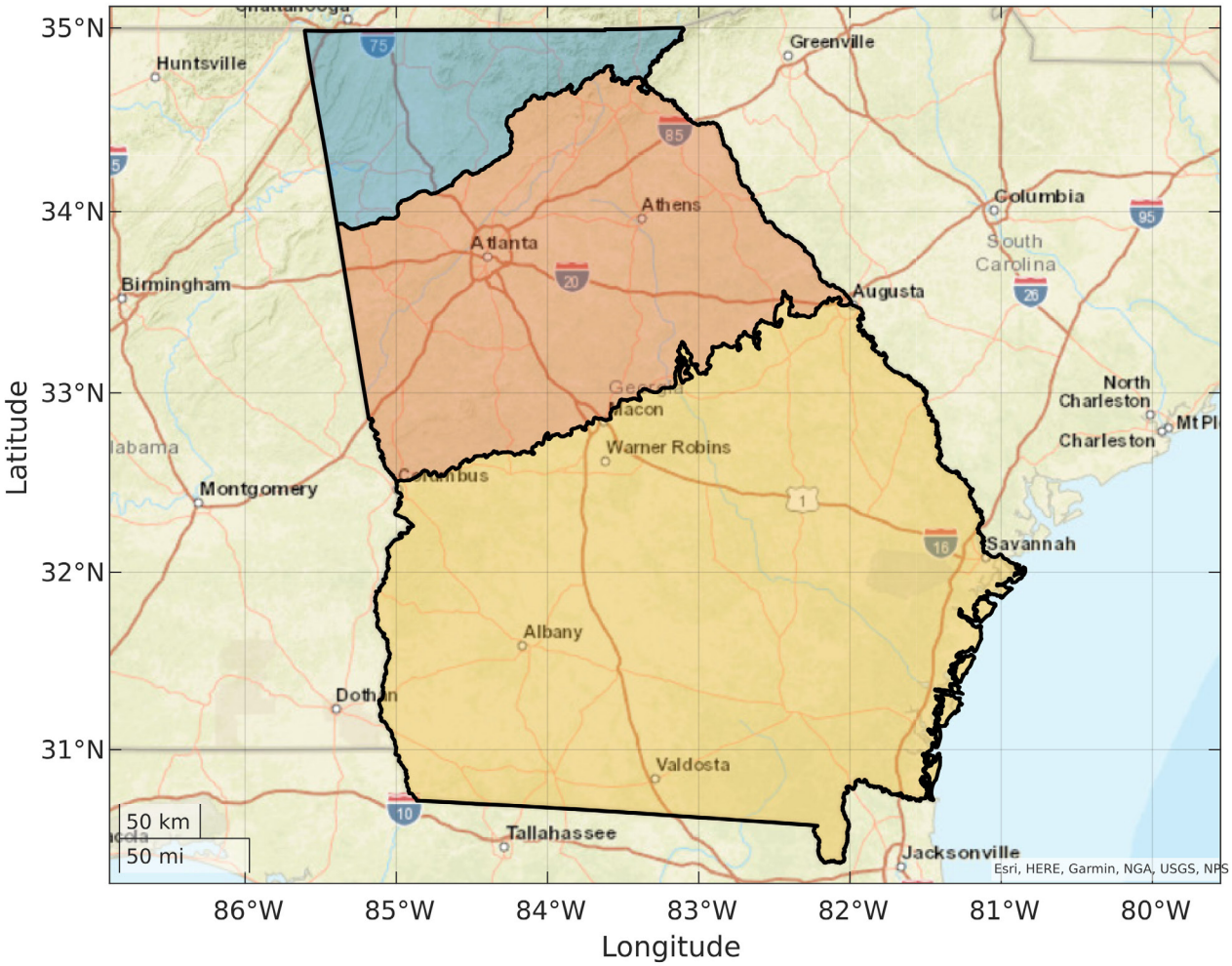

Figure 7. Three physiographic regions of Georgia: Blue Ridge Mountains (blue shading), Piedmont (orange shading), Coastal Plain (yellow shading).

ASSESSMENT OF AGRICULTURAL YIELD AND IRRIGATION DEMAND FOR THE ACF RIVER BASIN

Husayn El Sharif and Aris P. Georgakakos

REFERENCE: *Proceedings of the 2023 Georgia Water Resources Conference*, held March 30–31, 2023, at the University of Georgia.

Abstract. Biophysical crop models coupled with modern meteorological and soil data can support better crop planting strategies, more efficient irrigation water use, and more resilient drought management responses to climate variability and change. In this study, soil, crop, and meteorological gridded data are combined with the Decision Support System for Agrotechnology Transfer - Cropping System Model (DSSAT-CSM) [*Tsuji et al.*, 1994; *Hoogenboom et al.*, 2017] to assess the sensitivity of crop yield (peanuts, corn, soybeans, and cotton) and irrigation demand to historical climate conditions in the Apalachicola-Chattahoochee-Flint (ACF) River Basin. This assessment included normal, dry, and wet years. Then, using bias corrected General Circulation Model (GCM) climate projections, we estimate how crop yield and irrigation demand may materialize in the future.

For this study, the ACF is divided into 14 sub-basins as shown in **Figure 1**. Crop acreages for rainfed and irrigated peanut, corn, soybean, and cotton were obtained from the USDA Cropland Data Layer [*USDA NASS*, 2015] and the USDA Farm Service Agency. Annual crop yields and irrigation amounts for the control period 1980 – 2016 were simulated using the DSSAT-CSM model calibrated to the ACF region with the parameters listed in **Table 1**. Simulation results were then coupled with reanalysis climate data from the Climate Research Unit (CRU) to estimate typical crop yields and irrigation demand during dry, normal, and wet growing seasons as presented in **Tables 2** through **5**. Regression relationships were identified using these crop model runs between growing season precipitation, potential evapotranspiration, and modeled irrigation demand. These relationships were extended into the future using bias-corrected climate projections to assess the types of growing seasons, crop yield, and irrigation demand could materialize over the next thirty years to the end of the century.

Results based on the latest bias-corrected CMIP6 climate data indicate that over the next thirty years, the frequency of dry growing seasons will increase mildly throughout the ACF, and that after year 2050 dry growing seasons will constitute nearly half or more the growing seasons, suggesting that agricultural drought could become the “new normal” in the region (**Figure 2**). Crop model simulations assuming no change in irrigated acreages suggest that compensating for the increased frequency in dry seasons will require on average a 30 to 40 percent increase in irrigation volume over the next thirty years and a doubling or more of irrigation demand by the end of the century as illustrated in **Figures 3** and **4**.

Acknowledgements. This study was sponsored by the Georgia Water Resources Institute at Georgia Tech.

References:

Hoogenboom, G., et al. (2017), Decision Support System for Agrotechnology Transfer (DSSAT) Version 4.7, edited, DSSAT Foundation, Gainesville, Florida, USA.

Tsuji, G., G. Uehara, and S. Balas (1994), *DSSAT V3*, University of Hawaii, Honolulu.

USDA NASS (2015), USDA National Agricultural Statistics Service Cropland Data Layer, edited by USDA-NASS, Washington, DC. USA.

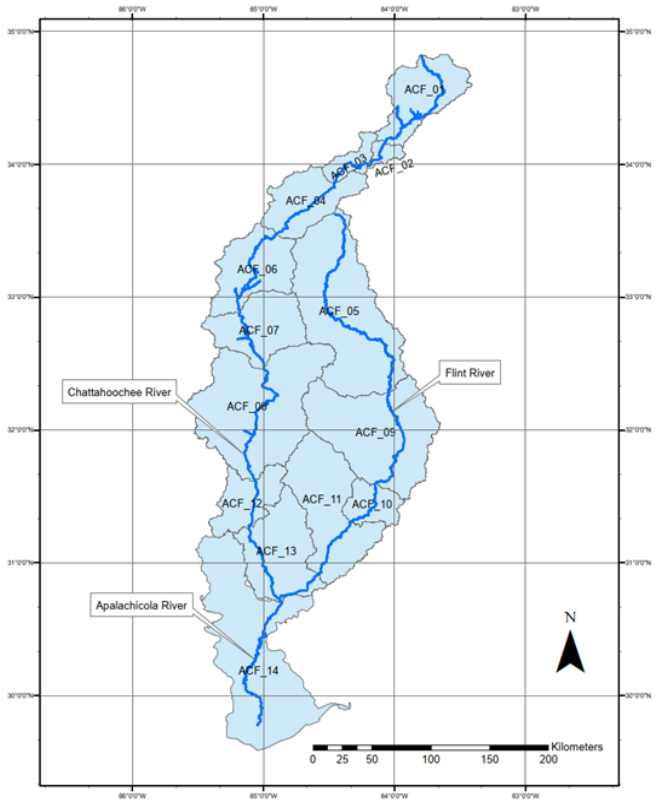

Figure 1. The Apalachicola-Chattahoochee-Flint (ACF) River Basin and its 14 sub-basins.

Table 1. Calibrated input parameters for DSSAT-CSM rainfed and irrigated crop simulations.

Model Parameter	Corn	Peanut	Cotton	Soybean
Planting Date (1980-2016)	March 29th	May 16th	May 5th	May 25th
Cultivar	B73 X MO17	Georgia Green	DP 555 BG/RR	DP 5634 (Maturity Group V)
Row Spacing	30 inches (76 cm)	36 inches (90 cm)	36 inches (90 cm)	30 inches (76 cm)
Plant Population	30,000 plants/acre (7.9 plants/m^2)	85,000 plants/acre (21 plants/m^2)	50,000 plants/acre (12.4 plants/m^2)	90,000 plants/acre (22.2 plants/m^2)
Irrigation: Soil Management Depth	12 inches (30 cm)	20 inches (50 cm)	12 inches (30 cm)	12 inches (30 cm)
Irrigation: Available soil water content threshold	50%	60%	50%	50%
Nitrogen Fertilizer	Nitrogen stress not simulated	Nitrogen stress not simulated	45 lbs/acre (50 kg/ha) of N fertilizer applied at 4 inch (10 cm) depth at planting and again at 46 days after planting	Nitrogen stress not simulated

Table 2. DSSAT-CSM Simulation results for rainfed and irrigated corn during typical dry, normal, and wet growing seasons in the ACF during the 1980-2016 control period.

ACF Basin	Corn								
	Rainfed Yield (kg/ha)			Irrigated Yield (kg/ha)			Irrigation Amount (mm)		
	Dry	Normal	Wet	Dry	Normal	Wet	Dry	Normal	Wet
1	6935	9413	12194	13696	13486	13772	196	147	78
2	5735	7508	11141	12064	12269	12751	212	169	99
3	5457	8064	11170	12191	12540	13153	211	160	105
4	4846	8104	10609	11263	11941	12254	216	146	90
5	3197	5579	9991	10527	10798	10895	261	189	93
6	5302	7607	11079	11332	11927	12319	216	156	89
7	5395	6842	10003	10294	10426	10347	186	147	86
8	4556	6269	9958	10859	11046	11378	237	170	104
9	3910	5936	9528	10494	10743	10303	253	179	100
10	4842	6525	8902	10319	10500	9861	230	158	113
11	4736	6746	9106	10492	10660	10047	230	159	104
12	4292	7227	9811	10514	11197	10507	231	152	99
13	4716	6532	8787	9887	10491	9616	224	162	105
14	5323	7675	8221	10317	10537	10458	200	143	116

Table 3. DSSAT-CSM Simulation results for rainfed and irrigated cotton in the ACF during typical dry, normal, and wet growing seasons in the ACF during the 1980-2016 control period.

ACF Basin	Cotton								
	Rainfed Yield (kg/ha)			Irrigated Yield (kg/ha)			Irrigation Amount (mm)		
	Dry	Normal	Wet	Dry	Normal	Wet	Dry	Normal	Wet
1	2206	2330	2414	2623	2700	2517	174	137	74
2	-	-	-	-	-	-	-	-	-
3	-	-	-	-	-	-	-	-	-
4	2273	2369	2564	2724	2723	2693	195	158	96
5	2272	2470	2971	2921	2959	3149	202	165	82
6	2250	2449	2580	2751	2764	2743	213	156	103
7	2230	2453	2655	2775	2800	2837	218	157	93
8	2250	2562	2756	2810	2872	2939	204	138	91
9	2336	2600	3116	3008	3072	3296	188	152	85
10	2618	2961	3154	3113	3261	3290	150	107	73
11	2582	2923	3114	3073	3223	3258	156	113	72
12	2383	2815	2907	2872	3013	2982	174	103	69
13	2562	2936	3070	3001	3205	3188	147	104	69
14	2644	2896	2916	2904	3039	2959	119	75	54

Table 4. DSSAT-CSM Simulation results for rainfed and irrigated peanut in the ACF during typical dry, normal, and wet growing seasons in the ACF during the 1980-2016 control period.

ACF Basin	Peanut								
	Rainfed Yield (kg/ha)			Irrigated Yield (kg/ha)			Irrigation Amount (mm)		
	Dry	Normal	Wet	Dry	Normal	Wet	Dry	Normal	Wet
1	3580	4128	5035	5297	5295	5292	197	166	91
2	-	-	-	-	-	-	-	-	-
3	-	-	-	-	-	-	-	-	-
4	-	-	-	-	-	-	-	-	-
5	2710	3237	4694	5222	5432	5337	274	221	122
6	2976	3682	4525	5445	5548	5693	272	205	136
7	2583	3385	4566	5295	5409	5509	287	213	128
8	2816	3804	4690	5259	5367	5395	266	185	125
9	2901	3544	4612	5165	5369	5271	253	202	121
10	3481	4228	4710	5191	5349	5293	212	157	111
11	3447	4189	4703	5187	5333	5269	218	162	106
12	3068	4319	4811	5227	5374	5313	240	157	100
13	3460	4328	4770	5070	5376	5252	210	152	101
14	3591	4547	4992	5116	5318	5305	201	123	84

Table 5. DSSAT-CSM Simulation results for rainfed and irrigated soybean in the ACF during typical dry, normal, and wet growing seasons in the ACF during the 1980-2016 control period.

ACF Basin	Soybean								
	Rainfed Yield (kg/ha)			Irrigated Yield (kg/ha)			Irrigation Amount (mm)		
	Dry	Normal	Wet	Dry	Normal	Wet	Dry	Normal	Wet
1	2057	2534	3222	3253	3344	3431	148	122	56
2	1651	2115	2815	3394	3358	3453	191	149	90
3	1689	2180	2848	3450	3348	3457	200	144	93
4	1735	2017	2603	3332	3331	3369	183	148	88
5	1485	1815	2501	3183	3210	3157	197	155	84
6	1550	2033	2486	3351	3356	3396	198	147	94
7	1419	1892	2481	3329	3276	3355	208	155	92
8	1393	1976	2455	3206	3143	3203	202	138	89
9	1522	1840	2376	3088	3113	3075	194	149	88
10	1817	2224	2550	3012	3017	3042	153	105	75
11	1629	2140	2539	3049	3052	3086	170	117	79
12	1501	2235	2560	3092	3035	3086	178	109	74
13	1841	2272	2558	2957	3006	3006	152	102	68
14	2067	2420	2781	3008	2921	3063	115	74	49

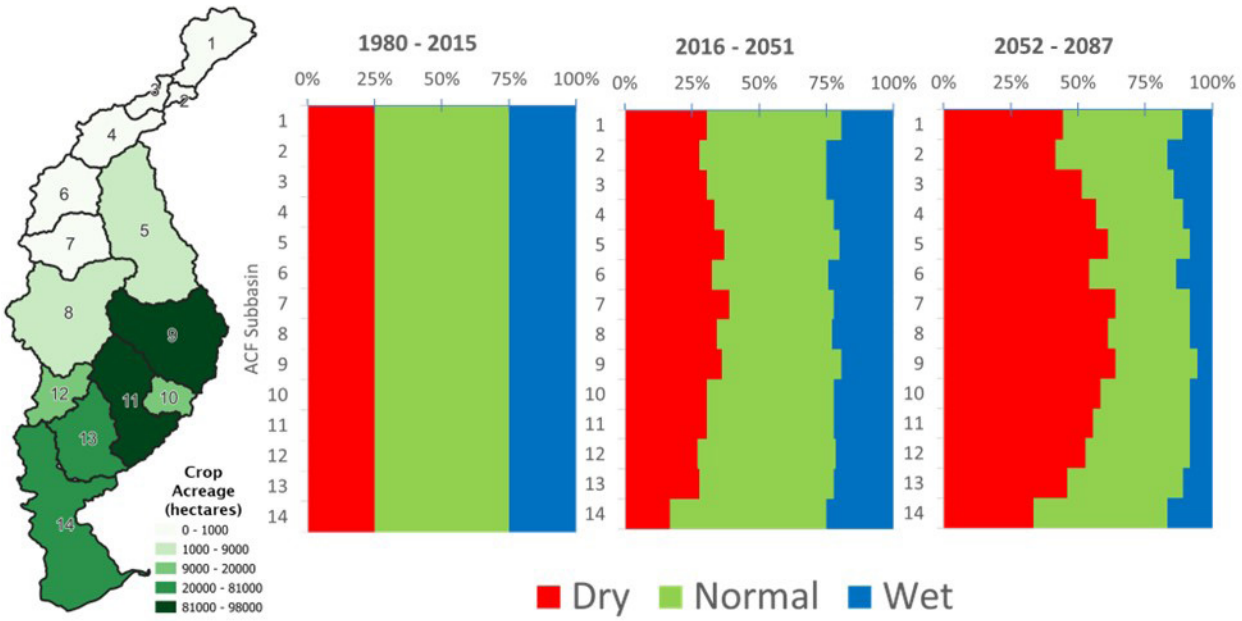

Figure 2. Classification of ACF growing seasons as dry, wet, or normal as a function of projected growing season precipitation and potential evapotranspiration.

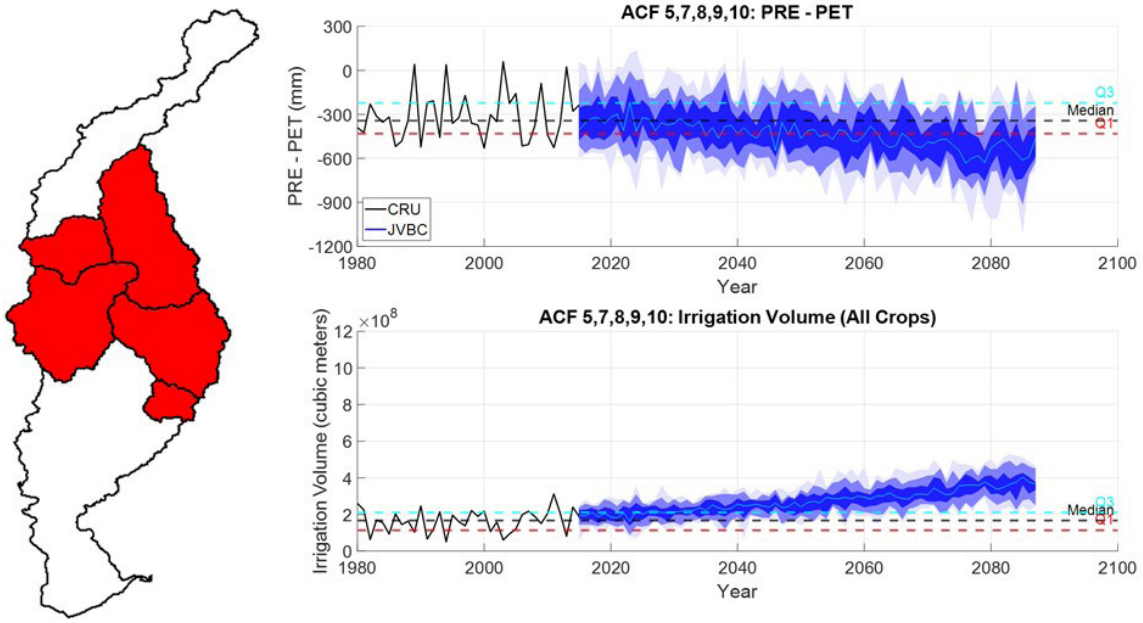

Figure 3. Projected irrigation volume for all crops (corn, cotton, peanut, and soybean) in the central ACF region as a function of projected growing season precipitation and potential evapotranspiration.

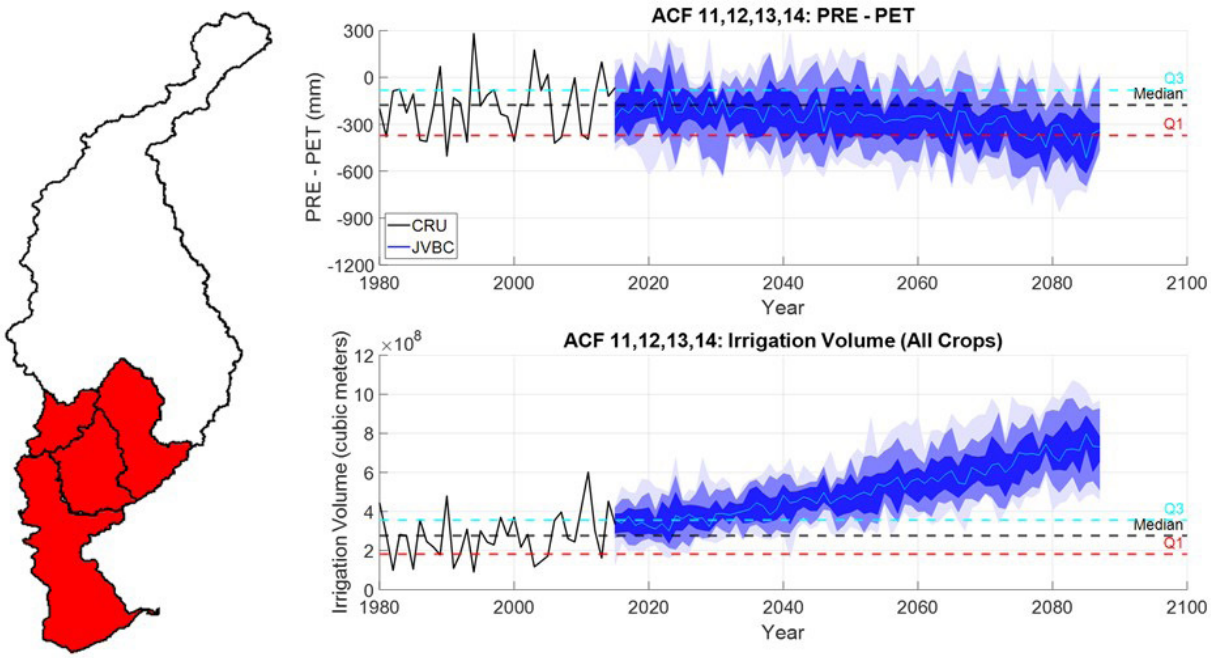

Figure 4. Projected irrigation volume for all crops (corn, cotton, peanut, and soybean) in the southern ACF region as a function of projected growing season precipitation and potential evapotranspiration.

FUTURE CLIMATE TRENDS IN GEORGIA

Husayn El Sharif and Aris P. Georgakakos

REFERENCE: *Proceedings of the 2023 Georgia Water Resources Conference*, held March 30–31, 2023, at the University of Georgia.

Abstract. According to the US EPA (2016), Georgia's climate is expected to usher in warmer temperatures and more severe floods and droughts in the coming years. Such changes can have critical impacts for the State's environment and economy, but the extent and severity of these impacts are still debated. In a separate article of this conference, the Georgia Water Resources Institute (GWRI) provided evidence that significant climatic shifts are clearly detectable in the State's historical data of temperature, precipitation, and potential evapotranspiration (Chougule *et al.*, 2023). In this study, we analyze the latest climate projections from 16 Global Circulation Models (GCMs) to assess whether the historical climate trends are likely to persist, intensify, or subside in the coming decades.

Our analysis of the future climate focuses on the monthly daily average temperature (TMP), monthly potential evapotranspiration (PET), monthly precipitation (PRE), and the difference between monthly precipitation and potential evapotranspiration (PRE - PET) projected to the end of the century under the Shared Socioeconomic Pathway 5 (SSP 5) fossil fuel emissions scenario (Nakicenovic *et al.*, 2014). The study assesses the climatic trends over three climatic Georgia regions: the Blue Ridge Mountain region in the north, the Piedmont plateau in the middle, and the coastal region in the south (**Figure 1**). Results are only presented for the Piedmont, but the identified trends are fairly similar for the Blue Ridge Mountain and the coastal regions. The GCM projections are analyzed at monthly, annual, bi-annual, and four-year time scales.

Systematic comparisons of the GCM-simulated climatic data for 1987–2014 versus the historical observations of the same period (Harris *et al.*, 2020; Climatic Research Unit, CRU, gridded data upscaled to the GCM spatial resolution) indicate that all GCMs contain significant biases that must be removed before any analysis of future climate trends can be undertaken. Bias correction is carried out via a new bias correction approach named Joint Variable Bias Correction (JVBC; Georgakakos and El Sharif, 2023, El Sharif and Georgakakos, 2023), designed to remove the simultaneous biases of statistically correlated climatic fields. The satisfactory performance of the JVBC algorithm is exemplified in **Figure 2**.

Figure 3 shows that all GCMs project rising temperature trends in the Piedmont region. Furthermore, the 1-, 2-, and 4-year rolling average sequences indicate that the interval (in years) during which temperatures *exceed* a specific threshold will rise sharply. For example, during the period from the 1980s to present, the 4-yr average temperature in the Piedmont region *never* exceeded 18 °C (64.6 °F). By contrast, all bias-corrected GCM projections indicate that beyond 2055, the region's 4-yr average temperatures will *always* exceed 18 °C. The rising temperature trends are expected to have important implications for agriculture, hydrology, water resources management, human health, and other socio-economic sectors.

The precipitation projections are shown on **Figure 4**. Precipitation is more variable (over all time scales) than temperature and PET, and its trends are more difficult to ascertain. However, the plots clearly indicate that heavy (maximum) precipitation is projected to increase considerably (see monthly and 1-yr plots), while average precipitation is expected to increase at a slower pace.

On the other hand, the Piedmont PET (**Figure 5**) is expected to rise sharply and outpace precipitation by 2040 (**Figure 6**). After 2040, the long-term difference between precipitation and PET (PRE - PET) is expected to exhibit growing deficits, more severe than any deficits experienced in the 1987–2014 historical period. This ominous trend implies adverse impacts for Georgia's agriculture, hydrology (surface and subsurface), and water resources management.

Bias-corrected climatic projections and similar assessments are currently been developed for all southeast river basins. GWRI plans to make this data publicly available through its website to facilitate detailed environmental and socio-economic impact studies.

Acknowledgements. This study was sponsored by the Georgia Water Resources Institute at Georgia Tech.

References:

Chougule, S., H. El Sharif, and A.P. Georgakakos (2023). Proceedings of the 2023 Georgia Water Res. Conference, held March 30–31, 2023, at the University of Georgia.

El Sharif, H., and A.P. Georgakakos (2023): A Bias-Corrected Climatic Projection Data Set for U.S. River Basins. Climatic Change, in review.

Georgakakos, A.P., and H. El Sharif (2023): Bias Correction of Correlated Climatic Variables. Climatic Change, in review.

Harris, I., Osborn, T. J., Jones, P., & D. Lister (2020). Version 4 of the CRU TS monthly high-resolution gridded multivariate climate dataset. Scientific Data, 7(1), 109. https://doi.org/10.1038/s41597-020-0453-3

Nakicenovic, N., Lempert, R. J., and A.C. Janetos (2014). A Framework for the Development of New Socio-Economic Scenarios for Climate Change Research: Introductory Essay, Climatic Change, 122, 351–361, https://doi.org/10.1007/s10584-013-0982-2.

U.S. Environmental Protection Agency, EPA (2016). What Climate Change Means for Georgia. US EPA. https://19january2017snapshot.epa.gov/sites/production files/2016-09/documents/climate-change-ga.pdf

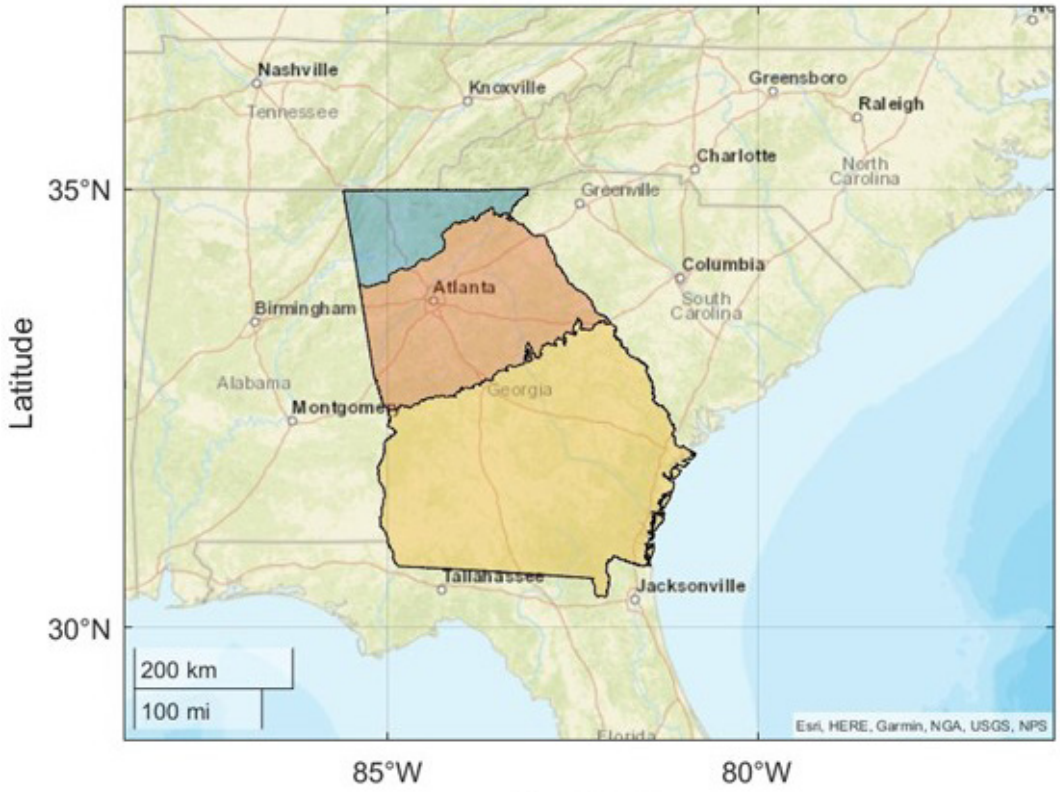

Figure 1. Three physiographic regions of Georgia: Blue Ridge Mountains (blue shading), Piedmont (orange shading), Coastal Plain (yellow shading).

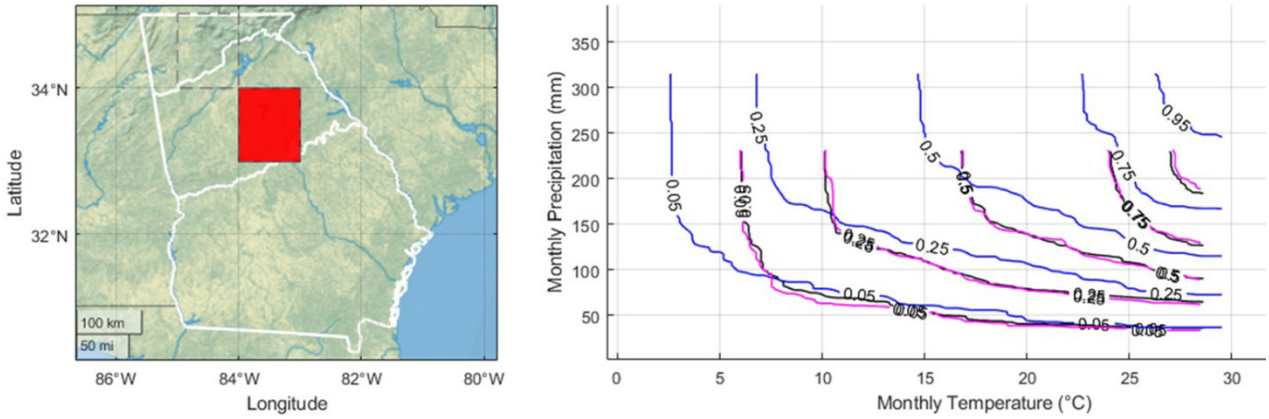

Figure 2. Typical Temperature-Precipitation joint cumulative distribution contours for a single GCM pixel (shown on the map) for the 1987–2014 historical period. Raw GCM contours without bias correction are plotted in blue, the target CRU-based contours in black, and the JVBC bias-corrected contours in magenta. These contours highlight the JVBC algorithm effectiveness in removing biases from raw GCM data.

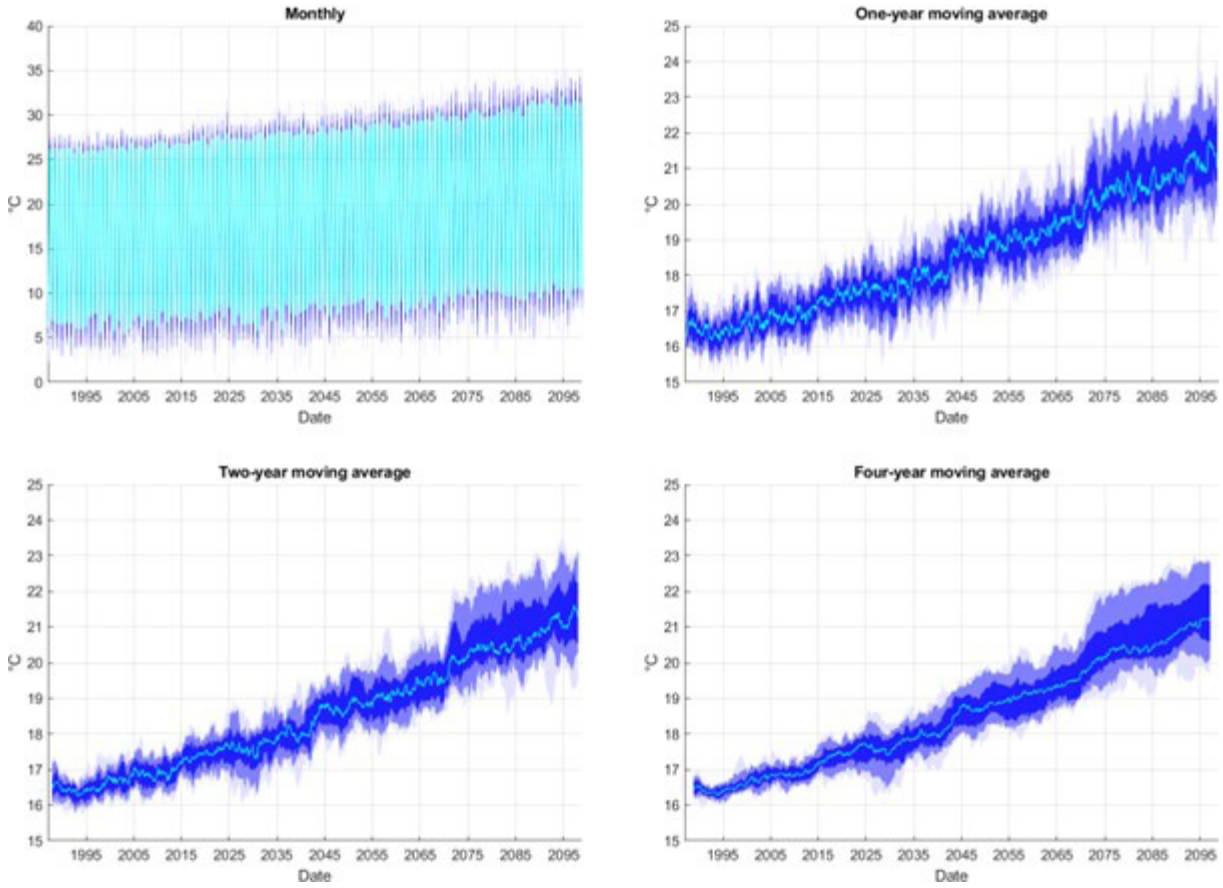

Figure 3. Time series of bias-corrected GCM monthly daily average temperature data for the Georgia Piedmont region. The shading delineates the 0th, 10th, 25th, 50th (cyan line), 75th, 90th, and 100th percentiles across 16 bias corrected CMIP6 GCM models under the aggressive SSP 5 emissions scenario.

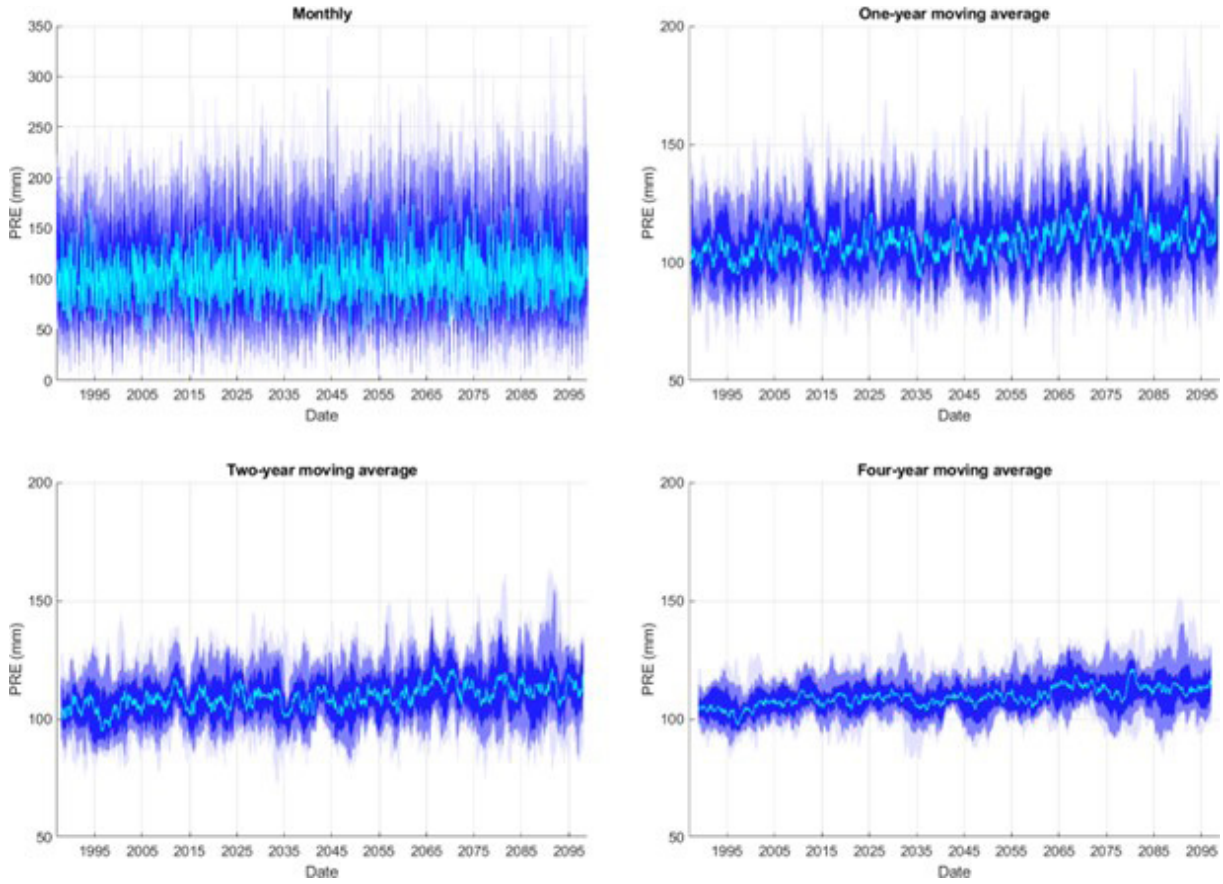

Figure 4. Time series of bias corrected GCM monthly precipitation (PRE) data for the Georgia Piedmont region. The shading delineates the 0th, 10th, 25th, 50th (cyan line), 75th, 90th, and 100th percentiles across 16 bias corrected CMIP6 GCM models under the aggressive SSP 5 emissions scenario.

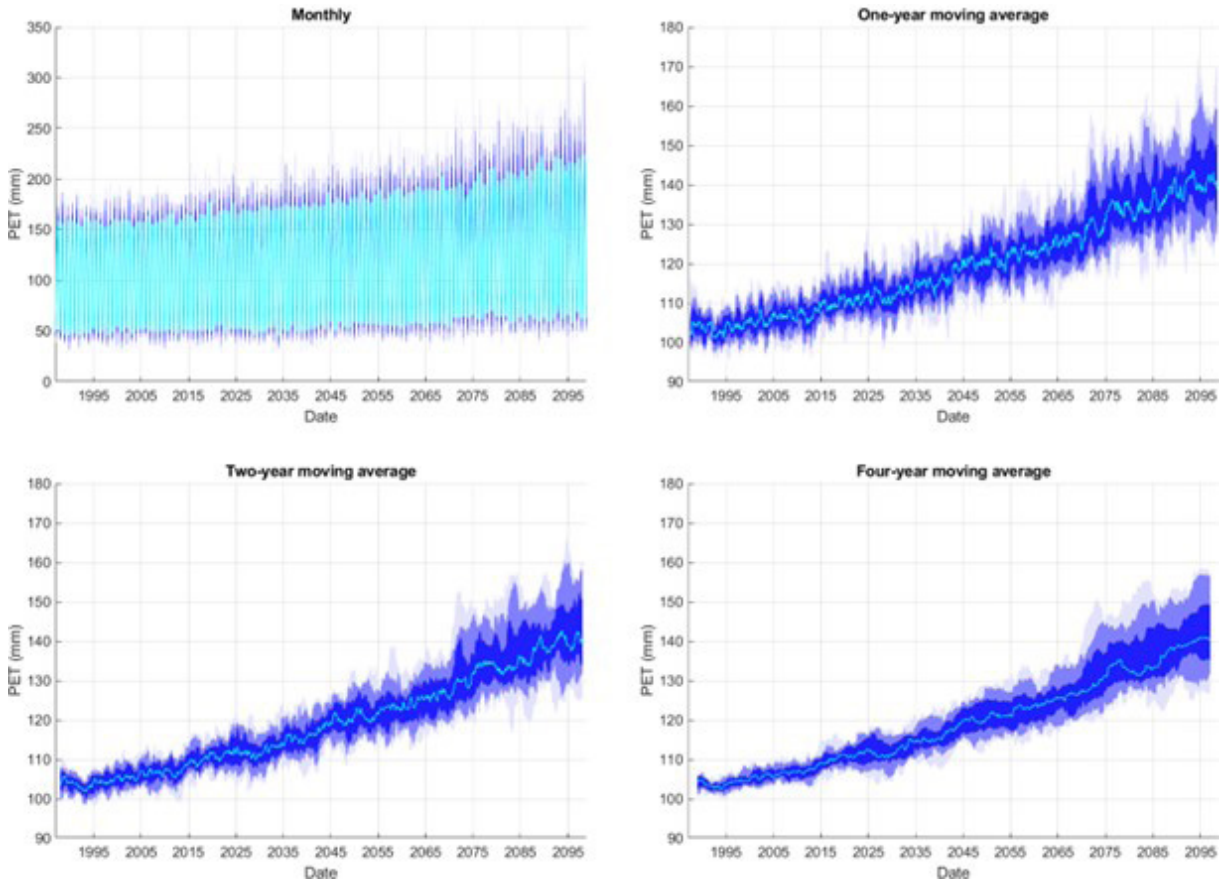

Figure 5. Time series of bias-corrected GCM monthly potential evapotranspiration (PET) data for the Georgia Piedmont region. The shading delineates the 0th, 10th, 25th, 50th (cyan line), 75th, 90th, and 100th percentiles across 16 bias corrected CMIP6 GCM models under the aggressive SSP 5 emissions scenario.

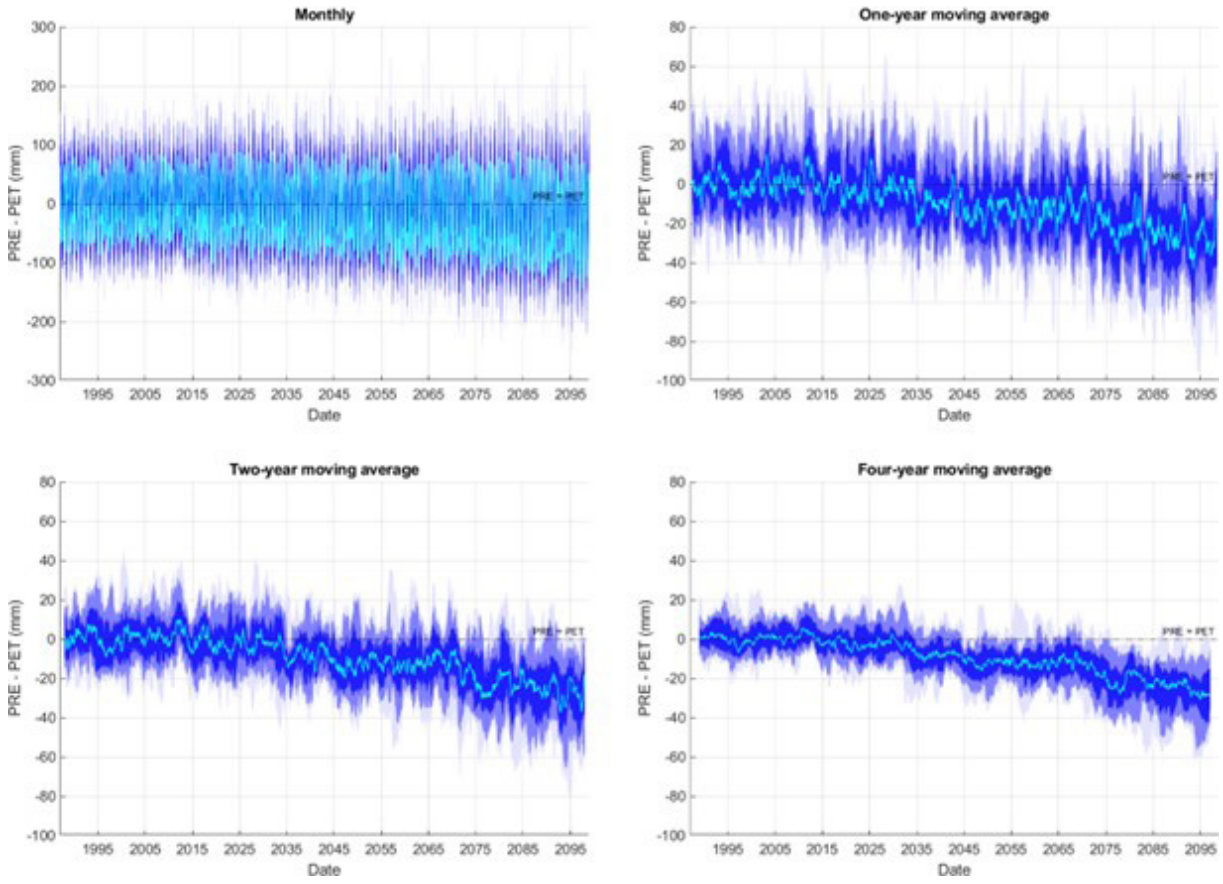

Figure 6. Time series of bias-corrected GCM monthly difference between precipitation and potential evapotranspiration (PRE ¬- PET) data for the Georgia Piedmont region. The shading delineates the 0th, 10th, 25th, 50th (cyan line), 75th, 90th, and 100th percentiles across 16 bias corrected CMIP6 GCM models under the aggressive SSP 5 emissions scenario.

Project ID	2022GA01B
Project Type	Research
Award Type	Base Grant (104b)
Project Title	Hydraulic transients in water distribution systems – the role of unsteady friction and GW contamination
Project PI	Lai, Chris
Academic Institution of PI	Georgia Institute of Technology
Congressional District of project	GA-5

Prepared by Dr. Chris Lai
School of Civil and Environmental Engineering
Georgia Institute of Technology, Atlanta

1 Summary

This report gives an account of the research activities done during the project period 10/1/2022 to 9/30/2023. As stated in the awarded proposal, this project consists of both experimental work and CFD code development. Each of them are separately discussed below. The research highlights are: (1) an operational reservoir-pipe-reservoir system built to study hydraulic transients (both accelerating and decelerating) in the presence of pipe roughness, (2) an experimental dataset demonstrating the effects of roughness in which the result interpretation is achieved by an analytical decomposition of the skin friction coefficient C_f, and (3) a set of MATLAB codes that implement 1D and 2D hydraulic transient calculations for pipe networks. These activities have been carried out by a first-year PhD student (Wei-Cheng Hung) who is supervised by PI Lai.

2 Experiments

2.1 Experimental setup

Figure 1 shows the current experimental setup in the Mason hydraulic lab located in the School of Civil and Environmental Engineering at Georgia Tech. The pipeline is 12m long and its nominal diameter is $D = 75$mm. The middle section is a 3.6m-long transparent octagonal test section where fluid flow measurements are made. The development length L_e for fully developed turbulent pipe flows was estimated using $L_e = 4.4Re^{1/6}D$. It is equal to $25.7D$ for the highest Re (=40000) achievable by this facility; our flows were all fully developed at the measurement station where $x = 80D > L_e$. Steady water flows in the system are generated and maintained by the difference in water levels between the upstream and downstream reservoir tanks. A butterfly valve installed near the downstream end controls the flowrate. The maximum Reynolds number Re achievable is 40,000 with a corresponding bulk velocity equal to 0.53 m/s.

Figure 2 shows a close-up of the test section. A rectangular water prism (0.15 m long) was built around the octagonal pipe to reduce unwanted op-

Figure 1: The reservoir-pipe-reservoir system used in this study.

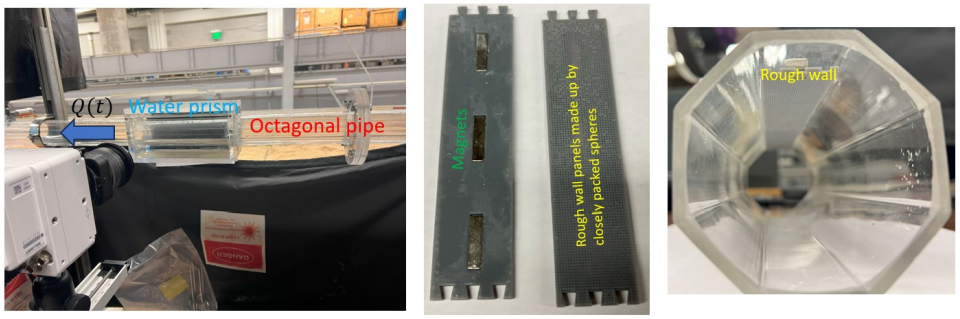

Figure 2: A closeup of the measurement station showing the octagonal pipe, water prism, 3D-printed uniformly roughness and its attachment to the top pipe wall.

tical distortions that would otherwise bias our particle image velocimetry (PIV) measurements. The acrylic octagonal pipe is hydraulically smooth. Roughness is introduced to the pipe by attaching 3D-printed panels on the inside of the pipe; figure 2 also shows an example of uniform roughness created by closely-packed 1 mm-diameter spheres. These panels are easily detachable because they are attached to the pipe walls using strong magnets. They remained securely in place (without motions) during experiments, enabling us to easily test different roughness patterns. We note that the roughness height/pipe radius ratio is $k/(D/2) = 1/37.5$ which according to [5] is sufficiently small to ensure the decoupling between the inner wall flow and the outer core flow. From table 1, flows considered in this study were all transitionally rough as the roughness Reynolds number k_s^+ falls between 5 and 70 (e.g. [8]). However, we expect our findings to be close to those of fully rough turbulent flows because the difference in friction factor (see Moody diagram) is only about 5% for the Re considered here; flows with a relative roughness $e = k/D \approx 0.01$ become fully rough at $Re = 10^5$.

Fluid velocities in the pipe centerplane during transient events were measured by 2D PIV where the illumination was provided by a 1 mm-thick laser sheet (created by a 5W, 532nm continuous wave laser and optics). A high-speed Phantom Research camera (VEO 440) was used to capture the PIV images with a field-of-view (FOV) measuring 54.4 mm tall and 87 mm long; it covered the near wall region to the pipe centerline. The sampling frequency was between 25 and 100 Hz, and the sampling duration was 60 s such that the whole flow transition was recorded. Since the flows were unsteady, each experiment (see Table 1) was repeated twenty times to obtain ensemble-averaged flow fields for subsequent analysis.

We have investigated both temporally accelerating and decelerating pipe flows. In either case, a turbulent pipe flow is forced to transition from one steady state to another. The required acceleration or deceleration was achieved by manually opening or closing the downstream butterfly valve. We found from experiments that this manual operation is highly repeatable and provides flow statistics that are suitable for ensemble averaging. Figure XX (a) shows a representative example of the time evolution of the bulk velocity ($U_b = Q/A$) during accelerations. It is seen that U_b increased nonlinearly with time and the flow transition with respect to U_b took about 4 s to complete; flow turbulence took longer (see later discussion). The corresponding acceleration-time graph is shown in figure 5. A similar situation happens during deceleration (figure 6). Table 1 gives the experimental con-

ditions of the three experiments conducted. These conditions were chosen to isolate the influence of uniform roughness (figure 2) on transients by keeping the pair of Reynolds numbers the same. T^{+0} is the dimensionless ramp up/down time and our values are about 10 to 40 times to those in [1]. Of most concern in PIV measurements of wall-bounded flows is the near-wall spatial resolution $\Delta y^{+1}_{\text{wall}}$. We did not try to make $\Delta y^{+1}_{\text{wall}} < 1$ but only ensured that it was close to or within the laminar sublayer ($\Delta y^{+1}_{\text{wall}} \leq 5$). The reason is that we have developed an equation that allows the use of noisy and resolution-limited PIV data to compute the unsteady friction coefficient C_f. This is explained in §2.3.

Case	$Re_{b,0}/Re_{b,1}$	$Re_{\tau,0}/Re_{\tau,1}$	k_s^{+0}/k_s^{+1}	T^{+0}	Δt^{+0}	γ	Δx^{+1}	$\Delta y^{+1}_{\text{wall}}$
A1S	9577/22983	299/643	0/0	352	3.5	4.6	9.5	5.1
A1R	9577/22983	353/817	7.2/16.6	495	4.8	5.5	12.0	6.4
D1R	22983/9577	817/353	16.6/7.2	495	4.0	5.7	6.0	2.8

Table 1: Experimental conditions - $\gamma = \frac{dU_b}{dt}(\frac{1}{U_{b,0}}\frac{D}{u_{*,0}})$ is the dimensionless parameter defined in He and Jackson (2000); when $\gamma >> 1$ the turbulent energy of the transient flow deviates from its initial quasi-steady value. Letter 'A' stands for accelerating flows whereas 'D' stands for decelerating flows. Letter 'S' indicates hydraulically smooth pipes and 'R' indicates hydraulically rough pipes. The superscript '+' stands for normalization by the shear velocity u_* and the fluid kinematic viscosity ν. The notation '0' means variables are calculated based on the initial steady flow whereas '1' means the ending steady flow conditions are used. Δt is the temporal resolution whereas Δx and Δy_{wall} are the streamwise spatial resolution and the first PIV grid point from wall, respectively. k_s^+ is the roughness Reynolds number. The hydraulic diameter of the octagonal test section is $D_H = 69.1$mm; it was used to calculate various Reynolds numbers.

2.2 PIV data processing

The captured images were first processed to remove stationary background (e.g. the non-moving pipe wall) prior to PIV cross-correlation. The background was constructed from the full image sequence by finding the minimum intensity level at each image pixel ([7]). Upon its subtraction from the raw images, strong laser light reflections at the wall were eliminated and therefore greatly minimized the PIV bias that would otherwise occur due to such stationary pixels of high intensity values. The PIV processing involved three iterative passes with image deformation of decreasing interrogation window (IW) size. The final IW had a 64 pix by 32 pix resolution and a

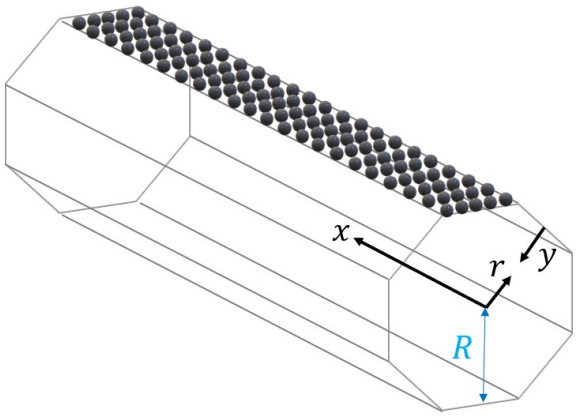

Figure 3: The coordinate system adopted in this study. The top wall of the octagonal pipe is lined with a uniformly packed of spheres.

75% overlap between windows. We used rectangular IWs to better resolve the steep velocity gradients in the wall-normal direction near the wall. By inspecting the raw images, there were 4-7 seeding particles at this resolution, lending confidence in the computed velocity fields. After each PIV pass, the universal outlier detection median filter ([10]) and a correlation peak ratio test (= 1.2) were applied to screen out unreliable PIV vectors. The created data gaps were not filled using interpolation to avoid biases; less than 4% of the total data were filtered out. The final 2D PIV vector spacing is 0.54 mm and 0.27 mm in the streamwise and wall-normal direction, respectively. All calculations were done using the open source PIV code PRANA ([2]).

2.3 Ensemble averaging of PIV data

Eq. (1) is the Reynolds averaged Navier-Stokes (RANS) equation for axisymmetric pipe flows; (x, r) are the streamwise and radial direction, respectively. It has been non-dimensionalized by the velocity scale $2U_b$ and the pipe radius R. $\overline{\mathbf{P}} = \overline{P}/\rho$ is the normalized pressure. $Re_b = 2U_bR/\nu$ is the bulk flow Reynolds number. The overbar notation $\overline{(\cdot)}$ indicates ensemble averaging.

$$\overbrace{\frac{\partial \overline{U}}{\partial t}}^{\overline{I_t}} + \overbrace{\frac{\partial \overline{U}^2}{\partial x} + \frac{1}{r}\frac{\partial r\overline{U}\overline{V}}{\partial r} - \frac{1}{Re_b}\frac{\partial^2 \overline{U}}{\partial x^2}}^{\overline{I_x}} = -\frac{\partial \overline{\mathbf{P}}}{\partial x} + \frac{1}{r}\frac{\partial}{\partial r}[\frac{1}{Re_b}\frac{r\partial \overline{U}}{\partial r} - r\overline{u'v'}] \quad (1)$$

Terms appearing in eq. (1) were computed from the PIV data by ensemble averaging the twenty repeated experiments for each experimental conditions. Turbulent fluctuation terms (e.g. $\overline{u'v'}$) are defined as the difference between an instantaneous variable and its average value i.e., $u' = u - \overline{U}$ and $v' = v - \overline{V}$. A schematic of our setup is shown in figure 3.

As derived in previous research (e.g. [3] and [1]), the bulk friction factor C_f can be analytically decomposed into different contributions that represent different forcings as shown in eq. (2) below.

$$C_f(x,t) = \frac{16}{Re_b} + 32\int_0^1 r'^2\overline{u'v'}dr' + 16\int_0^1 (1-r'^2)^2 Lr'dr' \tag{2}$$

where $L = I_t'' + I_x'' + \frac{\partial \mathbf{P}''}{\partial x} = \frac{1}{r}\frac{\partial}{\partial r}[\frac{1}{Re_b}\frac{r\partial\overline{U}}{\partial r} - r\overline{u'v'}] + C_f(x,t)/4 = \frac{1}{r}\frac{\partial r\tau_{\text{total}}}{\partial r} + C_f(x,t)/4$ where τ_{total} is the total fluid stress.

We now take a closer look at the last integral in eq. (2) - the term $\int_0^1 (1-r'^2)^2 Lr'dr' = \int_0^1 (1-r'^2)^2(\frac{1}{r}\frac{\partial r\tau_{\text{total}}}{\partial r} + C_f(x,t)/4)r'dr'$. Splitting the term into two yields:

$$\int_0^1 (1-r'^2)^2(\frac{1}{r'}\frac{\partial r\tau_{\text{total}}}{\partial r'} + \frac{C_f(x,t)}{4})r'dr' = \overbrace{\int_0^1 (1-r'^2)^2\frac{\partial r\tau_{\text{total}}}{\partial r'}dr'}^{I_1} + \overbrace{\int_0^1 (1-r'^2)^2 r'\frac{C_f}{4}dr'}^{I_2} \tag{3}$$

Since $C_f/4$ is independent of r', the value of I_2 can be straightforwardly found by integration and is equal to $\frac{1}{6}\frac{C_f}{4} = C_f/24$. And so from eq. (2), we found that C_f equals:

$$C_f(x,t) = 3[\frac{16}{Re_b} + 32\int_0^1 r'^2\overline{u'v'}dr' + 16I_1] \tag{4}$$

This means the integral I_2 is equal to:

$$I_2 = \frac{1}{6}\frac{C_f}{4} = \frac{1}{8}[\frac{16}{Re_b} + 32\int_0^1 r'^2\overline{u'v'}dr' + 16I_1]$$

Eq. (2) can be rewritten as:

$$C_f(x,t) = \frac{16}{Re_b} + 32\int_0^1 r'^2\overline{u'v'}dr' + 16(I_1 + I_2) \tag{5}$$

Then by definition, the bulk wall shear stress in physical units is computed as $\tau_w = 0.5\rho U_b(t)^2 C_f$:

$$\tau_w(x,t) = \frac{4\rho\nu U_b}{R} + 16\rho U_b^2 \int_0^1 r'^2 \overline{u'v'} dr' + 8\rho U_b^2 (I_1 + I_2) \tag{6}$$

Both eq.(5) and eq.(2) are inherently the same and will produce the same result when the input velocity data is error-free and of adequate spatio-temporal resolution. When applied to noisy PIV data with limited spatial resolution, eq.(5) has the clear advantage that the normalized bulk wall stress $2\tau_w^* = C_f/4$ (appearing in L in eq.(2)) needs not be computed, thus eliminating any inaccuracies that would have incurred from the finite difference approximation of $\partial\overline{U}/dr|_{r=1}$. *To the authors' knowledge, this form of the equation that is suitable for noisy PIV data has not been stated before.* Finally, one might argue that near wall velocity gradients still need to be computed when the integral I_1 is sought. While this is true we note that the weighting function $(1 - r'^2)^2$ effectively nullifies any errors stemming from the numerical approximation of the near wall gradients; $(1 - r'^2)^2$ is essentially zero in the near wall region. Thus, all terms appearing in eq. (4) and eq. (5) are large-scale flow quantities that are adequately resolved in most standard 2D PIV setup, including ours here. This is not surprising and is consistent with the integral analysis adopted in the FIK identity/approach of decomposing C_f.

3 Results

We start by showing the mean streamwise velocity profiles $\overline{U}(y)$ of the two steady end states ($Re_{b,0}$ and $Re_{b,1}$) where $y = 1 - r$ is the wall-normal distance (see figure 3). This is followed by the profiles of Reynolds stresses $\overline{u'^2}, \overline{v'^2}$ and $\overline{u'v'}$. We then present the time evolution of the above variables as a function of the normalized time $t^{+0} = t(u_{*,0}^2/\nu)$, starting with Case A1R. The FIK-decomposed C_f is shown next together with the predictions from the recently proposed unsteady friction model by [1].

3.1 Statistics of steady flows

Figure 4 shows the measured mean streamwise velocity profile against y in wall units. To objectively compare our data, the shear velocity $u_* = \sqrt{f/8}U_b$ has been computed with the established Colebrook equation and the bulk flow velocity U_b, not from fitting a presumed log-law profile to the data.

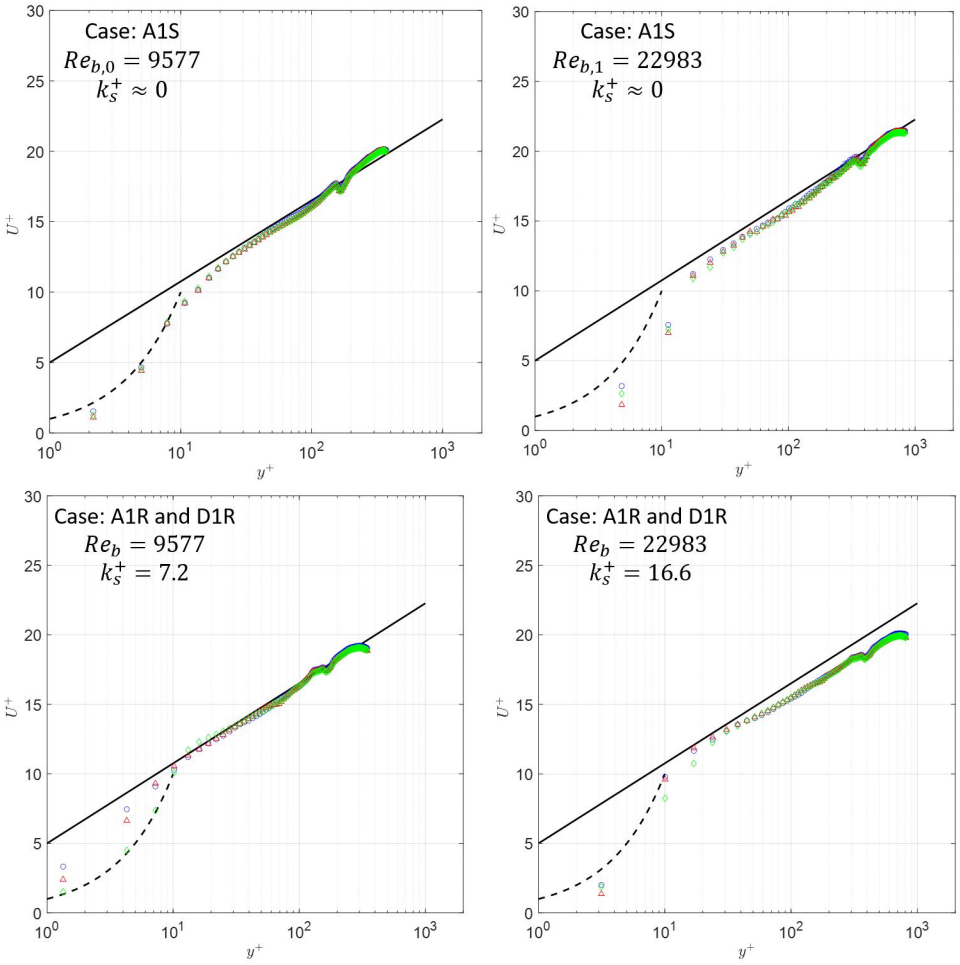

Figure 4: Mean streamwise velocity profile U^+ against y^+ for all cases. Symbols are experimental data points and the solid line represents the log-law $U^+ = 1/0.4\ln(y^+) + 5.0$

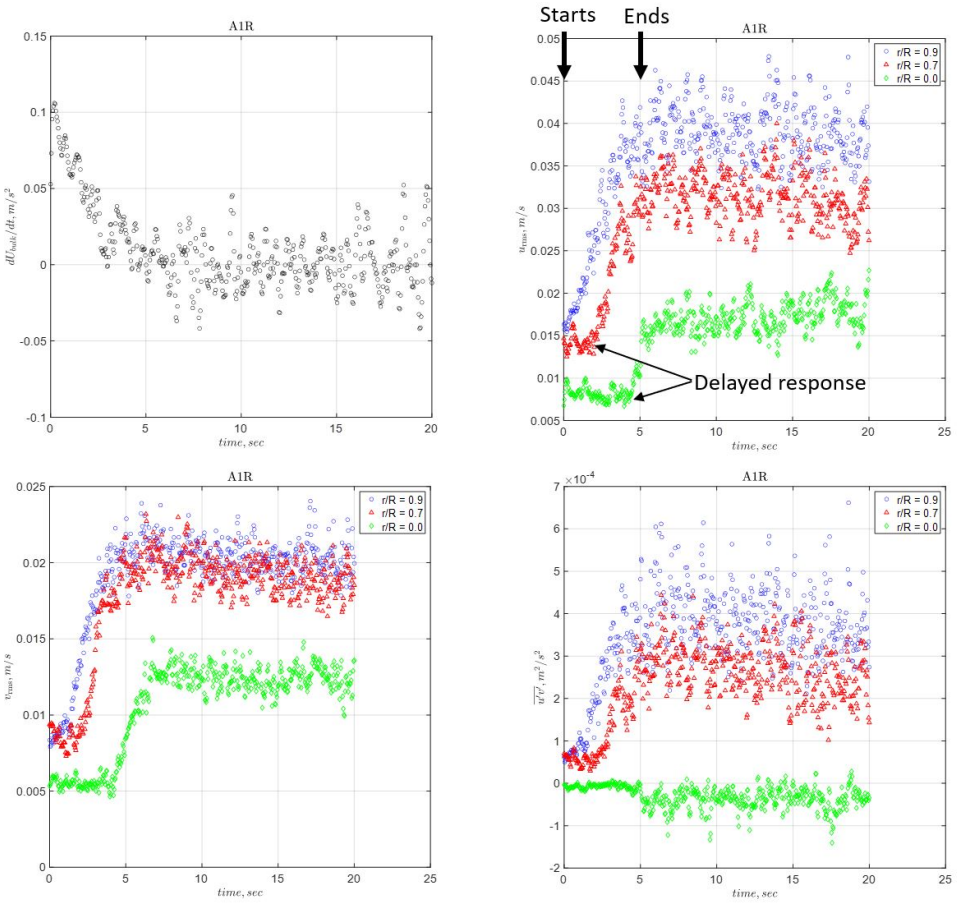

Figure 5: Time evolution of Reynolds stresses for accelerating flow case A1R.

Several observations can be made: (1) the first PIV data point from both smooth and rough wall was always within the laminar sublayer, (2) the laminar and buffer layer were resolved, (3) the rough pipe flow at the lower $Re_b = 9577$ was essentially hydraulically smooth, and (4) the rough pipe flow at the higher $Re_b = 22983$ was transitionally rough as reflected in the vertically shifted-down U^+ profile.

3.2 Statistics of unsteady flows

Figure 5 shows the time evolution of the Reynolds stresses in case A1R. From the acceleration-time graph (top left), it can seen that the flow took about 5 s to accelerate from $Re_{b,0}$ to $Re_{b,1}$. The acceleration peak was about

0.1 m/s^2 and the acceleration non-linearly decreased with time to zero at $t = 5$s. The Reynolds stresses at three radial positions ($r/R = 0.9, 0.7$ and 0) are shown in physical units; $r/R = 0.9$ corresponds to a position near the start of the log-law (overlapped) region, $r/R = 0.7$ is at the upper end of the overlapped region, and $r/R = 0$ is at the pipe center. As expected, they all increased in magnitudes as the initial flow was accelerated. The transient period seemed to have ended at around 10 s beyond which all stresses attained their new steady state values. Similar to previous observations, turbulent structures closer to the wall responded earlier to the imposed flow acceleration, with turbulence at the pipe center responding the slowest. By $t = 20$s, $\overline{u'v'} \sim 4 \times 10^{-4}\text{m}^2/\text{s}^2$ at $r/R = 0.9$. If we use the approximation $u_*^2 \approx \overline{u'v'}$, we get $u_* = 0.02$m/s which is close to the value (=0.214 m/s) calculated by $u_* = U_b\sqrt{f/8}$ with f found from the Colebrook equation.

Figure 5 shows the time evolution of the Reynolds stresses in the decelerating flow case D1R. In this case, the deceleration peak was about -0.6m/s^2 and the mean flow deceleration process ended at about $t = 1$s. The turbulence, however, took a longer time ($\sim$ 7s) to reach the new steady state ($Re_b = 9577$) as was observed in the accelerating flow case. Again, the near wall turbulent structures were responding earlier to flow transition than those at the pipe center. At $t = 7$s, $\overline{u'v'} \sim 0.5 \times 10^{-4}\text{m}^2/\text{s}^2$ at $r/R = 0.9$, giving an estimated $u_* = 0.0071$ m/s. This value is again comparable to $u_* = U_b\sqrt{f/8} = 0.0092$ m/s.

The results for the accelerating flow case A1S are qualitatively very similar to those of A1R and are therefore not shown for brevity.

3.3 Decomposition of C_f and τ_w

Before we show the decomposition of C_f, it is instructive to show C_f calculated directly from the measured streamwise velocity gradient at the wall i.e. $\tau_w = \mu\partial\overline{U}/\partial y|_{\text{wall}}$. Figure 7 shows the time evolution of C_f. It can be seen that C_f changed from an initial plateau to another one at large times in all cases. The two plateaus, of course, correspond to the initial and final steady states. Since C_f is related to the Darcy-Weisbach friction factor f by $f = 4C_f$, we can compare the experimentally found f to the predictions by the Colebrook equation. The differences between them were found to be within $\pm 20\%$. This supports our chosen near-wall PIV resolution $\Delta y^{+1}_{\text{wall}} \sim 5$ in which it was adequate to resolve τ_w. We have, however, computed the decomposition of C_f using eq.(6) instead of eq.(2) to avoid errors caused by

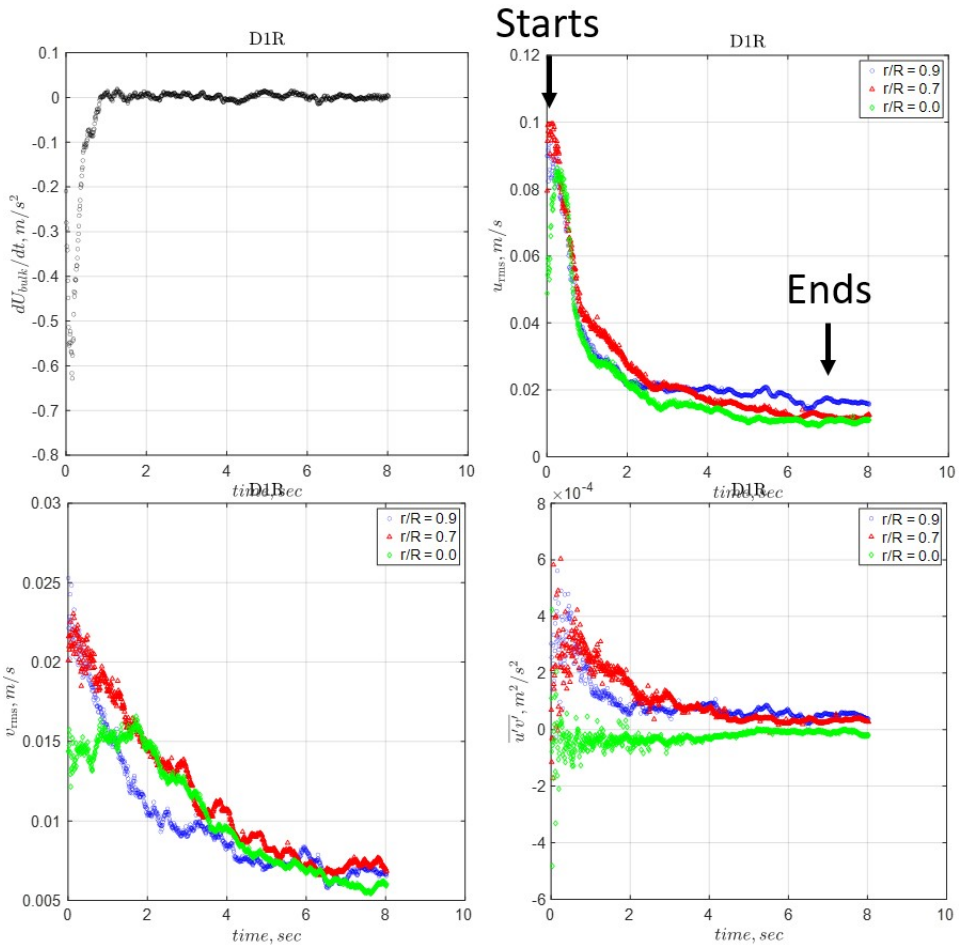

Figure 6: Time evolution of Reynolds stresses for decelerating flow case D1R.

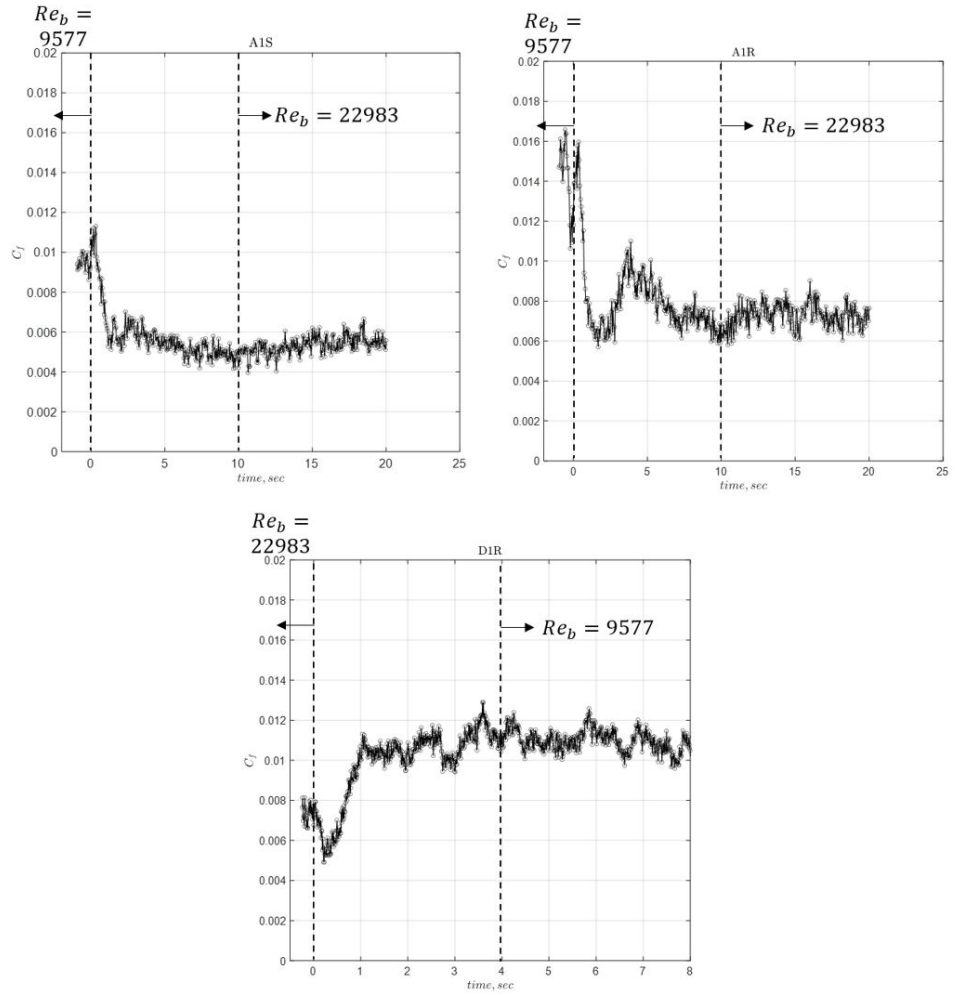

Figure 7: Time evolution of the skin friction coefficient $C_f = \tau_w/(0.5\rho U_b^2)$. The wall shear stress τ_w was directly computed using its definition $\tau_w = \mu\partial\overline{U}/dy|_{\text{wall}}$.

the rather noisy velocity-gradient-based wall stress measurements.

Case	$C_{f,0}/C_{f,1}$	$f = 4C_f$	$f_{\text{Colebrook}}$
A1S	0.009/0.0058	0.036/0.029	0.031/0.025
A1R	0.014/0.0077	0.056/0.031	0.043/0.041
D1R	0.008/0.0105	0.032/0.042	0.041/0.043

Table 2: Directly measured skin friction coefficient C_f from experiments and its conversion and comparison to the Darcy-Weisbach friction factor f.

Figure 8 shows the decomposition of the wall shear stress τ_w using eq.(6) for all three cases; τ_w is normalized by $\tau_{w,0}$ and time t by $\nu/u^2_{*,0}$. First, we look at the two accelerating flow cases A1S and A1R. Except for the small differences in the magnitudes, the decomposed stress terms behaved very similarly in both cases. At the start of valve opening $t^+ = 0$, the unsteady term rapidly increased to a maximum value of about 1.8 and then dropped gradually to zero at larger times when the turbulent term had reached its new plateau. It appears that the unsteady terms of both smooth and rough pipe flows reached their maxima at about the same time ($t^{+0} \sim 250 - 280$). However, the term became zero (or small compared to the turbulent term) earlier ($t^{+0} \sim 800$) in the smooth pipe than the rough pipe ($t^{+0} \sim 1000$).

In the case D1R of decelerating rough pipe flow, the unsteady term was negative. It responded immediately to the valve closure, reached its minimum value, then increased back to zero at large times. Compared to accelerating flows, it is seen that the non-dimensional time required for decelerating flows to complete its transition is much longer ($t^{+0} \sim 10^4$).

In the recent work by [1], the authors found that the semi-analytical unsteady friction model by Vardy and Brown ([9]) accurately predicts the unsteady term in hydraulically smooth pipe flows undergoing uniform acceleration/deceleration. After accounting for the different model coefficients in smooth and rough pipe flows, we have plotted the model τ_{VB} in figure 8. It is seen that τ_{VB} underpredicts the measured unsteady friction term by more than 50% in accelerating flows, regardless of roughness. For decelerating flow,τ_{VB} instead overpredicts by about 60%. Further, our measured data reached their peak/minimum value later than τ_{VB}. A possible reason for the observed discrepancy could be due to the violation of an assumption used in the Vardy and Brown model - they assumed $\gamma \gg 1$. Our experiments

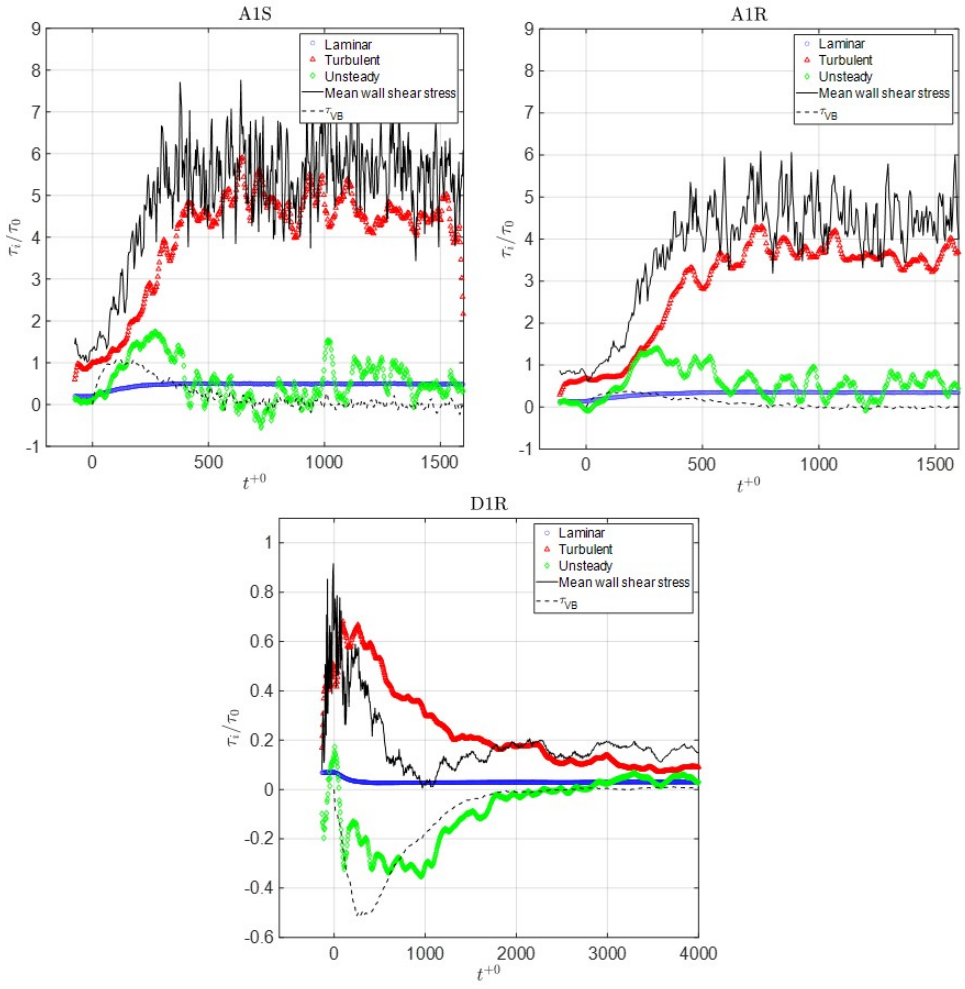

Figure 8: Time evolution of the decomposed wall shear stress using eq.(6).

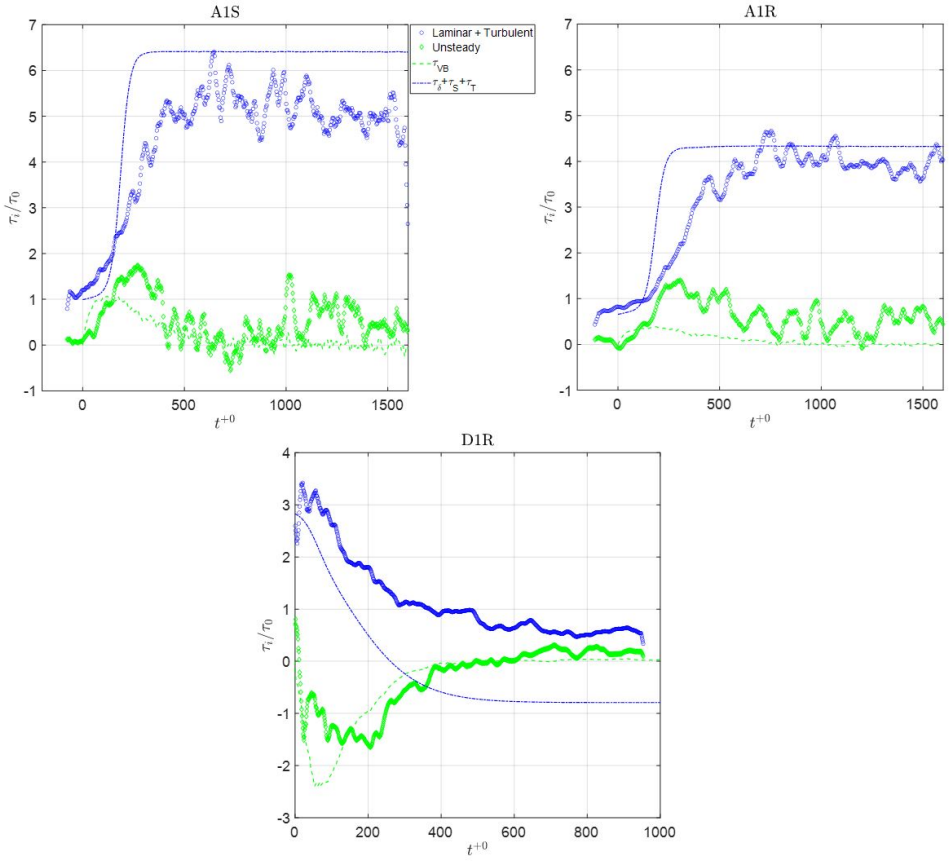

Figure 9: Comparison of the unsteady friction term and the sum of turbulent and laminar terms between measurements and the predictions by the recent model in [1].

had $\gamma \sim 5$ (see table 1). This value was based on the maximum magnitude of flow acceleration/deceleration. If we account for the non-uniform acceleration/deceleration time history, the average $\gamma_{\text{avg}} \approx \gamma/2 = 2.5$. The assumption $\gamma \gg 1$ enabled Vardy and Brown to treat the eddy viscosity distribution as frozen during the entire flow transition. To clarify this issue, we will later do an in-depth analysis on the eddy viscosity distribution with time for all cases.

Figure 9 shows a comparison of the various contributions to the unsteady wall shear stress between predictions from the recent model proposed by [1]

and our measured data. It can be seen that the sum of laminar and turbulent terms in accelerating flows (A1S and A1R) is not predicted well by the model. The predicted curve reaches the new steady state too quickly at $t^{+0} = 250$. Instead, our measured data show that the flow took two times the time predicted by the model ($t^{+0} = 500$) to reach the new steady state. As described previously, τ_{VB} is unable to accurately predict the unsteady term. In the case of decelerating flow (D1R), we found that the predicted sum of laminar and turbulent terms exhibits non-physical behavior (being negative) at large times. This suggests that the proposed model that is originally devised for smooth turbulent pipe flows is not applicable to the rough, decelerating flow studied here. One may ask why the model works reasonably well (at least being physically correct for displaying positive values) in our accelerating rough pipe flow case A1R. We remark that this flow began with a k_s^+ value of 7.2 that is just outside the hydraulically smooth regime. This means the roughness elements (almost) reside within the laminar sublayer. Their presence only increases the wall shear stress but do not disturb the overlying buffer layer and log layer. The near wall flow remains structurally the same as a flow without the roughness (i.e. case A1S), thus explaining the fair comparison between predictions and measured data. On the contrary, the decelerating flow case D1R began with $k_s^+ = 16.6$ that indicates transitionally rough regime. Any models that assume hydraulically smooth flows will not perform well.

In the next step, we will revise the model using our data.

4 Hydraulic transient simulations

In this section, we detail our coding efforts on simulating hydraulic transients in pipes and pipe networks. Although the numerical methods are not new, the developed codes are integral to the project and will be used to test our newly proposed unsteady friction model.

4.1 1D modeling

The governing equations for 1D modeling of hydraulic transients (e.g. [4]), including both unsteady friction and viscoelastic effects, are:

$$\frac{\partial H}{\partial t} + \frac{a^2}{g}\frac{\partial U}{\partial x} + \frac{2a^2}{g}\frac{d\epsilon_r}{dt} = 0 \tag{7}$$

$$\frac{\partial U}{\partial t} + g\frac{\partial H}{\partial x} + \frac{\tau_w \pi D}{\rho A} = 0 \tag{8}$$

where H is the pressure head, $U = Q/A$ is the bulk velocity, a is the pressure wave speed, and τ_w is the average wall shear stress. ϵ_r is the retarded viscoelastic response (strain) that viscoelastic pipes (e.g. PVC) develop during water hammers. These two equations are solved using the method of characteristics (MOC) with the wall shear stress parameterized as $\tau_w = \tau_{w,s} + \tau_{w,us}$. $\tau_{w,s}$ is the quasi-steady stress and can be specified using any established empirical formula for steady flows. $\tau_{w,us}$ is the unsteady stress and can be modeled in the number of ways. Here we use C_f, leading to $\tau_{w,us} = 0.5 C_f U|U|$.

Our numerical solver is written in MATLAB and can handle pipe networks with multiple junctions, reservoirs, valves, and pumps.

4.2 2D modeling

While 1D modeling has been successful in predicting H and U, it neglects the variations of the streamwise velocity across the pipe cross-section. This is undesirable in water quality modeling because mass transport is intimately linked to the radial profile, hence gradients, of the streamwise velocity. This is especially true in the pipe wall regions where contaminants are introduced into a pipe. To circumvent this problem, we need a 2D modeling of hydraulic transients for which we have followed the proposed formulation in [11]. The governing equations are:

$$\frac{\partial H}{\partial t} + \frac{a^2}{g}\left[\frac{\partial u}{\partial x} + \frac{1}{r}\frac{\partial r v}{\partial r}\right] = 0 \tag{9}$$

$$\frac{\partial u}{\partial t} + g\frac{\partial H}{\partial x} - \frac{1}{r\rho}\frac{\partial r \tau_{\text{total}}}{\partial r} = 0 \tag{10}$$

where $u = u(x, r, t)$ is the ensemble-averaged streamwise velocity and v is the radial velocity. These two equations are solved using the method of characteristics (MOC) in the streamwise direction x together with a finite difference discretization in the radial direction r for the radia flux rv and the total fluid stress τ_{total}.

To close the system of equations, it requires modeling of the Reynolds shear stress $-\overline{u'v'}$ in τ_{total}. This is commonly done using the eddy viscosity approach $-\overline{u'v'} = \nu_t(\frac{\partial u}{\partial y} + \frac{\partial v}{\partial x})$ where ν_t is the eddy viscosity that needs to be specified or computed. In our MATLAB code, we can choose between a constant eddy viscosity formulation and a variable viscosity formulation that is based on a two-equation $k-\epsilon$ turbulence model ([12]). As we analyze our experimental datasets further, this 2D code will allow us to test new formulations of the $k-\epsilon$ model that is suitable for rough pipes.

5 Summary and conclusions

In this one-year project, we have achieved the following:

1. Successfully designed an built an experimental setup suitable for studying hydraulic transients.
2. Derived and tested an analytical expression that is suitable for using noisy and resolution-limited PIV data to compute the friction coefficient C_f.
3. Elucidated the differences in hydrodynamic behaviors between accelerating and decelerating rough turbulent pipe flows and also between rough and smooth pipe flows.
4. Written a set of MATLAB codes that implements 1D and 2D hydraulic transient calculations

We plan to submit our first journal paper, entitled *An improved 1D unsteady friction model for turbulent rough pipe flows undergoing mild acceleration/deceleration: the case of closely packed uniform spheres* to the Journal of Hydraulic Engineering, ASCE by the end of November 2023.

To expand the results found in this one-year project, we propose the following tasks:

1. *Test random and irregular roughness patterns* - In this project year, we have only tested regular uniform roughness similar to those used by Nikuradse (1933) in his seminal experiments on steady rough pipe flows. Our experiments enabled us to test and validate our procedures and analysis framework. The next step will be to study random and irregular roughness as is commonly found in natural and man-made

surfaces. For this purpose, we will use 3D prints of single-valued self-affine fractal surfaces to mimic natural roughness ([6]).

2. *Increase the study range of Re and* γ - to develop an universal 1D unsteady friction model for general use.

References

[1] Guerrero B., M.F. Lambert, and Chin R.C. Extension of the 1d unsteady friction model for rapidly accelerating and decelerating turbulent pipe flows. *Journal of Hydraulic Engineering, ASCE*, 148(9):04022014, 2022.

[2] A. Eckstein and P.P. Vlachos. Digital particle image velocimetry (dpiv) robust phase correlation. *Meas. Sci. Technol.*, 20(5):055401, 2009.

[3] K. Fukagata, K. Iwamoto, and N. Kasagi. Contribution of reynolds stress distribution to the skin friction in wall-bounded flows. *Phys. Fluids*, 14(11):L73, 2022.

[4] M.S. Ghidaoui, M. Zhao, D.A. Mclnnis, and Axworthy D.H. A review of water hammer - theory and practice. *Applied Mechanics Review, ASME*, 58:49–75, 2005.

[5] J. Jimenez. Turbulent flows over rough walls. *Annual Review of Fluid Mechanics*, 36:173–196, 2004.

[6] V.I. Nikora, T. Stoesser, S.M. Cameron, M. Stewart, K. Papadopoulos, P. Ouro, R. McSherry, A. Zampiron, I. Marusic, and R.A. Falconer. Friction factor decomposition for rough-wall flows: theoretical background and applications to open-channel flows. *Journal of Fluid Mechanics*, 872:626–664, 2019.

[7] G.I. Roth and J. Katz. Five techniques for increasing the speed and accuracy of piv interrogation. *Meas. Sci. Technol.*, 12:238–245, 2001.

[8] H. Schlichting and K. Gersten. *Boundary-layer theory.* Springer, ninth edition, 2016.

[9] A.E. Vardy and J.M.B. Brown. Transient turbulent friction in fully rough pipe flows. *Journal of Sound and Vibration*, 270:233–257, 2004.

[10] J. Westerweel and F. Scarano. Universal outlier detection for piv data. *Exp. Fluids*, 39(6):1096–1100, 2005.

[11] M. Zhao and M.S Ghidaoui. Efficient quasi-two-dimensional model for water hammer problems. *Journal of Hydraulic Engineering, ASCE*, 129(12):1007–1013, 2003.

[12] M. Zhao and M.S Ghidaoui. Investigation of turbulence behavior in pipe transient using a $k - \epsilon$ model. *Journal of Hydraulic Research, IAHR*, 44(5):682–692, 2006.

Project ID	2022GA02B
Project Type	Research
Award Type	Base Grant (104b)
Project Title	Scenario Analysis of Flood Risk in Savannah by an Integrated Urban-Hydrology-Hydraulics Model – Phase II
Project PI	Luo, Jian
Academic Institution of PI	Georgia Institute of Technology
Congressional District of project	GA-5

FINAL REPORT

Scenario Analysis of Flooding Risk at City of Savannah by an Integrated Urban-Hydrology-Hydraulics Model – Phase II

Jian Luo

School of Civil and Environmental Engineering

Georgia Institute of Technology

Contents

Abstract:

This study is the second phase of our ongoing research, building upon prior support from the USGS 104B program. We have successfully developed a pilot-scale integrated urban-hydrology-hydraulics model, focused on simulating compound flood risks in downtown Savannah. In this new phase, our project expanded the model's scope to include residential areas and 2D Savannah River Basin hydrology, refine and calibrate this broader model, and leverage it for flood risk scenario analysis. Savannah faces an acute flood risk due to its low elevation, flat terrain, proximity to the coast, high tides, and the presence of numerous rivers, creeks, and streams. This risk is further exacerbated by the increasing frequency of extreme climate events and projected sea-level rise associated with 21st-century climate change. The expanded model encompasses both downtown Savannah and the uptown region, bounded by the Savannah River and coastal wetlands. It integrates a high-fidelity SWMM model for drainage systems, a HEC-RAS model for the Savannah River, and a SWMM model for surface runoff routing. The major outcomes of this project includes extensive datasets detailing hydrology and hydraulics parameters in Savannah, as well as a comprehensive flood risk assessment encompassing historical hurricane events and future climate change scenarios, which include coastal driving factors such as sea level rise, upstream driving factor such as reservoir management, and precipitation.

1. Introduction

Flooding in coastal regions, exacerbated by extreme weather events and sea level rise (SLR), has emerged as the most frequent and financially burdensome natural hazard in the United States. It presents a pressing national-security concern for emergency management. Various flood models have been crafted to gauge flood-hazard exposure in coastal areas, considering SLR, tides, and storms. These models include the hydrodynamic Sea, Lake, and Overland Surges from Hurricanes (SLOSH) model, designed to simulate storm surges from tropical cyclones (Zachry, 2015), and the recently developed Coastal Storm Modeling system (CosMoS) by the U.S. Geological Survey (USGS), which has been applied to urbanized regions in California (Barnard et al., 2019).

A primary assumption or constraint of such models is that coastal impacts overwhelmingly drive flooding. However, flooding in urbanized coastal areas results from an intricate interplay of urban hydrology, river and open channel hydraulics, coastal influences, and climate change. Unfortunately, there is a notable absence of modeling studies focusing on urbanized coastal regions. In our prior endeavors, partially supported by USGS 104B funding, we crafted an integrated urban-hydrology-hydraulics model based on SWMM to evaluate flood risks in the urbanized sectors of the City of Savannah (Figure 1). This project's objectives encompass conducting sensitivity and scenario analyses using the developed model to evaluate and predict compound flood risks in urbanized coastal regions. Additionally, it seeks to underscore the significance of integrating various disciplines to model coastal flood-driving processes, and to provide short-term mitigation strategies and long-term urbanization plans for enhancing community resilience to floods, thereby contributing to comprehensive hazard management and urban planning.

Situated in close proximity to both the Savannah River and the Atlantic Ocean (see Figure 1), the City of Savannah faces a significant vulnerability to flooding. This vulnerability extends to various infrastructures, roadways, wetlands, and properties, which are frequently inundated. This recurring flooding not only endangers public safety but also places tremendous pressure on emergency management efforts. The flood hazards experienced in this region encompass three main categories:

- Coastal Flooding: This results from the combined effects of high tides and storm surges (as depicted in Figure 1).

- Flash Floods: Localized areas are susceptible to flash floods triggered by heavy rainfall and subsequent surface water runoff.

- Riverine Floods: These occur due to the rising water levels in nearby rivers.

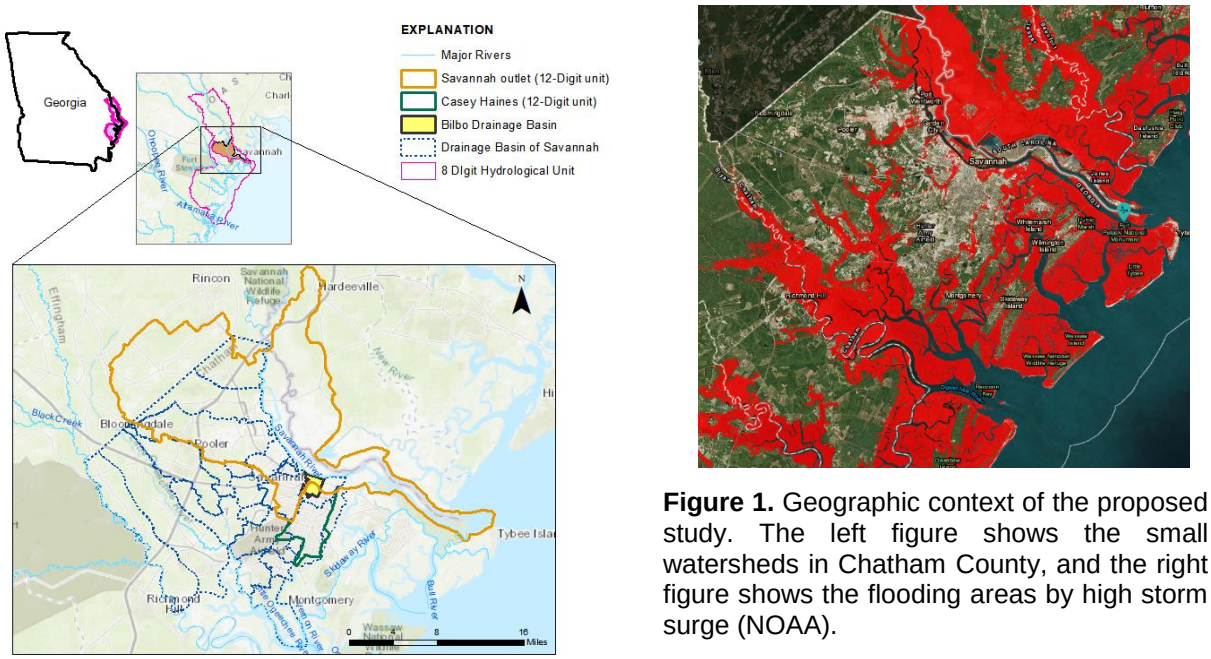

Figure 1. Geographic context of the proposed study. The left figure shows the small watersheds in Chatham County, and the right figure shows the flooding areas by high storm surge (NOAA).

The compound flood risk faced by Savannah is further exacerbated by the increasing frequency of extreme climate events and the anticipated sea-level rise associated with 21st-century climate change, as indicated in the Fourth National Climate Assessment (2018). For instance, we can observe the impact of these factors when comparing Hurricane Matthew in 2016 to Hurricane Dorian in 2019. Despite both being in the same category and following similar paths along the Georgia coast, Hurricane Matthew in 2016 resulted in more extensive flooding. This discrepancy was primarily due to Hurricane Matthew's significantly heavier rainfall, which led to runoff in the Savannah and Ogeechee rivers exceeding their capacity, causing numerous localized flooding incidents. These compounding processes not only increase the uncertainty surrounding flood control and mitigation but also pose a barrier to potential economic development in the region.

We have proposed to the USGS 104B program to develop a pilot-scale integrated urban-hydrology-hydraulics model has been developed to simulate flooding risks in downtown Savannah (Figure 2). This project is the second phase of research following previous support, extending the model (Figure 3) to include residential areas, refining and calibrating the extended model, and applying the calibrated model for compound flood risk scenario analysis.

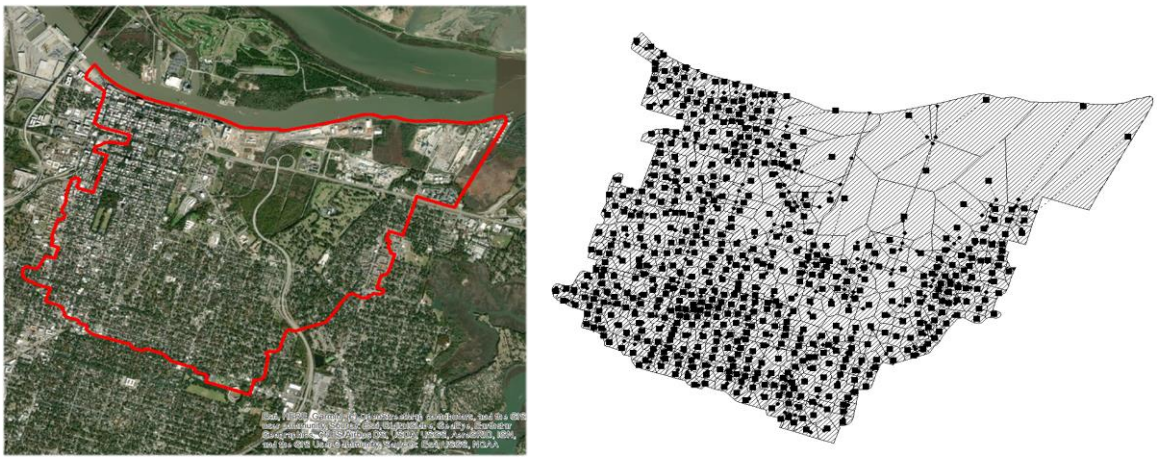

Figure 2. Pilot-scale urban-hydrology-hydraulic model for downtown Savannah.

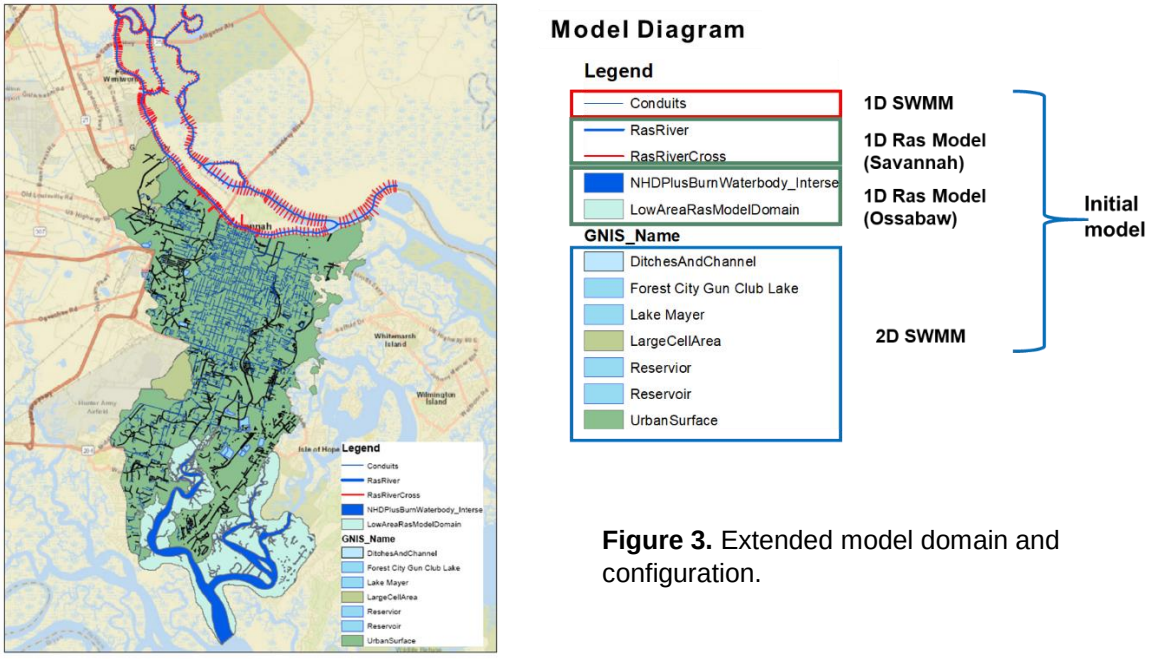

Figure 3. Extended model domain and configuration.

2. Scope and Objectives

As depicted in Figure 3, our research centers on downtown Savannah and adjacent residential areas that border wetlands, the Savannah River, and the coastline. The primary focus of this study is to simulate compound flood risks within this extended area using our developed model, encompassing both historical and future climate scenarios. Our specific research objectives are as follows:

- Data and Parameter Preparation for Model Development: To facilitate model development, we will prepare essential data and parameters. This includes the generation of parameter maps for the expanded area, incorporating factors such as land use, soil type, Manning coefficient, curve number, soil conductivity, soil moisture, and slope. Figure 4 illustrates some of the maps that have been generated and will be utilized in the model. We will gather historical climate data on precipitation, storms, and flooding from sources like USGS, NOAA, and local and federal agencies such as the Chatham Emergency Management Agency. Additionally, we will obtain future climate projections, specifically regarding rainfall and sea-level rise in Chatham County, from IPCC models (as referenced in the Fourth National Climate Assessment, 2018).
- Model Development and Validation: Our model will undergo further development to account for the influence of climate change and sea-level rise. This will involve integrating boundary condition impacts into the model. Two approaches will be explored: one will involve adjusting river water levels to manage discharge rates, and the other will consider inundation, which will affect the model's domain size. Subsequently, the developed model will undergo rigorous validation and calibration processes, utilizing historical and ongoing flooding events as benchmarks.

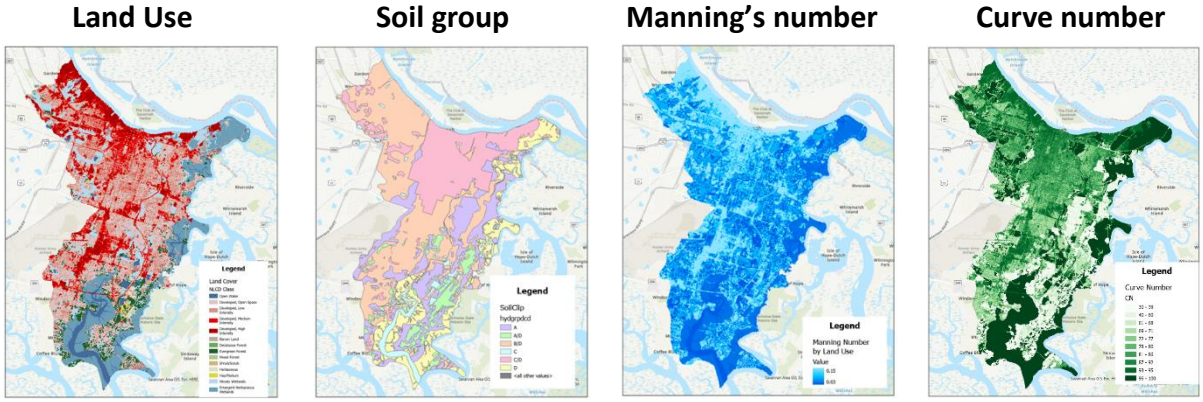

Figure 4. Input parameter map for the extended model.

- Flood Risk Scenario Analysis: Leveraging the capabilities of our developed model, we will conduct flood risk scenario analyses. These analyses will produce flood risk maps and identify "hot-spots" within the infrastructure, road networks, and specific areas. Our assessments will encompass historical climate data and consider the existing urbanization and stormwater management systems. Moreover, we will explore future scenarios that incorporate projected urban development, precipitation patterns, and sea-level rise.

3. Model Development

Fluvial Model for the Savannah River

Figure 5 depicts the riverine model utilized in this study, with the locations of data depots from USGS and NOAA indicated as Loc 1, Loc 2, Loc 3, Loc 4, and Loc 5. The model is delineated using NHDPlus HR Burned Water data, Water body data (WBD), and NHDPlus HR flow line data from USGS.

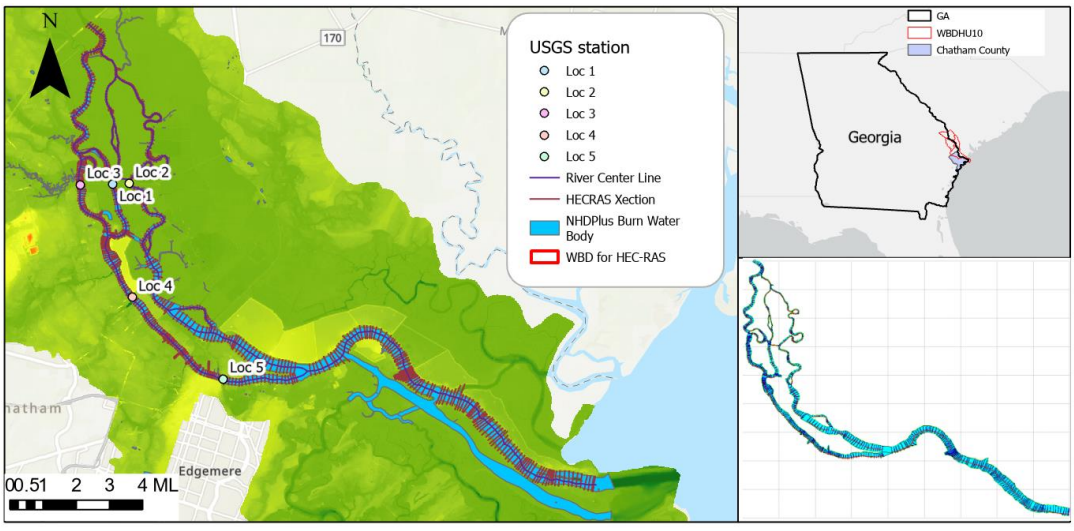

Figure 5. The left image shows HEC-RAS model with its data sets on DEM. The right upper image shows an approximate location of water body (WBD) of the Savannah River. The right lower image shows HEC-RAS model in HEC-RAS program GUI.

Table 1 outlines the critical data sets used in the construction of the model. The bathymetry data set and NHD Plus HD data set are particularly important as they determine the physical shape of the river model. The land use data from MRLC serves as a reference for Manning's roughness over the floodplain and open channel, which is a significant parameter used to calibrate the model. Historical flood data from USGS, presented as loc 1, loc 2, loc 3, and loc 4, are also used for model calibration. Flow rate and stage data at the upstream and downstream end locations provide information on the initial and boundary conditions for specific events, such as Hurricane Matthew (2016) and Hurricane Irma (2017), which serve as case studies for this research. Additionally, a hydro-enforced DEM generated from Light Detection and Ranging data (Lidar) provides the bathymetry data and floodplain elevation for the fluvial flood model.

Table 1. Key data sets for a fluvial flood model

Name	Description	Spatial resolution	Temporal resolution	Data Source
DEM	Hydro-enforced DEM(digital elevation model)	3m	N/A	NOAA
NHDPlus HR	National, geospatial watershed model	Various (1:24,000, 10m)	N/A	USGS
National Land Cover Data set (NLCD)	Land use data set	30m	Valid 2019	MRLC
USGS water data	A historical record of water stage/flow rate	N/A	15 mins	USGS/USACE

Unlike previous versions of HEC-RAS, the new HEC-RAS 6.0 Beta 2 allows for a 2D routing process, enabling the creation of a 1D-2D combined model. If revisions to the model are required, this could be another option for further research in line with our objectives.

Boundary conditions for the model are selected based on data availability from various sources, including NOAA, USGS, the Chatham County Hazard Mitigation Plan, Georgia Emergency Management Agent (GEMA), and FEMA. If coastal flooding records are available, the event period will be selected as a time window for the flooding case study. Data availability is then tested. Boundary data sets for upstream and downstream include river stage and flow rate data.

Calibration is conducted by changing the cross-section numbers between nodes and Manning's roughness along the fluvial flood model. Validation is performed by comparing the model output to real data measurements for several extreme weather cases.

GIS Integrated Urban Flooding Model

The urban flood model used in this study is a high-resolution, GIS-integrated model that employs a 2D distributed method. Due to the complex conditions of urban environments, including changes in surface elevation and multiple hydraulic components such as drainage networks, roads, stormwater headwalls, culverts, open channels, and weirs, a high-resolution model is required. The scale and resolution of the model are determined by the layers of surface and subsurface features. Figure 6 shows the conceptual model components, with details provided in Table 2.

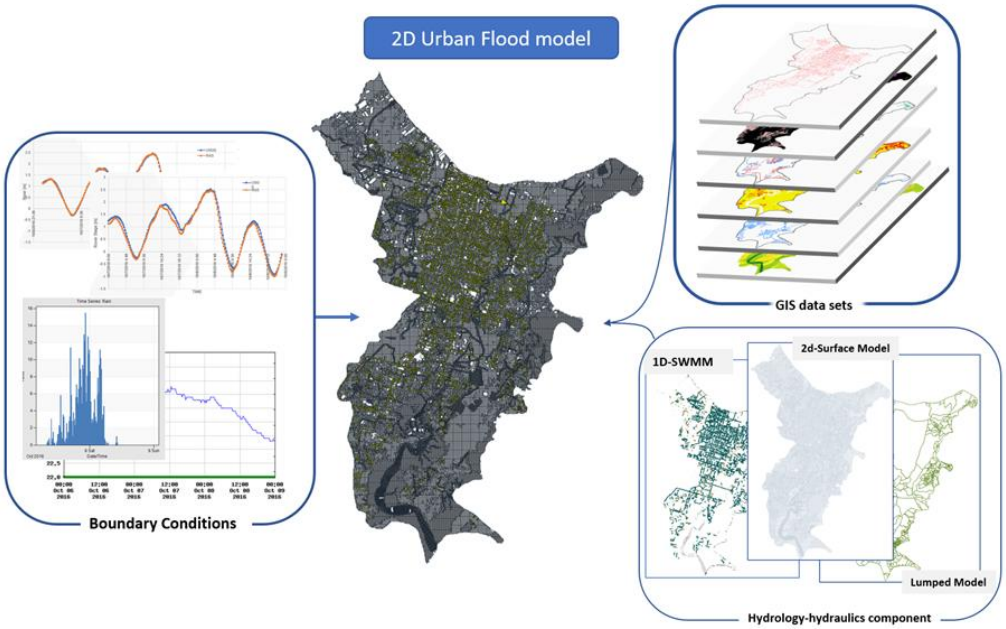

Figure 6. Conceptualized 2D urban model. The model components are parameter GIS data sets, hydrology-hydraulics components, and boundary conditions passed from HEC-RAS model and climate data sets. GIS data sets: Road, hydraulics structures, subsurface soil data.

Table *2.* Critical data sets for an urban flood model

NAME	Data products & parameters in SWMM	Spatial resolution	Temporal resolution	Data Source
DEM	Slope	3 m	N/A	NOAA
	Area			
NCLD	Manning's roughness	30 m	Valid 2019	MRLC
NHDPlus HR	Water Body	Various (1:24,000, 10 m)	N/A	USGS
	Burnwater data			
	Artificial/natural Channel			
SSURGO	Hydraulic Conductivity	Various	Valid 2016	USDA
	Suction Head			
	Porosity			
	Hydrological soil group			
	Wilting Point			
Stormwater structures	Pump station	N/A	Valid 2020	SAGIS
	Drainage system			
	Open Channel			
	Weir			
	Culvert			
	Stormhead wall			
	Canals			
	Tidal Gates			
Road centerline	Physical road data	1:24,000	Valid 2020	GDOT
Uran Imperviousness	Imperviousness	30 m	Valid 2020	MRLC
SMAP	initial soil moisture reference	3 km	Since 2015	NASA
eMODIS	Daily Evaporation	1.1 km	Since 2000	NASA/USGS

To construct the model, a 1D SWMM model was used for the drainage network, while PCSWMM was used for surface routing. The drainage network's location, material, and invert depth or elevation (pipe network) were mapped using a GIS data set. The SWMM model was constructed using drainage network data sets, inlet data, and manhole data sets, which were preprocessed before integration into the SWMM platform. The 2D surface routing model was constructed using

GIS data sets, which were separated into two groups based on their roles in the model. The first group comprised surface parameters used for the 2D distributed models, such as subsurface soil data, land use data, surface depression, and surface slope. The second group comprised data sets that described hydraulic structures, such as channels, culverts, inlets, pump stations, and tidal gates.

The 1D model and 2D model were connected using orifices for the 2D surface node and 1D SWMM nodes and direct connections for the surface nodes and other hydraulic structures, such as open channels, headwalls, and culverts. Based on the model's resolution, the 1D SWMM model becomes simplified and detailed. This model construction has the benefit that GIS data sets can fully present hydraulic structures in Table 2. Complex urban hydraulic structures require detailed information, such as location, dimension, and capacities, in the case of pump stations. Without these information sets, the model cannot simulate compound urban flooding. The surface routing models contain only surface components, such as DEM, and surface parameters (infiltration rate, soil types) and cannot perform simulations that should contain subsurface 1D drainage systems.

Table 2 presents critical datasets used in the construction of the urban model and their roles in the SWMM/PCSWMM model. The urban model is built upon various GIS datasets to capture the complexity of urban environments. The hydro-enforced digital elevation model (DEM) is based on LiDAR data sets and includes elevations of artificial impediments such as road fills or railroad grades to simulate hydraulics systems such as channels, culverts, and bridges, allowing continuous downslope flow (Poppenga, Worstell et al. 2014). The DEM was edited to contain only terrain values, excluding building elevations using building polygons generated from LiDAR point data. One of the core datasets used is the NHDPlus HR dataset containing the National Hydrography Dataset (NHD), Watershed Boundary Dataset (WBD), and 3D Elevation Program digital elevation model (3DEP). It helps identify the smallest watershed in the urban model domain and construct the whole model domain, including subsurface pipe and surface water systems.

Figure 7 illustrates the NHDPlus HR watershed data and the 1D SWMM pipe system in the domain.

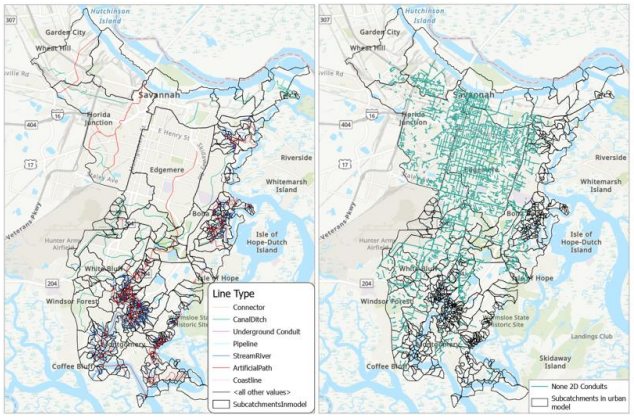

Figure 7. NHDPlus Subcatchments (right) and drainage system (left) built on SWMM in the model domain

Multi-Scale Modeling and Stepwise Simulation

The multiscale structure of the urban flood model takes into account two important factors: computational cost and model accuracy. To avoid high computational costs, the model is constructed with various resolution sets per surface type, optimized to achieve accuracy while minimizing cost. The resolution for each model is determined by the total number of cells in each model, as this is a determining factor for computational cost. For example, a flat urban area has a resolution of 50m, while open channels functioning as conduits have a resolution of 15m in the same model. The resolution for flat areas is determined based on their slight slope and role in surface routing as catchments that can be simplified in the modeling. However, the resolution of channels in the urban model is much finer than those of flat areas due to their significance in surface routing. Additionally, the resolution of each model is selected based on the maximum

number of nodes suggested by PCSWMM (total node number below 200,000) to maximize model accuracy.

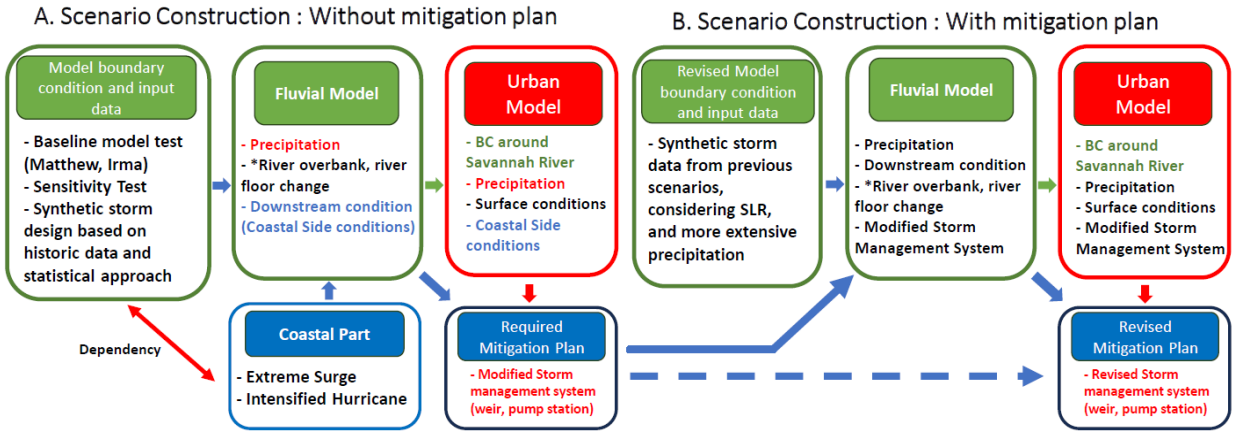

Figure 8. Scenario variables considered in this study.

4. Scenarios

Figure 8 shows Scenario variables considered in this study include the precipitation intensity, downstream water level height driven by sea level rise and tidal activities, and upstream water level height driven by basin hydrology and hydraulics control. Investigation of mitigation plans are underway and not included in this report.

For the sea level rise scenario, we consider the following (shown in Figure 9):

- Moderate Emission Scenario (RCP4.5): This assumes greenhouse gas emissions peak around the mid-century and decline afterward.
- High Emission Scenario (RCP6.0): Emissions peak in the latter half of the 21st century and then decline. Global mean sea level (GMSL) rise by 2100, roughly similar to RCP4.5 but possible slightly higher.
- Very High Emissions Scenario (RCP8.5): “Business-as-usual” scenario where emissions continue to rise throughout the 21st century. GMSL Rise by 2100, between 0.45-0.82 m, with higher values not ruled out.

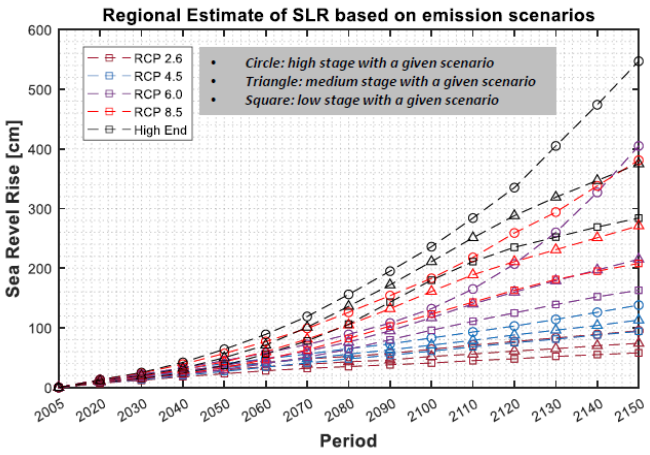

Figure 9. Local sea level rise based on greenhouse gas emission conditions.

Precipitation scenarios are based on the precipitation record during Hurricane Mathew. We consider no precipitation, true precipitation, and increased precipitation by 30%, 50%, 70%, and 120%.

5. Simulation Results

Model Validation by Hurricane Mathew

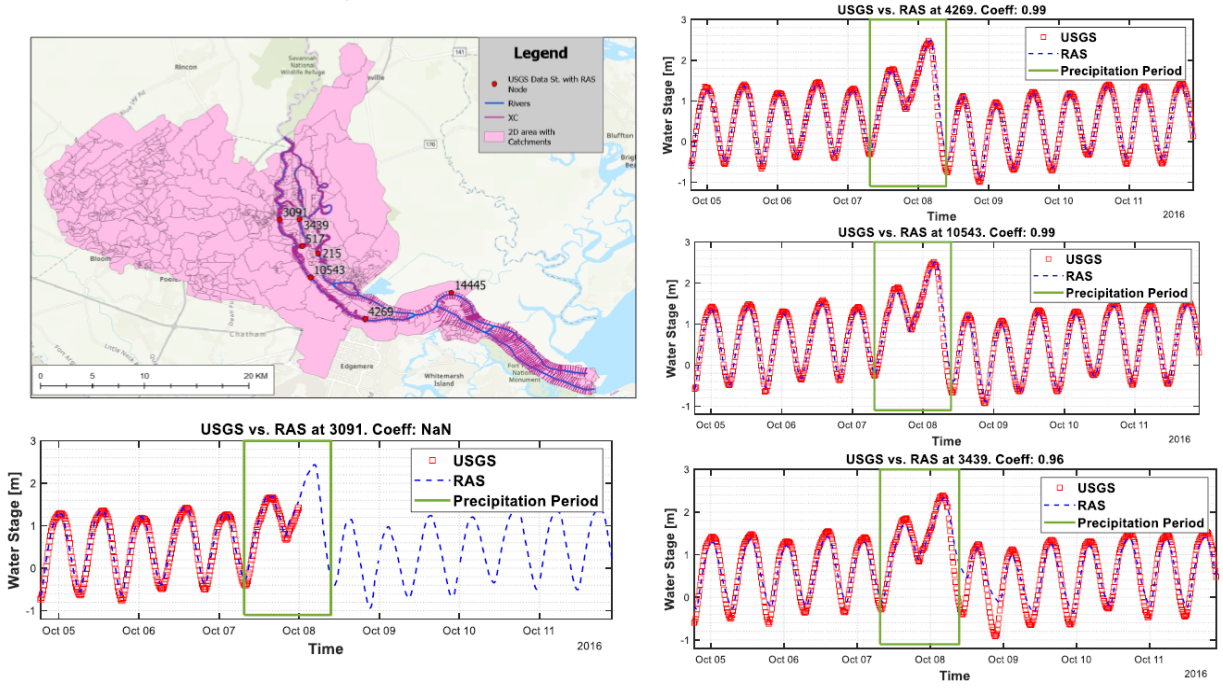

Figure 10. Model validation by local measurements along the riverbank of the Savannah River during Hurricane Mathew.

Figure 10 compares the model simulation and ground-based measurements of water levels during Hurricane Mathew. The comparison clearly shows that the model simulation matches the measurements, demonstrating the developed physics-based model provides satisfactory ability for simulating the flooding cases.

In addition, Phase I study presented visual comparison between model simulation results and social media report. For completeness, we included Figure 11 to demonstrate the effectiveness of the developed model. Figure 11 shows flood recordings as articles and photo records. The maximum water depth of the nearest node (nodes A, B, C, and D) at each location in Figure 11 was compared with the flood record from various sources. As mentioned in the literature review, one of the most significant challenges in urban flooding is the paucity of the flood record and its absence of details like measured water depths. So currently, the confirmed record of the flooding is the existence of flooding and images recorded by mass media and official records.

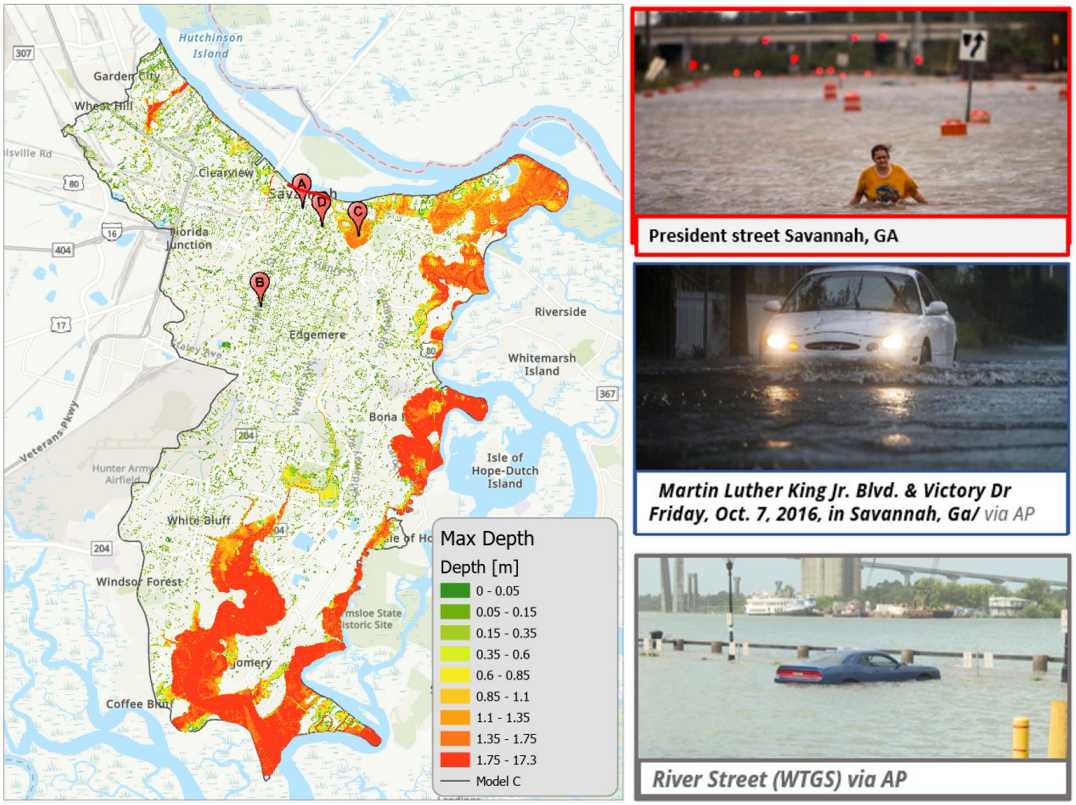

Figure 11. Model simulation of Matthew (left) and flood photos from various source (right).

Impacts of Downstream Condition Changes – Coastal Flood Driver

Figure 12 shows the simulated time series data at four monitoring locations for different downstream water levels driven by sea level rise and tidal activities. Figure 13 shows the maximum water levels almost change linearly with the downstream increment in water levels, indicating that coastal driving factors can significantly influence the fluvial flooding situations.

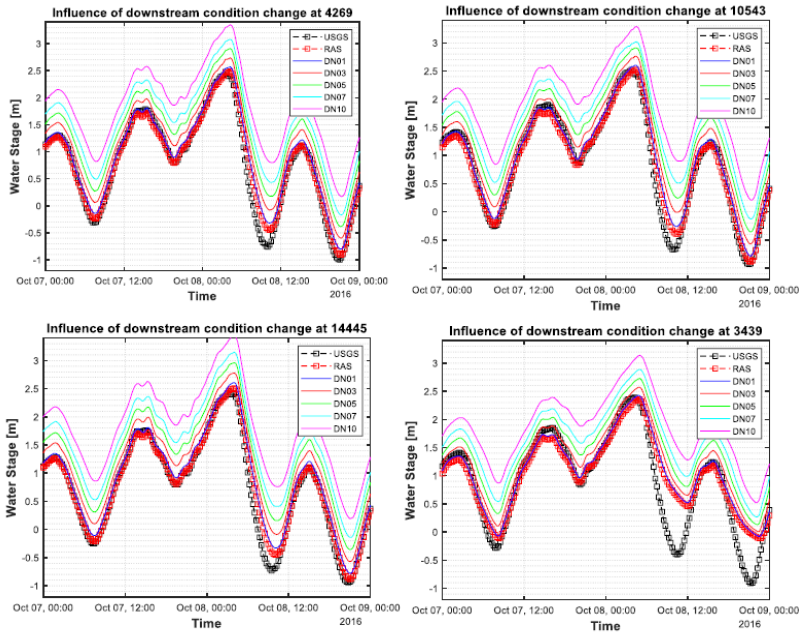

Figure 12. Time series simulations at different monitoring locations for different downstream water levels.

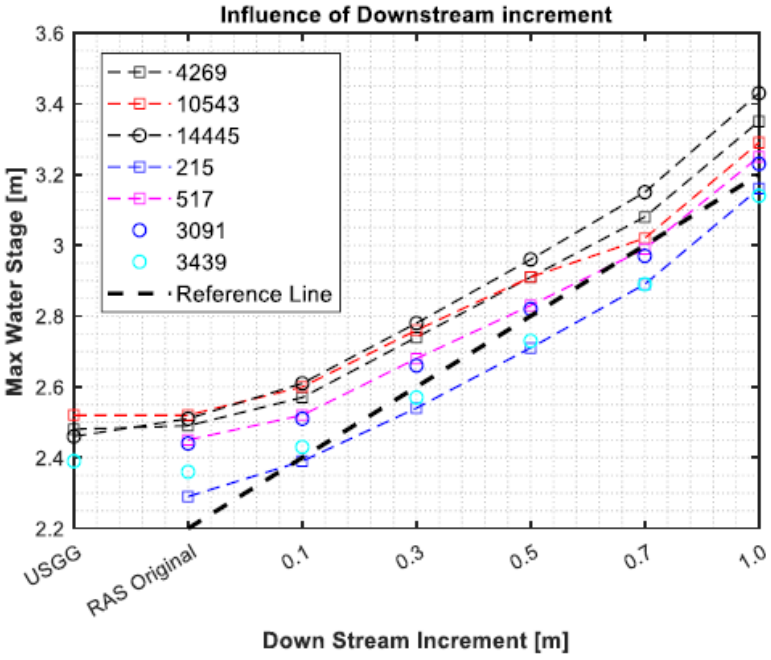

Figure 13. Simulated maximum water levels at different monitoring stations for different downstream water levels.

Impacts of Upstream Condition Changes – Fluvial Flood Driver

Figure 14 shows the simulated time series data at four monitoring locations for different upstream water levels driven by the Savannah River Basin hydrology and upstream reservoir management. Figure 15 shows the maximum water levels almost change linearly with the upstream increment in water levels, indicating that upstream water levels slightly influence the fluvial flooding situations compared with the coastal driving factors at the downstream.

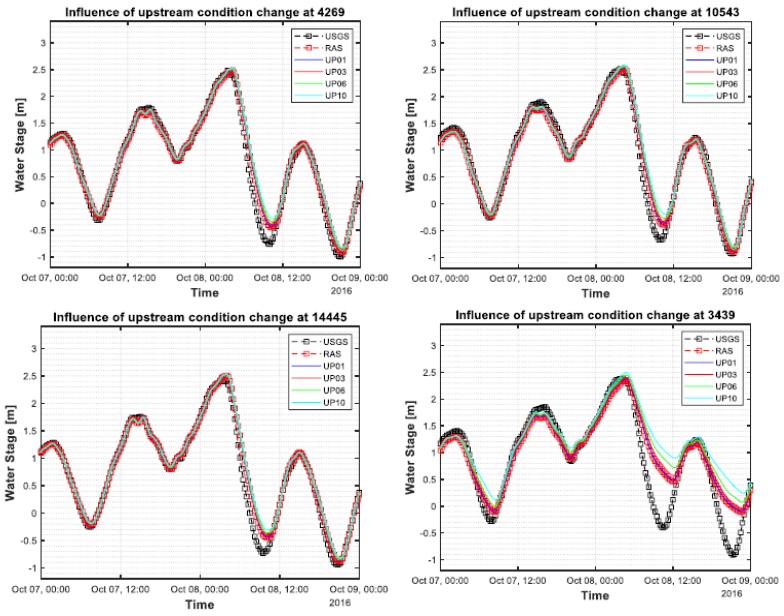

Figure 14. Time series simulations at different monitoring locations for different upstream water levels.

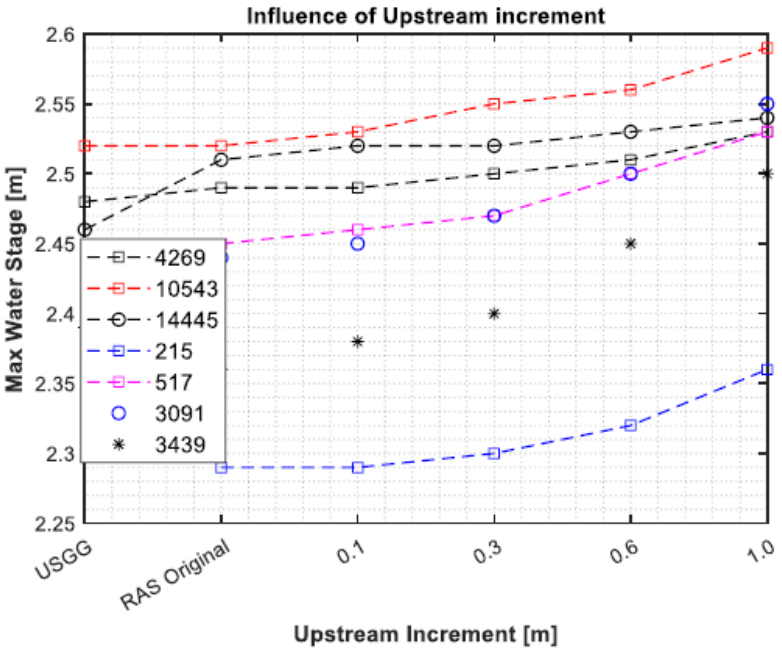

Figure 15. Simulated maximum water levels at different monitoring stations for different upstream water levels.

Impacts of Precipitation Increment – Pluvial Flood Driver

Figure 16 shows the simulated time series data at four monitoring locations for different precipitation scenarios. The base scenario is the precipitation record for Hurricane Mathew. Figure 17 shows the maximum water levels changes with the precipitation amount. Its impact is not as important as the downstream water levels, but is more significant than upstream water levels.

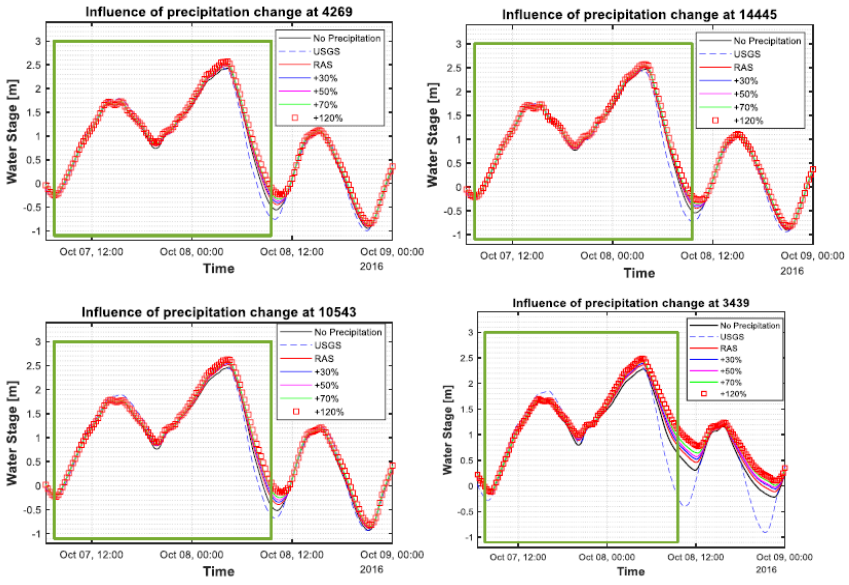

Figure 16. Time series simulations at different monitoring locations for different precipitation scenarios.

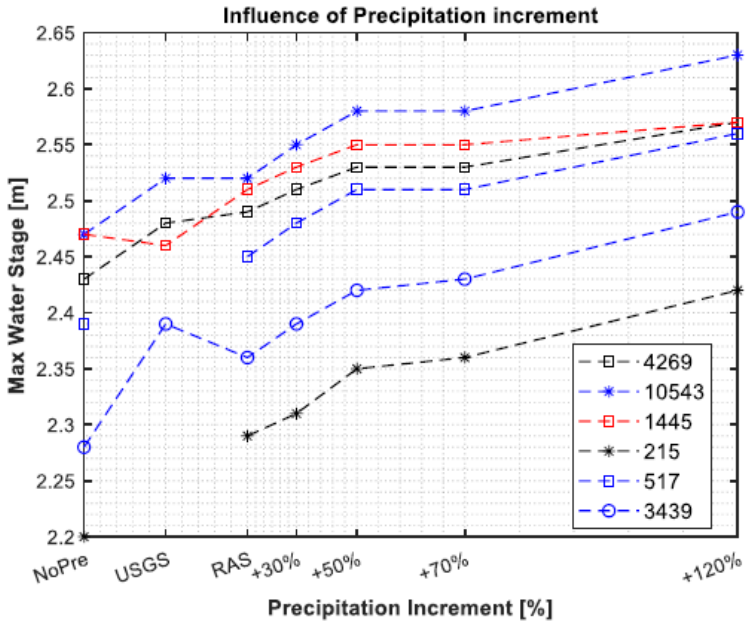

Figure 17. Simulated maximum water levels at different monitoring stations for different pumping scenarios.

Combined Impact

The investigation of combined impact of different driving factors is undergoing. Figure 18 shows some scenario analysis for the maximum water level by combining downstream water levels and precipitation.

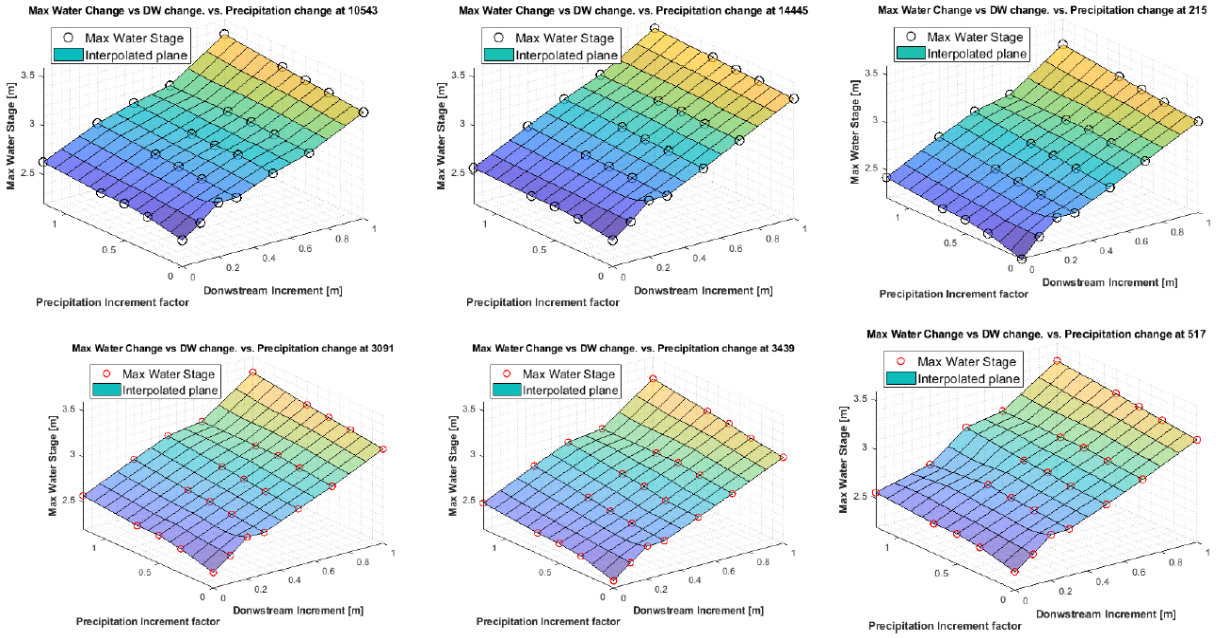

Figure 18. Combined impact of downstream water level and precipitation on the maximum water level.

6. Conclusion and Future work

This project extended our previously developed integrated urban flooding model to large basin areas including upstream river basin and downtown residential areas. The model consists of a 2D/1D HEC-RAS model for the Savannah River Basin (2D for the river basin hydrology and 1D for the river hydraulics) and a large-scale SWMM model for the urban surface runoff and drainage system to assess compound coastal flooding risks for storm water management in City of Savannah. Project products take into account the most accurate and up-to-date data from both inland urban hydrology, hydraulics in storm water management systems (drainage, pipes, canals and rivers), tides and sea level rise, and high-resolution digital data of urban development.

Major simulation results include:

(1) Validated the new 2D/1D HEC-RAS model by Hurricane Mathew
(2) Integrated HEC-RAS and SWMM model
(3) Validation of the integrated model using media reported flooding cases
(4) Generate climate change scenarios including downstream water levels driven by coastal flooding factors such as sea level rise, upstream water levels driven by fluvial flooding factors, and precipitation
(5) Comparison and analysis of simulation results of maximum water depth for different scenarios

The key findings derived from this study highlight the primary drivers of coastal flooding as having the most substantial impact on flooding scenarios, with precipitation ranking second, and upstream water levels exhibiting the least influence. This conclusion is substantiated by the validated fluvial model applied to the Savannah River.

Additionally, the study is currently assessing the cumulative impacts arising from the intricate interactions among multiple influencing factors. It is crucial to emphasize that the developed model encompasses the urban drainage system, although it has not yet been incorporated into the scenario analysis; this specific aspect of the research is also presently in progress. Additionally, the investigation of mitigation strategies to address flooding risks is a crucial next step in this research endeavor.

Acknowledgment

The authors thank to the support from Georgia Water Resources Institute and Director Dr. Georgakakos. Their help and guidance facilitates the completion of the study. Minjae Kim as a Ph.D. was supported by the funds to conduct most of the research.

References

Baig, M. H. A., et al. (2014). "Derivation of a tasselled cap transformation based on Landsat 8 at-satellite reflectance." Remote Sensing Letters **5**(5): 423-431.

Barco, J., et al. (2008). "Automatic Calibration of the U.S. EPA SWMM Model for a Large Urban Catchment." Journal of Hydraulic Engineering **134**(4): 466-474.

Bedient, Philip B. and Wayne C. Huber. "Hydrology and Floodplain Analysis." (1989).

Bisht, D. S., et al. (2016). "Modeling urban floods and drainage using SWMM and MIKE URBAN: a case study." Natural Hazards **84**(2): 749-776.

Chatham County Floodplain Management Plan, http://engineering.chathamcounty.org/Portals/Engineering/forms/Chatham%20County%20FMP%20Final.pdf, 2018

City of Savannah, http://ga-savannah.civicplus.com/DocumentCenter/View/6678/Section_03_Hazard_Identification_and_Analysis_FINAL, 2009

Crockett, C. 2007. The regulated perspective of stormwater management. Presentation to the NRC Committee on Stormwater Discharge Contributions to Water Pollution. January 22, 2007. Washington, DC

Dasgupta, S., et al. (2013). "A megacity in a changing climate: the case of Kolkata." Climatic Change **116**(3): 747-766.

Environmental Protection Agency, Storm Water Management Model User's Manual Version 5.1, EPA/600/R-14/413b, 2015.

Fourth National Climate Assessment, https://nca2018.globalchange.gov/chapter/19/, 2018

FEMA, https://msc.fema.gov/portal/search?AddressQuery=47108%20&%2047%20N%20CHERRY%20ST%20Hammond,%20LA#searchresultsanchor, 2019

Huong, H. T. L. and Pathirana, A.: Urbanization and climate change impacts on future urban flooding in Can Tho city, Vietnam, Hydrol. Earth Syst. Sci., 17, 379–394, https://doi.org/10.5194/hess-17-379-2013, 2013.

Jelesnianski, C. P., Chen, J. & Shaffer, W. A. SLOSH: Sea, Lake, and Overland Surges from Hurricanes. *NOAA Tech. Rep.* NWS 48 (1992)

Niazi, M., et al. (2017). "Storm Water Management Model: Performance Review and Gap Analysis." Journal of Sustainable Water in the Built Environment **3**(2): 04017002.

NOAA, https://water.weather.gov/ahps/inundation.php, 2019

Office for Coastal Management, 2019: NOAA Office for Coastal Management Sea Level Rise Data: 1-6 ft Sea Level Rise Inundation Extent, https://inport.nmfs.noaa.gov/inport/item/48106

Ornl, D. (2018). MODIS and VIIRS Land Products Global Subsetting and Visualization Tool, ORNL Distributed Active Archive Center.

Pazwash, H. (2016). Urban Storm Water Management. Boca Raton: CRC Press, https://doi.org/10.1201/b19658

Smart Sea Level Sensors, https://www.sealevelsensors.org, 2019

Tuppad, P., et al. (2011). "Soil and Water Assessment Tool (SWAT) hydrologic/water quality model: Extended capability and wider adoption." Transactions of the ASABE **54**(5): 1677-1684.

U.S. Geological Survey, 2016, National Water Information System data available on the World Wide Web (USGS Water Data for the Nation), accessed [June 10, 2012], at URL [http://waterdata.usgs.gov/nwis/]

Vermote, E., et al. (2016). "Preliminary analysis of the performance of the Landsat 8/OLI land surface reflectance product." Remote Sensing of Environment **185**: 46-56.

Yuan, F. and M. E. Bauer (2007). "Comparison of impervious surface area and normalized difference vegetation index as indicators of surface urban heat island effects in Landsat imagery." Remote Sensing of Environment **106**(3): 375-386.

Project ID	2022GA03B
Project Type	Research
Award Type	Base Grant (104b)
Project Title	Development of a Green Infrastructure by Using Biochar Amended Topsoil for On-Site Stormwater Runoff Treatment
Project PI	Fu, George
Academic Institution of PI	Georgia Southern University
Congressional District of project	GA-12

Georgia Water Resources Institute (GWRI) Project ID #2022GA03B

under the National Water Resources Research Act (104b – State Research)

Final Report

DEVELOPMENT OF A GREEN INFRASTRUCTURE BY USING BIOCHAR AMENDED TOPSOIL FOR ON-SITE STORMWATER RUNOFF TREATMENT

By

George Yuzhu Fu, Ph.D., P.Eng., Professor

Ayesha Sadia, Master Student

Department of Civil Engineering and Construction

Georgia Southern University

September 2023

TABLE OF CONTENTS

Pages

LIST OF FIGURES

Pages

LIST OF TABLES

Pages

LIST OF ABBREVIATIONS

BMPs	Best Management Practices
COD	Chemical Oxygen Demand
DO	Dissolved Oxygen
DOT	Department of Transportation
EPA	Environmental Protection Agency
GI	Green Infrastructure
GDOT	Georgia Department of Transportation
USDOT	US Department of Transportation
TKN	Total Kjeldahl Nitrogen
TN	Total Nitrogen
TP	Total Phosphorus
TS	Total Solids
TSS	Total Suspended Solids
WERL	Water and Environmental Research Laboratory

EXECUTIVE SUMMARY

Modern urbanization has transformed the natural landscape and increased the number of impervious surfaces, such as roads and buildings, which prevent the infiltration of rainwater into the ground. As a result, stormwater runoff has become a major issue in urban areas. This increased runoff contributes to flooding, erosion, and water pollution. In fact, urban stormwater runoff is one of the largest contributors to non-point source pollution. Due to its vast path of flow, it often carries a variety of pollutants including suspended solids, nutrients, heavy metals, oil and grease, etc.. These pollutants will ultimately end up in rivers and other nearby bodies of water, which can have detrimental effects on the health of the public and environment.

Green infrastructure (GI) is one way to quell this issue and has found increasing implementation in recent years. It involves the use of natural systems, such as trees or wetlands to capture, treat, and store stormwater. The pollutants in the runoff can be removed by these setups and are exemplified by existing infrastructure such as rain gardens or green roofs. The most important components for these GI filters are the type of grass and soil properties of the ground. One of the more promising materials that can be used in these filters is biochar. Biochar is a charcoal-like material produced by combusting waste organic biomass. It has high internal porosity and surface area, which makes it a favorable material for storm runoff treatment. Small scale tests have been conducted that show promising results for the capability of biochar amended topsoil to filter runoff, but full-scale testing still needs to be completed before its full potential is realized. High pollutant removal performance is made possible using biochar as performance-enhancing devices (PEDs) for best management practices (BMPs).

The proposed objectives of this research project are to design, build, operate and maintain, and monitor a new GI using biochar-amended topsoil for on-site stormwater runoff treatment in urban areas and to evaluate the removal efficiencies of pollutants from stormwater runoff such

as total suspended solid (TSS), nutrients including nitrogen and phosphorous, heavy metals including lead (Pb), zinc (Zn) and copper (Cu) and oil and grease etc. The goal of this research project is to investigate the feasibility of using biochar-amended topsoil as a new GI solution for on-site treating stormwater runoff in urban areas. Based on this assessment, guidelines will be developed for the implementation of similar systems in urban areas. The findings of this study will contribute to the understanding of biochar application in GI which is cost-effective and broaden the spectrum of sustainable stormwater treatment strategies.

The Phase I Project started in September 2022 and is scheduled to conclude in August 2023. Extensive preparations were undertaken to facilitate fieldwork including designing, installation, operation, sampling, laboratory analyses, and monitoring the Field Test Site during this time. The design was fabricated and approved by the Department of Facilities at GSU. In this Phase I Project, a 500 ft^2 full-scale Field Test Site with 1 ft depth was constructed to on-site treat stormwater runoff from a parking lot on Georgia Southern University (GSU) campus in Spring 2023. This Field Test Site consists of two identical cells, called the Control Cell and the Test Cell, each with an area of 250 ft^2 for a direct comparison purpose. Control Cell consists of topsoil only and Test Cell with 5% (weight percent, wt%) biochar amended topsoil. The local topsoil from Statesboro, GA, identified as Pelham series (very deep, poorly drained, moderately permeable soils with majority of sands), and the Soil Reef Biochar (Soil Reef Company, 1125 Lancaster Avenue, Berwyn, PA 19312) were used at the Field Test Site with switchgrass planted and growing at the Site also. By the end of Spring Semester, 2023, the building of the Field Test Site was completed. According to the findings from a GDOT Research Project, switchgrass was selected for this Project. All grass plants were planted by June 9, 2023. The emphasis for the Phase I Project was to design, build, maintain, and monitor

a cost-effective GI using biochar-amended topsoil for on-site treating stormwater runoff from the parking lot.

In this research project water quality (WQ) parameters of concern were suspended solids, nutrients (i.e., nitrogen and phosphorus), heavy metals (i.e., Pb, Zn, and Cu), oil and grease, and chemical oxygen demand (COD). These WQ parameters were selected based on the knowledge of these pollutants in stormwater runoff. During heavy rainfall events, the parking lot stormwater runoff was pumped by a submersible pump and sprayed onto to the Field Test Site via sprinklers, infiltrated and treated through the 1 ft layer of topsoil or biochar amended topsoil in Control/Test Cell. The treated stormwater runoff seeped into the corrugated perforated pipes and flowed into the end cylindrical catch basin drums, where the treated effluent samples were collected and tested for pollutants. The raw stormwater runoff was collected as the influent from the parking lot and the treated stormwater was collected as the effluent from Control Cell and Test Cell and tested for the concentration of the pollutants. The concentration of pollutants in the influent and the effluent were used to calculate the removal efficiencies by the new GI using biochar amended topsoil. The raw stormwater runoff sampled after the heavy rainfall period had the highest concentration of TSS, nutrients, and oil and grease.

According to lab test result, the addition of biochar (5% by wt) into the topsoil significantly increased its saturated hydraulic conductivity to 1.78E-05 m/s from 1.05E-06 m/s for topsoil only, allowing stormwater runoff to infiltrate through the media of biochar amended topsoil much faster. The results for on-site soil moisture content monitoring also showed that the 5% biochar amended topsoil in Test Cell had much higher moisture contents than the topsoil only in Control Cell. Based on the preliminary test results in Summer 2023, for the initial about 11

gallons of the parking lot stormwater runoff treated by each Control and Test Cell, the removal efficiencies are summarized as follows: TSS: 80% for Control Cell versus 84% for Test Cell; NH3-N: 5% vs. 83%, NO3--N: -1.3% vs 88%, TKN: 73% vs 95%; TN: 57% vs 91%; TP: 62% vs 81%; Oil and grease: 57% vs 88%. Overall, the removal efficiencies of pollutants by Test Cell are much higher than those by Control Cell.

The biochar addition to the topsoil has the potential to improve soil quality, increase water retention, reduce erosion, and provide a medium for plants. The porous structure of the biochar should work to capture and store pollutants, some of these being nutrients. Elements such as nitrogen, phosphorus, and potassium can be absorbed and slowly released over time. This helps to promote plant growth in the area, which in turn will bolster the landscape and contribute to filtering properties of this green infrastructure. Based on research completed by Ahmed I. Yunus (2022), we know that a 5% biochar addition to the topsoil is the best mixing ratio to topsoil to maximize these pollutant removal abilities. This led to the ultimate selection of our mixing ratio of biochar to topsoil. Overall, the project aims to create a sustainable and cost-effective solution for treating on-site stormwater runoff through this new GI, which could serve as a model for future urban projects.

Given the experience gleaned from the progress on this project, some recommendations can be made for the construction and implementation of this new GI system using biochar-amended topsoil for on-site stormwater runoff treatment. Firstly, a thorough site analysis should be conducted to determine the most suitable location for the system. This analysis should consider factors such as soil type, topography, and proximity to existing infrastructure. Secondly, it is important to select the appropriate biochar for the specific soil and site conditions. Different types of biochar have varying properties, so it is important to choose one that is compatible

with the soil and site. Native vegetation is also an important consideration and should be used in this new GI system to reduce maintenance requirements. It is also crucial to implement regular maintenance to ensure the long-term performance of the new GI system. This includes tasks such as monitoring soil moisture, pruning vegetation, and removing any debris that may accumulate in the system. Finally, it is important to educate the community on the benefits of this new GI and the importance of stormwater treatment. This can help to promote a culture of sustainability and encourage community involvement in the project. Getting the community involved allows for the education of this new GI to expand for generations to come.

Overall, the development of this new GI system using biochar-amended topsoil has the potential to provide a wide range of benefits, including improved stormwater treatment, soil health, and urban aesthetics. In our study, we considered multiple sites on campus for testing pollutants such as TSS, nutrients, heavy metals and oil and grease, etc. We specifically selected our Field Test Site because of the presence of these pollutants from the stormwater runoff from a nearby parking lot, as we intended to examine removal efficiency. The perimeter curb surrounding the parking lot made it impossible for its stormwater runoff to enter the Field Test Site with gravity, so we took advantage of a nearby catch basin as a starting point to draw the stormwater runoff from the parking lot. We utilized a submersible pump and sprinkler system to simulate stormwater runoff on the Field Test Site. In general, this new GI using biochar-amended topsoil can be implemented at any time, including during routine maintenance and retrofitting of existing landscapes. This approach can benefit a wide range of stakeholders, including property owners, developers, municipalities, and members of the general public. The use of biochar-amended topsoil can provide ecosystem services such as water quality. It can also improve soil fertility, and reduce soil erosion and compaction.

Furthermore, it can support plant growth and reduce the need for chemical fertilizers and pesticides. Overall, this new GI using biochar-amended topsoil has the potential to provide numerous benefits for both the environment and society.

CHAPTER 1. INTRODUCTION

1.1 Overview

Urban stormwater runoff, as a significant human-made source of pollution, poses a considerable threat to water quality (Qin 2023). It carries pollutants from the impervious surfaces such as streets, parking lots, and roofs when it rains. Generally, soil acts as a filtering medium, effectively removing the pollutants like total suspended solids (TSS), total dissolved solids (TDS), total solids (TS), nutrients including nitrogen (N) and phosphorus (P), and even heavy metals from stormwater runoff during the infiltration process (Choi 2017). The stormwater runoff with the remaining pollutants is transported to receiving water bodies and can severely impact their water quality. This stormwater runoff carries a large amount of nutrients (N and P) that can cause eutrophication in water bodies. If not properly managed, this excessive nutrient loading can create "dead" zones or hypoxic areas in slow-moving rivers or lakes (McCarthy, 2013). Hypoxic zones, characterized by low or no oxygen levels in water bodies, lead to the migration of aquatic life away from these areas or, in severe cases, cause death. Species that are already endangered or dependent on these water bodies, including aquatic species and birds that feed on fish, are at an elevated risk of mortality if the waterbodies continue to be polluted by highway stormwater runoff, which may contain high concentration of nutrients and heavy metals, etc. The pH and biochemical oxygen demand (BOD) of receiving water bodies are influenced by the significant buildup of deicing compounds including sodium (Na), magnesium (Mg), and chlorine (Cl) in soils and water which are used on the highway during cold winter for preventing ice forming. Stormwater runoff carries these substances into bodies of water. BOD refers to the quantity of oxygen needed for the natural breakdown of a substance by biological processes (Wyman 2018). TSS is a contaminant that

over time harms and clogs roadway drainage systems and established best management practices (BMPs). TSS degrades water quality by making water bodies more turbid, which limits the quantity of sunlight that reaches aquatic plants and fish. Photosynthetic processes are hampered when little to no sunlight is permitted to reach the water's surface, which lowers the concentration of oxygen. The water may appear murky, muddy, or discolored when TSS concentrations are high. The water bodies are less appealing to visitors and recreational activities as a result, which has a negative impact on their aesthetic attractiveness.

1.2 On-Site Stormwater Runoff Treatment

The accumulation of pollutants from paved surfaces like total nitrogen (TN), total phosphorus (TP), total suspended solids (TSS), heavy metals, and chemical oxygen demand (COD), can lead to water body contamination. The primary contributors to pollutant contamination on paved surfaces are vehicles, which introduce a wide range of chemicals into on-site stormwater runoff. Green grasses control stormwater runoff, which helps to reduce the quantity of stormwater. Increasing stormwater regulations on nutrient loads are compelling state DOTs to undertake stormwater restoration to reduce nutrient loads and where possible stormwater volume. While existing stormwater technologies such as detention ponds and new Low Impact Development features can remove nutrients, the required increase in load removal and runoff volume reduction will be costly on a watershed scale since more real estate is required for increased treatment using current technologies.

On-site stormwater runoff treatment is the process of treating stormwater runoff before it enters natural water bodies or drainage systems. There are several types of BMPs utilized by the Department of Transportation (DOTs) to on-site treat stormwater runoff to prevent the transportation of pollutants into the receiving water bodies. They are summarized as follows:

Permeable Pavement: Using permeable surfaces for roads, parking lots, and walkways allows more stormwater to infiltrate into the ground, while reducing runoff. The infiltration process helps with stormwater's natural treatment by removing pollutants as the water travels down the soil profile (Imran 2013).

Bioretention Ponds: Swales and other aquatic plants are used in bioretention ponds, which are constructed ponds with infiltration media for holding a large volume of water after a storm. This technique lowers the risk of flooding by allowing TSS to settle and aquatic plants to remove nutrients from the stormwater runoff (Zanin 2018).

Infiltration: There are various infiltration BMP types such as dry wells, infiltration trenches, and basins. As stormwater runoff penetrates the soil profile, these structures collect, store, and treat it. To treat particular pollutants including nutrients, heavy metals, TSS, TDS, TS, and organic compounds, performance-enhancing devices (PEDs) like iron filings, charcoal which also carbon rich material like biochar, and other geo media can be applied to the bed's profile of these BMPS (Laurenson, 2013).

Filtration: Filtration BMPs such as bioretention BMPs employ PEDs like grass swales, sand filters, activated carbon, charcoal, iron fillings, and filtering media. These PEDs are used to build filter strips that gather and treat stormwater runoff before delivering it to an underground drainage system or water body. The majority of filter strips are constructed from vegetal filters. Stormwater runoff is slowed down by vegetative filter strips, which are built on an even slope. It is simple to build, manage, and sustain and goes by the name of buffer stripes as well. Pollutants such nutrients, TSS, TDS, and heavy metals are typically removed (Ekka 2021).

Stormwater Ponds: Stormwater ponds are built to hold runoff from storms to minimize flooding and to allow area for TSS sedimentation before treating effluent is transported to

surrounding water bodies or drainage. Dry and wet ponds are the two different forms of stormwater ponds. In contrast to the dry ponds, which have little to no water stored and only collect highway stormwater runoff following a significant precipitation event, the wet ponds have water stored for the majority of the year (Beckingham, 2019).

Stormwater Wetlands: Construction and maintenance of stormwater wetlands are exceedingly laborious. These need a sizable space as well as a greater range of plant types. These plant species must be prepared to thrive in soils with high water content. It is similar to a wet pond, however there are differences in the water depths. In addition, they offer a long-term natural habitat for numerous animal species as well as a natural aesthetic to the environment. Wetlands frequently beyond their original size, hence they are typically built in less developed locations. They assist in gathering TSS and nutrients that are then used by aquatic plant species (Sharma 2021).

Bioslope: To treat stormwater runoff of pollutants like TSS, TDS, and nutrients, Bioslope is a highway stormwater BMP constructed on the side slopes of the road. In the majority of the time, they are made of an engineered topsoil mixture and laid on the ROW of roadways. The components that make up the topsoil mix include dolomite, gypsum, perlite, and stone aggregates. Stormwater infiltrates the media, where the materials are placed to filter and adsorp pollutants from the stormwater runoff. The designed topsoil mix's composition is expensive, necessitates specialized storage, and cannot be applied over long distances (Georgia Department of Transportation (GDOT) Drainage Design Manual 2020).

1.3 Problem Statement

According to the Georgia Environmental Protection Division (EPD), stormwater runoff, which can contain dangerous pollutants, influences thousands of miles of rivers throughout Georgia. In fact, stormwater contamination poses the biggest risk to Georgia's water quality. Stormwater runoff over streets, parking lots, and roofs is the greatest non-point source of pollution. The stormwater runoff flow carries a variety of pollutants including TSS, heavy metals, nutrients (N and P), oil and grease, etc. These pollutants are detrimental to the water quality of receiving water and public health and they must be removed. For onsite stormwater runoff treatment, BMPs are utilized to long-term infrastructures such as biofilters/bioretention basins, bio-slope, sand filters, infiltration trenches, and grass channels. These facilities frequently experience issues such as the necessity to purchase additional property, the complexity of their construction, and ongoing maintenance. One of the effective ways to combat the adverse effects of stormwater runoff is to remove the harmful pollutants, using biochar amended topsoil which is a cost-effective and sustainable GI before they reach these receiving water bodies.

The design of GI is a combination of qualitative and quantitative approaches and provides a more understanding of a research problem. GI using biochar amended topsoil will be used for on-site stormwater runoff treatment. The pollutants in stormwater runoff can be removed by sheet flowing over a land with grass, filtering out and uptaking pollutants by grass, and infiltrating into the ground. The most important components for an effective green infrastructure include the type of grass and soil properties in the ground. It is necessary to explore new engineered soil materials for an effective green infrastructure.

The application of biochar improves the topsoil's ability to increase soil's hydraulic conductivity. Due to the distinctive carbon structure, high internal porosity, and high internal surface area of biochar, resulting from a variety of small and large pores in granules of biochar, biochar can be used as an adsorbent to remove the pollutants from stormwater runoff. Meanwhile, a microorganism community would develop in the biochar amended topsoil that serves as the filter, removing pollutants such as heavy metals and nutrients from stormwater runoff biologically.

At the end of this Section, the challenge aiming to address involves the cost-effective and straightforward solutions to determine the feasibility and effectiveness of using biochar-amended topsoil in the context of GI for on-site stormwater runoff treatment within urban areas. There is now a lot of study on on-site stormwater runoff treatment systems, however, there is a significant lack in research about the use of biochar amended topsoil in on-site stormwater runoff treatment applications. Biochar amended topsoil can remove the pollutants from stormwater runoff from paved surfaces. Moreover, because of the availability of free on-site topsoil and the low cost of biochar, this is an economically viable solution.

1.4 Objectives of the Project

The objectives of the project are:

- To design and build a full-scale Field Test Site including Control Cell with topsoil only and Test Cell with 5% (Weight percent, wt%) biochar amended topsoil;
- To grow grass on the Field Test Site;
- To operate and maintain, monitor, and collect and test water samples from the Field Test Site;

- To evaluate and determine the removal efficiencies of pollutants from the stormwater runoff using the Field Test Site; and
- To develop guidelines for designing, building, and operating and maintaining a GI using biochar amended topsoil for on-site stormwater runoff treatment.

1.5 Scope and General Tasks of the Project

Refer to Phase I Proposal: Section 13 on 4 Tasks, the project aims to design, build, maintain, and monitor a cost-effective green infrastructure using biochar-amended topsoil as a natural solution for managing stormwater runoff in urban areas. The project commenced in September 2022 and is scheduled to conclude in August 2023, encompassing a duration of 11 months. During this time, extensive preparations were undertaken to facilitate fieldwork, laboratory analyses, and monitoring activities essential for the study. The project involved various components such as field installations, operation, sampling, laboratory analyses, and monitoring. The goal of this research is to assess the viability and effectiveness of utilizing biochar-amended topsoil as a green infrastructure approach for the treatment of on-site stormwater runoff within urban areas.

In this research project, two Cells are designed and built for a direct comparison purpose: a Control Cell with topsoil only and a Test Cell with biochar-amended topsoil at 5% biochar by weight (size of each Cell is 20ft x 12.5ft x 1ft). After installation of whole system, GI was operated during several rainfall events and collected influent and treated effluent. Different water quality parameters were tested, including heavy metals, nutrients, solids, COD, oil and grease, pH, dissolved oxygen (DO), and conductivity aiming to compare the pollutant removal efficiency of on-site stormwater runoff. According to field and lab results, the removal efficiency of all pollutants was over 80% and the removal efficiency of nutrients was over

85%. In July, there was less moisture because it rained almost every day, but August was mostly dry.

In this research project, the Georgia Southern (GS) Research Team has completed the design, ordered and obtained materials, and built the proposed Full-Scale Field Test Site (simply called "Test Site" hereafter) with an area of $500 ft^2$by 1 ft depth on GS campus, including Control Cell ($250 ft^2$) with topsoil only and Test Cell ($250 ft^2$) with 5% (wt%) biochar amended topsoil. Grasses were planted identically at both Cells during summer season. The Test Site is used for comparing the pollutant removal efficiency between Test Cell (topsoil mixed with 5% biochar) and Control Cell (only topsoil). Stormwater runoff from GS Parking lot goes into inlet and by operating a submergible pump stormwater was simulated over the Test site through two sprinklers to treat the stormwater runoff.

The raw stormwater runoff samples were collected as the influent from the nearby GS Parking Lot while the treated stormwater runoff samples were collected as the effluent from the Test Site. These water samples were tested at GS Water and Environmental Research Lab (WERL) for the concentration of the pollutants. The concentration of pollutants in the influent and the effluent were used to calculate the removal efficiency by the GI with biochar amended topsoil. The water quality parameters of concern were heavy metals (i.e., lead Pb, zinc Zn, and copper Cu), chemical oxygen demand (COD), nutrients (i.e., nitrogen (N) and phosphorus (P)), solids, oil and grease, pH, dissolved oxygen (DO), and conductivity.

CHAPTER 2. LITERATURE REVIEW

2.1 Overview

Water scarcity is a global phenomenon, and over the past ten years, there has been a huge increase in the use of resources to prevent the contamination of surface water (Liu 2017). Urban livability is promoted via GI, sometimes known as nature-based solutions. It reduces the volume of stormwater runoff and enhances the quality of surface water as well as delivering numerous additional environmental, economical, and social advantages at the same time. Rainwater that spills over the ground is known as stormwater runoff. It runs over roads and parking lots and picks up oil and other pollutants before entering a river or stream nearby is referred to as stormwater runoff. Stormwater can be held and filtered in more natural locations, such as wetlands and forested regions. Green space reduces the number of pollutants carried by stormwater runoff flows. There are different GI such as green roofs, rain gardens, bioretention ponds, bioswales etc. GI can reduce runoff volume and peak discharges, which will reduce localized urban flooding. Additionally, GI approaches' infiltration, evapotranspiration, and gradual release can regulate flood flows across a watershed. The decreased costs of flooding-related damage and the lower cost of building stormwater management and drainage infrastructure together constitute the economic benefits. Urban stormwater management has changed over the past 20 years from approaches that treat runoff as waste in end-of-pipe systems to those that regard stormwater as a resource that may be absorbed, stored, and/or reused at the site (Fletcher 2015). These systems use plants, soil, and/or infiltration to hold runoff and naturally filter out pollutants.

For a storm event that occurs once every two years and lasts for one hour, an analysis of the stormwater infiltration basin's ability to remove pollutants was done. Zeolite and coarse, pure

quarzitic sand with a mean diameter of 2 mm were combined in a 1 to 6 ratio to create the base of the infiltration basin. An autosampler was used to collect the stormwater effluent from a stormwater drainage pipe that connected to a nearby creek. The results showed that TSS had a weighted average removal efficiency of 50% and heavy metals like Pb, Cu, and Zn had a removal efficiency of 68%. whereas metals like Cr, iron (Fe), Ni, and manganese (Mn) were either the same as the influent or more significant and can be attributed to the leaching of heavy metals from clay particles or accumulation of metal infiltration bed, they were present in greater amounts than the influent (93% and 53%, respectively). There was a remarkable high efficiency in the removal of fecal coliform, which was initially concentrated at 70,000 colony forming units (CFU) (100 mL) and reduced to 2,000 CFU (100 mL), at 96%. Total phosphorus (TP) and TKN were removed at 51% and 68%, respectively (Birch 2005).

Urban areas reduce on-site infiltration and increase stormwater runoff, which introduces pollutants into surrounding surface waters, as they encroach on natural land cover in a watershed. Enhancing built-in stormwater treatment infrastructure with GI is a topic of continuous debate in both developed and developing countries. For on-site stormwater runoff treatment, there are many different types of GIs, however, biochar-based GI is a new technique that is not yet widely studied and adopted. Due to its advantageous effects on the environment and economy, biochar is being used more and more in engineered infrastructures like GIs (slopes and; landfill covers) (Lehmann 2015). The development of a GI using biochar amended topsoil is a promising approach for on-site stormwater runoff treatment. Biochar is a porous, carbon-rich material that can be added to soil to enhance its water holding capacity, reduce erosion, and improve plant growth. By combining biochar with topsoil, stormwater can be filtered and retained on site, reducing the amount of runoff that enters into local waterways.

The benefits of this approach extend beyond stormwater treatment. Biochar-amended topsoil also promotes soil health, increases carbon sequestration, and reduces greenhouse gas emissions. Additionally, this GI approach can enhance the aesthetic value of urban areas by promoting the growth of vegetation and improving air quality.

As this GI with biochar-amended topsoil will be cheap, the most likely potential users will be homeowners. They can build a stripe of the GI by using biochar-amended topsoil for on-site stormwater runoff treatment along the perimeter of their house. They can also expand it to their yards with lawns. The other potential users will include the park departments of each city, campuses of schools, and commercial areas with parking lots, etc.

2.2 On-Site Stormwater Runoff Treatment with GI

Precipitation, primarily in the form of rain, snow, or sleet, is how water first enters a watershed (Figure 1). This liquid or frozen precipitation enters the watershed generally pollutant-free, however it may pick up some pollutants from the atmosphere during its descent. Also, a range of other pollutants are picked up as this rainwater or meltwater travels across an urban environment and stormwater runs over roads and parking lots. Common pollutants include nutrients, metals, suspended solids (or total suspended solids, TSS), total dissolved solids, (TDS), chloride/salinity, , polychlorinated biphenyls (PCBs), pathogens, pesticides, and heat (Keeley 2011). In accordance with Phases I and II of the 1987 Clean Water Act, these are subject to regulatory threshold concentrations (in the United States). The need to improve stormwater quality is critical since stormwater runoff is a major contributor to surface water pollution (in developed countries).

The sources of urban stormwater pollution include cars, roads, buildings, lawns, industrial parks, and other man-made structures (Davis 1999, Polukarova 2020). With the deterioration of brake pads as well as component rust, vehicles can produce solid metal particles and also produce oils and grease. Building siding and roofing materials have the potential to leach metals into rainwater. With the help of grass clippings and other vegetative matter, lawns can produce solids that, when they decay, release nutrients. Stormwater runoff is also enriched with nutrients by fertilizer from urban turf areas. Although many of these pollutants are received by green stormwater infrastructure (GSI) techniques, some activities may be more effective at treating particular pollutants than others, and each activity has its own performance restrictions (Clark 2012, McFarland 2019). To be effective, GSI design, implementation, and maintenance must focus on particular pollutants of interest (Payne 2019).

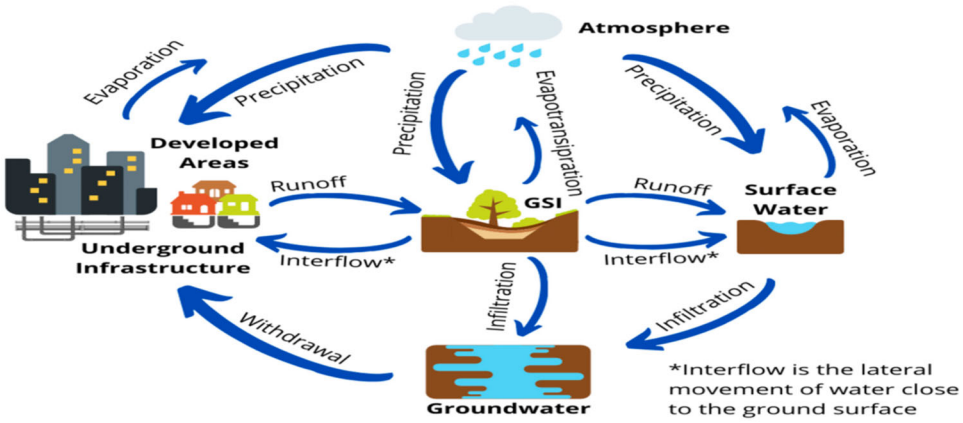

Figure 1. Conceptual diagram of water flow paths in the context of GSI (Taguchi 2020)

2.2.1 Development of GI

Stormwater runoff in urban settings can cause difficulties with water quantity and quality, which can be solved by GI. GI is a strategy that seeks to save receiving waterbodies in urban watersheds and lessen the quantity of stormwater that enters combined or stormwater sewer networks. By allowing plants to use the stormwater and/or allowing the stormwater to seep

into the natural soils, GI tries to replicate pre-development circumstances. GI is frequently referred to in the literature as low impact development (LID) or best management practice (BMP), but all these terms pertain to the same concept. Yet, choosing a specific type of GI system for a specific location in a complicated metropolitan water network can be difficult for designers and decision-makers (McFarland 2019). The biophysical qualities of the site, its location within the watershed, the connection of the current urban water system, and potential contaminants from the site and its surroundings must all be taken into account in order to maximize the efficacy of GI.

The concept of GI originated from the BMPs proposed by the United States in the mid1980s, to accomplish more holistic stormwater quantity management goals for runoff volume reduction, erosion prevention, and ground-water recharge (Schueler 1987), and the term formally emerged in 1990s. Moreover, similar strategies for stormwater control have been devised and adopted in numerous nations using various terminology (Vogel 2015). From the 1990s, stormwater problems have been reduced because of the adoption of sustainable urban drainage systems (SUDS), which were initially developed in the UK and Germany (Keeley 2011). Australia developed the idea of water sensitive urban design (WUSD) in the 1960s, but the formal national WUSD guidelines weren't published until the early 1990s (Fletcher 2015). WUSD is being utilized more and more over the world, especially in the UK and New Zealand (Ashley 2013).

According to the available literature, in contrast to conventional storm water treatment systems, GI techniques use a combination of plant, topography, soil, and bioengineered systems to regulate and control storm water runoff, which helps to reduce the quantity of stormwater (Bowman 2012). By minimizing stormwater runoff and prolonging the lag time,

GI practices can significantly lower the risks of urban flooding and the associated property losses because of the pervasive natural and semi-natural landscape elements.

Numerous research studies and practical applications came to the conclusion that GI approaches could successfully mitigate urban hydrology issues while providing significant environmental, social, and economic benefits to communities, businesses, and citizens (Gregoire 2011, Roseen 2015). Moreover, cost assessments of the installation and upkeep of LID procedures show that using these methods is less expensive than using standard end-of-pipe methods (Roseen 2015). In order to conserve or restore the hydrologic and biological functioning of an urban ecosystem, GI can be deployed at a wide range of landscape scales instead of or in addition to conventional storm runoff control measures (Liu 2014). As a result, the extensive use and widespread adoption of GI practices may lessen the demand for pricey gray stormwater drainage systems as well as the strain that stormwater runoff places on urban infrastructure, changing stormwater management in favor of a more distributed and at-source strategy (Liu 2014).

2.2.2 Benefits of GI

GI is a relatively new approach to stormwater treatment that uses natural systems, such as plants and soil, to manage and reduce the impact of stormwater runoff. Current research on GI and its benefits for stormwater runoff treatment has focused on several areas, including:

Hydrologic performance: Researchers have investigated the ability of GI to reduce the volume and velocity of stormwater runoff, as well as its ability to promote infiltration and groundwater recharge (Woznicki 2018)

Water quality: Studies have examined the ability of GI to remove pollutants from stormwater runoff, including nutrients, sediment, and heavy metals (Tirpak 2019)

Economics: Studies have looked at the cost-effectiveness of GI compared to traditional stormwater management techniques (Jiang 2015)

Social benefits: Researchers have investigated the potential for GI to provide social benefits, such as improved community aesthetics and increased recreational opportunities (Mei 2018)

Overall, research has shown that GI can provide numerous benefits for stormwater runoff treatment, including reduced flooding, improved water quality, increased groundwater recharge, enhanced urban aesthetics, increased biodiversity, and cost savings. However, the effectiveness of GI can vary depending on the specific design and implementation of the system, as well as the local climate, soil, and hydrologic conditions. Current research suggests that GI can be an effective and cost-efficient strategy for managing stormwater runoff in urban areas, while also providing a range of additional benefits for communities and the environment.

2.2.3 Different GIs for On-Site Stormwater Runoff Treatment

The major GIs for on-site stormwater runoff treatment are summarized as follows:

Bioretention:

A bioretention system, which includes many layers of vegetation, filter media, storage, and an optional underdrain, is a planted depression created to collect stormwater runoff from impermeable surfaces (Ahiablame 2012). By increasing evapotranspiration through vegetation uptake and the lag time through soil infiltration, plants, microbes, and soils within a bioretention cell remove pollutants from urban stormwater runoff, reduce peak flow and runoff volume (Lucke 2015). Water begins to pool on the ground surface when the inflow rate is higher than the pace at which the soil column is infiltrating. Most water that is collected by vegetation and held in depressions eventually turns into vapor and is released back into the environment through evapotranspiration (Figure 2) (Chui 2016). Consequently, improving soil

infiltration as well as vegetation evapotranspiration and interception can lessen rainfall-runoff processes (Davis 2009).

Green roof

According to various studies, green roofs also known as vegetative roofs or eco-roofs are typically built with three main layers: a vegetation layer, a lightweight growing medium layer, and a storage or drainage layer placed on top of a waterproof membrane (Carson 2013). As they are light, inexpensive, and require no care, extensive green roofs are typically used and researched more (Carson 2013). Due to their ability to store water, green roofs can greatly reduce the peak flow of the majority of rainfall-runoff and postpone the initial period of runoff production (Karteris 2016). The test bed (3 1m) makes use of a standard commercial extensive green roof system (Alumasc/Zinco), which consists of a layer of sedum vegetation growing in 80 mm of substrate. Green roofs have the ability to make a substantial impact on reducing the amount of stormwater runoff that occurs during frequent periods of heavy rainfall (Figure 2). The roof retained 50.2% of the annual cumulative rainfall, with a total volumetric retention of 30% during the major occurrences. The annual performance values are at the lower end of a range of global data, which is likely due to the possibility of larger rainfall depths and lower evapotranspiration rates than in certain more continental climate situations (Karteris 2016).

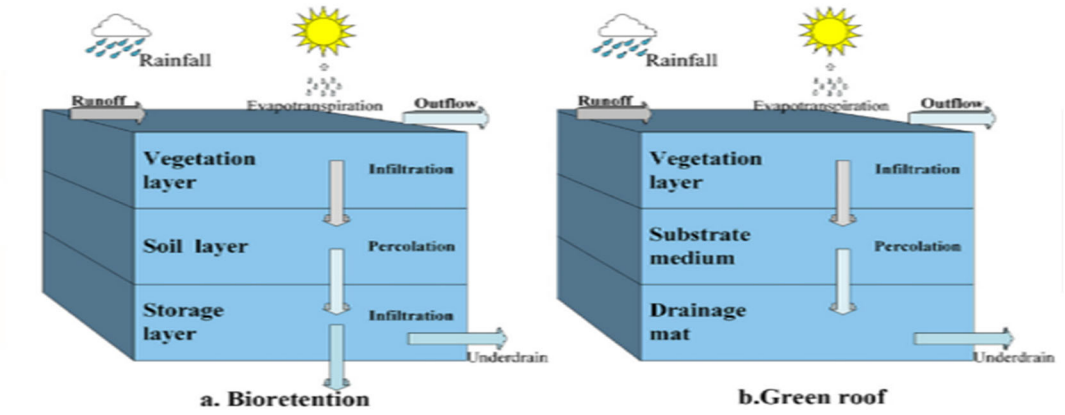

Figure 2. Green Infrastructure practices: (a) bioretention (Chui 2016) (b) green roof (Stovin 2012)

Rain Garden:

GI installations such as rain gardens and bioswales are increasingly regarded as viable tools to mitigate stormwater runoff at the parcel level (Figure 3) (Chaffin 2016). Rain gardens, a GI, play a vital role in reducing rainwater volume and flow, preventing asset's destruction, remove pollutants from urban runoff, and recharge groundwater (Sharma 2021). Physio-chemical and biological features of rain gardens positively help in remediating contaminants, storing runoff water, reducing peak-flow, nutrient cycling, sequestering heavy metals and also provides supplementary benefits such as recreational facilities (Malaviya 2019)

Figure 3. Cleveland Botanical Garden rain garden (Chaffin 2016)

2.3 On-site Stormwater Runoff Treatment by GI Using Biochar Amended Topsoil

2.3.1 Introduction

Biochar is a charcoal-like material rich in carbon and is fabricated from waste biomass at an elevated temperature (200 - 600 °C) and in an oxygen-controlled (pyrolysis) environment. Due to its advanced features, biochar can remove water contaminants using physical, chemical, and biological adsorption processes. High pollutant removal performance is made possible using biochar as performance-enhancing devices (PEDs) for BMPs (Ouedraogo 2023). On roadway bioslopes and filter strips, topsoil can be amended with biochar to improve soil quality and promote the penetration of pollutants. The application of biochar amended topsoil improves the topsoil's ability to increase hydraulic conductivity. Biochar produced at a high temperature has improved pollutant removal ability as a result of having a high surface area and pore volume (Cairns 2022). Biochar can also be produced naturally during a forest fire. For many years biochar has been used as a soil enhancer to help grow crops by creating biodiversity in the soil. The problem is when removing the leftovers after picking crops like corn stalks a lot of carbon is emitted out into the atmosphere from burning them in the open area. The burning of them in an enclosed environment like a kiln will allow for more biochar to be produced and less carbon emission into the atmosphere (Golisano Institute for Sustainability, 2021)

Every year in the United States rain causes billions of dollars in damage and also destroys many ecosystems. The ecosystems are destroyed from the stormwater runoff caused by the rain. Storm water runoff is when the water isn’t able to soak into the ground, so it picks up any loose materials in its way and transports them to where it’s going. The stormwater runoff will pick up anything from trash to oil and grease from a car and move them to the body of water it’s heading toward. Trash can be very harmful to the animals in the ecosystem, because they can mistake it as food or get caught on it and die from it. Also, other nutrients can cause

increased growth to plant life in the body of water which would deplete the oxygen in the water killing many of the fish and other water living animals. These issues can cause significant problems to communities, because there would be way less recreational uses of the body of water causing significant financial losses.

When it comes to the health of soil, biochar has been used to help poor soil regain its nutrients. The pH of normal soil has an average of 6.5 to 7.0 but in a lot of places in the world, the pH of soil is between 4 and 5.5, making the soil acidic and extremely unhealthy. The use of biochar has helped soil gain its nutrients. “In soils this acidic, most plants cannot take up nutrients, even if they are present in the soil. Stick some biochar in this soil, however, and you can push the pH as much as a whole point higher. As pH rises, more and more nutrients become available for crops”. This allows an ecosystem to thrive.

Water filtration has primarily been done mostly using coal /anthracite and sand. Biochar is a substance made from waste wood and other biomass that resembles coal in its qualities. Water pollutants can be removed by using biochar. In order to remove urban usage pesticides and trace organic contaminants, biochar has been added to biofilters that have been modified to do so. Stormwater runoff pollution can be treated with biochar since it is affordable, effective, and environmentally beneficial. The U.S. Department of Transportation (USDOT) takes actions to lessen the pollution caused by stormwater runoff from highways. In the US, polluted stormwater runoff poses a threat to the environment, particularly to lakes, rivers, reservoirs, and estuaries that support aquatic life. More contaminants are transferred into waterbodies through stormwater runoff as a result of rising urbanization and daily traffic. Stormwater runoffs wash pollutants from roadways and other paved ways (parking spaces, parks) including SS, fertilizers, heavy metals, and organic contaminants. Vehicle emissions and atmospheric

deposition are closely linked to these contaminants. Numerous research has identified biochar as a low-cost and effective material for treating on-site stormwater runoff as the need to eliminate these water contaminants grows (Gwenzi 2017, Ashoori 2019). On-site stormwater runoff treatment utilizing GI with biochar-amended topsoil is a new method that will be discussed in this section.

2.3.2 Biochar as a Substrate of GI

Biochar generated from biomass and biosolids can be utilized in substrates appropriate for urban GI, particularly green roofs, green parking lots, and green walls. Biochar can be utilized as a substrate for GI because it promotes plant growth, fertilizer effectiveness, and rainwater collection (Novotný 2023).

Biochar is a type of charcoal that is produced by a pyrolysis of heating organic material in a low-oxygen environment. When added to topsoil, biochar can help to improve the soil's water-holding capacity and reduce erosion, making it a valuable tool for stormwater treatment. Biochar, which is a carbon-negative material, appears to be an essential soil amendment in green roof due to its water-holding capacity and stability. Green roof with 5% Biochar amended soil (BAS) has highest runoff reduction and longest peak outflow delay (Gan 2021). Some of the benefits of biochar-amended topsoil for stormwater treatment include:

Increased water infiltration: Biochar-amended topsoil (unsieved biochar) has been shown to increase the hydraulic conductivity of soil, increasing water infiltration (Trifunovic 2018).

Improved soil structure: Biochar can help to improve soil structure by increasing soil porosity and reducing compaction, which can lead to better infiltration and reduced erosion (Blanco-Canqui 2017, Are 2019).

Reduced nutrient leaching: Biochar has been shown to help retain nutrients in the soil (Beck 2011, Major 2012), reducing the amount of nutrients that are lost to leaching during storm events.

Carbon sequestration: Biochar is produced by pyrolysis process. This pyrolysis process produces a high carbon biochar that can be sequestered almost permanently in soil, and energy that substitutes for fossil fuels (Winsley 2007).

Reduced pollutants from stormwater runoff: Biochar can help to filter pollutants from stormwater runoff, reducing the number of pollutants that enter nearby waterways (Mohanty 2018).

Overall, the use of biochar-amended topsoil for stormwater treatment can provide numerous benefits, including improved water retention, reduced erosion, increased plant growth, and carbon sequestration. These benefits can help to improve the health of local ecosystems and reduce the negative impacts of stormwater runoff on the environment.

2.3.3 On-site stormwater runoff treatment by GI using biochar amended topsoil and its performance

According to Wolfand's research, biofilters with a volume of 33% biochar totally eliminated the target contaminants (fipronil, bifenthrin, benzotriazole, and other pesticides used in urban areas) from the water (Wolfand 2019). Similar investigations showed that biochar columns in biochar-amended biofilters had a more than 99% removal of a trace organic pollutant, while granular activated carbon had less than 70% removal (Ashoori 2019). Imhoff and Nakhli (2017) showed the effect of biochar (produced through pyrolysis of southern yellow pine) on biochar-amended soil on highway side slopes from the edge of the pavement in Delaware (Imhoff 2017). In their simulated stormwater runoff event, 4% biochar–amended soil reduced runoff volume 13% lesser than biochar free soil and reduced dissolved organic carbon (DOC)

due to reduced leaching in the biochar-amended soil as well as efficiency of approximately 83% was achieved in the removal of nutrients and TSS based on an average of 83% reduction of stormwater runoff volume. Similar research prepared for Virginia Center for Transportation Innovation and Research titled "Removing Nitrate from Stormwater with Biochar Amendment to Roadway Soils" was conducted under the same principal investigator (P.I.) in 2019 (Imhoff 2017) . Imhoff et. al (2019) also studied composted amended soil and showed a higher drainage rate but less effective moisture retention and compaction resistance. Compost is relatively enriched in available nutrients compared to biochar because most of the available nutrients in biochar are lost during pyrolysis (Jílková 2022). After 1.5 years of installing biochar amended soil on-site in Delaware, it showed comparable results in water retention hydraulic conductivity to the newer on-site installation in Virginia (Imhoff 2019). Results demonstrated increased efficiency in removing nitrate and total nitrogen and suggested that recent installations of biochar-amended topsoil may result in the mobilization of nutrients and microbial activity (Imhoff 2019). The most important components for an effective GI include the type of grass and soil properties in the ground. It is necessary to explore new engineered soil materials for an effective GI. GI using biochar amended topsoil is a new approach for on-site stormwater runoff treatment. Numerous studies confirm that vegetated filters achieve higher removals of nutrients when compared to non-vegetated filters (Bratieres 2008). Vegetation also helps to maintain the hydraulic conductivity of biofilters over time (Hatt 2009), and a thicker root morphology may decrease the impact of clogging (Le Coustumer 2012). An extensive study of 20 different Australian native grasses adapted to low nutrient concentrations in native soils determined that grasses vary greatly in their ability to uptake nitrogen and phosphorus (Read 2008). One recent study demonstrated significant differences in nitrogen removal based on

vegetation type (Burns 2015). Switchgrass typically had a very high performance with all nutrients when compared to other species (Burns 2015). Different GDOT grass 35 species were analyzed to assess nutrient removal performance, and switchgrass had the highest nitrogen removal percentage (18%) (Burn 2015). A detailed study was conducted to analyze the removal of nutrients, heavy metals, and TSS from contaminated highway stormwater runoff. Two different grass swale designs were tested in 52 storm events over 4.5 years. The experiment also tested the design's efficiency by including vegetative check dams and filter strips. The grass swale was influential in the removal of TSS, nutrients (nitrogen, phosphorus), and heavy metals (Pb, Cu, Zn, Cd) from the influent stormwater runoff. Removal of nutrients had inconsistency in a few storm events and can be attributed to other nutrient sources such as fertilizer application and landscape management. Nitrite was the only nutrient removed with consistency. The inclusion of pretreatment filters such as the vegetative check dams and filters negatively affected the results (Stagge 2012). The addition of filter strips only aided in removing nitrate, which can be due to the uptake of the grass through infiltration. Structures like GI serve many important roles in the drainage, with one of the most important being the filtration of stormwater runoff. The EPA reports that urban stormwater runoff is the leading cause of water quality problems in the United States. “Green infrastructure improves water quality by decreasing the amount of stormwater that reaches waterways and by removing contaminants from the water that does. Soil and plants help capture and remove pollutants from stormwater in a variety of ways, including adsorption, filtration, plant uptake, and the decomposition of organic matter. These processes break down or capture many of the common pollutants found in runoff, from heavy metals to oil to bacteria” (Denchak 2019).

In all this research, they did not show 5% biochar amended soil experimental results both in lab scale and field scale experiment. In Imhoff et. al (2017) research, in the bench-scale experiment, they used 2% to 6% biochar with soil and in field scale experiment, biochar was added at 4% to a sandy loam along a four-lane divided highway (0.12 acres) in Delaware. Our field scale experiment focused on reducing pollutants from stormwater runoff and stormwater runoff volume. At 5% biochar amended soil also increased the soil hydraulic conductivity which increased infiltration rate. Also, GI may increase soil hydraulic conductivity after long term period due to grass growth (Ni 2020). Although many pollutants can be removed by using current stormwater best management techniques (BMPs), they are expensive and usually require the purchase of additional land. But Existing GI using biochar amended topsoil can be extended to provide stormwater treatment rather than capturing stormwater for treatment in new treatment systems. This eliminates the expense of building new infrastructure.

Among all the commercial biochars, Soil Reef Biochar is the most effective biochar among the three commercial biochar products selected (Yunus 2022). Soil Reef Biochar is a type of biochar derived from southern yellow pine trees using pyrolysis at a temperature of 550℃ for 10 minutes. It has a specific area of approximately 350 ±30 m2/g and an internal porosity of 0.83 mL/g. Its bulk density is 9.0 lbs/cft. The company is located in Berwyn, PA, USA, and offers online purchasing options for commercial use in multiple states. In this research project Soil Reef Biochar was used with local topsoil, established a Control Cell and a Test Cell where Control Cell was made with only topsoil and Test Cell was made with topsoil, mixed by 5% biochar. Switchgrass was grown at these two Cells identically to see the comparison of the stormwater pollutant's removal efficiency.

CHAPTER 3. MATERIALS AND METHODS

3.1 Overview

The main materials and methods used to carry out this project are covered in this Chapter. Design, construction and installation, operation and maintenance, and sampling and testing of Full-Scale Field Test Site are all been thoroughly described here. Lab test methods for topsoil, biochar, biochar amended topsoil, and water quality parameters are also reported here.

3.2 Full-Scale Field Test Site for On-Site Stormwater Runoff Treatment by GI Using Biochar Amended Topsoil

For Phase I, the project's main focus was on design, construction and installation, operation and maintenance, and sampling and testing of a GI using biochar amended topsoil for on-site stormwater runoff treatment.

3.2.1 Design

The Full-Scale Field Test Site needed to be 500 ft^2 in total. Two Cells are designed and built for a direct comparison purpose: Control Cell with topsoil only and Test Cell with biochar-amended topsoil at 5% biochar by weight. The two Cells were 250 ft^2 each, specifically 20 ft x 12.5 ft (see Figure 4, the top view), Test Cell was made up of 95% topsoil and 5% biochar by weight. Each cell was also excavated 1 ft deep with 2 ft trench running down the middle of each Cell for laying perforated corrugated pipe (0.5 ft diameter) (see Figure 5, the front and rear view), otherwise called a French Drain Collection System. There was 1% slope for the center drain collection pipe (see Figure 6, the side view). Two (2) cylindrical catch basin drums, with a standing water capacity of 5 gallons, were installed at the ends of corrugated pipes, one for each Cell. Control Cell and Test Cell were prepared and constructed almost

identically: Control Cell with topsoil only while Test Cell with biochar amended topsoil. After constructing, both Control Cell and Test Cell were stabilized and grassed.

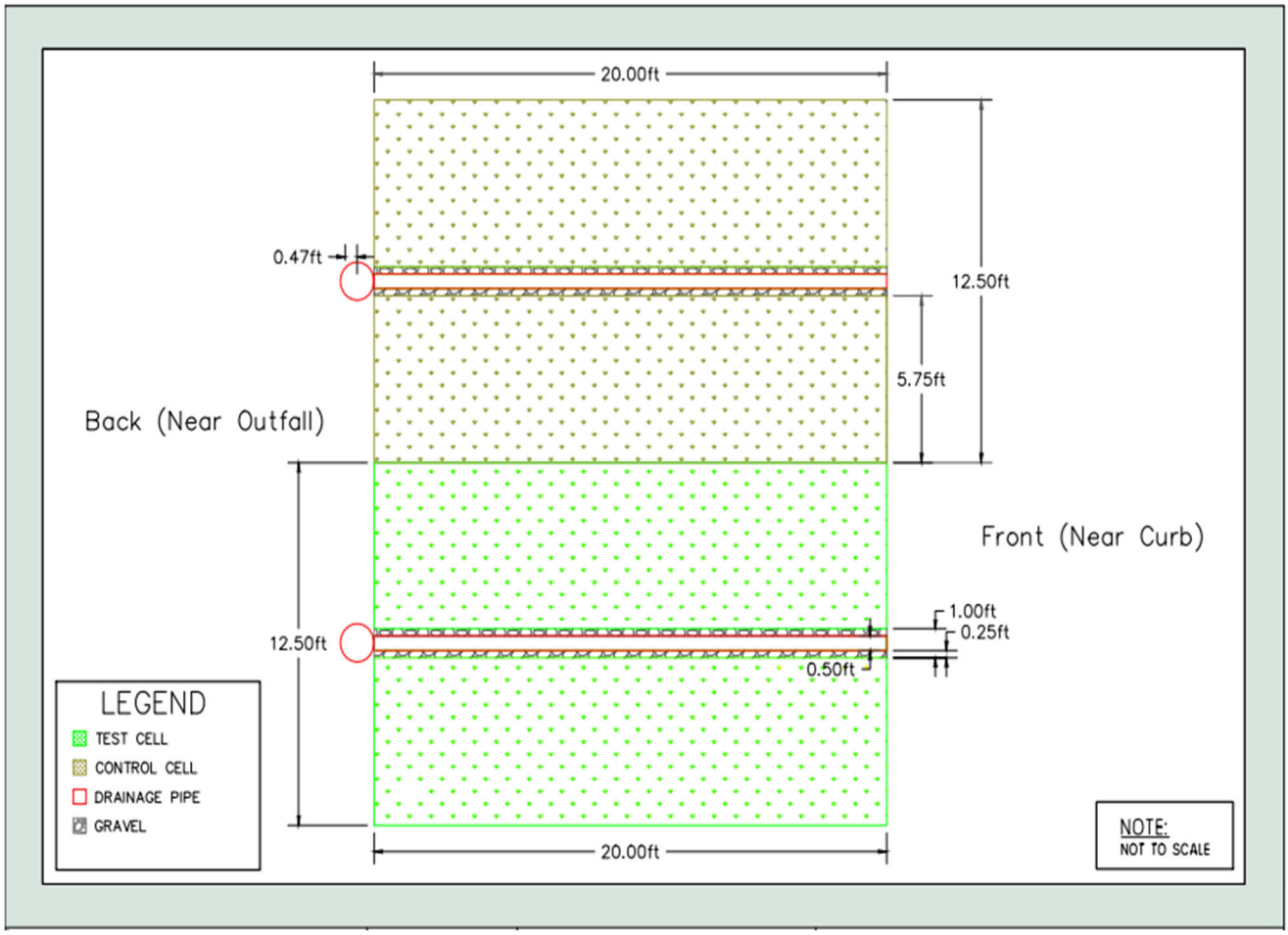

Figure 4. Top View of Field Test Site with Control and Test Cells

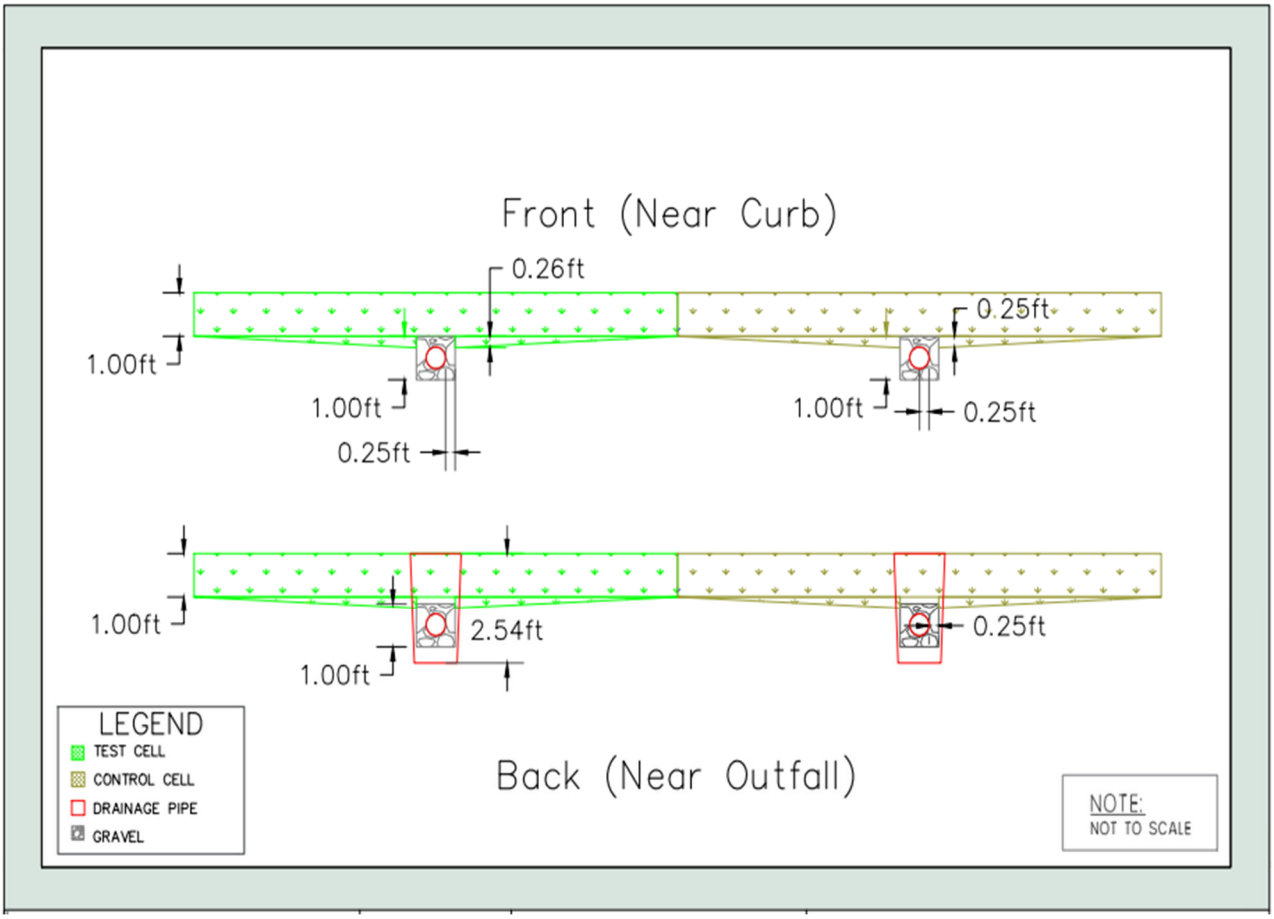

Figure 5. Front and Rear View of Field Test Site with Control and Test Cells

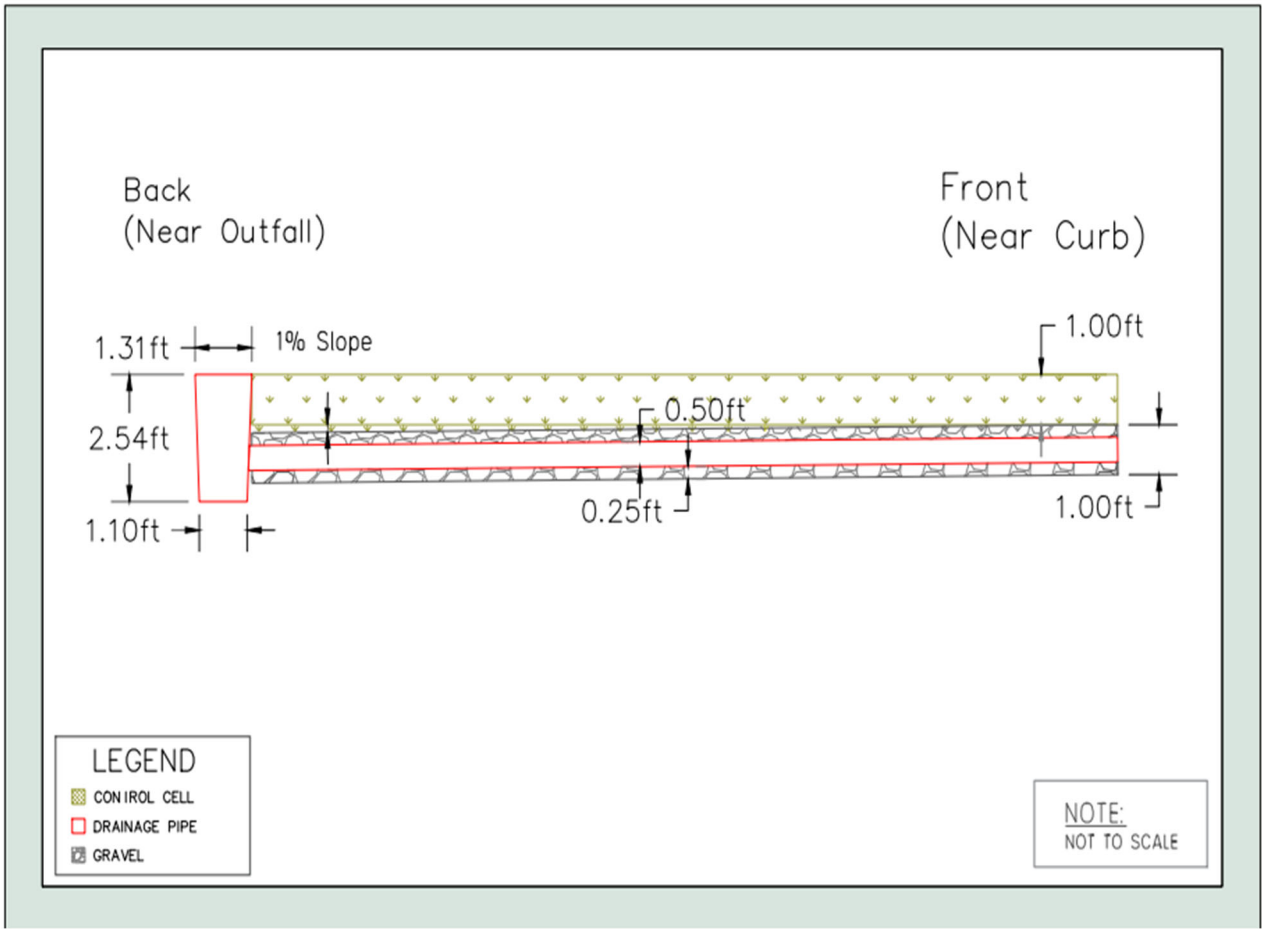

Figure 6. Side View of Field Test Site with Control Cell (Test Cell almost identical side view)

3.2.1.1 Site Selection

To get the project started, a location of Field Test Site needed to be applied for and approved by the Facilities Department of GSU. There were three locations that were considered for the project to be placed. The first one was to use the shoreline of the pond in front of the new Engineering and Research Building. That location was turned down because Facilities thought that it is very visible for the public and is often used for marketing purposes and live feed streams (weather). The second location was close to the Engineering Building. There is a creek that could have been utilized to receive treated stormwater runoff but there was not enough

work area that was desired. The last location was in between the Hendricks Hall (Jiann-Ping Hsu College of Public Health Student Services Center) and the Center for Art and Theatre. The coordinates for the project location are as follows: (32.4260589, -81.7852243). Considered the space for the desired work area, this location was ultimately chosen because Veazy Hall Parking Lot (about 1.3 Acres) is nearby. The Parking Lot was on a slope that would collect the stormwater runoff, which has an abundance of pollutants and can serve as raw influent for the Field Test Site. Figure 7 represents the location of the project with Full-Scale Field Test Site for on-site treatment of stormwater runoff from the Veazy Hall Parking Lot on GSU Campus and Figure 8 is the Inlet of the GSU Parking Lot from where stormwater runoff was collected and pumped by a submergible pump to the Field test Site.

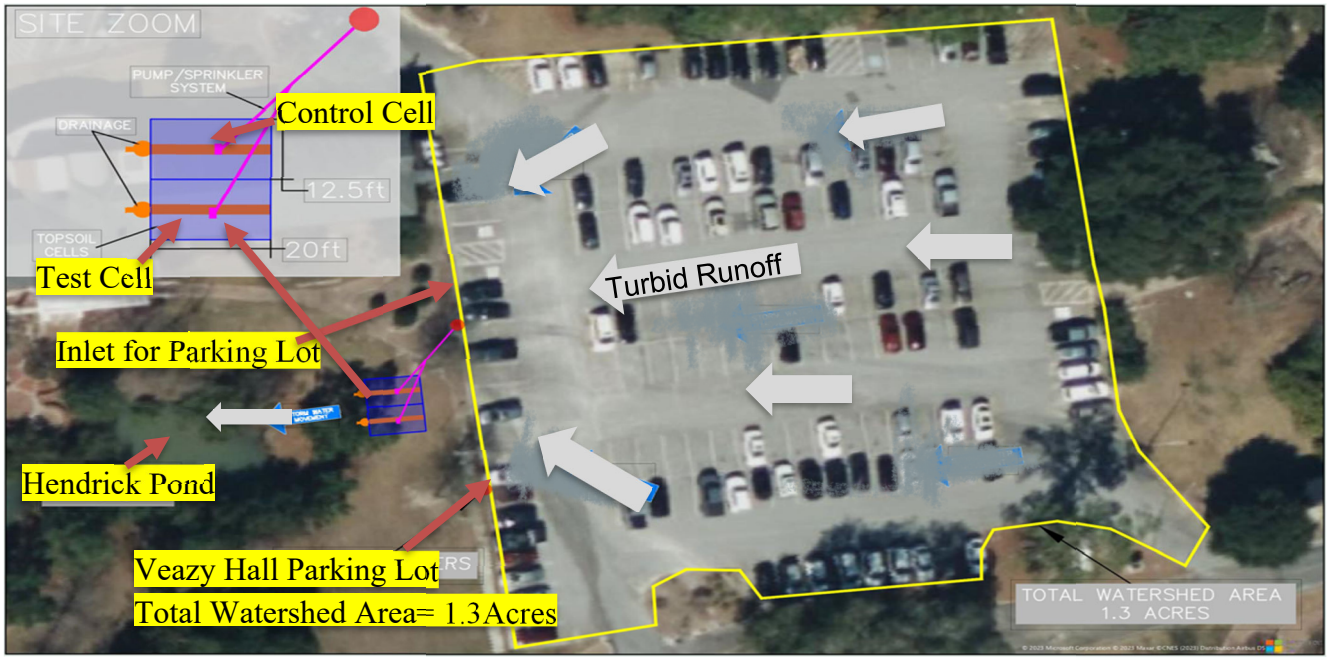

Figure 7. Full-Scale Field Test Site for On-Site Treatment of Stormwater Runoff from Veazy Hall Parking Lot (GSU Campus)

Figure 8. Inlet for Parking Lot from where Stormwater Runoff was Pumped by a Submergible Pump to Field Test Site

3.2.1.2 Pumping, Sprinkler, Infiltration and Treated Effluent

There had a plan for how to collect the Parking Lot stormwater runoff and make sure that it would be able to reach the Field Test Site due to a couple gutter systems and the parking lot being curbed off. What was decided on was to install a submersible pump into a inlet that was connected to a sprinkler (see Figure 7). The inlet is used to collect the Parking Lot stormwater runoff and discharge it into Hendrick Pond. In order to keep certain volume of the Parking Lot stormwater runoff in the inlet for pumping, a piece of plywood board, with a height greater than diameter of the discharge pipe, was installed against the inlet of the discharge pipe in the inlet. During a significant rainfall event, the Parking Lot stormwater in the inlet was pumped to the Field Test Site and sprayed through two sprinklers separately: one for Control Cell while the other one for Test Cell. A RAINPOINT Water Flow Meter was installed for each sprinkler to monitor the flowrate and accumulated volume of stormwater runoff applied onto Control/Test Cell. Then, the Parking Lot stormwater runoff was infiltrated/treated through the 1 ft layer of topsoil or biochar amended topsoil in Control/Test Cell and seeped into the

corrugated perforated pipes and flow into the end cylindrical catch basin drums, where the treated effluent samples were collected and tested for pollutants. The corrugated perforated pipes had designed holes to let the treated effluent seep into the pipes and flow into the end cylindrical catch basins.

3.2.1.3 Topsoil Selection

The local topsoil from Statesboro was used in this project. It was top layer of soil from the earth's surface in Southeast Georgia. It was purchased from Mulch & More, 22659 US Highway 80 E Statesboro GA 30461. Figure 9 represents the topsoil collection location (blue symbol), ga031 represents soil survey area for Bulloch County, Georgia and Figure 10 shows the piles of topsoil obtained from the earth's surface in Southeast Georgia and used for this project. This topsoil is under Pelham series soil. The Pelham series consists of very deep, poorly drained, moderately permeable soils that formed in unconsolidated Coastal Plain sediments. The composition of the topsoil is given in Table 1.

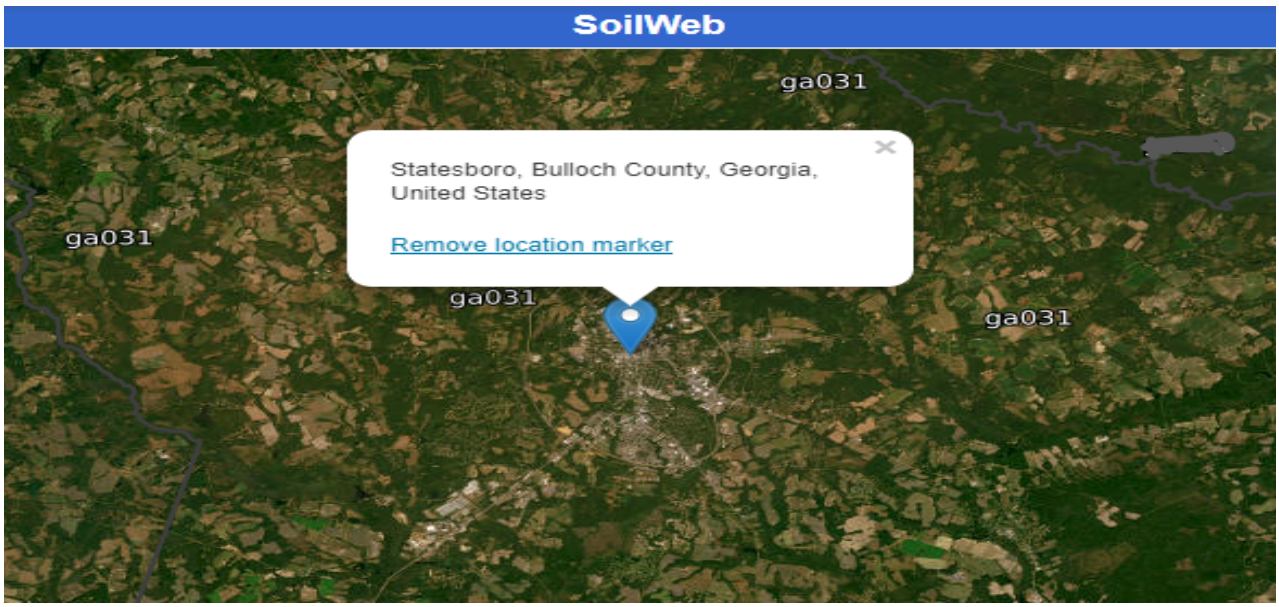

Figure 9. Map illustrating sampling location of topsoil for Field Test Site (source: UC-Davis Soil Web https://casoilresource.lawr.ucdavis.edu/gmap/)

Figure 10. Pile of Topsoil at our Field Test Site before use

Table 1. Topsoil samples and composition (source: UC-Davis Soil Series Extent Explorer)

Sample Location	Description	Organic % @ 1 ft depth	Sand% @ 1 ft depth	Clay% @ 1 ft depth
Statesboro, GA	Pelham series (very deep, poorly drained, moderately permeable soils)	1.5%	83.5%	7.5%

3.2.1.4 Biochar Selection

Based on the previous Master research project completed by Ahmed Yunus, what was the effective biochar he found was Soil Reef Biochar with a 5% addition to the topsoil which

achieved the maximum pollutant removal efficiencies (Yunus 2022). In this Phase I project, the Soil Reef Biochar with 5% addition to topsoil was used. It was purchased from Soil Reef Company, 1125 Lancaster Avenue, Berwyn, PA 19312. Figure 11 shows the Soil Reef biochar received and left at our Field Test Site.

Figure 11. Soil Reef Biochar received and left at our Field Test Site

3.2.1.5 Grass selection

According to GDOT Research Project Report (RP 11-23) on Treatment of Highway Runoff: Engineered Filter Media for Pollutant Removal through Enhanced Sorption, on average across all experiments, total nitrogen was removed at the highest percentage of 18% with Switchgrass. These plants have extensive, dense root networks that covered the whole biofilter column. A saturated zone improved nitrate removal while decreasing ammonium removal (Burns 2015). In this Phase I Project, Switch grass was selected. A total of 13 Switchgrass plants were purchased from Lowe's and each was in an individual pot. They were planted at the Control Cell and Test Cell identically on June 9th, 2023. Figure 12 represents the Switchgrass plants at our Field Test Site.

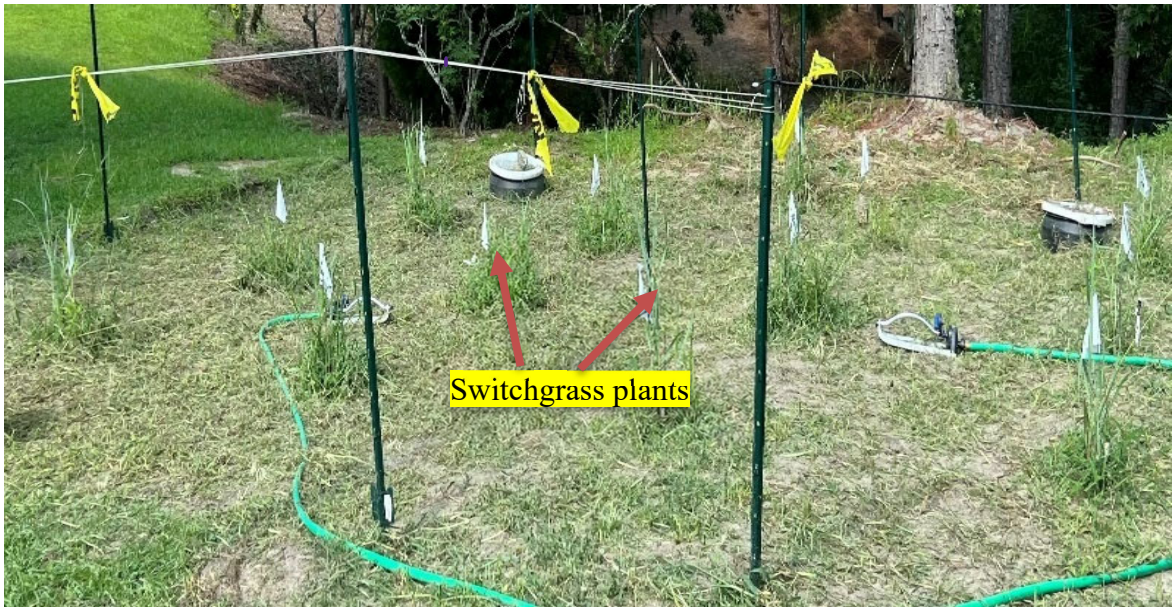

Figure 12. Switchgrass Plants at our Field Test Site

3.2.2 Construction and Installation

3.2.2.1 Site Layout

Site layout was performed for 20ft x 12.5ft for Control Cell and 20ft x 12.5ft for Test Cell on February 9th, 2023. A measurement tape was used to make the rectangular layout of the Field Test Site. A White marker was used to mark the layout for Control Cell and Test Cell. Figure 13 represents the site layout marking for Field Test Site near GSU Parking Lot.

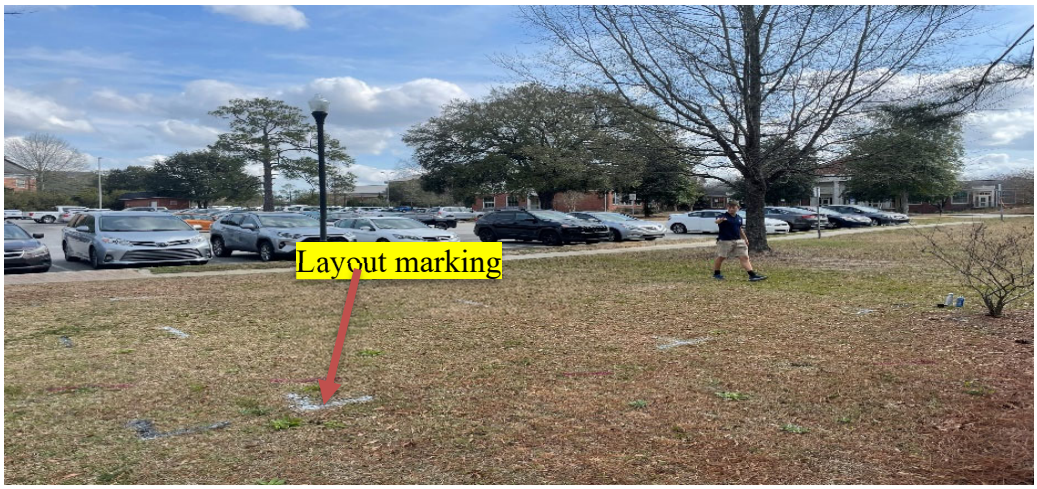

Figure 13. Layout marking for Field Test Site near GSU Parking Lot

3.2.2.2 Excavation

Each Cell was excavated 250 ft^2 area and 1 ft depth by excavator (see Figure 14) on April 15th 2023. A middle trench was dug for the corrugated perforated pipe in the Control Cell and Test Cell respectively. Facilities Department from GSU campus helped excavate the Field Test Site.

Figure 14. Excavating by Excavator/Backhoe at Field Test Site

3.2.2.3 Installation of corrugated perforated pipe and end cylindrical catch basin drums for collecting treated effluent

Two cylindrical catch basin drums (see Figure 15 a) were installed in both Cells, one for each Cell. They were connected with the upstream corrugated perforated pipes from Field Test Site for sampling treated effluent (see Figure 15 b). and the downstream corrugated perforated pipes discharging extra treated effluent into the Hendricks Pond. Each drum was capable of holding about 5 gallons of treated effluent sample. These pipes (see Figure 15 b) were equipped with specific openings to allow water to seep inside and be directed towards the drums. To prevent sediment from entering the pipes and reaching the catch basins drums, the pipes were surrounded by gravel and wrapped with a layer of landscaping fabric (see Figure 15 c).

Figure 15. a) Two cylindrical drums b) Corrugated perforated pipe c) Cylindrical drum and perforated pipe installation

3.2.2.4 Preparation of biochar amended topsoil

5% of biochar was added in a weight ratio to the topsoil to form the biochar amended topsoil (see Figure 16). In preparing the biochar amended topsoil, a total weight of 14472.29lb (25 ft^3) mixture of topsoil and biochar was utilized for Test Cell. For preparing 5% biochar ratio, two bucket was used (red bucket was for biochar and orange bucket was for topsoil) (see Figure 16). To measure the mass marketable lab scale was used. Orange bucket was filled with topsoil

and weight was taken by scale. 5% of that weight was calculated and red bucket was filled with that weighted biochar. A level was marked at both of the buckets as a consistent measurement could be done for the mixing. The mixture was hand-mixed for 15 minutes to ensure even distribution before transferring the mixture of biochar amended topsoil into the Test Cell.

Figure 16. Mixing topsoil and biochar

3.2.2.5 Earth filling

The Control Cell was filled with topsoil only and the Test Cell was filled with 5% biochar and 95% topsoil mixing (see Figure 17). Corrugated perforated pipes were surrounded by gravel at every Cell (see Figure 17).

Figure 17. Earth Filing at Field Test Site

3.2.2.6 Grass Growing

Switchgrass plants were planted with 5 ft spacing from each other (see Figure 18). These plants are 5 ft taller after growing. In addition to switchgrass, natural grasses grew swiftly as well. The natural grass was removed regularly from the Field Test Site in order to make clear and tidy. The switch grass plants were marked by white flags and the metal posts were installed around the whole Field Test Site (see Figure 18).

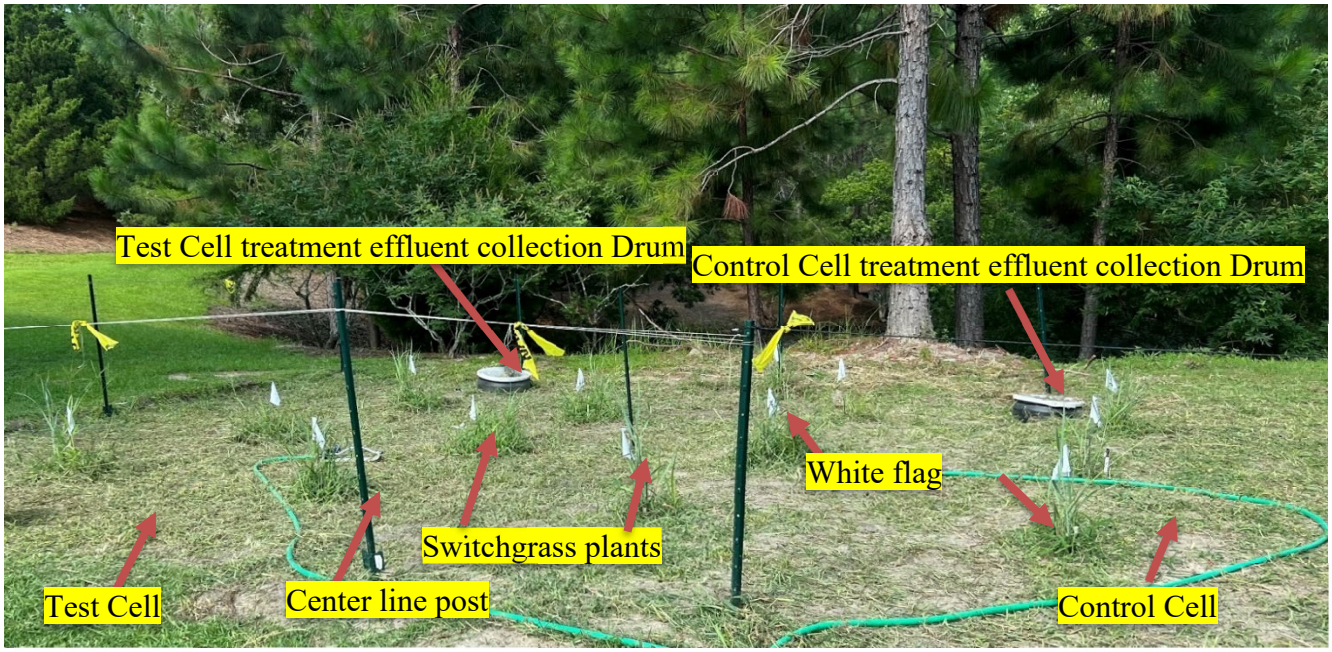

Figure 18. Field Test Site after growing grass

3.2.3 Operation, maintenance and monitoring of the field test site

3.2.3.1 Introduction

Operating the Field Test Site, performing maintenance, and monitoring are thoroughly covered in this section. A submersible pump which is 1/3-HP 115-Volt Submersible Utility Pump, was installed inside the inlet for the Veazy Hall Parking Lot on GSU campus, it is connected to a sprinkler system for the Field Test Site (see Figure 19). This setup aimed to simulate a rainfall scenario: the stormwater runoff from the Parking Lot was pumped and applied onto the Field Test, Site for treatment whenever it rained. An average 5.5-gallon stormwater runoff from the inlet was pumped at an average flow rate of 3.44 gallon/hr. at every rainfall event. the applied stormwater runoff from the Parking Lot were infiltrated and treated through the Field Test Site, collected through the corrugated pipes, and flowed into the catch basin drums. In these drums,

samples of treated effluent were collected and tested for the concentrations of pollutants. After every rainfall event, two collection drums were emptied, and ready for next rainfall event.

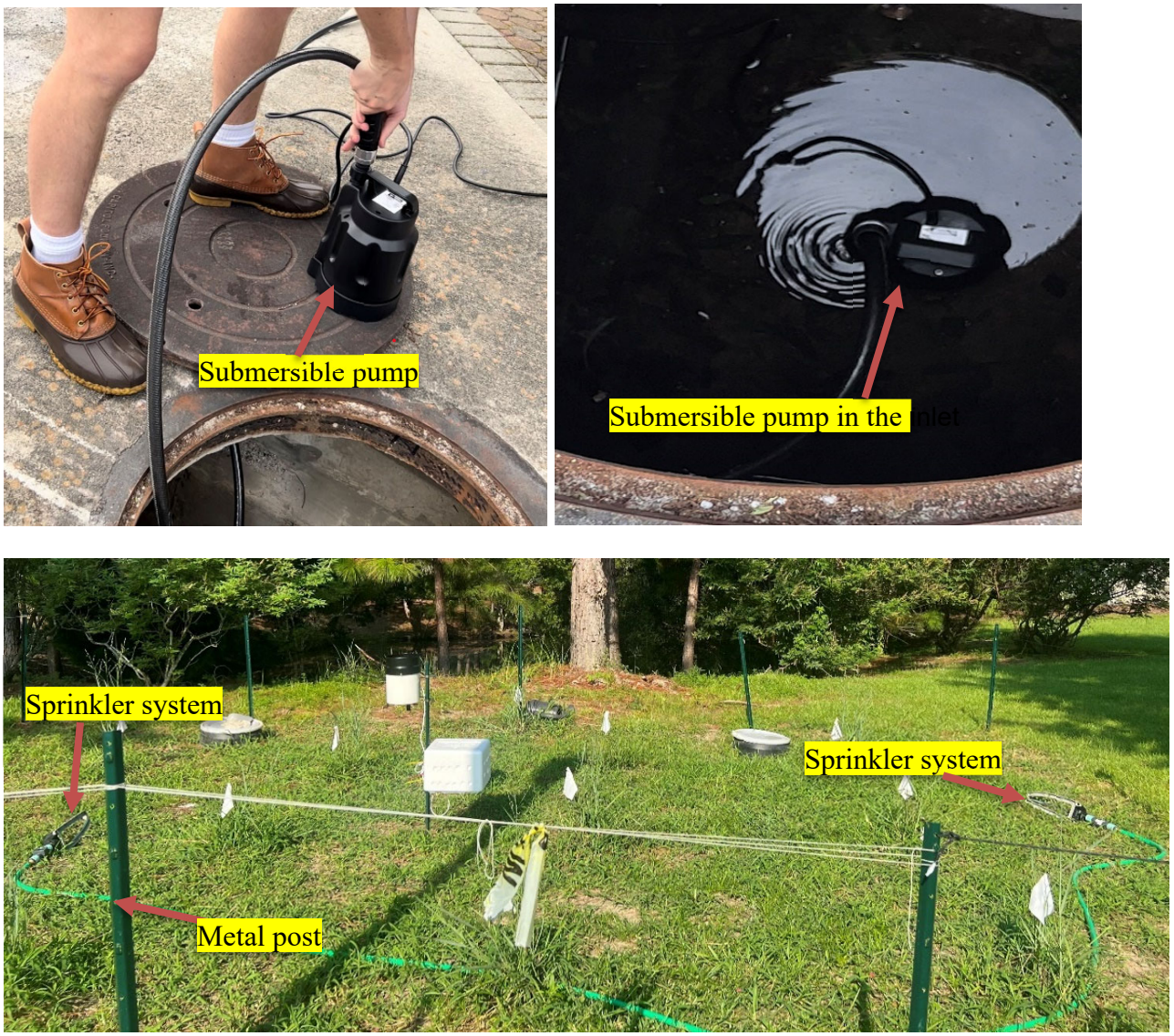

Figure 19. 1/3-HP 115-Volt Submersible Utility Pump with sprinkler system

3.2.3.2 Pumping

The average flow rate of the pump was 3.44gal/hr, while the amount of water in the inlet applied to the Field Test Site was around 5.45gal.

3.2.3.2 Sprinklers

Two sprinklers are linked with the submersible pump. Stormwater runoff was identically applied onto each Cell when the pump was operated (see Figure 18).

3.2.3.3 On-site monitoring

The flow rate of the stormwater runoff applied onto each Cell was measured using a Rainpoint flow meter which can provide both flow rate and water volume (see Figure 20). To keep track of the intensity of the rainfall events, a rain gauge was set up on-site (see Figure 20). A HOBO onset rain gauge was installed at the test site on August 8th 2023. This rain gauge provides rainfall data as well as temperature data. There is a pendant logger with the rain gauge, which is used for storing and transferring all the data to any device by a HOBO logger base station. To get the temperature reading, the pendent data logger was kept under an insulative box. The pendant data logger is used for both temperature and rainfall data. HOBO ware software was used to get rainfall and temperature data from the logger. Additionally, a HOBO soil moisture logger that was operated with HOBO connect software was used at the Field Test Site to monitor and record soil moisture data (see Figure 20).

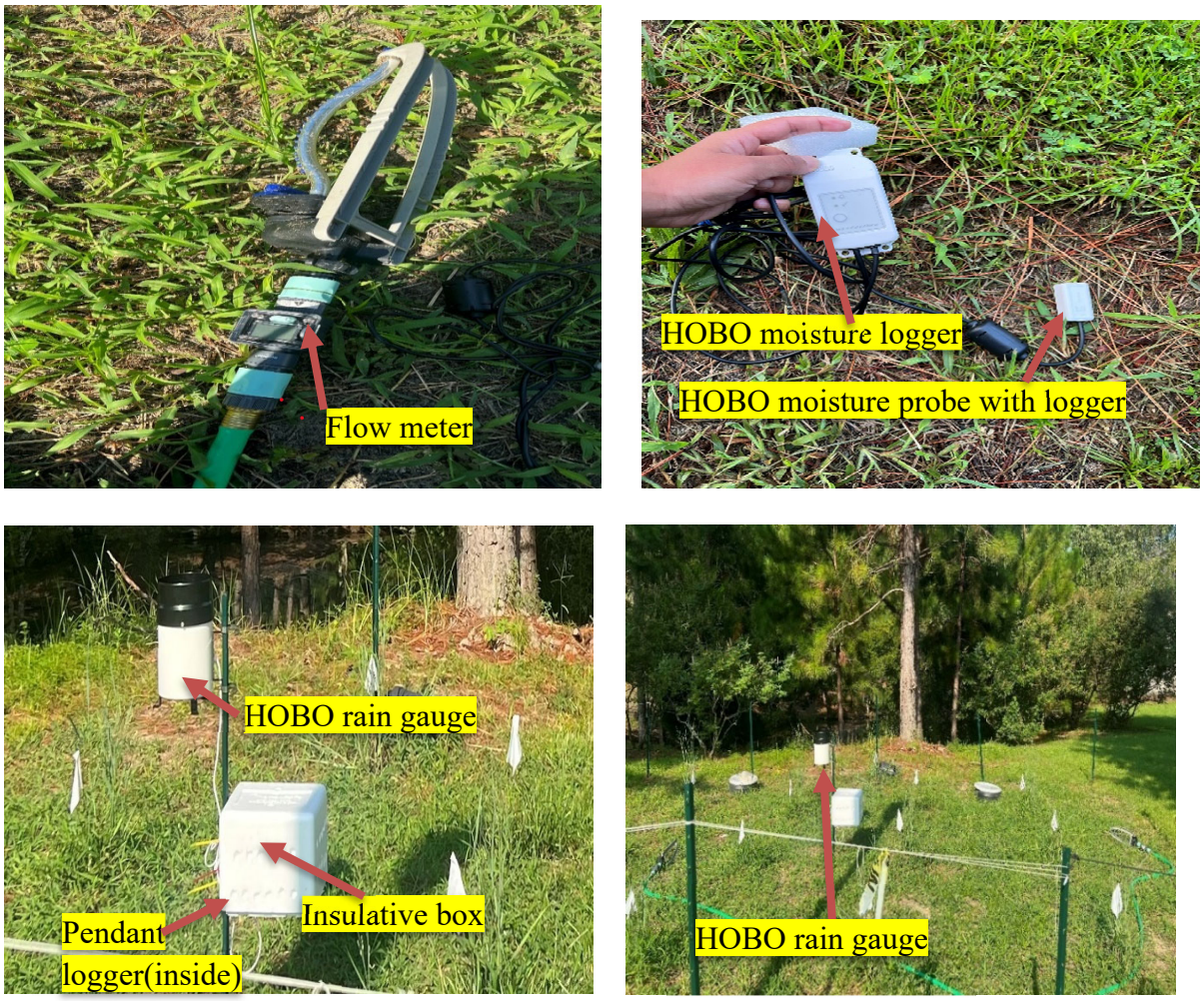

Figure 20. Flow meter, HOBO moisture logger and HOBO Rain gauge set up at Field Test Site

3.2.4 Water sampling

3.2.4.1 Introduction

The stormwater runoff was sampled from GSU parking lot. The rainwater samples were collected in a bucket, the raw stormwater runoff samples were collected from the Inlet for the Parking Lot using a pole sampler and the treated stormwater runoff samples were collected from the two end drums at the Field Test Site. The Veazey Parking Lot was repaired from July 9th to July 31st, 2023, using sealant, asphalt, and road markings (see Figure 21). During each

major rainfall event, one gallon of each water sample was collected and stored in a refrigerator at the refrigerator room in the Engineering and Research Building (ERB) at GSU (see Figure 22).

Figure 21. GSU Veazey Parking lot repairing work

Figure 22. All Samples stored in Refrigerator in ERB at GSU

3.2.4.2 Rainwater only sampling

Rainwater samples were collected on July 10th, 15th, 28th, 29th and 30th, 2023, respectively. While raining without operating the pump, only rainwater directly hit the Field Test Site. During operating the pump, both rainwater and raw stormwater runoff from the Parking Lot were applied onto the Field Test Site for infiltration and treatment.

3.2.4.3 Raw stormwater runoff sampling from GSU Parking Lot

On July 10th, 15th, 28th, 29th, 30th, and August 6th, and 15th, 2023, raw stormwater runoff samples were collected from the Inlet for the Parking Lot (see Figure 23). A pole sampler was used to collect the sample. After every rainfall event, the water from the two drums was removed. Raw stormwater runoff was a little bit colored due to the repair work (road marking color) before sampling days.

Figure 23. Raw stormwater runoff sampling at the Inlet for Parking Lot

3.2.4.4 Treated effluent sampling at the end drum in the Field Test Site

The treated effluent samples were collected from the two end drums for the Control and Test Cells, respectively, at the Field Test Site on July 28th, 29th, 30th, and August 15th, 2023. at field test site on July 28, July 29, and July 30, 2023. A ladle was used to collect the treated effluent from the end drums. While the treated effluent from the Test Cell was clear, that from the Control Cell was tinted, giving it a soil-like appearance (see Figure 24). Before every rainfall event the two end barrels were emptied by a vacuum pump, cleaned and were ready to store new samples.

Figure 24. Treated effluent samples from Test Cell and Control Cell

3.3 Lab tests

3.3.1 Topsoil, biochar and biochar amended topsoil properties

3.3.1.1 Bulk Density

The sampling ring of the KSAT was used to sample the topsoil in the aquarium tank 14 days after the tap water infiltration (see Figure 26). The volume (V) of the sampling ring was 250 mL, and the initial weight of the sampling ring (W_1) and final weight of both the sampling ring and dry topsoil (W_2) were recorded. The topsoil in the sampling ring was placed in an oven at 105℃ for 2h. The bulk density was calculated as: Bulk Density = $\frac{W_2 - W_1}{V}$

The same procedure was followed for measuring bulk density for biochar and biochar amended topsoil.

3.3.1.2 Saturated Hydraulic conductivity

The KSAT Saturated Conductivity Meter (benchtop) was used to evaluate the ability of the saturated topsoil with and without biochar to transmit water when subjected to a hydraulic gradient (see Figure 25 and 26). The measurement of saturated hydraulic conductivity illustrates the soil pore and fractures' ability to release saturated water. This physical property

helps explain an idea about the soil water holding capacity undersaturation. The sampling ring of the KSAT was used to sample the topsoil in the aquarium tank (see Figure 26). The topsoil in the sampling ring was saturated for an hour and then set up on the instrument, illustrated below (see Figure 25 and 26). KSAT VIEW software was used to measure hydraulic conductivity. For setting zero point, the fill cock was opened and the measuring dome was filled slowly with water-burette cock needed to be open. A water lense was set up by opening and closing the burette cock and he setting zero-point button was pressed. The soil ring was put slightly tilled and fixed the measuring set up with screw cap. The burette was filled with up to 5cm water column. The KSAT was turned on, and the hydraulic conductivity was measured. The range of R2 value of the read saturated hydraulic conductivity of the topsoil samples was 0.98 to 1. The same procedure was followed for measuring bulk density for biochar and biochar amended topsoil.

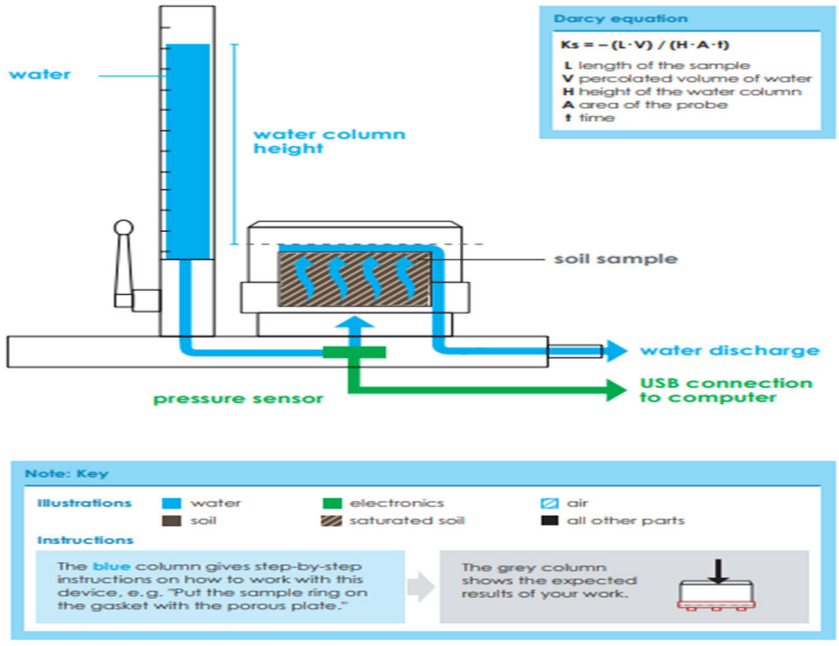

Figure 25. KSAT Saturated Hydraulic Conductivity Meter (benchtop) and its working mechanism (Adopted from KSAT manual)

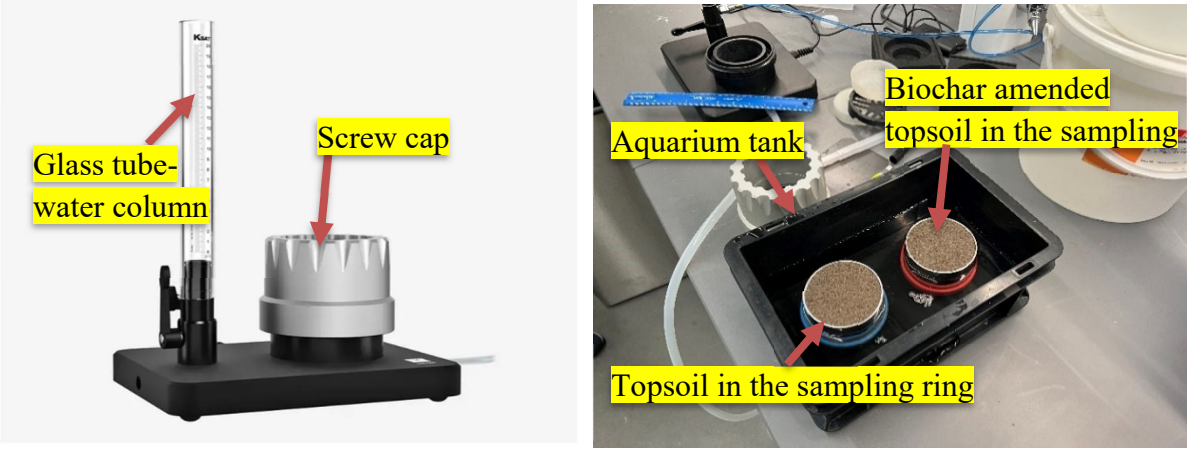

Figure 26. The KSAT Saturated Conductivity Meter (benchtop) used in WERL lab at GSU

3.3.2 Water quality (WQ) parameters

3.3.2.1 Overview of standard experimental methods for testing WQ parameters

The major instruments utilized in the WERL at GSU are listed here. Additionally, the standardized methods employed for testing WQ parameters' concentrations are presented and discussed here. Duplicate samples were used to test each WQ parameter's concentration, and the average values were utilized to calculate the efficiency of pollutant removal.

Major Instruments:

• DR Hach 5000 Spectrophotometer for testing Color, COD, Nutrients (nitrogen and phosphorous)

• Shimadzu AA-7000 graphite furnace atomic absorption spectroscopy for testing heavy metals of Pb, Zn, and Cu.

Standard experimental methods utilized:

• Heavy metals (Pb, Zn, and Cu; Standard Method EPA-NERL: 200.9).

• Chemical oxygen demand (COD) (Standard Method Hach 8000 [USEPA 5220 D]).

• Total nitrogen (TN) (Standard Method Hach 10071).

• Ammonia nitrogen (NH_3-N) (Standard Method Hach 10031).

• Total Kjeldahl nitrogen (TKN) (Standard Method Hach 10242)

• Nitrate (NO_3^--N) (Standard Method Hach 8192).

• Total Phosphorus (TP) (Standard Method Hach 8190 [USEPA 4500-P E]).

• Solids (Standard Method EPA 1684).

• Oil and grease (Standard Method EPA 1664A).

• pH (Standard Method EPA 150.2).

• Dissolved oxygen (DO)(Standard Method EPA-NERL: 360.1).

• Conductivity (Standard Method EPA D1125-14 A).

• Color (Hach Platinum-Cobalt Standard method

3.3.2.2 Basic WQ Parameters

- **pH**

A Thermo Fisher Orion Star A216 dual pH/DO electrode was used to measure the pH of the water samples (see Figure 27). Before measuring, the Thermo Fisher pH standards of pH 4.00, 7.00, and 10.00 were used for instrument calibration. The pH probe was directly inserted into the sample, the sample was stirred gently, and the pH was recorded after reading.

Figure 27. Orion pH/DO meter

- **Dissolved Oxygen (DO)**

A Thermo Fisher Orion Star A216 dual pH/DO electrode was used to measure DO of water samples. Before that, a sealed BOD bottle filled with distilled water was used for the instrument calibration. The DO probe was directly put into the sample, and the DO was recorded after reading.

- **Conductivity**

A Fisher Scientific Traceable Conductivity/TDS Pocket Tester was used to measure the conductivity of the water samples directly after inserting them into the samples (see Figure 28). A sensitivity check was done by measuring the known conductivity of laboratory-produced DI water.

Figure 28. Fisher Scientific Traceable Conductivity/TDS Pocket Tester

- **Color**

The Hach Platinum-Cobalt Standard method was utilized to analyze the color of the water samples. 50 mL of deionized water was filtered through a 0.45 µm Whatman filter paper, and

10 mL of the filtrate was collected and set as the blank sample on the DR 5000 Spectrophotometer (Figure 31 a) using the 120 Color, 455 nm program. The water sample to be analyzed was filtered, and 10 mL was added to the cell and measured.

3.3.2.3 WQ Parameters of Concern

- **Solids**

Total solids (TS) in stormwater runoff consist of both suspended (TSS) and dissolved (TDS) solids. In order to determine the concentration of these solids, a Whatman filter paper of 0.45 µm was used to filter 100 mL of the water sample (see Figure 29).

- **TSS**

To begin the process, the weight of a ceramic dish along with the filter paper was measured using an Electronic Balance (AG204) and recorded as W1. After filtration, the filter paper containing the solids and the ceramic dish were placed in a Fisher Scientific oven and heated at 105°C for one hour. Following the heating process, the filter paper and ceramic dish were allowed to cool down to room temperature. Once cooled, the weight of the filter paper and ceramic dish was measured and recorded as W2 (see Figure 30b).

Figure 29. Vacuum Pump for filtration

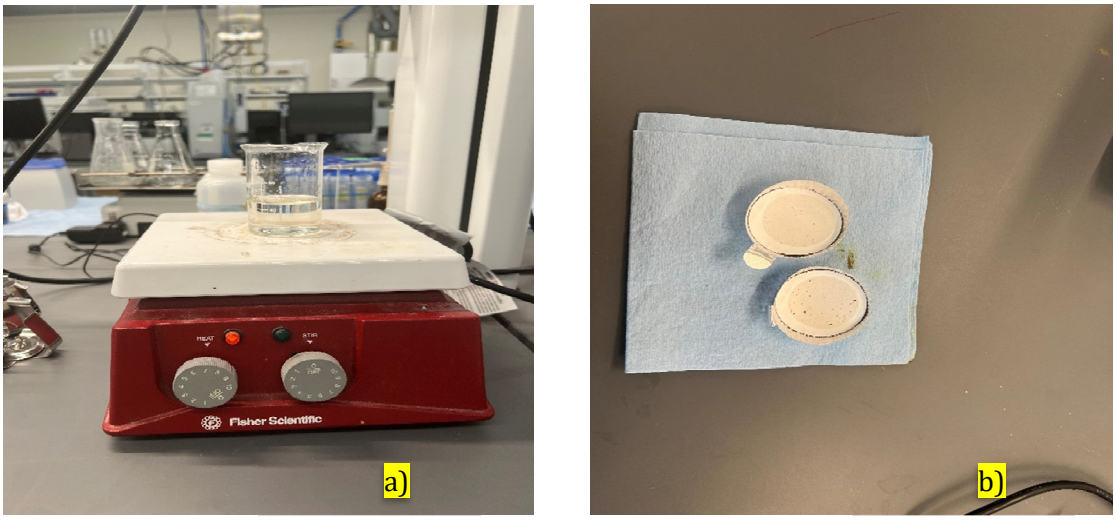

Figure 30. a) Fisher Scientific Hot plate and b) Filter paper with solids after drying

The difference between W1 and W2 represented the weight of the solids retained by the filter paper. This difference was then divided by the volume of the water sample (100 mL) to obtain the concentration of TSS.

- **TDS**

To determine the concentration of TDS, 50 mL of the filtrate obtained from the previous filtration step was taken and added to a pre-weighed beaker (W1). The beaker containing the filtrate was placed on a hot plate and heated to evaporate the water (see Figure 30a). After the evaporation process, the beaker was allowed to cool to room temperature and then reweighed as W2. The difference in weight between W1 and W2 divided by the volume of the filtrate (50 mL) provided the concentration of TDS.

- **Nutrients**

➢ **Nitrogen**

▪ **NH_3-N**

The concentration of NH_3-N in the water samples was determined using the Hach photometric method. For this analysis, a Hach TNT 832 test kit was employed. To perform the test, the foil on the screwed-on DosiCap Zip was removed, the DosiCap was then removed. Then, 5 mL of the water sample was added to the vial. The DosiCap was immediately overturned and screwed back on, after which the vial was vigorously shaken 2-3 times. Subsequently, the vial was allowed to sit for 15 minutes and cleaned before being read using the DR 5000 Spectrophotometer. Prior to reading the samples, the Hach DR 5000 Spectrophotometer (see Figure 31 a) was zeroed using Deionized (D.I.) water specifically for the NH_3-N measurement.

▪ **NO3−-N**

The Hach photometric method was utilized to measure the concentration of NO3−-N in the water samples. Specifically, the Hach TNT 835 test kit was employed for this parameter.

To perform the analysis, the vial was opened, and 1 mL of the water sample was carefully pipetted into the vial. Subsequently, 0.2 mL of solution A from the test kit was also pipetted into the same vial, and the vial was sealed. The mixture inside the vial was then inverted several times until there were no streaks present, and it was allowed to sit for 15 minutes to complete the reaction. Following the reaction period, the vial was cleaned to remove any residue or contaminants before being placed in the DR 5000 Spectrophotometer for reading. Prior to reading the samples, the Hach DR 5000 Spectrophotometer (see Figure 31 a) was calibrated to zero for the nitrate measurement using D.I. water.

- **TKN**

The Hach photometric method was utilized to measure the concentration of TKN in the water samples. TKN is a parameter that quantifies both organic and NH_3-N in water samples. To conduct the analysis, the Hach TNT 880 combined vials test kit was employed. The procedure involved adding 1.3 mL of the water sample to a separate digestion vial. Then, 1.3 mL of solution A and one tablet B were added to the vial. The mixture was immediately sealed and placed in the DRB 200 Digestor (see Figure 31 b) for a duration of 60 minutes at a temperature of 100°C. After digestion, the vial was taken out and allowed to cool down to a room temperature range of 20-23°C. To continue the analysis, one MicroCap C from the test kit was added to the mixture, and the vial was inverted several times until all the content in the MicroCap was dissolved. Then, 0.5 mL of the digested mixture was transferred to the red vial, followed by the addition of 0.2 mL of Solution D. The red vial was sealed, inverted a few times, and left to sit for 15 minutes.

Simultaneously, 1 mL of the raw, undigested water sample was added to the green vial, followed by the addition of 0.2 mL of Solution D. The mixture in the green vial was also inverted several times until there were no streaks, and it was left to sit for 15 minutes. Both the red and green vials were cleaned and inserted into the DR 5000 Spectrophotometer (see Figure 31 a) for reading. The reading value of the red vial represented the total nitrogen, while the green vial represented nitrate plus nitrite. The TKN value of the sample was determined by subtracting the reading value of the green vial from that of the red vial. Prior to reading the samples, the Hach DR 5000 Spectrophotometer was zeroed for the TKN measurement using D.I. water.

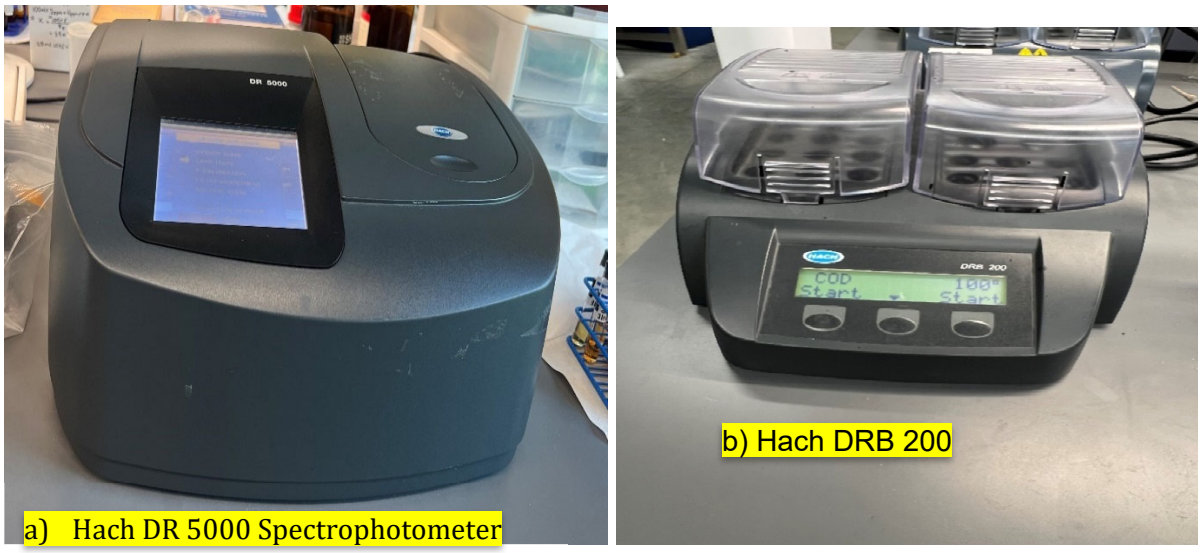

Figure 31. a) *Hach DR 5000* Spectrophotometer and b) Hach DRB 200

- **TN**

The total nitrogen value was recorded from the simplified TKN Hach method above. The red vial represents the TKN value.

- **TP**

The Hach photometric method was employed to measure the concentration of TP in the water samples. For this parameter, the Hach TNT 844 test kit was specifically used. To begin the analysis, the foil cap of the vial was removed, and the DosiCapTM Zip was unscrewed. Then, 0.5 mL of the water sample was added to the vial, and the DosiCapTM Zip was screwed back on, but overturned. The vial was vigorously shaken until a uniform mixture was formed. Next, the vial with the mixture was placed in the DRB 200 Reactor and kept at a temperature of 100°C for a duration of 1 hour. After the reaction, the vial was allowed to cool for approximately 20 minutes at room temperature, which ranged between 20 and 23°C. Following the cooling period, 0.2 mL of Reagent B was added to the vial, and the vial was sealed using the DosiCapTM Zip. The mixture inside the vial was shaken and then left to sit for a few

seconds. Subsequently, the vial was measured using the Hach DR 5000 Spectrophotometer (see Figure 31a). Before reading the samples, the Hach DR 5000 Spectrophotometer was zeroed for the phosphorus measurement using D.I. water.

- **Heavy Metals**

In the study, the analysis of heavy metal pollutants in the on-site stormwater runoff was conducted. Three specific heavy metals namely Pb), Zn, and Cu, were monitored. These heavy metals were measured after the infiltration treatment of the on-site stormwater through Test Cell and Control Cell, respectively. Additionally, the analysis of these three heavy metals was also performed on the raw stormwater runoff during various rainfall events. The Shimadzu AA-7000 Atomic Absorption Spectrophotometer (see Figure 32) was used for this purpose. It is important to note that the AA-7000 Atomic Absorption Spectrophotometer is located in the WERL at GSU, and unfortunately it didn't work properly during this test period for this Project. Currently, the Shimadzu is working on diagnosis and repair.

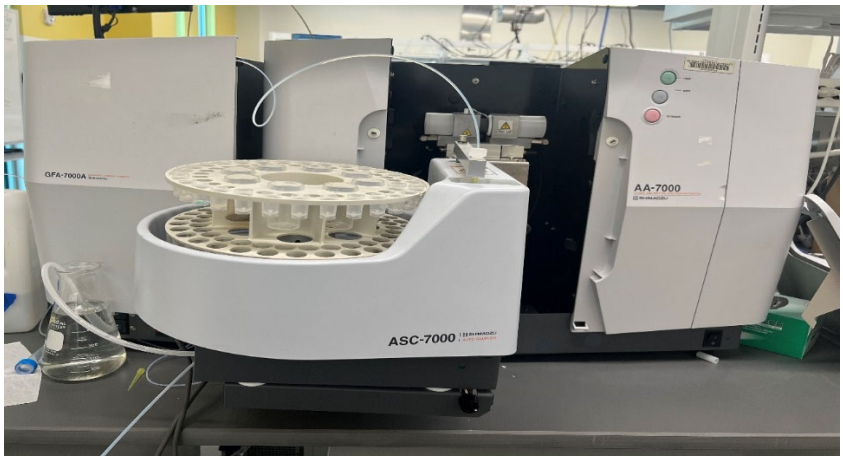

Figure 32. AA-7000 Atomic Absorption Spectrophotometer

To measure the total and dissolved concentrations of heavy metals in the samples, the water samples were prepared by filtering them through a 0.45 µm Pall membrane filter and a vacuum

filtration system. Before testing, the water samples were acidified with concentrated nitric acid. The concentration values of each sample were measured in parts per billion (ppb) using the AA-7000 instrument, following the development of a three-point calibration curve that employed a 1,000 μg/l "High Purity Standard" solution for each heavy metal element.

- **Oil and Grease**

To determine the amount of oil and grease in the stormwater runoff from the parking lot, the gravimetric procedure was employed. Firstly, a 100 mL water sample was transferred into a beaker. Then, 2.5 mL of HCl was added to the water sample in the beaker, followed by transferring the mixture to a separatory funnel. Next, 20 mL of n-Hexane organic solvent (with a purity of 95-99%) was added to the mixture in the separatory funnel, and the contents were vigorously shaken for 2 minutes. After shaking, the mixture was allowed to settle for approximately 15-20 minutes, enabling the separation of the oil phase from the liquid phase. The liquid phase was carefully transferred into another beaker, while the upper portion containing the oil phase was transferred into a previously weighed and tared beaker (W1). The beaker with the oil phase was then placed in a hot environment at a temperature of 70°C to facilitate the evaporation of the n-Hexane solvent.

The liquid phase was transferred back into the separatory funnel to repeat the extraction, adding the oil phase into the same tarred beaker. Once the n-Hexane had completely evaporated, the beaker was allowed to cool at room temperature for approximately 15 minutes and then reweighed (W2). The concentration of oil and grease was calculated by subtracting the weight obtained at W2 from the weight measured at W1 and dividing the result by the volume of the water sample (100 mL).

- **COD**

To analyze the presence of oxidizable organic compounds in the water samples, COD tests were conducted. The Hach DR 5000 Spectrophotometer (see Figure 31 a), located in the WERL at GSU (as shown in Figure 32), was used in the Hach photometric method. To perform the test, a TNT 820 test kit was used, following the Hach photometric method. For each test, 2 mL of the water sample was added to vials containing either HACH TNT 821 (low range: 0.00-150.00 mg/l) or TNT 822 (high range: 30.00 mg/l-1,500.00 mg/l). The samples in the vials were digested using the Hach DRB 200 (see Figure 31 b) for 2 hours at a temperature of 150°C and subsequently cooled to room temperature (20-23°C) before measurement with the Hach DR 5000 Spectrophotometer. Prior to reading the samples, the Hach DR 5000 Spectrophotometer was calibrated to zero using D.I. water specifically for the COD measurement.

CHAPTER 4. RESULTS AND DISCUSSION

4.1 Overview

The study findings and analysis from the Full-Scale Field Test Site using a new GI with biochar-amended topsoil for on-site stormwater runoff treatment are presented in this Chapter.

4.2 Topsoil, Biochar and Biochar Amended Topsoil

4.2.1 Topsoil properties

- **Bulk Density**

The volume of the soil particles and the volume of the void spaces between the soil particles are represented by bulk density, which also shows how compacted the topsoil is. Water and air are trapped in the gaps between the soil particles. Duplicate measurements of bulk density were taken. The average bulk density of topsoil was 1.65 gm/cm^3.

- **Hydraulic conductivity**

The saturated conductivity of the topsoil was evaluated and the measured data in the study represented the specific saturated hydraulic conductivity of the topsoil. The saturated hydraulic conductivity from laboratory measurement of the topsoil was 1.05E-06 m/s.

4.2.2 Biochar properties

- **Bulk Density**

The volume of the biochar particles and the volume of the void spaces between the biochar particles are represented by bulk density, which also shows how compacted the biochar is. Duplicate measurements of bulk density were taken. The average bulk density of biochar was 0.143 gm/cm^3.

- **Hydraulic conductivity**

The saturated conductivity of the biochar was evaluated and the measured data in the study represented the specific saturated hydraulic conductivity of the biochar. The saturated hydraulic conductivity from laboratory measurement of the biochar was 2.41E-04m/s which is more than the topsoil's hydraulic conductivity (see Figure 33).

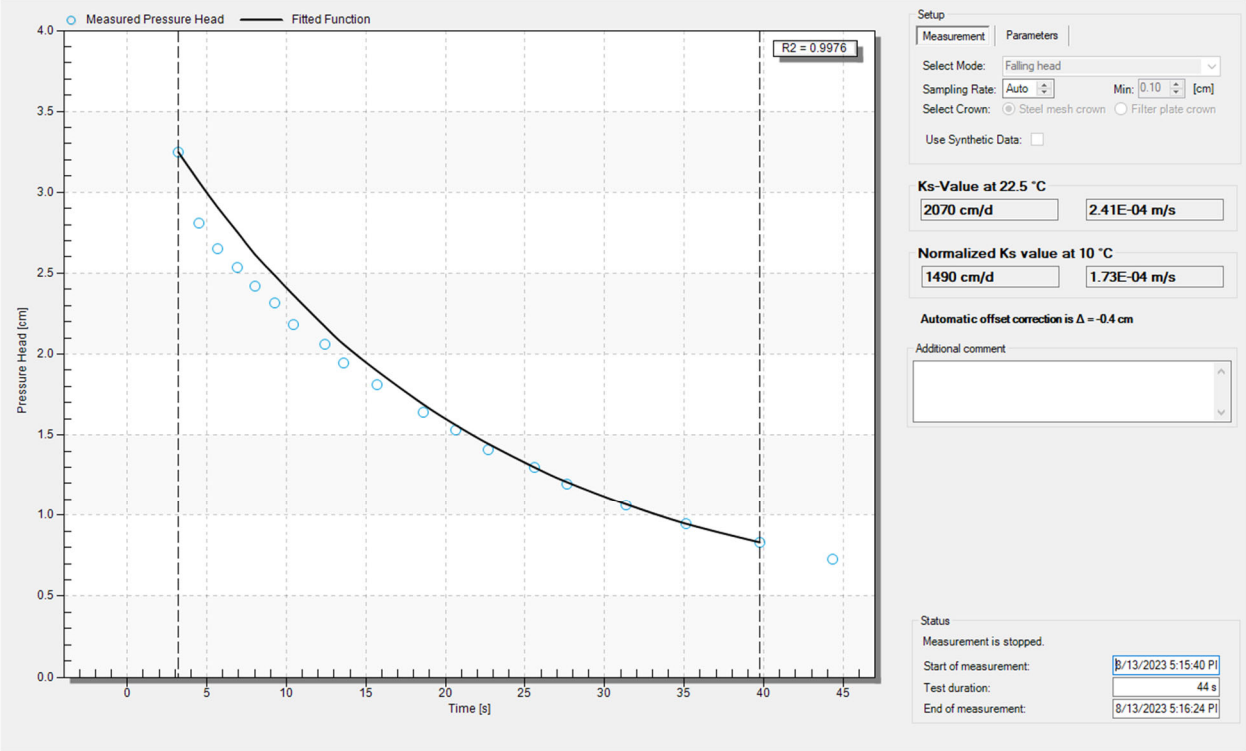

Figure 33. KSAT saturated hydraulic conductivity measurement of biochar

4.2.3 5% Biochar amended topsoil properties

- **Bulk Density**

The bulk density of the biochar-amended topsoil was then determined. Duplicate measurements of bulk density were taken. The average bulk density of biochar was 0.215 gm/cm^3.

- **Hydraulic conductivity**

After the topsoil was amended with 5 % biochar, the saturated hydraulic conductivity of biochar-topsoil mixer was measured. The saturated hydraulic conductivity from laboratory measurement of the 5% biochar-amended topsoil was 1.78E-05 m/s (see Figure 34). The addition of biochar at 5% to topsoil, increased the saturated hydraulic conductivity of the topsoil. The saturated hydraulic conductivity tested on the topsoil with no biochar addition had lesser hydraulic conductivity (1.05E-06 m/s) therefore the stormwater runoff infiltrated much faster.

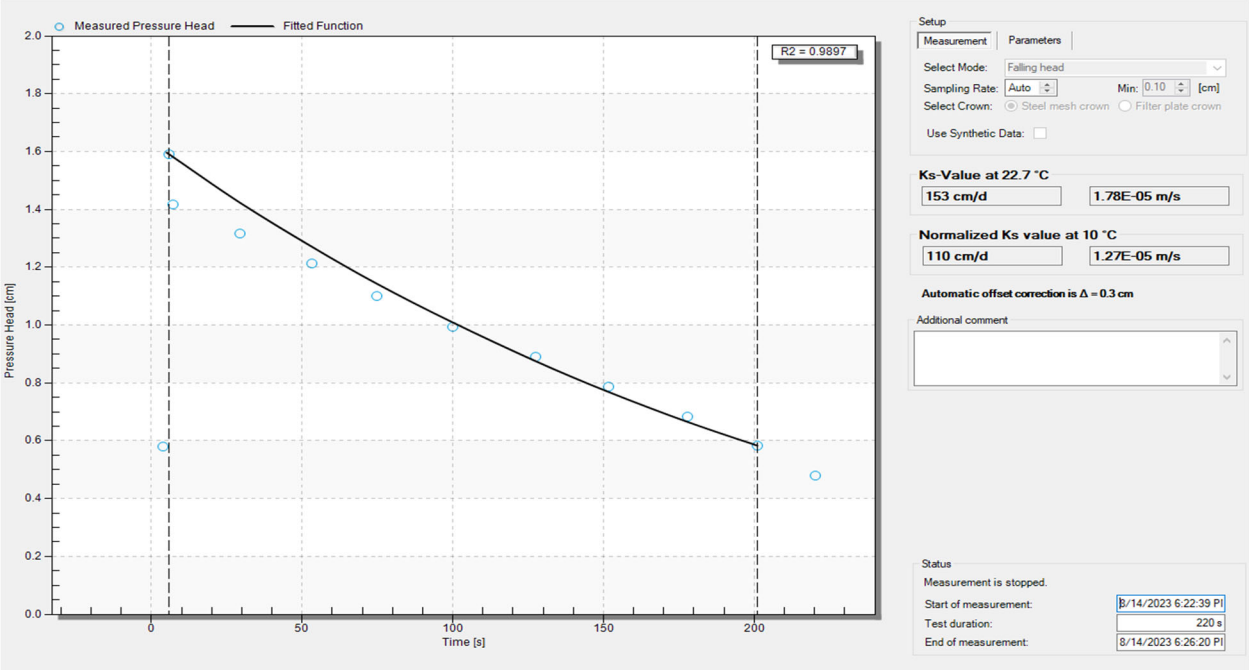

Figure 34. KSAT saturated hydraulic conductivity measurement of topsoil with 5% biochar

4.3 Field Monitoring Results

The moisture content of the topsoil and 5% biochar amended topsoil, ambient temperature and rainfall depth were monitored at the Field Test Site.

4.3.1 Moisture Content Monitoring at Field Test Site

Moisture Content was monitored by HOBO moisture logger weekly at same points (see Figure 35) at Field Test site. HOBOconnect software is used to monitor moisture and temperature. It was observed that the moisture content increased gradually at Test Cell (Table 2). When it was more dry environment moisture content was decreased a little bit.

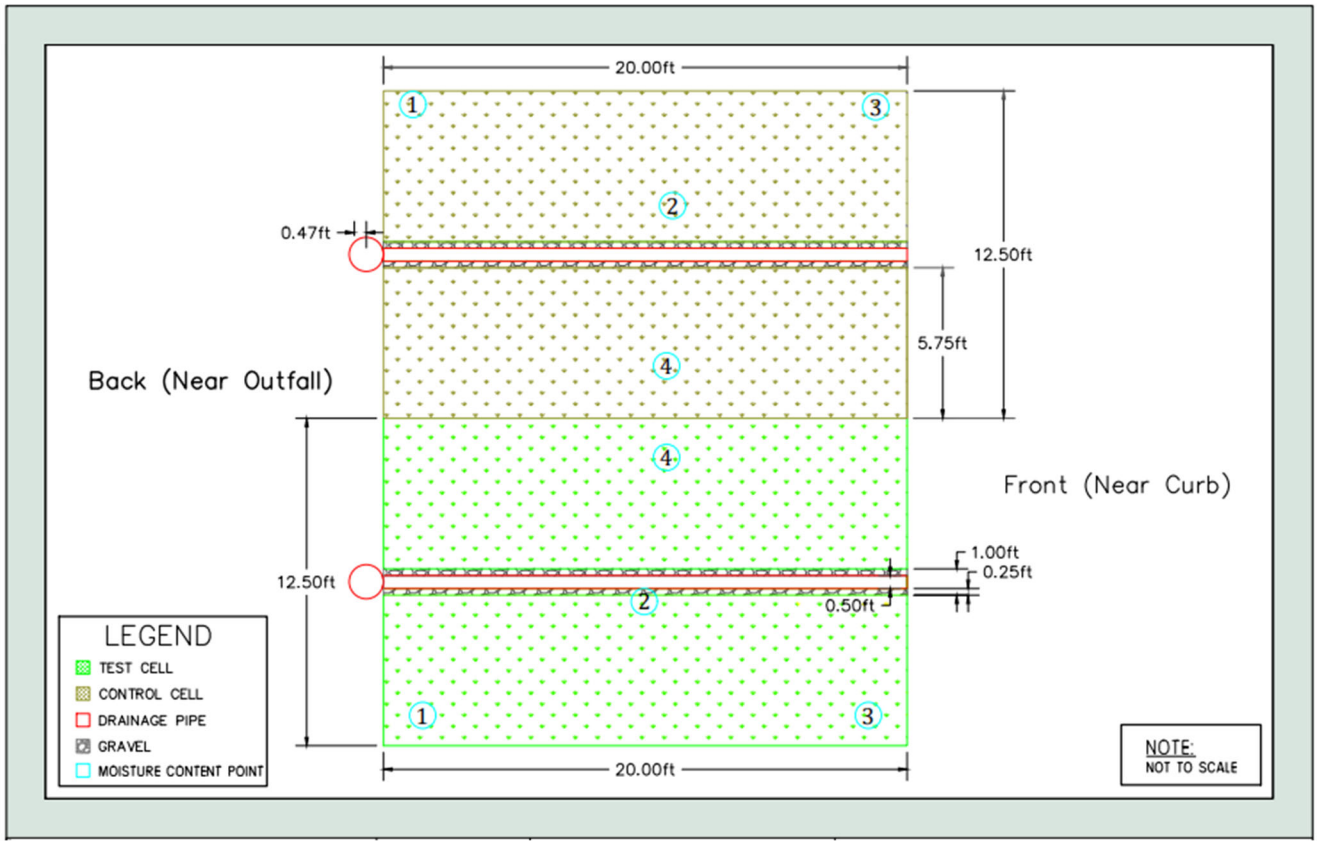

Figure 35. Field Test Site showing Moisture content points

Table 2. Monitoring Moisture Content data at Field Test Site

Date	Soil Temparature (°C)	Moisture Content							
		Control Cell				Test Cell			
		01	02	03	04	01	02	03	04
7/29/2023	27.56	0.189	0.303	0.210	0.320	0.326	0.346	0.203	0.308
8/6/2023	24.29	0.111	0.108	0.107	0.193	0.227	0.195	0.295	0.327
8/14/2023	30.58	0.041	0.084	0.008	0.085	0.159	0.165	0.192	0.344

4.3.2 Rain Gauge

A HOBO RG-3 Rain gauge was installed to monitor the rainfall events which has a pendant logger that stored the data. HOBOware software was used to collect the data (see Table 3).

Table 3. Raingauge data from HOBO rain gauge

Date	Ambient Temp, °F	Rainfall depth (inch)
8/8/2023	76.26	0.065
8/10/2023	77.52	0.155
8/15/2023	75.6	0.92

4.4 Pollutants in Stormwater and Stormwater Runoff from the Parking Lot, Respectively

On July 28th, 2023, the first samples of stormwater and stormwater runoff from GSU parking lot were taken and tested with higher pollutant concentrations in the stormwater runoff than those in stormwater. The rainfall events on July 28th and August 15th, 2023 also caused an increase in pollutants in the stormwater runoff. Overall, the stormwater runoff samples had much higher levels of color, DO, COD, solid pollutants, oil and grease, and all nutrient pollutants compared with pollutants in stormwater samples. It was observed that all the samples of stormwater runoff had color concentrations and low pH level during this time of period for repair and maintenance of the parking lot using sealer and road marking paint.

4.4.1 Basic WQ Parameters

- **pH**

The sstormwater samples showed lower pH in a range of 6.1 - 6.2 than the stormwater runoff samples did (6.4-6.6) (see Figure 36).

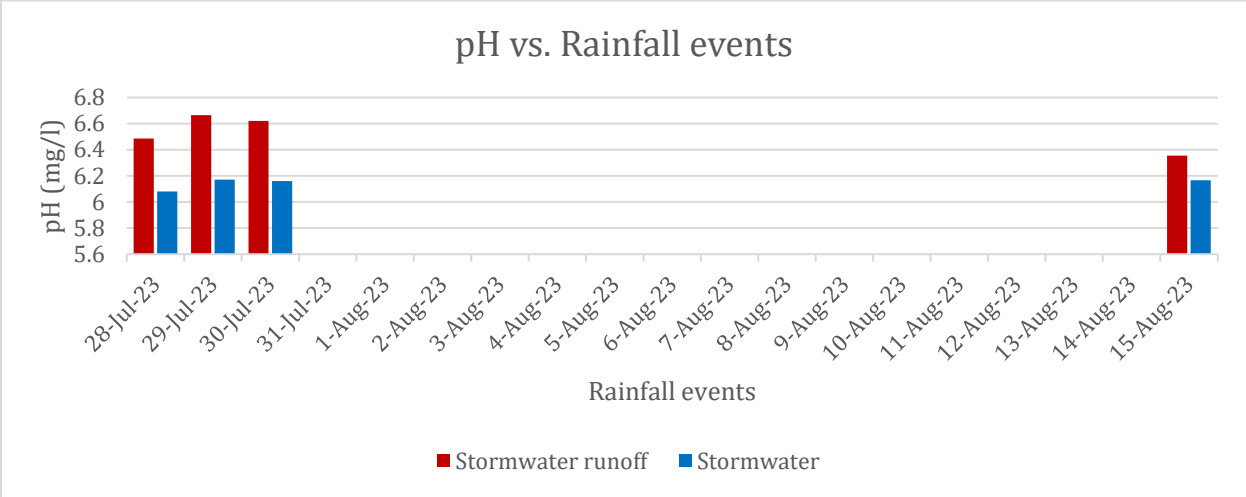

Figure 36. pH readings for stormwater and stormwater runoff

- **DO**

The bar graph below shows DO levels are higher in the stormwater samples (8.5-9.3mg/l) than those in the stormwater runoff samples (7.2-9.0 mg/l).

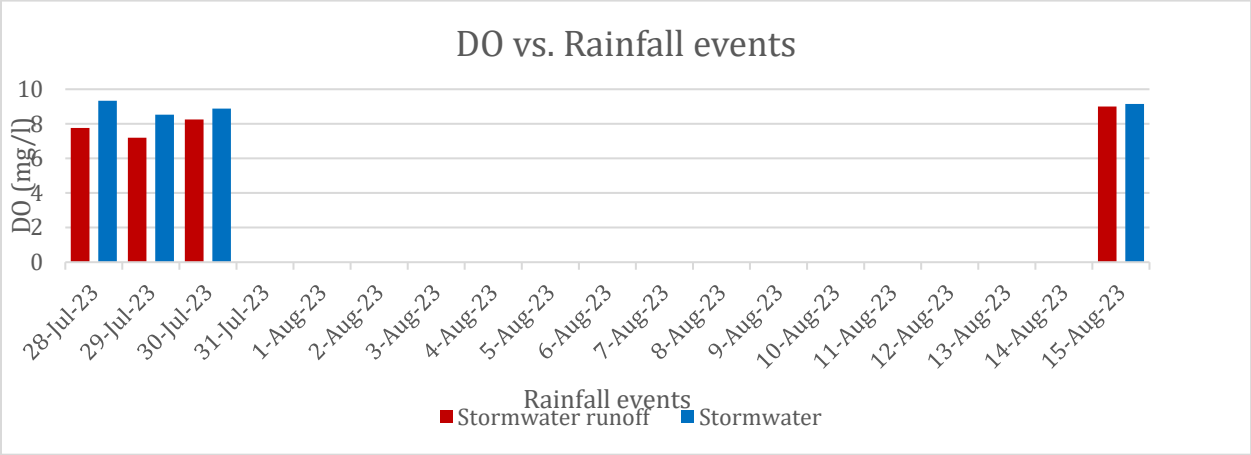

Figure 37. DO readings for stormwater and stormwater runoff

- **Conductivity**

The conductivities of stormwater samples were much lower (9.0-13.5µs/cm) than those of the stormwater runoff samples (37.5-47.5µs/cm) (see Figure 38).

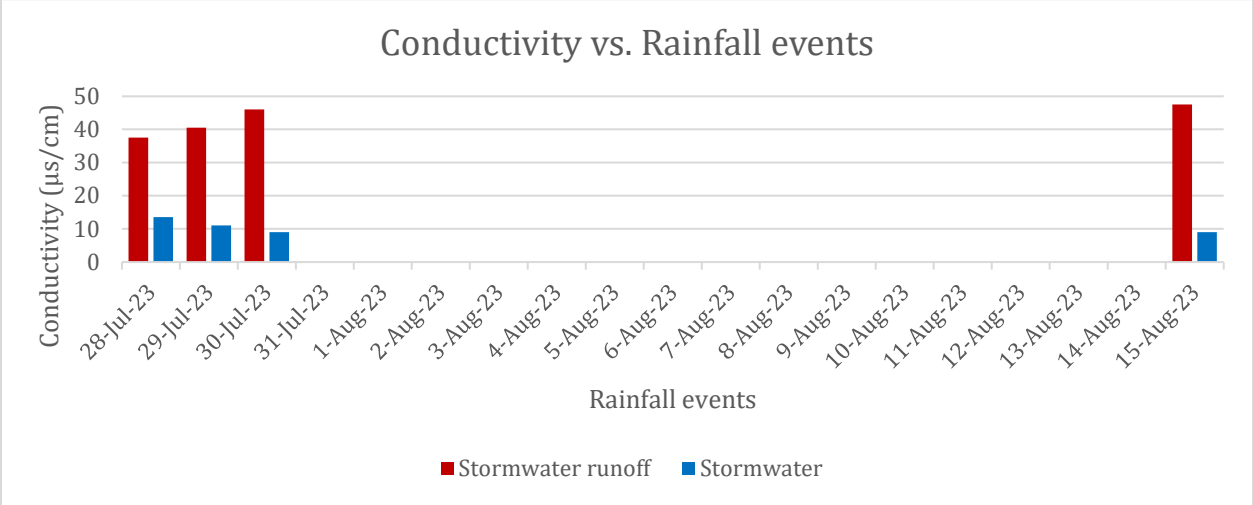

Figure 38. Conductivity readings for stormwater and stormwater runoff

- **Color**

The stormwater samples had much lower color (3-4.5 Pt.Co) than the stormwater runoff samples had (30.5-69.5 Pt.Co) (see Figure 39).

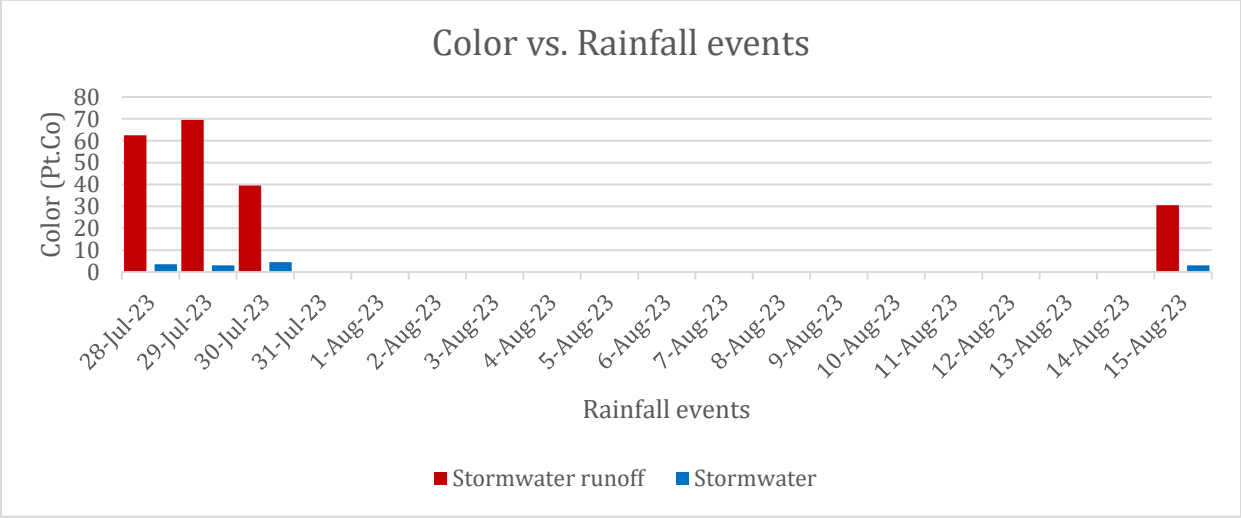

Figure 39. Color readings for stormwater and stormwater runoff

4.4.2 WQ Parameters of Concern

- Solids

The concentrations of suspended solids and dissolved solids in the stormwater samples were much lower (8-9 mg/l for TSS and 5-7 mg/l for TDS) than those in the stormwater runoff samples (47-69 mg/l for TSS and 15-26 mg/l for TDS) (see Figure 40 and 41).

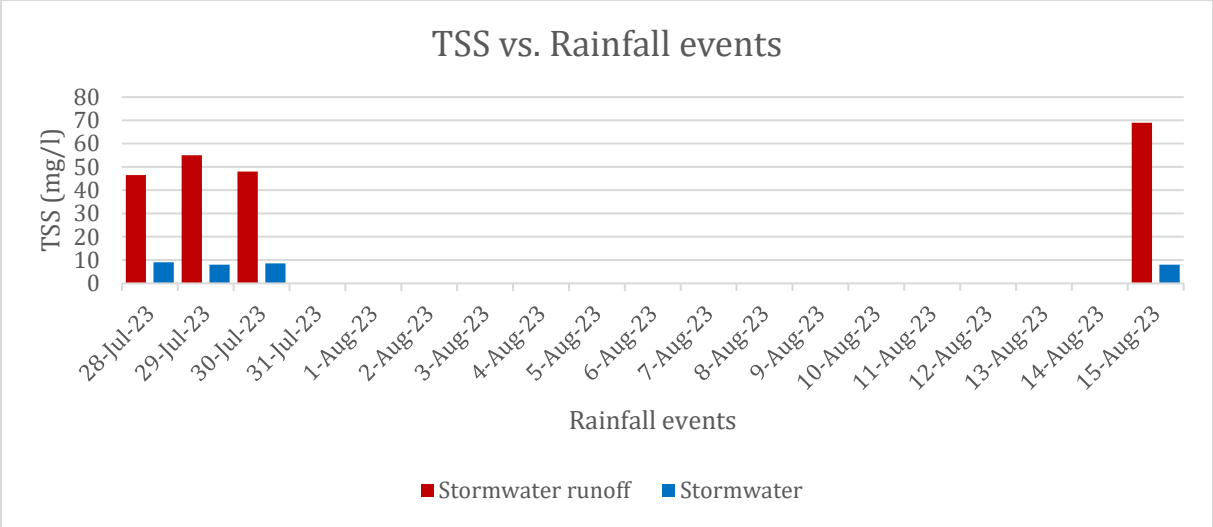

Figure 40. TSS readings for stormwater and stormwater runoff

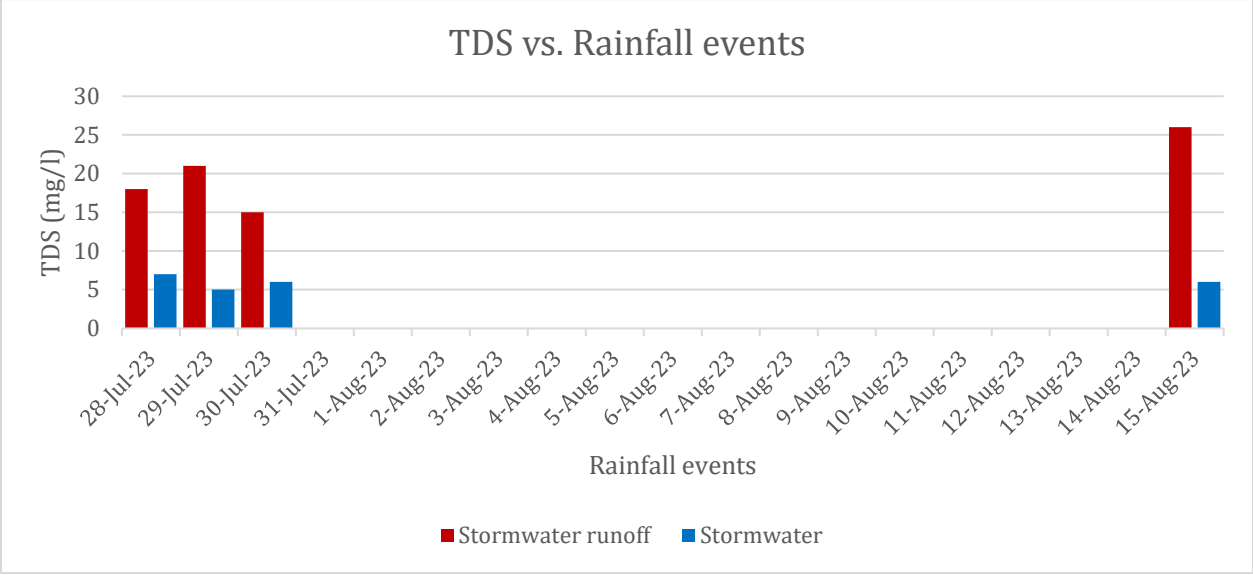

Figure 41. TDS readings for stormwater and stormwater runoff

- Nutrients

In general, the stormwater samples carried lower level of nutrients than the stormwater runoff samples did. It also observed that the stormwater samples had higher levels of nitrogen than phosphorus (see Figure 42, 43, 44 and 45) because nitrogen is the significant component of atmosphere.

- **NH_3-N**

The stormwater samples had much lower NH_3-N (0.05-0.06 mg/l) than the stormwater runoff samples had (0.16-0.3 mg/l) (see Figure 42).

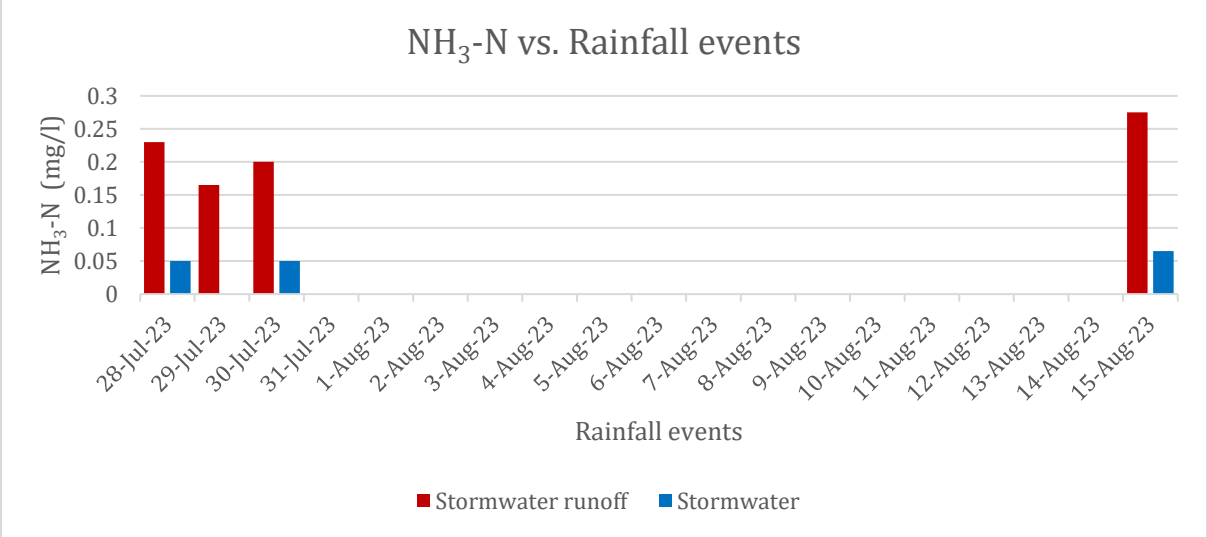

Figure 42. NH3-N readings for stormwater and stormwater runoff

- **NO_3^--N**

The stormwater samples had much lower NO_3^--N (0.1-0.25 mg/l) than the stormwater runoff samples had (0.3-0.6 mg/l) (see Figure 43).

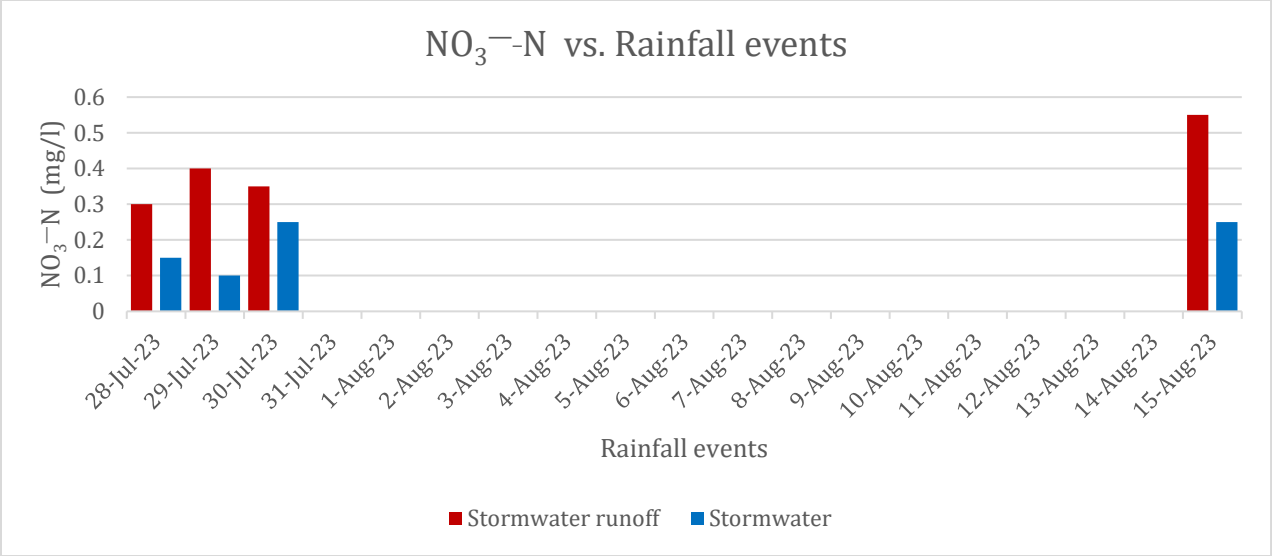

Figure 43. NO_3^--N readings for stormwater and stormwater runoff

- TKN

TKN is the sum of NH_3-N and total organic nitrogen. The stormwater samples had much lower TKN (0-1 mg/l) than the stormwater runoff samples had (2.5-4.0 mg/l) (see Figure 44).

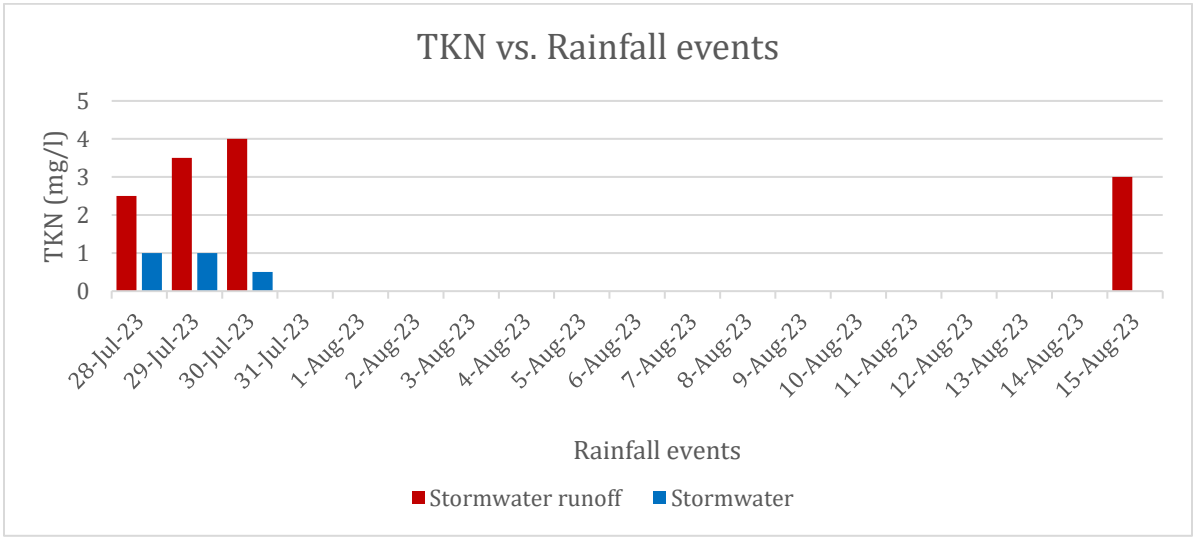

Figure 44. TKN readings for stormwater and stormwater runoff

- TN

The stormwater samples had much lower TN (1.0-2.0 mg/l) than the stormwater runoff samples had (3.5-4.5 mg/l) (see Figure 45).

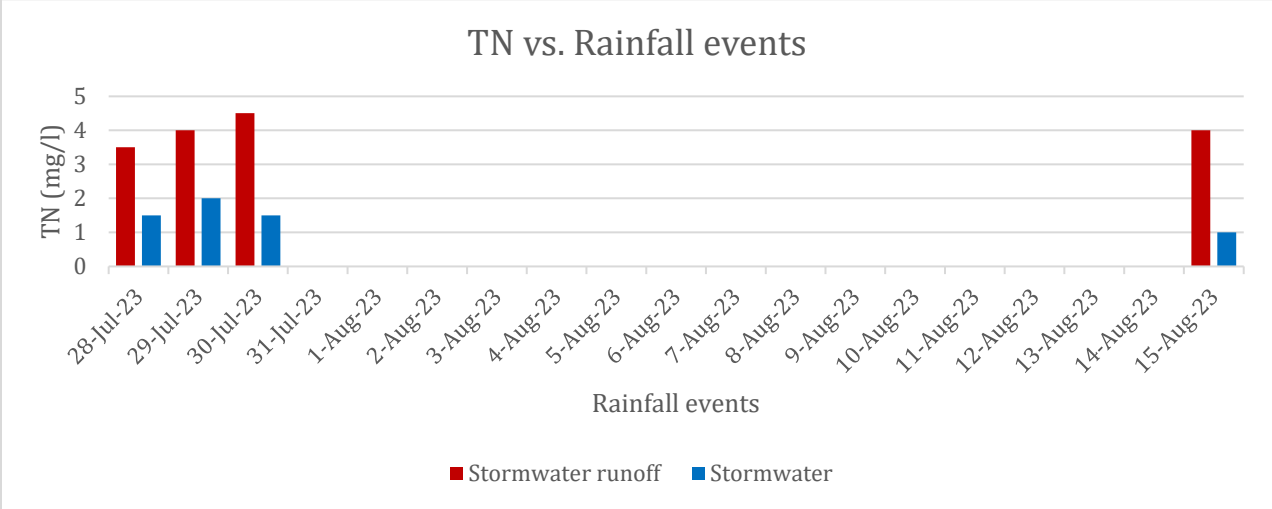

Figure 45. TN readings for stormwater and stormwater runoff

- TP

The stormwater runoff samples had higher TP concentration (0.45-0.65 mg/l) (see Figure 46) while stormwater had zero TP concentration.

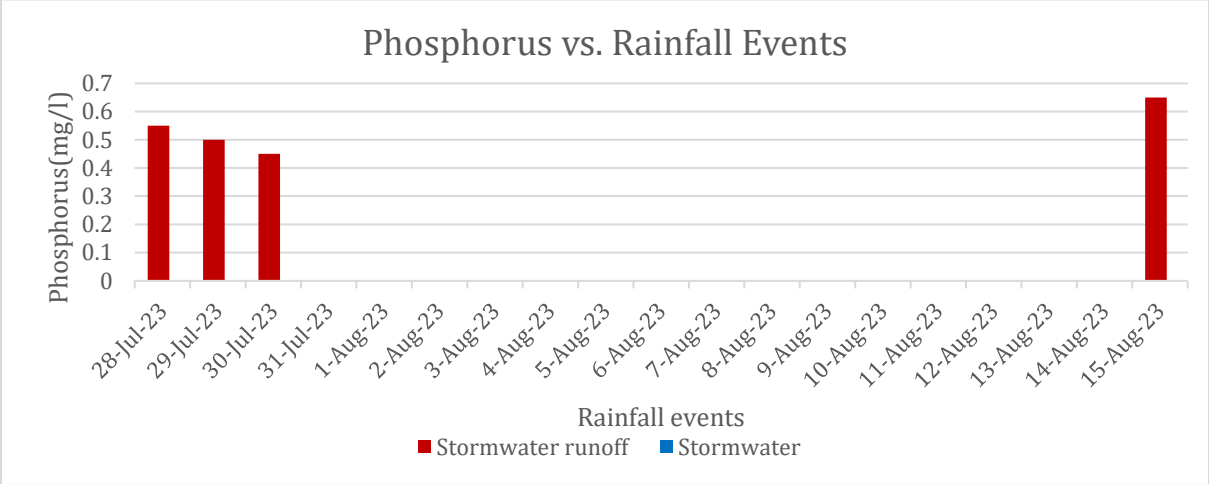

Figure 46. Phosphorus readings for stormwater and stormwater runoff

- Oil and grease

There is no oil and grease concentration in stormwater samples. Stormwater runoff from the parking lot carries a high level of oil and grease concentration (10.0-15.5 mg/l) (see Figure 47).

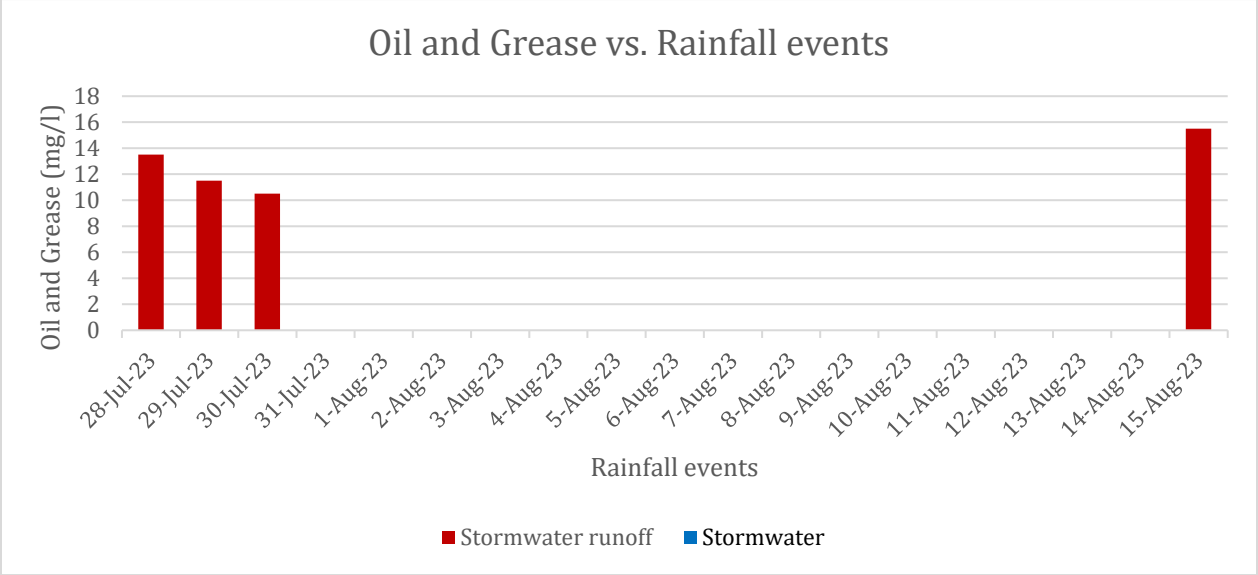

Figure 47. Oil and Grease readings for stormwater and stormwater runoff

- COD

COD is a measure of the amount of oxygen required to chemically oxidize organic and inorganic compounds in water. The stormwater samples typically had a very low COD or can be considered to have no measurable COD (see Figure 48) as they were considered as "clean" water and had a short contact time with surfaces of potential contaminants. Stormwater runoff from the parking lot carries a high level of oil and grease concentration (15.0-19 mg/l).

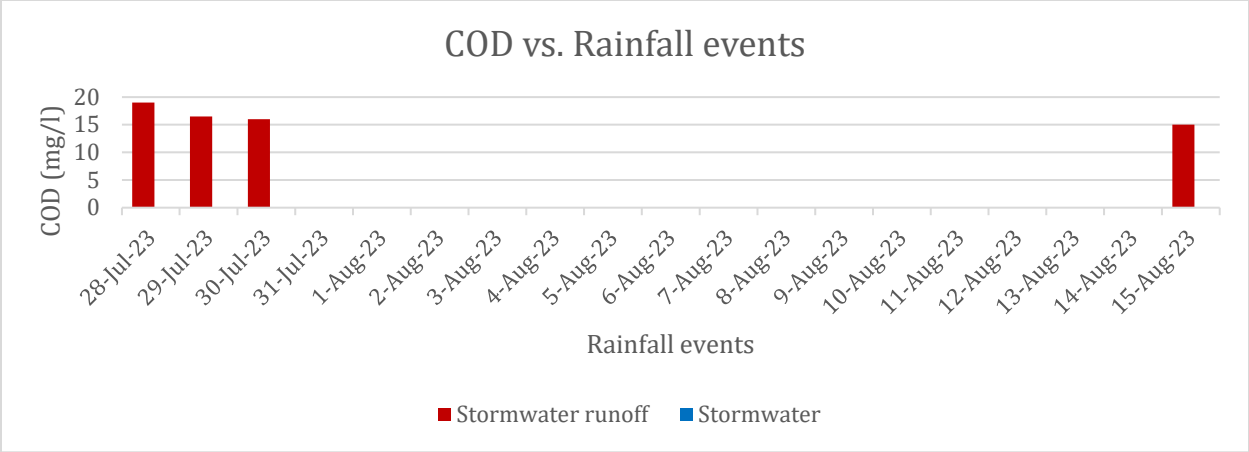

Figure 48. COD readings for stormwater and stormwater runoff

4.5 Estimate Volume of the Parking Lot Stormwater Runoff Treated by the Field Test Site

The submersible pump was operated during the following dates (Table 3). Total volume of 21.7-gal stormwater runoff from the parking lot was treated by the Field Test Site in this Phase I project, 10.85 gal for Control Cell or Test Cell.

Table 4. Operation record for Pumping

Operation record for Pumping					
Date	**Start time (hr)**	**End time (hr)**	**Duration (hr)**	**Flow rate (Gal/hr) at Control cell and Test Cell**	**Volume V (Gal)**
7/28/2023	8:00pm	10:00pm	2	4.17	8.33
7/29/2023	6:30am	8:00am	1.7	2.50	4.25
7/30/2023	6:30am	8:00am	1.7	2.92	4.96
8/15/2023	7:00pm	8:00pm	1	4.16	4.16
Total Influent Volume					**21.7**

4.6 Removal Efficiencies of Pollutants from the Parking Lot Stormwater Runoff Using the Field Test Site

4.6.1 Overview

The WQ parameters listed in this section are tested on all raw influent of the parking lot stormwater runoff and the treated effluent to determine the removal efficiencies of these pollutants. The pollutants' removal efficiencies were consistent, and are presented in Tables of Appendix-A.

Raw stormwater runoff samples from GS parking lot were tested at WERL lab in GSU. Nutrients, COD, TSS, TDS, Oil and grease were at a high level during heavy stormwater runoff while pH, DO and conductivity were at lower level during heavy rainfall. To evaluate the performance of the GI with biochar amended topsoil, the efficiency in pollutants removal was analyzed for GSU parking lot stormwater runoff. A clear comparison of two Cells (Control Cell and Test Cell) has been described. The addition of biochar at a rate of 5% in the topsoil resulted in pollutant removal efficiencies over 80%. The high efficiencies seen in the removal of organic pollutants can be attributed to the effective removal of total suspended solids (TSS), which serve as significant indicators and carriers of organic contaminants in water. The GI which consists of biochar-amended topsoil, has enhanced filtering and adsorption capabilities, resulting in a more efficient removal of COD pollutants from stormwater runoff originating from parking lot. The removal efficiency of total Kjeldahl nitrogen (TKN) was found to be the highest among all nutrient contaminants, exhibiting a 95% removal efficiency. The removal of nutrients is due to the great removal of TSS through physical filtration, as suspended particles provide surface attachment of nutrients and other organic pollutants in water. Adsorption of nutrient pollutants onto the surface of the biochar

increased pollutant removal. Retardation of pollutants as the on-site stormwater runoff infiltrated the GI media mix of topsoil and biochar also explains the good nutrients pollutant removal efficiencies. For Control Cell, nutrients increase after stormwater infiltration. DO and conductivity increased for both Control and Test Cell after infiltration through the GI (see Figure 50 and 51). Color decreased for Test Cell treated effluent but for Control Cell, color increases more because of the soil color (see Figure 52). The removal of TSS, TS, and TDS was consistency or increasing in removal efficiency. Oil and grease removal efficiency in topsoil with biochar amendment increased or consistent after every infiltration of on-site stormwater runoff. Rainwater also added with the stormwater runoff from parking lot at the Field Test Site. Rainwater contains solids which also infiltrated through the GI.

4.6.2 Basic WQ Parameters

- **pH**

It was observed that the pHs of treated effluent from Test Cell significantly increased to 7.2–7.8 while those of treated effluent from Control Cell insignificantly increased to 6.5 -7.0 compared with the pH of raw influent from the parking lot stormwater runoff in a range of 6.4 – 6.6 for all the four (4) rainfall events (see Figure 49).

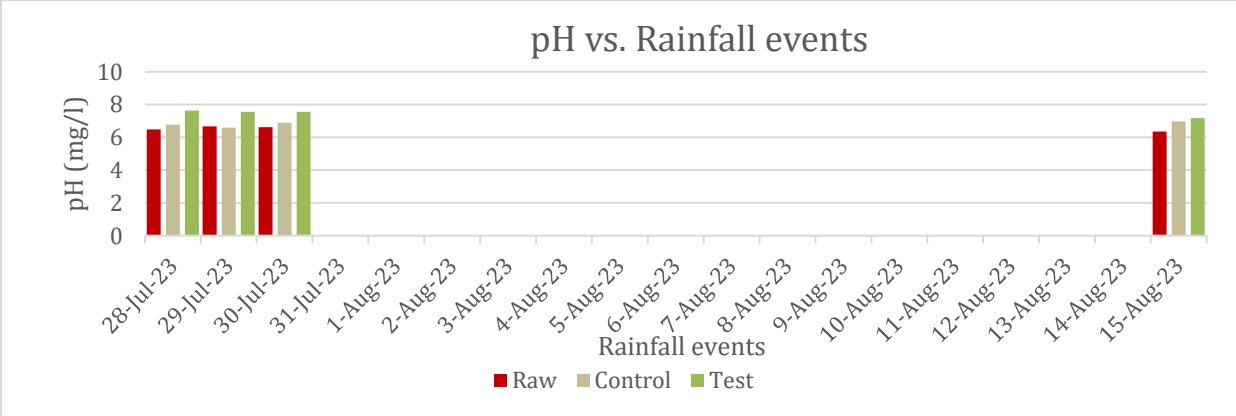

Figure 49. pH readings for raw influent and treated effluent from each Sampling Date

- DO

The DO concentrations in the treated effluents from Test Cell were observed to significantly increase in a range of 28-32 mg/l while those from Control Cell also increased to a range of 11 to 12.8 mg/L compared with the DO concentrations in a range of 7.76 to 8.99 mg/Lin raw influent (see Figure 50).

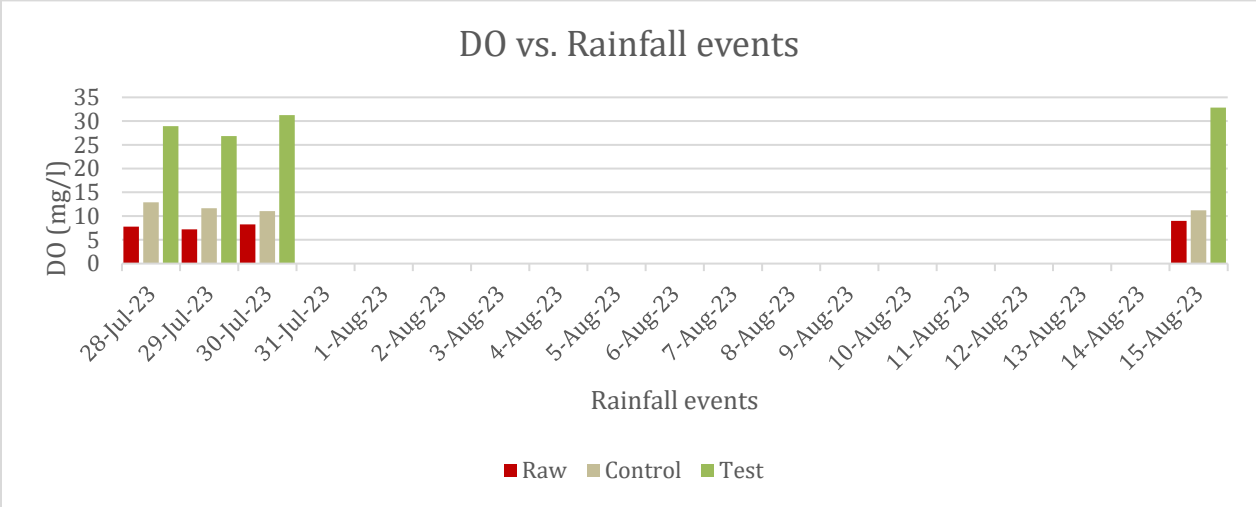

Figure 50. DO readings for raw influent and treated effluent (Control Cell and Test Cell) from each Sampling Date

- Conductivity

The conductivity in the treated effluents from Test Cell were observed to significantly increase in a range of 158.5 - 252.5 µs/cm while those from Control Cell also increased to a range of 131 – 157.5 µs/cm compared with the conductivities in a range of 37.5 – 547.5 µs/cm in raw influent (see Figure 51).

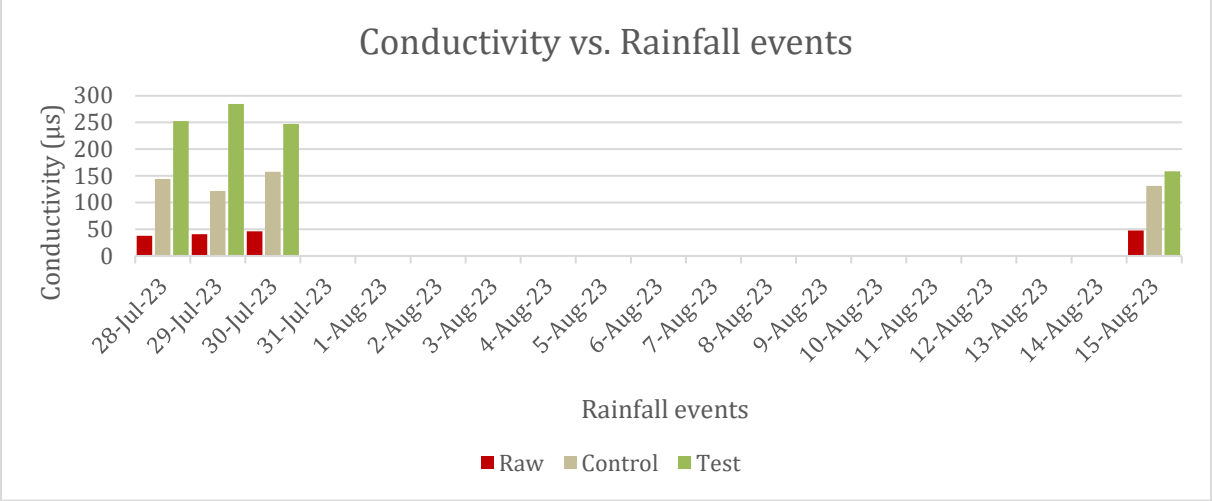

Figure 51. Conductivity readings for raw influent and treated effluent from each Sampling Date

- Color

The color in the treated effluents from Test Cell were observed to decrease in a range of 35-44 Pt.Co and a little bit color increase was observed at August 15th, 37.5 Pt.Co while those from Control Cell significantly increased to a range of 290-327 Pt-Co color units compared with the color in a range of 30.5-69.5 Pt-Co color units in raw influent (see Figure 52). High colors in the treated effluent from Control Cell were consistent among all the four (4) rainfall events due to the color leaching out from the topsoil (see Figure 52).

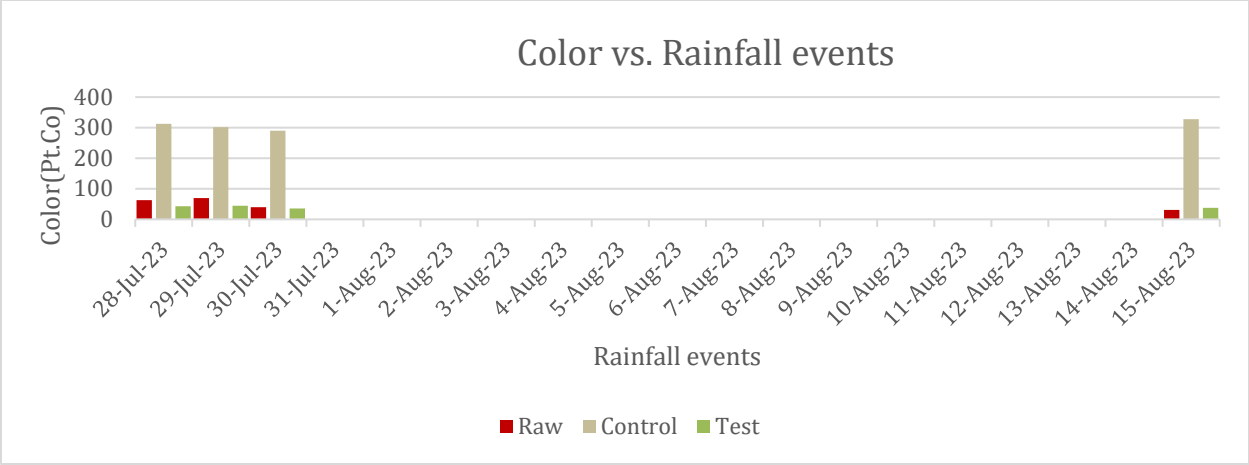

Figure 52. Color readings for raw influent and treated effluent (Control Cell and Test Cell) from each Sampling Date

4.6.3 WQ Parameters of Concern

For each of WQ parameter of concern, the results of concentrations in raw influent of stormwater runoff and treated effluent from Control Cell and Test Cell at the Field Test Site are presented first while those of removal efficiencies from Control Cell and Test Cell are given second.

- Solids

➢ **`TSS**

It was observed that the TSS concentrations of treated effluent from both Control Cell and Test Cell significantly decreased to 7.5-12.5 mg/l and 5.0– 11.0, respectively, compared with the TSS concentrations of raw influent from the parking lot stormwater runoff in a range of 46 – 69 for all the four (4) rainfall events (see Figure 53). TSS as a pollutant is of significant concern for GDOT, with the permit performance for its removal targeted at 80%. It was observed that Test Cell achieved an average of 84.1% removal efficiency while Control Cell achieved 79.7% removal efficiency (see Figure 55). TSS removal efficiency by Test Cell exceeded the permit

performance goal of 80%. Figure 54 represents a comparison among raw stormwater runoff, Control Cell and Test Cell for TSS concentration.

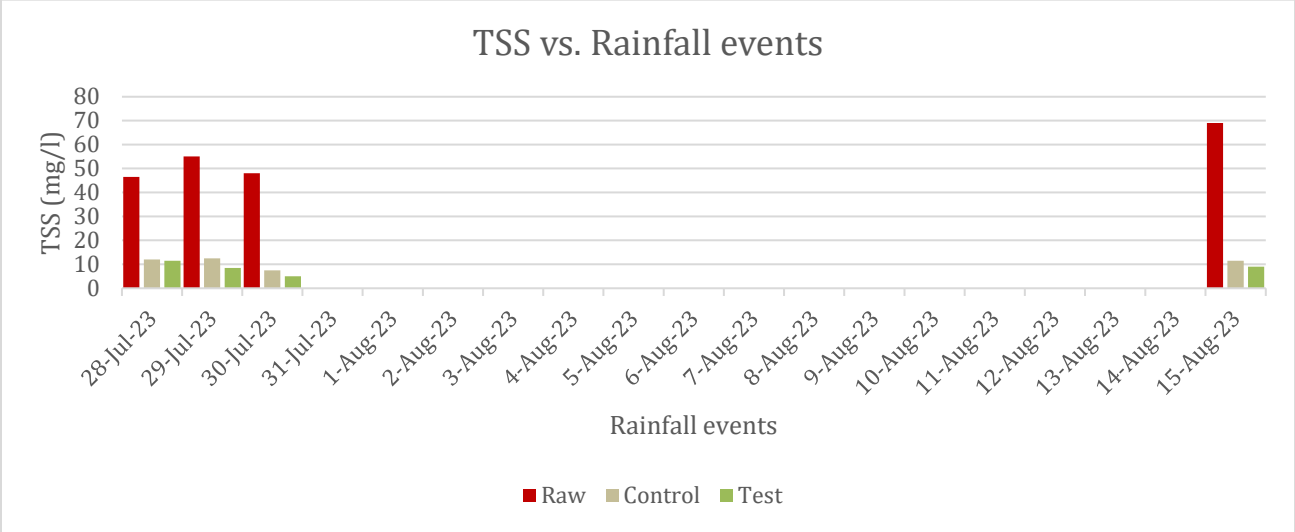

Figure 53. TSS readings for raw influent and treated effluent (Control Cell and Test Cell)

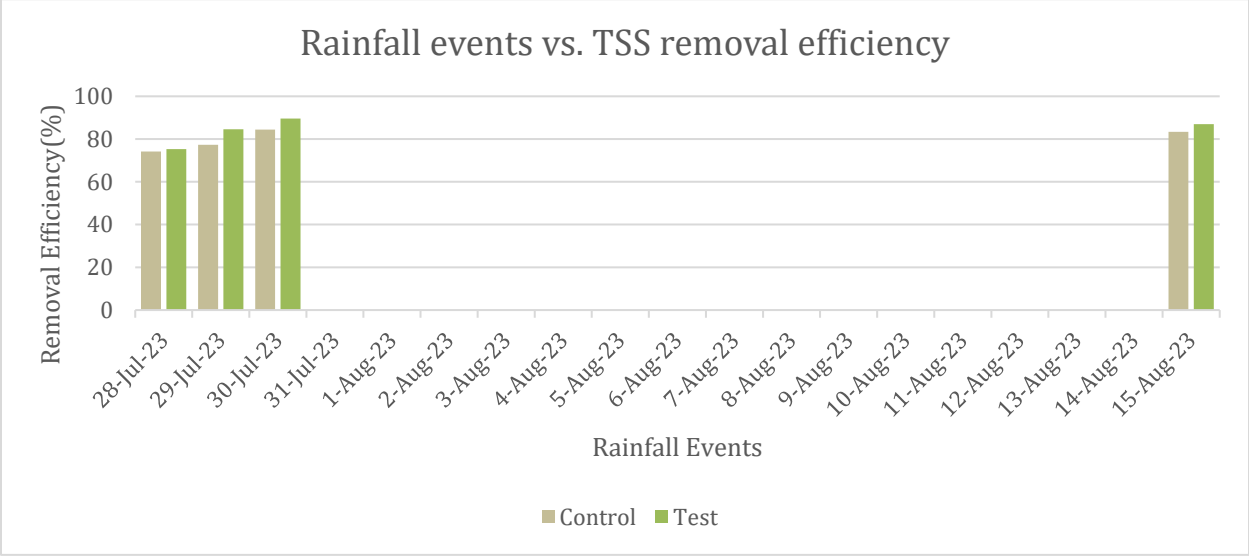

Figure 54. TSS removal efficiency of Control Cell and Test Cell vs. Rainfall events

- TDS

For all the four (4) rainfall events, it was observed that the TDS concentrations of treated effluent from Test Cell significantly decreased in a range of 2.0 to 4.0 mg/L while those from Control Cell also decreased to a range of 6.0 to 10.0 mg/L compared with the TDS concentrations in a range of 15.0 to 26.0 mg/Lin raw influent (see Figure 55).

For the removal efficiencies of TDS concentrations, Test Cell achieved an average of 83.6% while Control Cell achieved an average of 62.0% (see Figure 56).

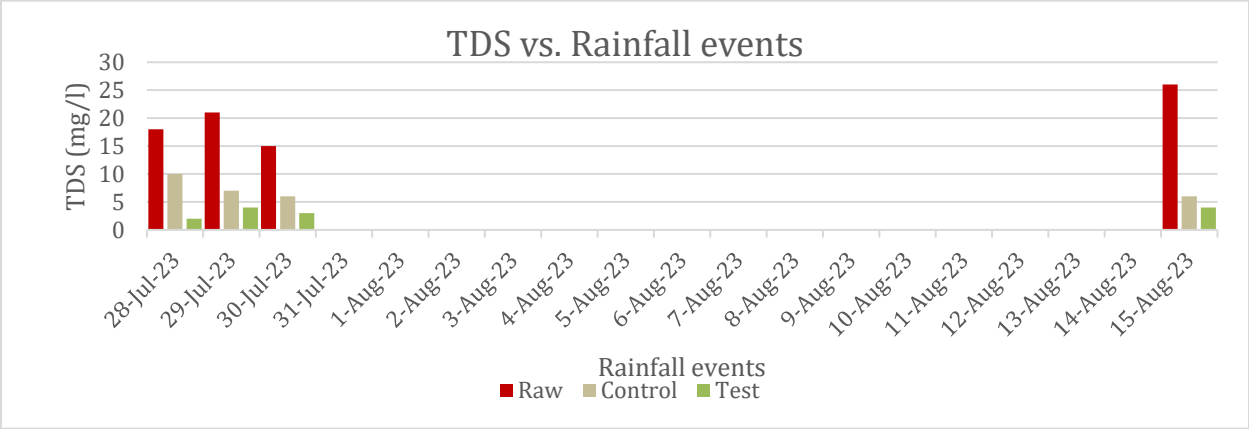

Figure 55. TDS readings for raw influent and treated effluent (Control Cell and Test Cell) from each Sampling Date

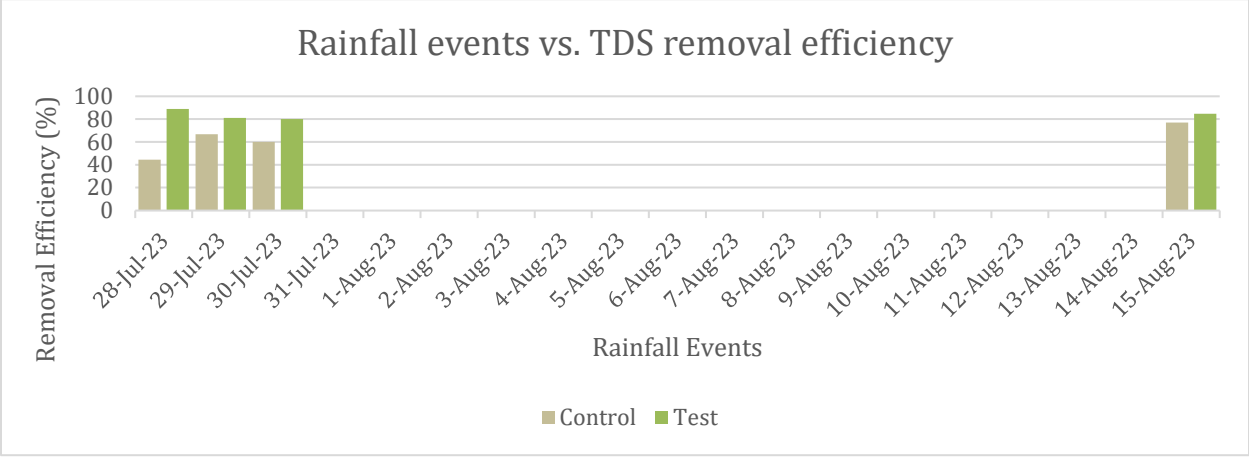

Figure 56. TDS removal efficiency of Control Cell and Test Cell vs. Rainfall events

- TS

For all the four (4) rainfall events, it was observed that the TS concentrations of treated effluent from Test Cell significantly decreased in a range of 8.0 to 13.0 mg/L while those from Control Cell also decreased to a range of 13.0 to 22.0 mg/L compared with the TS concentrations in a range of 63.0 to 95.0 mg/L in raw influent (see Figure 57).

For the removal efficiencies of TS concentrations, Test Cell achieved an average of 84.0% while Control Cell achieved an average of 75.0% (see Figure 58). TSS removal followed the same trend as the TSS and TDS removal and is attributed to the overall high removal efficiencies of TSS and TDS.

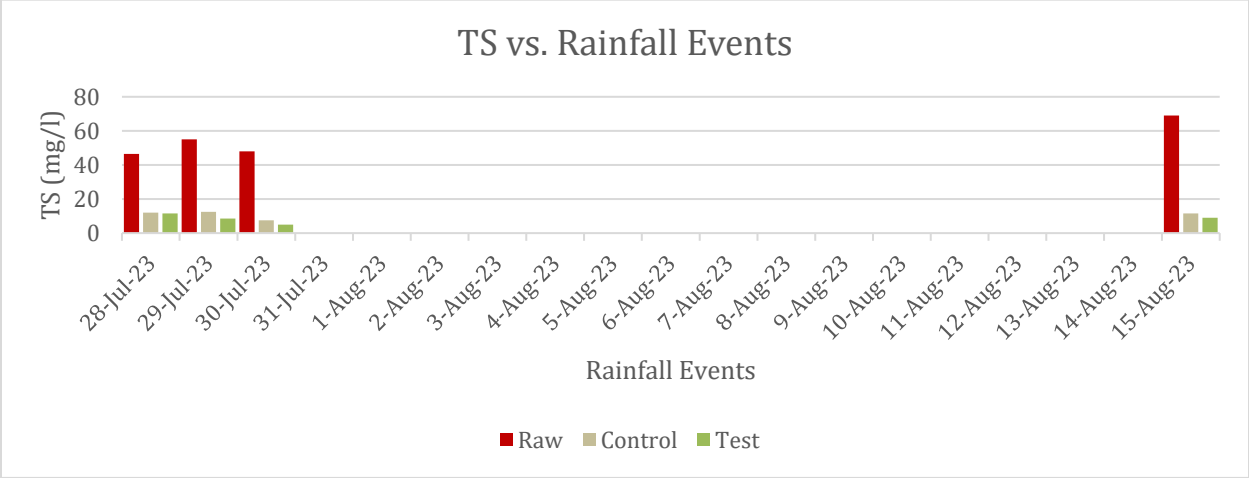

Figure 57. TS readings for raw influent and treated effluent (Control Cell and Test Cell) from each Sampling Date

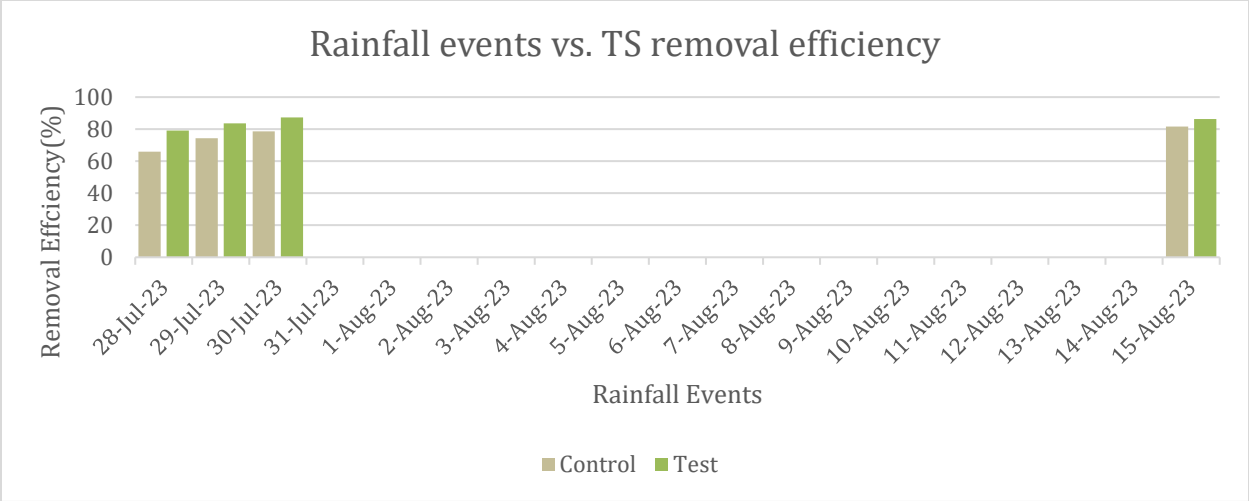

Figure 58. TS removal efficiency of Control Cell and Test Cell vs. Rainfall events

- **Nutrients**

The biochar amended topsoil illustrated removal efficiency of nutrients pollutants as discussed in this section. The removal of nutrients is due to the great removal of TSS through physical filtration, as suspended particles provide surface attachment of nutrients and other organic pollutants in water. Adsorption of nutrient pollutants onto the surface of the biochar increased pollutant removal.

- **Nitrogen**

- **NH_3-N**

For all the four (4) rainfall events, it was observed that the NH_3-N concentrations of treated effluent from Test Cell significantly decreased in a range of 0.0 to 0.07 mg/L while those from Control Cell insignificantly decreased to 0.15 – 0.25 mg/L and a little increased to a range of 0.17 to 0.25 mg/L compared with the NH_3-N concentrations in a range of 0.16 to 0.27 mg/L in raw influent (see Figure 59).

For the removal efficiencies of NH_3-N concentrations, Test Cell achieved an average of 83.2% while Control Cell achieved an average of 5.0% (see Figure 60).

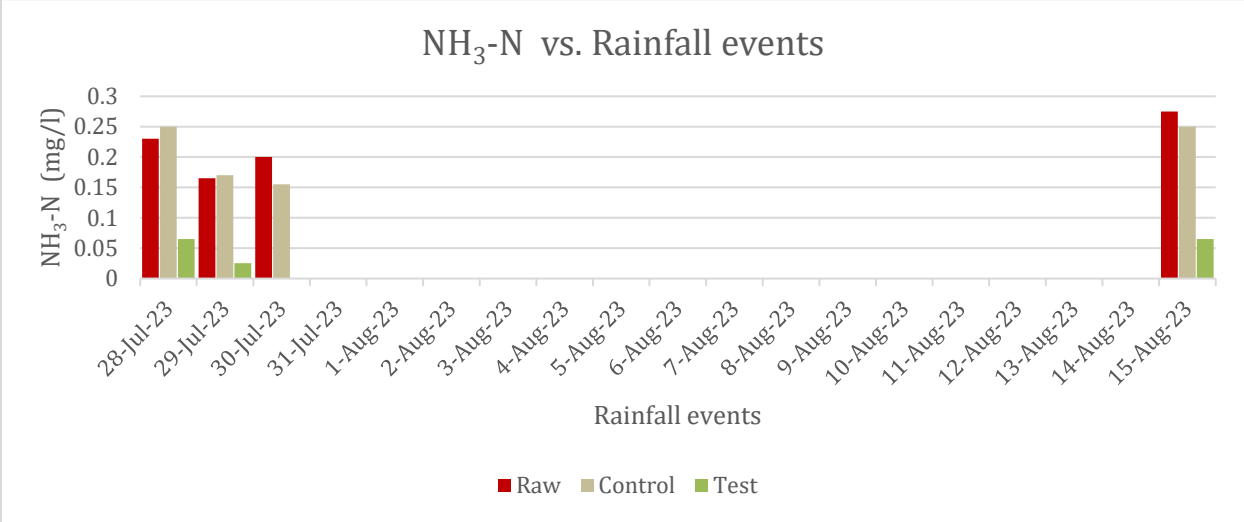

Figure 59. NH_3-N readings for raw influent and treated effluent (Control Cell and Test Cell) from each Sampling Date

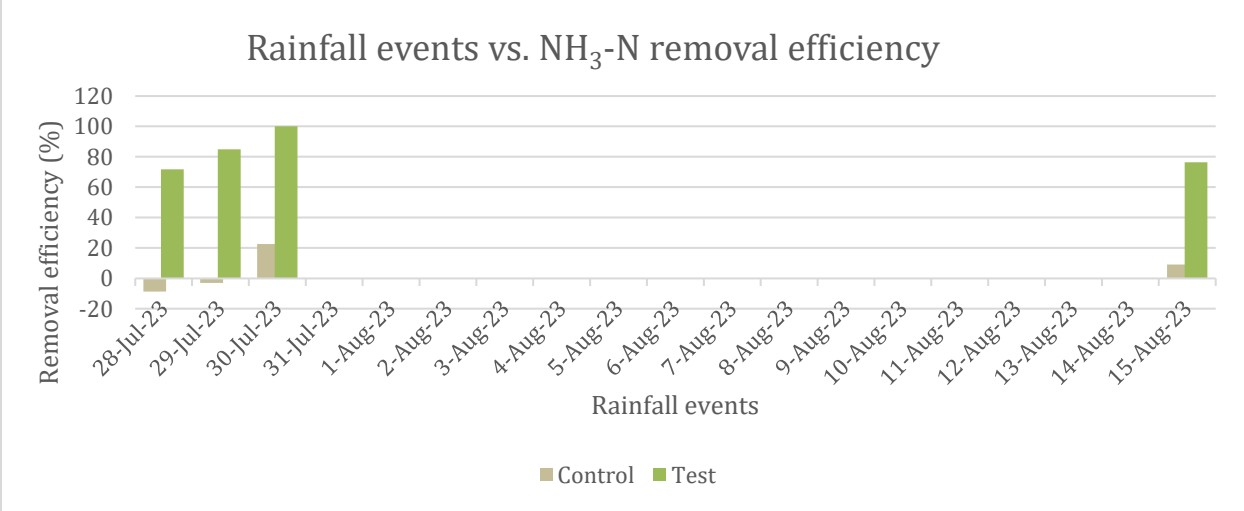

Figure 60. NH_3-N removal efficiency of Control Cell and Test Cell vs. Rainfall events

- **NO_3^--N**

For all the four (4) rainfall events, it was observed that NO_3^--N concentrations of treated effluent from Test Cell significantly decreased to a range of 0.0 to 0.1 mg/L while those from Control Cell significantly increased to 0.85 mg/L for the first rainfall event on July 28th, 2023, then decreased to 0.15 – 0.20 mg/L for the remaining three rainfall events, compared with NO_3^--N concentrations in a range of 0.3 to 0.55 mg/L in raw influent of stormwater runoff from the parking lot (see Figure 61).

For the removal efficiencies of NO_3^--N concentrations, Test Cell achieved an average of 88.2% while Control Cell achieved an average of -1.3% (see Figure 62) indicating some leaching out of NO_3^--N from the topsoil in Control Cell.

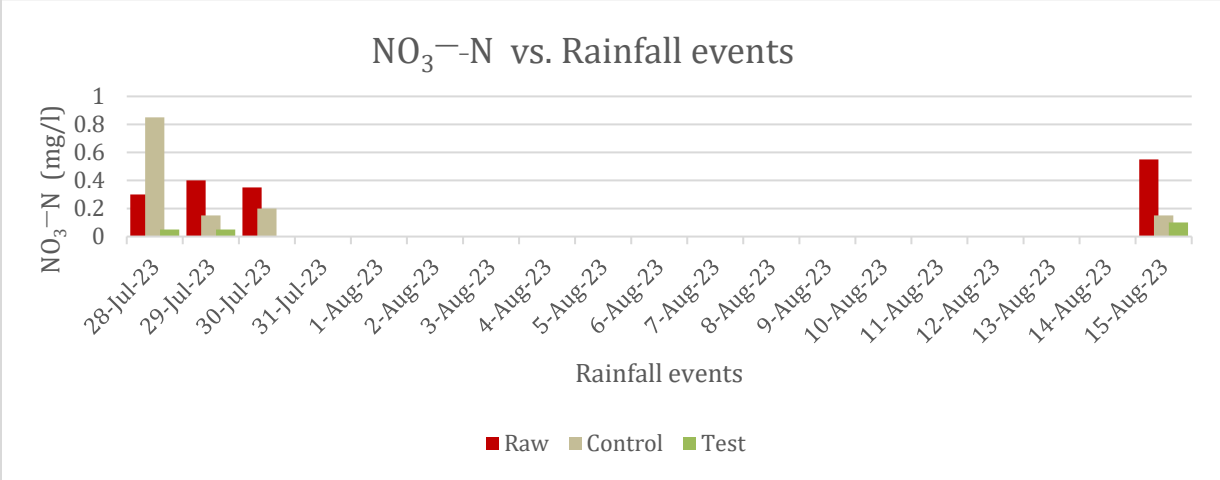

Figure 61. NO_3^--N readings for raw influent, and treated effluent (Control Cell and Test Cell) from each Sampling Date

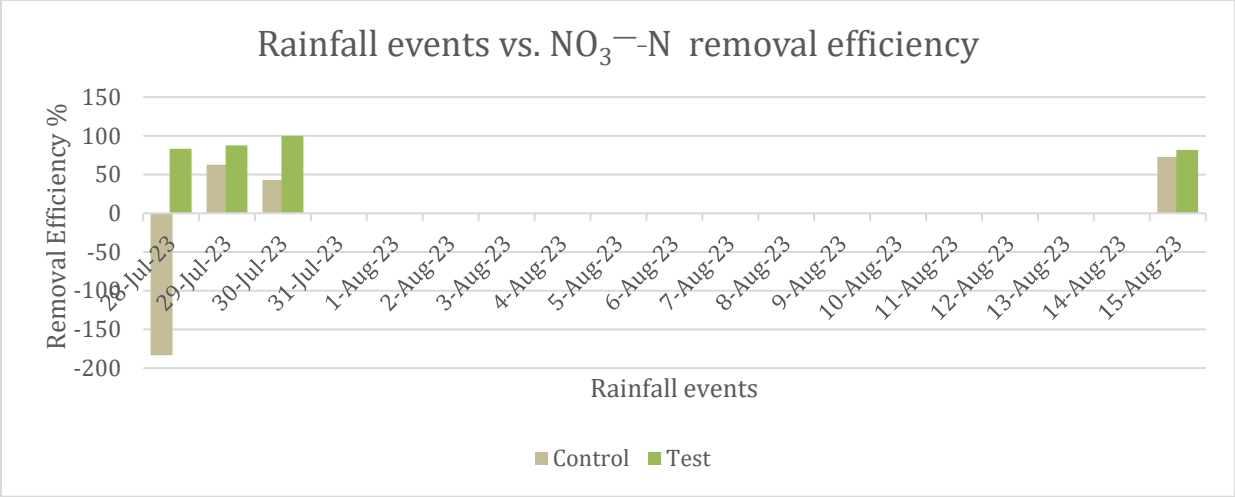

Figure 62. NO_3^--N removal efficiency of Control Cell and Test Cell vs. Rainfall events

- **TKN**

For all the four (4) rainfall events, it was observed that the TKN concentrations of treated effluent from Test Cell significantly decreased in a range of 0.0 to 0.5 mg/L while those from Control Cell also decreased to a range of 0.0 to 2.0 mg/L compared with the TKN concentrations in a range of 2.5 to 4.0 mg/L in raw influent from the parking lot (see Figure 63).

For the removal efficiencies of TKN concentrations, Test Cell achieved an average of 95.0% while Control Cell achieved an average of 72.7% (see Figure 64).

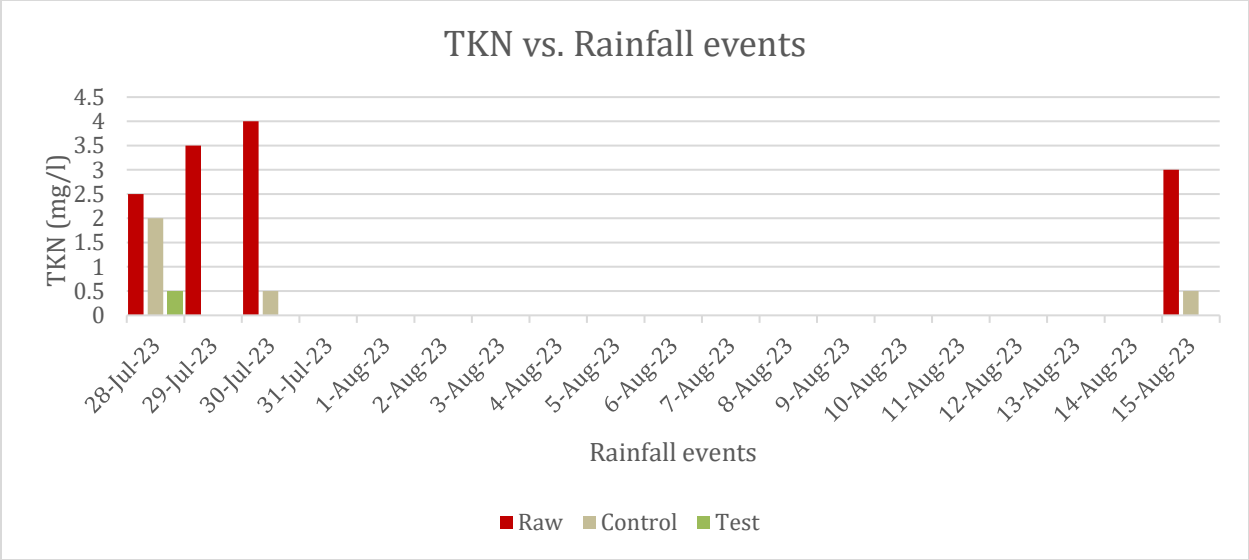

Figure 63. TKN readings for raw influent and treated effluent (Control Cell and Test Cell) from each Sampling Date

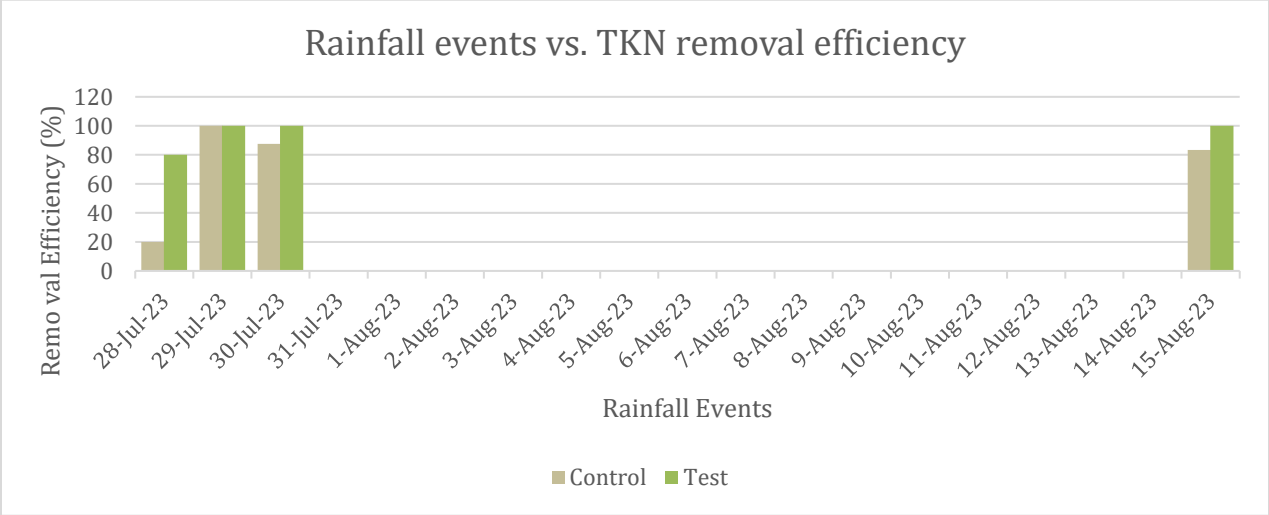

Figure 64. TKN removal efficiency of Control Cell and Test Cell vs. Rainfall events

- **TN**

For all the four (4) rainfall events, it was observed that the TN concentrations of treated effluent from Test Cell significantly decreased in a range of 0.0 to 0.5 mg/L while those from Control

Cell also decreased to a range of 1.0 to 3.0 mg/L compared with the TN concentrations in a range of 3.5 to 4.5 mg/L in raw influent from the parking lot (see Figure 65).

For the removal efficiencies of TKN concentrations, Test Cell achieved an average of 90.5% while Control Cell achieved an average of 57.39 % (see Figure 66). TN removal is attributed to the overall removal efficiencies of TKN and TDS.

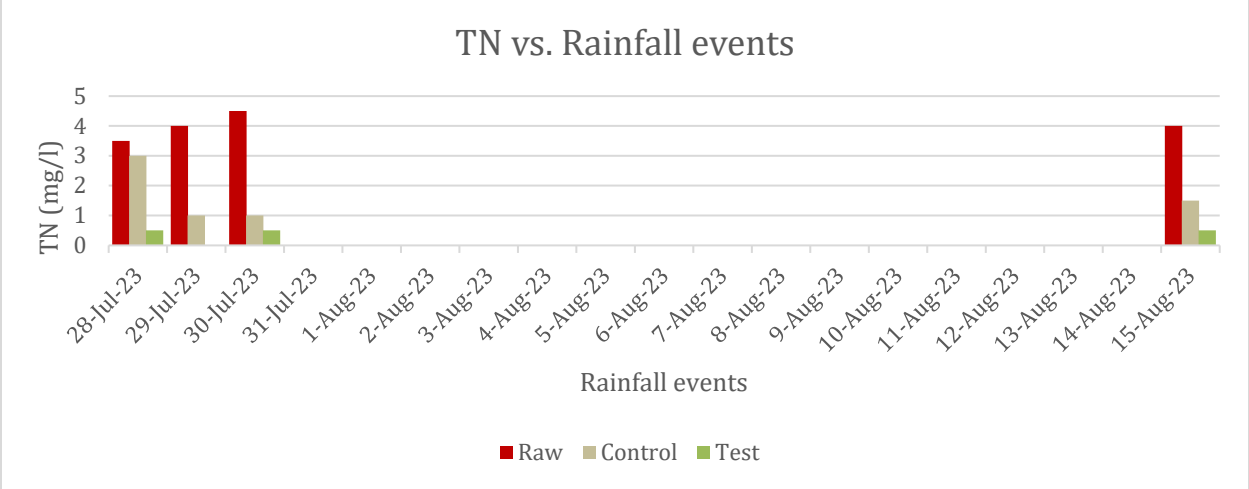

Figure 65. TN readings for raw influent and treated effluent (Control Cell and Test Cell) from each Sampling Date

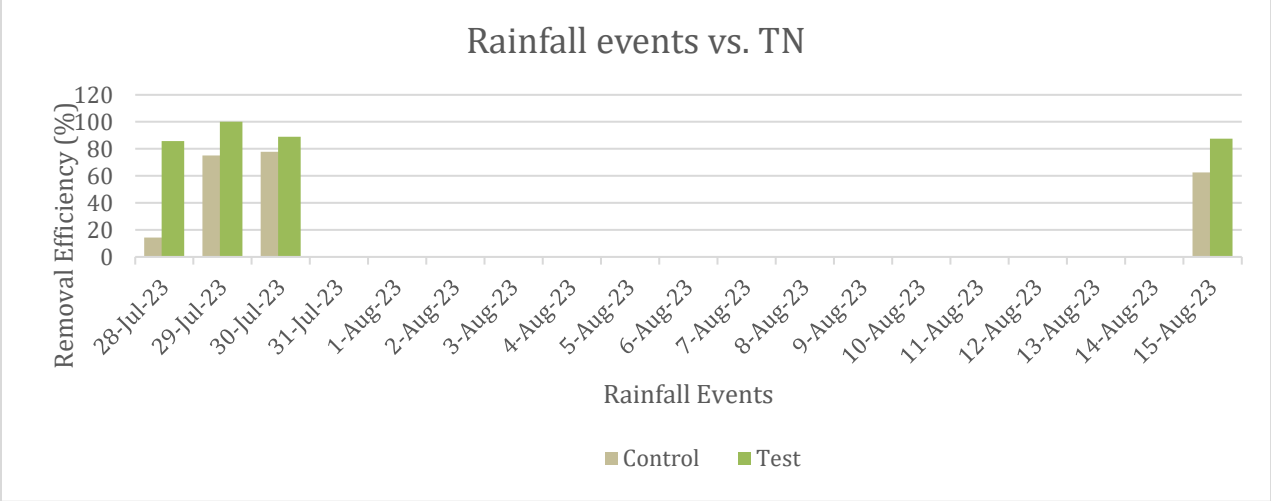

Figure 66. TN removal efficiency of Control Cell and Test Cell vs. Rainfall events

- **TP**

For all the four (4) rainfall events, it was observed that the TP concentrations of treated effluent from Test Cell significantly decreased in a range of 0.1 to 0.1 mg/L while those from Control Cell also decreased to a range of 0.15 to 0.3 mg/L compared with the TP concentrations in a range of 0.45 to 0.65 mg/L in raw influent from the parking lot (see Figure 67).

For the removal efficiencies of TP concentrations, Test Cell achieved an average of 81.1% while Control Cell achieved an average of 62.26% (see Figure 68).

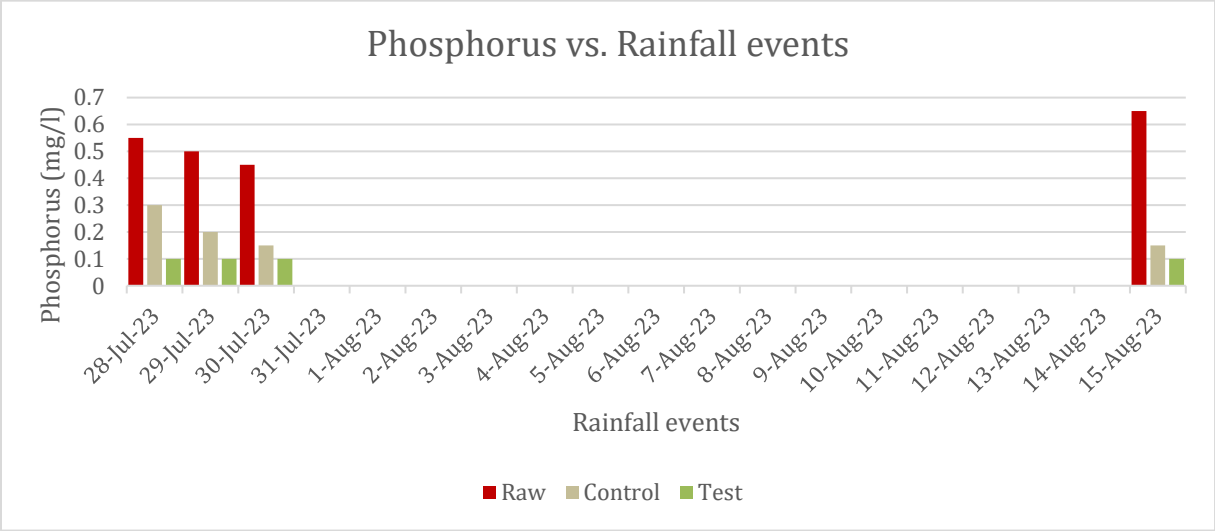

Figure 67. Phosphorus readings for raw influent and treated effluent (Control Cell and Test Cell) from each Sampling Date

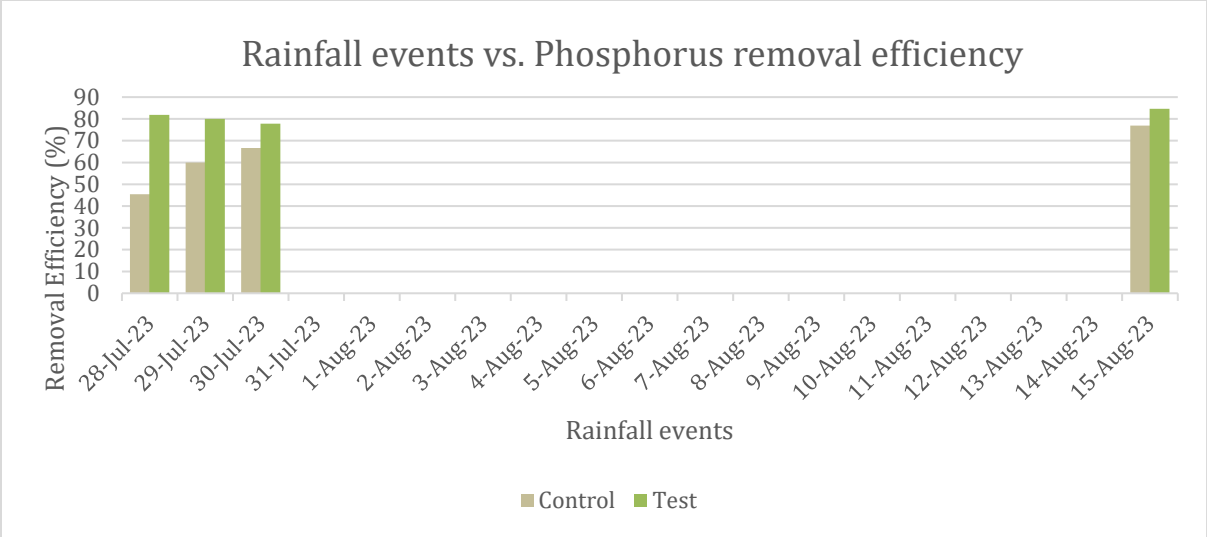

Figure 68. Phosphorus removal efficiency of Control Cell and Test Cell vs. Rainfall events

- **Oil and grease**

For all the four (4) rainfall events, it was observed that the oil and grease concentrations of treated effluent from Test Cell significantly decreased in a range of 1.0 to 3.0 mg/L while those from Control Cell also decreased to a range of 4.0 to 7.5 mg/L compared with the oil and grease concentrations in a range of 10.5 to 15.5 mg/L in raw influent from the parking lot (see Figure 69).

For the removal efficiencies of oil and grease concentrations, Test Cell achieved an average of 87.83% while Control Cell achieved an average of 57.48% (see Figure 70).

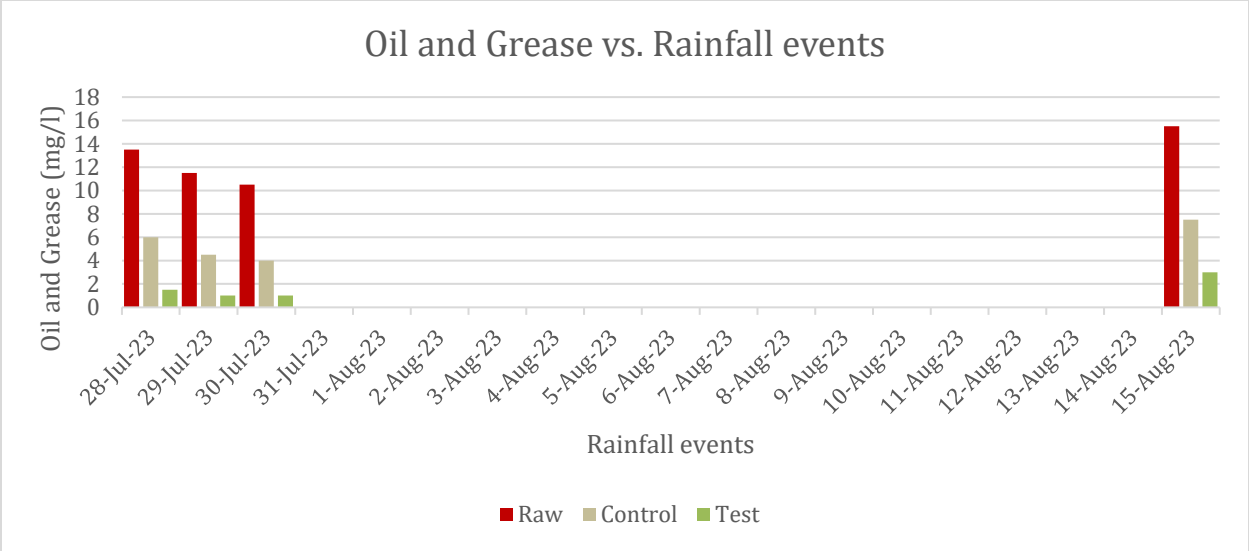

Figure 69. Oil and Grease readings for raw influent and treated effluent (Control Cell and Test Cell) from each Sampling Date

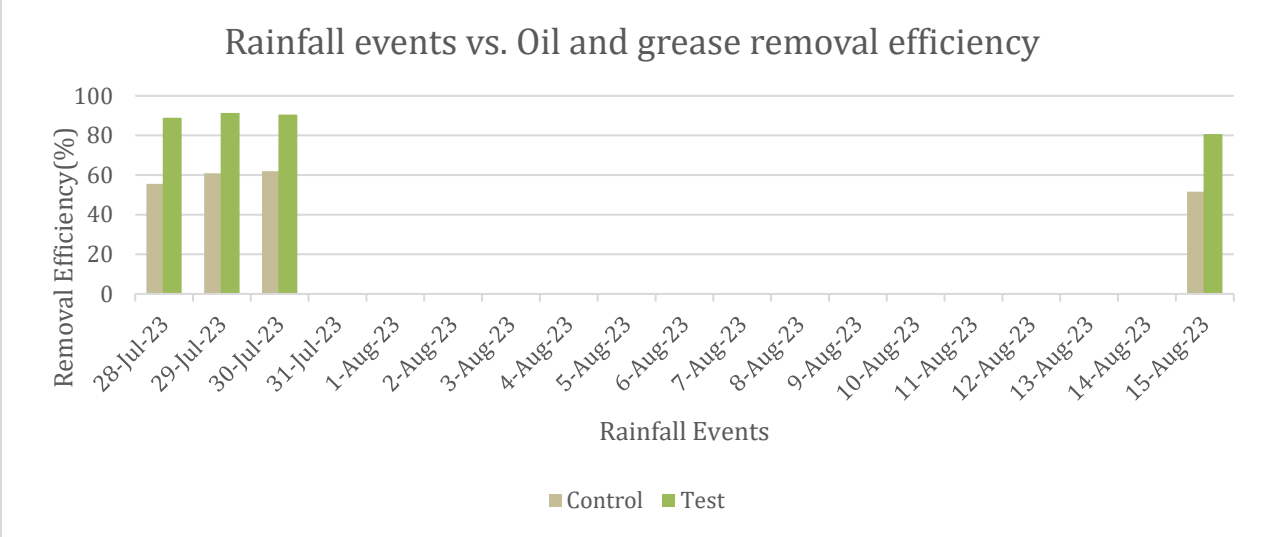

Figure 70. Oil and grease removal efficiency of Control Cell and Test Cell vs. Rainfall events

- **COD**

For all the four (4) rainfall events, it was observed that the COD concentrations of treated effluent from Test Cell significantly decreased in a range of 2.5 to 3.0 mg/L while those from

Control Cell also decreased to a range of 6.5 to 8.5 mg/L compared with the COD concentrations in a range of 15.0 to 19.0 mg/L in raw influent from the parking lot (see Figure 71).

For the removal efficiencies of oil and grease concentrations, Test Cell achieved an average of 83.25% while Control Cell achieved an average of 56% (see Figure 72).

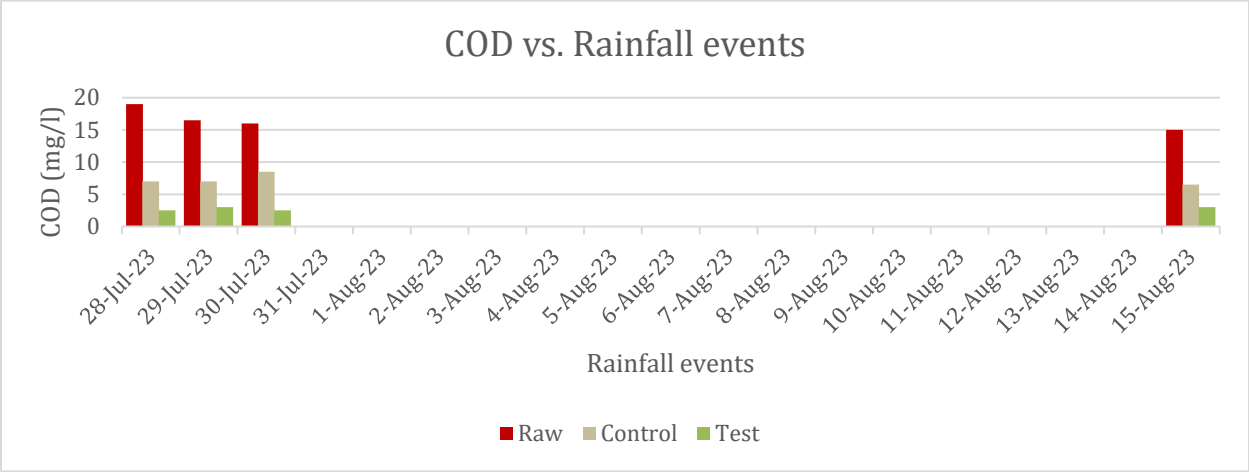

Figure 71. COD readings for raw influent and treated effluent (Control Cell and Test Cell) from each Sampling Date

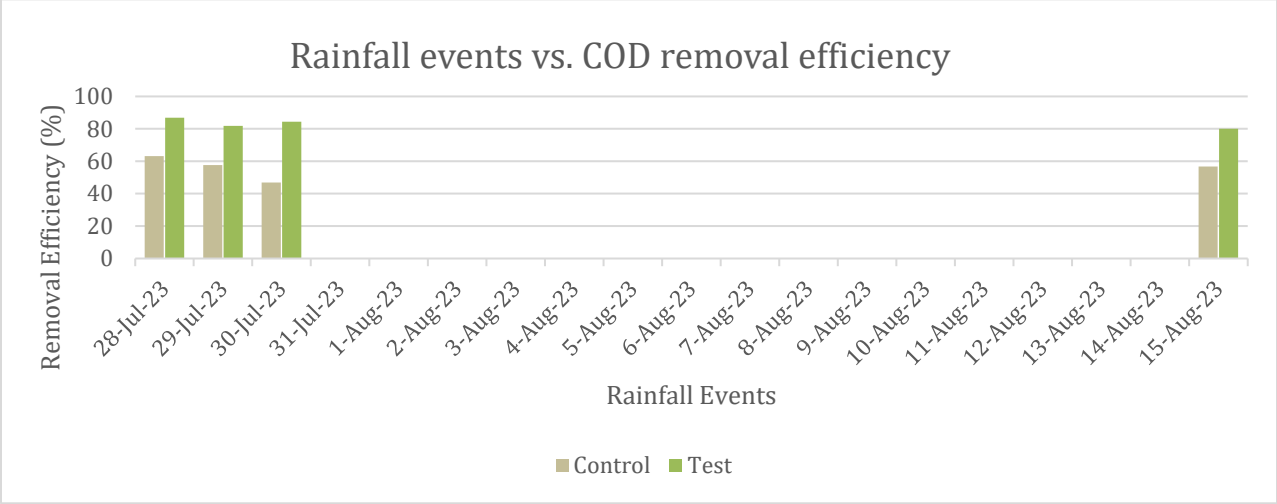

Figure 72. COD removal efficiency of Control Cell and Test Cell vs. Rainfall events

4.6.4 Comprehensive Analysis

The results analysis is further summarized in this section under two (2) categories: the basic WQ parameters including pH, Color, Conductivity, and DO and the WQ parameters of concern including solids (TDS, TSS, TS), nutrients (N and P), and heavy metals (Cu, Zn, and Pb), oil and grease and COD.

4.6.4.1 Basic WQ parameters including pH, Color, Conductivity, and DO

The basic WQ parameters including pH, Color, Conductivity, and DO, are discussed in this section. For Test Cell, it was observed that the treated effluent conductivity correlated well with the pH (see Figure 73).

.

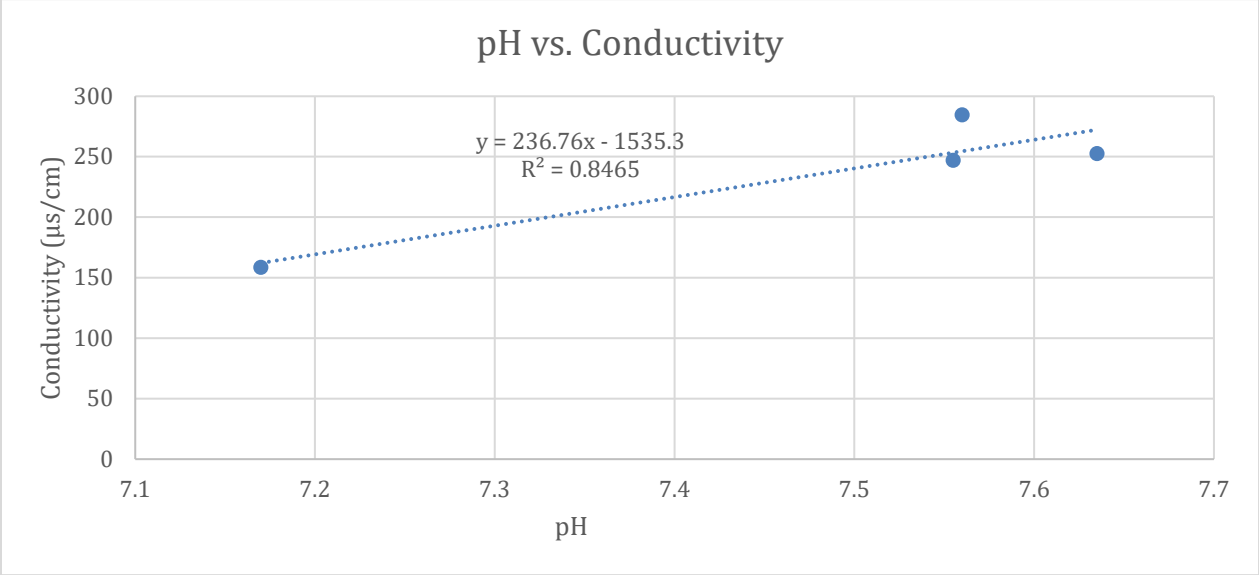

Figure 73. Graph illustrating the linear relationship between pH and conductivity of treated effluent from Test Cell

For Test Cell, a higher color removal efficiency was expected. But an average low color removal efficiency of 14.2% was observed. One reason could be that the raw stormwater runoff

from the parking lot was more colored than normal due to parking lot repairing work and using road marking color during the sampling period (see Figure 21).

On the other hands, DO concentrations in the treated effluent after infiltration from Test Cell were significantly higher (see Figure 50). Biochar produced through pyrolysis of biomass used in water treatment can increase the DO concentration of the water (Mopoung 2020).

4.6.4.2 TSS, TDS, TS, and Oil and Grease

The removal efficiency of oil and grease in treated stormwater effluent strongly correlated with TS removal efficiency (see Figure 74). TS comprises the suspended (TSS) and dissolved solids (TDS); therefore, a correlation of removal efficiency between TS and oil and grease is advantageous in using biochar to treat stormwater runoff with these pollutants. In removing oil and grease from the stormwater runoff, Test Cell achieved an average of 87.83% removal efficiency. The removals of TSS, TDS, TS, oil, and grease were consistently high from Test Cell.

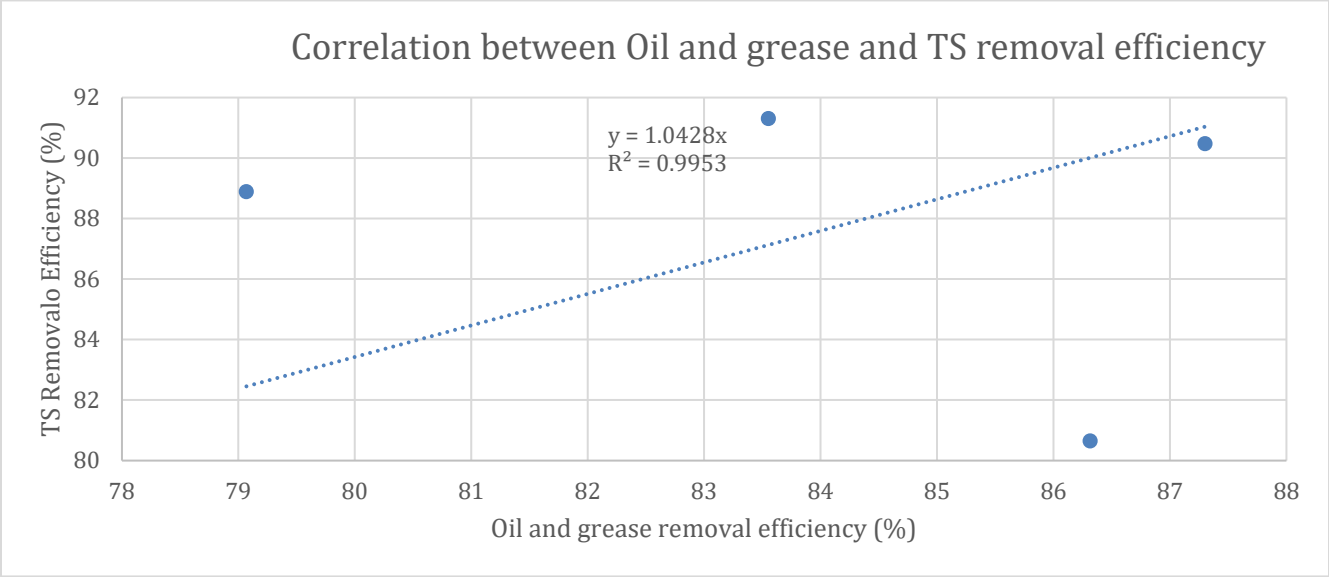

Figure 74. Graph illustrating the relationship between TS and oil & grease of treated effluent from the biochar amended topsoil media

4.6.4.3 COD and Nutrients (Nitrogen and Phosphorus)

Nutrients are of primary concern regarding pollutants in urban stormwater runoff. BMPs are designed and can remove nitrogen, phosphorous, and oxidizable pollutants (COD) from stormwater runoff. Study incorporating biochar and topsoil amendment as a treatment media have reported 50 - 60% NO_3^-–N and NH_3-N removal from urban stormwater runoff after 140 days while dissolved phosphorus and organic removal performance were between 20 to 30% (Afrooz 2017). This indicates consistent nutrient removal performance using biochar as a topsoil amendment to treat urban stormwater runoff. Biochar produces high removal efficiency (89.35 ± 0.5% and 95.5 ± 0.5% for single and combined modified biochar respectively) in removing COD from wastewater (Khurshid 2021). The combined modified biochar has higher oxygen-containing functional groups (-OH and -COOH), surface area and pore volume compared to single modified biochar (Khurshid 2021). This study shows high removal efficiencies, all greater than 80%, for NH_3-N, NO_3^--N, TKN, TN, TP and COD from the stormwater runoff of the parking lot using biochar amended topsoil media, Test Cell (see Figures 75).

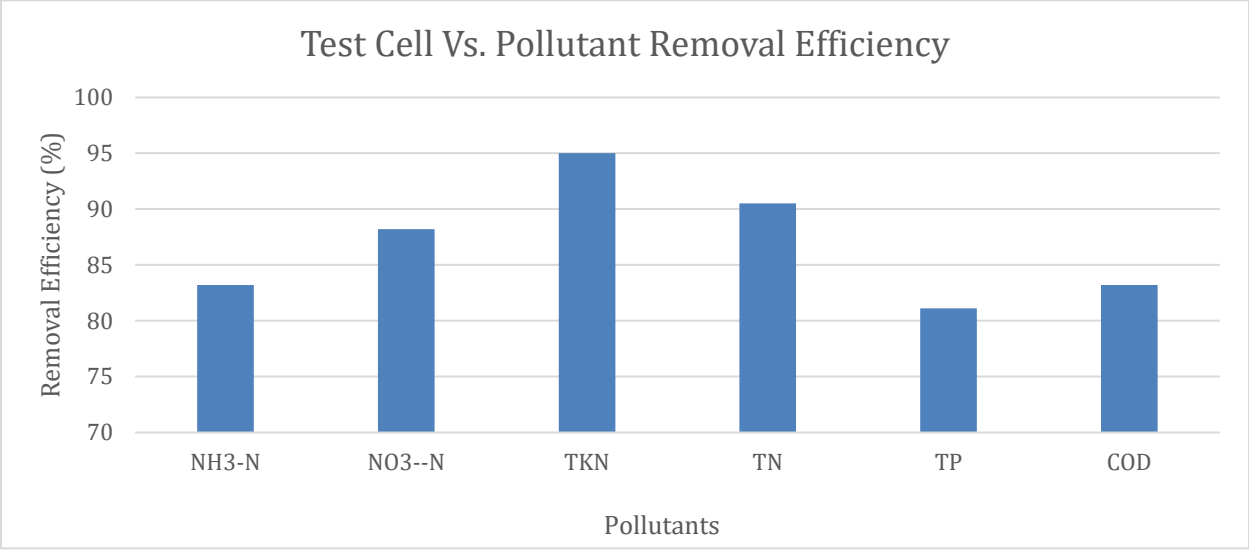

Figure 75. Nutrient Removal Efficiency vs. Biochar Amended Topsoil Media

4.7 Economic Analysis

To estimate the economic feasibility of this new GI using biochar amended topsoil, the total cost of materials and equipment installed at the Field Test Site with an area of of 500 ft^2 is used to calculate how much it costed to on-site treat the stormwater runoff from GSU parking lot. In Table 4, the cost of land and topsoil were $0.00 due to the donation from GSU Facilities Department, the cost of labor and construction equipment were free from a Senior Project Team of three (3) CE Seniors and help from GSU Facilities Department, while the biochar cost in terms of volume was $300.00 with 5% (wt%) biochar application and other equipment and materials costs were about $ 2,500.00. The total material and equipment cost was about $ 2,800.00 for building the Field Test Site for this Phase I Project.

Table 5. Material and equipment cost for Phase I Project

SL No	Item Name	No. of item	Unit price ($)	Total price ($)
01	Topsoil	$500ft^3$	0	0
02	Construction equipment		0	0
03	Labor cost		0	0
04	Biochar	1	300	300
05	Drum barrel	2	62.93	125.86
06	HOBO data logging rain gauge, 0.01" per tip	1	446.5	446.5
07	HOBO optic USB base station	1	133	133

SL No	Item Name	No. of item	Unit price ($)	Total price ($)
08	HOBO MX soil moisture & temperature logger, 2m cable	1	379.05	379.05
09	Utility Pump 1/3HP	1	159	159
10	3000sqft OSC Sprinkle	2	8.98	17.96
11	Acurate glass Rain guage	2	2.58	5.16
12	PS brass Y shut off cone	1	10.98	10.98
13	Scotts 4ft X50ft pro feb	1	24.98	24.98
14	15ft utility hose	2	16.98	33.96
15	50 ft utility hose	1	29.98	29.98
16	100ft utility hose	2	25.98	51.96
17	gravel			112
18	Perforated Pipe			280
19	Glass tube for KSAT	1	142	142
20	flow meter	2	27	54
21	lifting manhole tool	1	28	28
22	small vaccume pump	1	28	28
23	plant	13	28	364
24	post	13	5	65
Total Construction Cost				**$2,800**

4.8 Guidelines for Designing, Building, and Operating and Maintaining this New GI Using Biochar Amended Topsoil for On-Site Stormwater Runoff Treatment

A number of essential requirements must be followed in order to effectively and sustainably design, construct, and operate this new GI using biochar-amended topsoil for on-site stormwater runoff treatment. Here are some general and important guidelines:

- Site Assessment and Planning: Areas need to be identified where stormwater runoff has potential sources of pollutants.
- Design Considerations: Size of the Test Site needs to be calculated and the treated effluent collection path needs to be determined. The depth of the media of biochar amended topsoil may be varied and 1 ft depth will be the minimum. A minimum 6-inch diameter of perforated pipe needs to be selected for installation. Local topsoil needs to be used as it can be free to get for the project.
- Plant Selection for GI: Native grasses/plants need to be used in this new GI system to promote biodiversity and reduce maintenance requirements. Plant needs to be installed at appropriate depths to maximize stormwater pollutant removal.
- Biochar Selection and Application: High quality and effective biochar needs to be selected. The appropriate and effective biochar amendment rate needs to be determined. 5% (by wt) biochar amendment with topsoil is recommended. Biochar needs to be mixed thoroughly with topsoil to ensure even distribution.
- Construction and Installation: Necessary construction equipment and machineries are necessary such as excavator loaders, and mixer etc. Best practices should be followed to minimize soil compaction and disturbance.

Proper measurements are needed to install the perforated pipe and catch basins for collecting treated effluent.

- Maintenance and Monitoring: A regular maintenance plan should be developed that includes regular inspections, monitoring soil moisture and rainfall events, weeding. Any issues should be addressed promptly such as plant die-off, proper electricity for operation. The performance of this new GI should be monitored to ensure it meets stormwater runoff treatment goals.
- WQ Testing: Stormwater runoff samples (influent and effluent) needs to be tested as much as possible for key pollutants to assess the effectiveness of this new GI.
- Community Engagement: Engage with the local community to raise awareness about the benefits of this new GI and involve them in maintenance efforts. Also, educate stakeholders about the importance of stormwater treatment using this new GI with biochar amended topsoil.
- Documentation and Record-Keeping: Maintain detailed records of construction, operation and maintenance, and monitoring activities. Any modification or improvements made to this new GI over time for on-site stormwater runoff treatment should be documented.
- Training and Education: Training section can be developed for the personnel responsible for operation and maintenance in the best practices of this new GI management. Continuously educate staff and stakeholders on the benefits and importance of this new GI.

CHAPTER 5. CONCLUSIONS

In this Project, a full-scale Field Test Site with a total area of 500 ft^2 and 1 ft depth was built to on-site treat stormwater runoff from a parking lot on Georgia Southern University (GSU) campus in Spring 2023. It includes two (2) cells: Control and Test Cells, 250 ft^2 each, for a direct comparison purpose. Control Cell consists of topsoil only and Test Cell with 5% (weight percent, wt%) biochar amended topsoil. The local topsoil with majority of sands from Statesboro, GA, and the Soil Reef Biochar were used at the Field Test Site with switchgrass planted and growing at the Site also. During heavy rainfall events, the parking lot stormwater runoff was pumped and sprayed onto to the Field Test Site via sprinklers, infiltrated and treated through the 1 ft layer of topsoil or biochar amended topsoil in Control/Test Cell, and seeped into the corrugated perforated pipes and flowed into the end cylindrical catch basin drums, where the treated effluent samples were collected and tested for pollutants.

The testing results showed that the addition of biochar (5% by wt) into the topsoil significantly increased its saturated hydraulic conductivity to 1.78E-05 m/s from 1.05E-06 m/s for topsoil only, which resulted in stormwater runoff infiltrating through the media of biochar amended topsoil much faster. The results for on-site soil moisture content monitoring also showed that the 5% biochar amended topsoil in Test Cell had much higher moisture contents than the topsoil only in Control Cell.

Based on the preliminary test results in Summer 2023, for the initial about 11 gallons of the parking lot stormwater runoff treated by each Control and Test Cell, the removal efficiencies are summarized as follows: TSS: 80% for Control Cell versus 84% for Test Cell; NH_3-N: 5% vs 83%; NO_3^--N: - 1.3% vs 88%; TKN: 73% vs 95%; TN: 57% vs 91%; Phosphorus: 62% vs 81%; and Oil and Grease: 57% vs 88%. Overall, the removal efficiencies of pollutants by Test Cell are much higher than those by Control Cell.

In summary, this new GI using biochar amended topsoil for on-site stormwater treatment is cost-effective and sustainable.

CHAPTER 6. FURTHER STUDIES

Future research should be needed to continually operate, maintain, sample and test the Test Site on-site treating the stormwater runoff from the parking lot; and continually investigate and determine performance of the Test Site on removal efficiencies of the pollutants under different weather conditions including frequencies of rainfall events and dry and wet seasons. Even after completion of this Project, the Test Site with grass growing can be still used as a demonstration site for a show case, and continually operated to study long-term treatment performance beyond 1-2 year operation.

ACKNOWLEDGMENTS

The authors would like to thank the Georgia Water Research Institute (GWRI) under the National Water Resources Research Act (104b-StateResearch) for funding this project, the Department of Civil Engineering and Construction (CEC) and the Department of Facilities, -Planning, Design, and Construction at Georgia Southern University (GSU) for their support in selecting and providing the Field Test Site on campus and excavating the site. The GSU Research Team offers special thanks to GSU Senior Projects Team in Springs 2023 for their participating in designing and building the Field Test Site which is critical for this research project; and Mr. Shawn Jackson, Laboratory Coordinator of Civil Engineering in the Department of CEC, for his valuable help with site installations and support on instruments used in this research project.

REFERENCES

Afrooz, A. N. and A. B. Boehm (2017). "Effects of submerged zone, media aging, and antecedent dry period on the performance of biochar-amended biofilters in removing fecal indicators and nutrients from natural stormwater." Ecological Engineering **102**: 320-330.

Ahiablame, L. M., et al. (2012). "Representation and evaluation of low impact development practices with L-THIA-LID: An example for site planning." Environment and Pollution 1(2): 1.

Are, K. S. (2019). "Biochar and soil physical health." An Imperative Amendment for Soil and the Environment; Abrol, V., Sharma, P., Eds: 21-33.

Ashley, R., et al. (2013). Water-sensitive urban design: opportunities for the UK. Proceedings of the Institution of Civil Engineers-Municipal Engineer, Thomas Telford Ltd.

Ashoori, N., et al. (2019). "Evaluation of pilot-scale biochar-amended woodchip bioreactors to remove nitrate, metals, and trace organic contaminants from urban stormwater runoff." Water research 154: 1-11.

Bakr, A. R., et al. (2020). "Water quality impacts of bridge stormwater runoff from scupper drains on receiving waters: A review." Science of the Total Environment 726: 138068.

Beck, D. A., et al. (2011). "Amending greenroof soil with biochar to affect runoff water quantity and quality." Environmental pollution 159(8-9): 2111-2118.

Beckingham, B., et al. (2019). "Stormwater ponds in the southeastern US coastal plain: hydrogeology, contaminant fate, and the need for a social-ecological framework." Frontiers in Environmental Science 7: 117.

Birch, G., et al. (2005). "Efficiency of an infiltration basin in removing contaminants from urban stormwater." Environmental Monitoring and Assessment 101: 23-38.

Blanco-Canqui, H. (2017). "Biochar and soil physical properties." Soil Science Society of America Journal 81(4): 687-711.

Bowman, T., et al. (2012). "Resident, developer, and city staff perceptions of LID and CSD subdivision design approaches." Landscape and Urban Planning 107(1): 43-54.

Bratieres, K., et al. (2008). "Nutrient and sediment removal by stormwater biofilters: A large-scale design optimisation study." Water research 42(14): 3930-3940.

Brogowski, Z., et al. (2014). "Calculating particle density, bulk density, and total porosity of soil based on its texture." Soil science annual 65(4): 139.

Burns, S. E. and N. T. Caruso (2015). Treatment of highway runoff: engineered filter media for pollutant removal through enhanced sorption, Georgia. Dept. of Transportation. Office of Research.

Cairns, S., et al. (2022). Engineered biochar as adsorbent for the removal of contaminants from aqueous medium. Engineered Biochar: Fundamentals, Preparation, Characterization and Applications, Springer: 353-381.

Carson, T., et al. (2013). "Hydrological performance of extensive green roofs in New York City: observations and multi-year modeling of three full-scale systems." Environmental Research Letters 8(2): 024036.

Chaffin, B. C., et al. (2016). "A tale of two rain gardens: Barriers and bridges to adaptive management of urban stormwater in Cleveland, Ohio." Journal of Environmental Management 183: 431-441.

Choi, J., et al. (2017). "Strategies to improve reference databases for soil microbiomes." The ISME journal 11(4): 829-834.

Chui, T. F. M., et al. (2016). "Assessing cost-effectiveness of specific LID practice designs in response to large storm events." Journal of Hydrology 533: 353-364.

Clark, S. E. and R. Pitt (2012). "Targeting treatment technologies to address specific stormwater pollutants and numeric discharge limits." Water research 46(20): 6715-6730.

Davis, A. P. and M. Burns (1999). "Evaluation of lead concentration in runoff from painted structures." Water research 33(13): 2949-2958.

Davis, A. P., et al. (2009). "Bioretention technology: Overview of current practice and future needs." Journal of environmental engineering 135(3): 109-117.

Ekka, S. A., et al. (2021). "Next generation swale design for stormwater runoff treatment: A comprehensive approach." Journal of Environmental Management 279: 111756.

Fletcher, T. D., et al. (2015). "SUDS, LID, BMPs, WSUD and more–The evolution and application of terminology surrounding urban drainage." Urban water journal 12(7): 525-542.

Gan, L., et al. (2021). "Influence of biochar amendment on stormwater management in green roofs: experiment with numerical investigation." Acta Geophysica 69: 2417-2426.

Gregoire, B. G. and J. C. Clausen (2011). "Effect of a modular extensive green roof on stormwater runoff and water quality." Ecological engineering 37(6): 963-969.

Gwenzi, W., et al. (2017). "Biochar-based water treatment systems as a potential low-cost and sustainable technology for clean water provision." Journal of Environmental Management 197: 732-749.

Hatt, B. E., et al. (2009). "Hydrologic and pollutant removal performance of stormwater biofiltration systems at the field scale." Journal of Hydrology 365(3-4): 310-321.

Imhoff, P. T., et al. (2019). "Removing Nitrate from Stormwater with Biochar Amendment to Roadway Soils."

Imhoff, P. T. and S. A. A. Nakhli (2017). Reducing stormwater runoff and pollutant loading with biochar addition to highway greenways.

Imran, H., et al. (2013). "Permeable pavement and stormwater management systems: a review." Environmental technology 34(18): 2649-2656.

Jiang, Y., et al. (2015). "A review of applicability and effectiveness of low impact development/green infrastructure practices in arid/semi-arid United States." Environments 2(2): 221-249.

Jílková, V. and G. Angst (2022). "Biochar and compost amendments to a coarse-textured temperate agricultural soil lead to nutrient leaching." Applied Soil Ecology 173: 104393.

Karteris, M., et al. (2016). "Towards a green sustainable strategy for Mediterranean cities: Assessing the benefits of large-scale green roofs implementation in Thessaloniki, Northern

Greece, using environmental modelling, GIS and very high spatial resolution remote sensing data." Renewable and Sustainable Energy Reviews 58: 510-525.

Keeley, M. (2011). "The Green Area Ratio: an urban site sustainability metric." Journal of environmental planning and management 54(7): 937-958.

Khurshid, H., et al. (2021). "Adsorptive removal of COD from produced water using tea waste biochar." Environmental Technology & Innovation 23: 101563.

Laurenson, G., et al. (2013). "The role of bioretention systems in the treatment of stormwater." Advances in agronomy 120: 223-274.

Le Coustumer, S., et al. (2012). "The influence of design parameters on clogging of stormwater biofilters: A large-scale column study." Water research 46(20): 6743-6752.

Lee, H., et al. (2004). "Seasonal first flush phenomenon of urban stormwater discharges." Water research 38(19): 4153-4163.

Lehmann, J. and S. Joseph (2015). Biochar for environmental management: an introduction. Biochar for environmental management, Routledge: 1-13.

Liu, J., et al. (2017). "Water scarcity assessments in the past, present, and future." Earth's future 5(6): 545-559.

Liu, W., et al. (2014). "Assessing the effectiveness of green infrastructures on urban flooding reduction: A community scale study." Ecological Modelling 291: 6-14.

Lucke, T. and P. W. Nichols (2015). "The pollution removal and stormwater reduction performance of street-side bioretention basins after ten years in operation." Science of the Total Environment 536: 784-792.

Major, J., et al. (2012). "Nutrient leaching in a Colombian savanna Oxisol amended with biochar." Journal of environmental quality 41(4): 1076-1086.

Malaviya, P., et al. (2019). "Rain gardens as stormwater management tool." Sustainable green technologies for environmental management: 141-166.

McCarthy, M. J., et al. (2013). "Oxygen consumption in the water column and sediments of the northern Gulf of Mexico hypoxic zone." Estuarine, Coastal and Shelf Science 123: 46-53.

McFarland, A. R., et al. (2019). "Guide for using green infrastructure in urban environments for stormwater management." Environmental science: Water research & technology 5(4): 643-659.

Mei, C., et al. (2018). "Integrated assessments of green infrastructure for flood mitigation to support robust decision-making for sponge city construction in an urbanized watershed." Science of the Total Environment 639: 1394-1407.

Mohanty, S. K., et al. (2018). "Plenty of room for carbon on the ground: Potential applications of biochar for stormwater treatment." Science of the total environment 625: 1644-1658.

Mopoung, S., et al. (2020). "Water treatment for fish aquaculture system by biochar-supplemented planting panel system." The Scientific World Journal 2020.

Novotný, M., et al. (2023). "The use of biochar made from biomass and biosolids as a substrate for green infrastructure: A review." Sustainable Chemistry and Pharmacy 32: 100999.

Ouedraogo, A. S., et al. (2023). "Treatment of Highway Stormwater Runoff Using Sustainable Biochar: A Review." Journal of Environmental Engineering 149(2): 03122005.

Payne, E. G., et al. (2019). "Biotreatment technologies for stormwater harvesting: critical perspectives." Current opinion in biotechnology 57: 191-196.

Polukarova, M., et al. (2020). "Organic pollutants, nano-and microparticles in street sweeping road dust and washwater." Environment international 135: 105337.

Qin, Y., et al. (2023). "Optimization of a compact on-site stormwater runoff treatment system: Process performance and reactor design." Chemosphere 315: 137767.

Roseen, R. M., et al. (2015). "Economic and adaptation benefits of low impact development." Low Impact Development Technology: Implementation and Economics: 74-92.

Schueler, T. R. (1987). Controlling urban runoff: A practical manual for planning and designing urban BMPs, Metropolitan Washington Council of Governments Washington, DC.

Sharma, R. and P. Malaviya (2021). "Management of stormwater pollution using green infrastructure: The role of rain gardens." Wiley Interdisciplinary Reviews: Water 8(2): e1507.

Stagge, J. H., et al. (2012). "Performance of grass swales for improving water quality from highway runoff." Water research 46(20): 6731-6742.

Stovin, V., et al. (2012). "The hydrological performance of a green roof test bed under UK climatic conditions." Journal of hydrology 414: 148-161.

Taguchi, V. J., et al. (2020). "It is not easy being green: Recognizing unintended consequences of green stormwater infrastructure." Water 12(2): 522.

Tirpak, R. A., et al. (2019). "Investigating the hydrologic and water quality performance of trees in bioretention mesocosms." Journal of Hydrology 576: 65-71.

Trifunovic, B., et al. (2018). "Dynamic effects of biochar concentration and particle size on hydraulic properties of sand." Land Degradation & Development 29(4): 884-893.

Vogel, J. R., et al. (2015). "Critical review of technical questions facing low impact development and green infrastructure: A perspective from the Great Plains." Water Environment Research 87(9): 849-862.

Winsley, P. (2007). "Biochar and bioenergy production for climate change mitigation." New Zealand Science Review 64(1): 5-10.

Wolfand, J. M., et al. (2019). "Occurrence of urban-use pesticides and management with enhanced stormwater control measures at the watershed scale." Environmental science & technology 53(7): 3634-3644.

Woznicki, S. A., et al. (2018). "Effectiveness of landscape-based green infrastructure for stormwater management in suburban catchments." Hydrological processes 32(15): 2346-2361.

Yunus, A. I. (2022). "Highway Stormwater Runoff On-site Treatment Using Bioslope With New Media Of Biochar Amended Topsoils."

Zanin, G., et al. (2018). "Assessing stormwater nutrient and heavy metal plant uptake in an experimental bioretention pond." Land 7(4): 150.

APPENDIX A: ADDITIONAL TABLES

Table A-1. pH readings of Stormwater Runoff samples from each Sampling Date.

Sample	Sampling Date	Average pH
01	7/10/2023	5.45
02	7/15/2023	6.08
03	7/28/2023	6.49
04	7/29/2023	6.67
05	7/30/2023	6.62
06	8/6/2023	6.11
07	8/15/2023	6.36

Table A-2. Conductivity readings of Stormwater Runoff samples from each Sampling Date

Sample	Sampling Date	Average Conductivity (µs/cm)
01	7/10/2023	39.50
02	7/15/2023	43.50
03	7/28/2023	37.50
04	7/29/2023	40.50
05	7/30/2023	46.00
06	8/6/2023	46.50
07	8/15/2023	47.50

Table A-3. Color readings of Stormwater Runoff samples from each Sampling Date

Sample	Sampling Date	Average Color (Pt.Co)
01	7/10/2023	48.50
02	7/15/2023	46.00
03	7/28/2023	62.50
04	7/29/2023	69.50
05	7/30/2023	39.50
06	8/6/2023	41.50
07	8/15/2023	30.50

Table A-4. DO readings of Stormwater Runoff samples from each Sampling Date.

Sample	Sampling Date	Dissolved oxygen (DO) (mg/l)
01	7/10/2023	8.62
02	7/15/2023	8.72
03	7/28/2023	7.76
04	7/29/2023	7.20
05	7/30/2023	8.25
06	8/6/2023	8.42
07	8/15/2023	9.00

Table A-5. COD readings of Stormwater Runoff samples from each Sampling Date

Sample	Sampling Date	Average COD (mg/l)
01	7/10/2023	13.50
02	7/15/2023	10.00
03	7/28/2023	19.00
04	7/29/2023	16.50
05	7/30/2023	16.00
06	8/6/2023	11.00
07	8/15/2023	15.00

Table A-6. Phosphorus readings of Stormwater Runoff samples from each Sampling Date

Sample	Sampling Date	Average Phosphorus (mg/l)
01	7/10/2023	0.20
02	7/15/2023	0.50
03	7/28/2023	0.55
04	7/29/2023	0.50
05	7/30/2023	0.45
06	8/6/2023	0.40
07	8/15/2023	0.65

Table A-7. NH_3-N readings of Stormwater Runoff samples from each Sampling Date.

Sample	Sampling Date	Average NH_3-N (mg/l)
01	7/10/2023	0.29
02	7/15/2023	0.22
03	7/28/2023	0.23
04	7/29/2023	0.17
05	7/30/2023	0.20
06	8/6/2023	0.24
07	8/15/2023	0.28

Table A-8. Total Nitrogen (TN) and Total Kjeldahl Nitrogen readings of Stormwater Runoff samples from each Sampling Date

Sample	Sampling Date	Average TKN (mg/l)	Average TN (mg/l)
01	7/10/2023	1.50	2.50
02	7/15/2023	2.30	3.50
03	7/28/2023	2.50	3.50
04	7/29/2023	3.50	4.00
05	7/30/2023	4.00	4.50
06	8/6/2023	2.00	3.50
07	8/15/2023	3.00	4.00

*Note TN = Total Nitrogen, TKN = Total Kjeldahl Nitrogen

Table A-9. NO_3—N readings of Stormwater Runoff samples from each Sampling Date

Sample	Sampling Date	Average NO_3—N (mg/l)
01	7/10/2023	0.50
02	7/15/2023	0.30
03	7/28/2023	0.30
04	7/29/2023	0.40
05	7/30/2023	0.35
06	8/6/2023	0.30
07	8/15/2023	0.55

Table A-10. Total Suspended Solids, Dissolved Solids, and Total Solids readings of Stormwater Runoff samples from each Sampling Date

Sample	Sampling Date	Average TSS (mg/l)	Average TDS (mg/l)	Average TS (mg/l)
01	7/10/2023	66.00	38.00	104.00
02	7/15/2023	46.00	16.00	62.00
03	7/28/2023	46.50	18.00	64.50
04	7/29/2023	55.00	21.00	76.00
05	7/30/2023	48.00	15.00	63.00
06	8/6/2023	34.50	11.00	45.50
07	8/15/2023	69.00	26.00	95.00

*Note: TDS = Total Dissolved Solids, TSS = Total Suspended Solids, TS = Total Solids.

Table A-11. Oil and Grease readings of Stormwater Runoff samples from each Sampling Date.

Sample	Sampling Date	Average Oil and grease (mg/l)
01	7/10/2023	13.50
02	7/15/2023	11.00
03	7/28/2023	13.50
04	7/29/2023	11.50
05	7/30/2023	10.50
06	8/6/2023	11.00
07	8/15/2023	15.50

Table A-12. Stormwater Runoff Treated Effluent Parameter concentrations for Test Cell and Control Cell

Sample No.		**01**	**02**	**03**	**04**
Sample Date	**Date**	**7/28/2023**	**7/29/2023**	**7/30/2023**	**8/15/2023**
Average pH	**Control**	6.77	6.59	6.90	6.97
	Test	7.64	7.56	7.56	7.17
Conductivity (µs/cm)	**Control**	144.00	121.50	157.50	131.00
	Test	252.50	284.50	247.00	158.50
Color (Pt.Co)	**Control**	312.50	301.50	290.00	327.50
	Test	42.50	44.00	35.50	37.50
Dissolved oxygen (DO) (mg/l)	**Control**	12.88	11.64	11.05	11.20
	Test	28.95	26.85	31.26	32.84
Average COD (mg/l)	**Control**	7.00	7.00	8.50	6.50
	Test	2.50	3.00	2.50	3.00
Average Phosphorus (mg/l)	**Control**	0.30	0.20	0.15	0.15
	Test	0.10	0.10	0.10	0.10

Average NH_3-N (mg/l)	**Control**	0.25	0.17	0.16	0.25
	Test	0.07	0.03	0.00	0.07
Average TKN (mg/l)	**Control**	2.00	0.00	0.50	0.50
	Test	0.50	0.00	0.00	0.00
Average TN (mg/l)	**Control**	3.00	1.00	1.00	1.50
	Test	0.50	0.00	0.50	0.50
Average NO_3^-N (mg/l)	**Control**	0.85	0.15	0.20	0.15
	Test	0.05	0.05	0.00	0.10
Average TSS (mg/l)	**Control**	12.00	12.50	7.50	11.50
	Test	11.50	8.50	5.00	9.00
Average TDS (mg/l)	**Control**	10.00	7.00	6.00	6.00
	Test	2.00	4.00	3.00	4.00
Average TS (mg/l)	**Control**	22.00	19.50	13.50	17.50
	Test	13.50	12.50	8.00	13.00
Average Oil and grease (mg/l)	**Control**	6.00	4.50	4.00	7.50
	Test	1.50	1.00	1.00	3.00

*Note: TN = Total Nitrogen, TKN = Total Kjeldahl Nitrogen, TDS = Total Dissolved Solids, TSS = Total Suspended Solids, TS = Total Solid

Table A-13. Efficiency Removal of Stormwater Runoff Pollutants

Sample No.			**01**	**02**	**03**	**04**
Sample Date	**Removal Efficiency (%)**	**Date**	**7/28/2023**	**7/29/2023**	**7/30/2023**	**8/15/2023**
Average COD (mg/l)		**Control**	63.16	57.58	46.88	56.67
		Test	86.84	81.82	84.38	80.00
Average Phosphorus (mg/l)		**Control**	45.45	60.00	66.67	76.92
		Test	81.82	80.00	77.78	84.62
Average NH_3-N (mg/l)		**Control**	-8.70	-3.03	22.50	9.09
		Test	71.74	84.85	100.00	76.36
Average TKN (mg/l)		**Control**	20.00	100.00	87.50	83.33
		Test	80.00	100.00	100.00	100.00
Average TN (mg/l)		**Control**	14.29	75.00	77.78	62.50
		Test	85.71	100.00	88.89	87.50
Average NO_3—N (mg/l)		**Control**	-183.33	62.50	42.86	72.73
		Test	83.33	87.50	100.00	81.82

Average TSS (mg/l)		**Control**	74.19	77.27	84.38	83.33
		Test	75.27	84.55	89.58	86.96
Average TDS (mg/l)		**Control**	44.44	66.67	60.00	76.92
		Test	88.89	80.95	80.00	84.62
Average TS (mg/l)		**Control**	65.89	74.34	78.57	81.58
		Test	79.07	83.55	87.30	86.32
Average Oil and grease (mg/l)		**Control**	55.56	60.87	61.90	51.61
		Test	88.89	91.30	90.48	80.65

*Note: % Removal = % removal of pollutants after treatment, (-) values= % increase of pollutant concentration after treatment

Project ID	2022GA04B
Project Type	Outreach and Engagement
Award Type	Base Grant (104b)
Project Title	The 2023 Biennial Georgia Water Resources Conference
Project PI	Wegner, Seth
Academic Institution of PI	University of Georgia
Congressional District of project	GA-10

U.S. Department of the Interior/Geological Survey
Research Grant 2022GA04B
The 2023 Biennial Georgia Water Resources Conference
FINAL REPORT – 21 September 2023

Award Amount: $9,990

UGA River Basin Center
203 D.W. Brooks Drive
Athens, GA 30602-5017

Summary: Since its inception in 1989, the biennial Georgia Water Resources Conference has provided an open forum for the discussion of water policies, research, and management strategies within the state of Georgia and surrounding states. The high-profile meeting attracts diverse attendance from government, private, academic and non-profit sectors. The 2023 meeting was the largest ever, with 400 total registrants, 130 oral presentations, 10 panels and 47 posters. The meeting attracted 27 sponsors in addition to GWRI (the lead sponsor); these additional sponsors contributed a total of $30,350. A total of 116 students (mostly graduate and undergraduate, plus a few high school students) attended the meeting.

Objectives
The objectives for which the conference sought funding in 2023 were:

1) Development of internal and external sponsorship opportunities.
2) Creation and coordination of a Conference Technical Planning Committee consisting primarily of faculty from University System of Georgia schools.
3) Creation and coordination of a Conference Steering Committee consisting of representatives of state agencies, non-government organizations, and significant private sector water users.
4) Regular meetings of both committees to develop technical sessions and conference tracks, selection of keynote speakers and invitation of other speakers, promotion of the conference through their personal and professional contacts, including social media.
5) Solicitation of abstracts from a wide range of scientists, engineers, and other water professionals across Georgia and surrounding states.
6) Public outreach to identify conference topics and invited speakers that reflect current and emerging water resources issues at the state level and attract new constituencies to present at the conference.
7) Development of GWRC branding and advertising including emails, graphics, web-based articles, flyers and posters.
8) Regular communication with the Technical Planning and Steering Committees and water experts assigned to review abstracts and manuscripts.
9) Dissemination of GWRC branded materials via social media channels, email, and flyers.
10) Planning and preparation for all physical aspects of the conference, including facility reservations, banquet catering, and social events; execution of the conference itself.

Results
All project objectives were met. Highlights and critical statistics are listed below.

Sponsorships: Although the Georgia Water Resources Institute remains the prime sponsor and provides support that is critical for sustaining the conference, we rely on additional sponsorships to keep student registration fees low. This year's additional sponsors include six UGA units; four other Georgia universities; 10 private companies, including Southern Company/Georgia Power, Tetra Tech, and Kleinschmidt Associates; and seven nonprofits, including The Nature Conservancy of Georgia and The Longleaf Alliance. Total funding from our 27 additional sponsors (not including GWRI) amounted to $30,350.

Steering Committee: We established a 26-member steering committee spanning a broad range of sectors. It included professionals from ARC/Metro Water Planning District, Corblu Ecology Group, US Geological Survey, Georgia DNR, Chemours, Georgia Conservancy, Chattahoochee Riverkeeper, and faculty from multiple institutions.

Conference Execution: The conference was the largest on record, with 400 total registrants, 130 oral presentations, 10 panels, and 47 posters. This represents a 26% increase in registrations since 2019 (the most recent in-person conference), a 20% increase in presentations and 30% increase in posters. Of the non-student attendees, 35% were from the academic sector, 29% from government entities, 18% from the private sector, and 18% from NGOs.

The meeting attracted 15 exhibitors: In-Situ, Nutter and Associates, Georgia Southern University, Storm Water Systems, YSI/Xylem, Odum School of Ecology, Corblu, College of Coastal Georgia, American Rivers, Oconee Rivers Greenway Commission, U.S. Geological Survey, Kleinschmidt, Georgia Water Planning and Policy Center, Upper Oconee Watershed Network, GDNR Adopt a Stream. The USGS conducted a series of well-attended outdoor equipment demonstrations.

Student engagement:
116 students—undergraduate, graduate and a small contingent of high schoolers—attended the 2023 meeting, making up about 29% of our total registrants. Almost 30% of our talks and 75% of our posters were presented by students, for a total of 74 student presenters. Additionally, several panelists were students, and the conference provided professional development opportunities to 19 student volunteers from multiple universities. Because attendance is highly diverse, including representatives from consulting firms, government agencies, NGOs and academia, the meeting was an exceptional opportunity for student training, education, and networking with water professionals.

Conference Proceedings: Presenters were invited to submit brief papers, or "extended abstracts," for compilation into the Proceedings of the 2023 Georgia Water Resources Conference. Fifteen papers were ultimately submitted. These were peer reviewed by volunteers from the steering committee, compiled, formatted and transferred to GWRI for publication.

Project ID	2022GA01G
Project Type	Research
Award Type	104g - General
Project Title	Monitoring and modeling expanding risk of hydrilla, neurotoxic Aetokthonos hydrillicola, and vacuolar myelinopathy
Project PI	Gerrin, Wesley
Academic Institution of PI	University of Georgia
Congressional District of project	GA-10

Monitoring and modeling expanding risk of hydrilla, neurotoxic *Aetokthonos hydrillicola*, and vacuolar myelinopathy

Interim Year Technical Report FY22

Susan Wilde, Associate Professor and Wesley Gerrin, Research and Outreach Professional.

Warnell School of Forestry and Natural Resources. swilde@uga.edu

Abstract

Cyanobacterial harmful algal blooms are common in freshwater ecosystems, and joint efforts continue to manage risks to water quality, wildlife, and human health. Field and laboratory evidence confirmed that vacuolar myelinopathy was caused by aetokthonotoxin (AETX), a novel neurotoxin produced by cyanobacterium *Aetokthonos hydrillicola* growing on highly invasive aquatic plants, especially *Hydrilla verticillata (Figure 1.)*

We have continued to document expansion of hydrilla, *A. hydrillicola*, and vacuolar myelinopathy (VM) disease since this emerging disease was defined following a mass dieoff of eagles on DeGray Lake, AR (1994). Clinical signs of the disease include tremors, excitability, seizures, and eventual paralysis. The characteristic intramyelinetic edema has been documented in birds, fish, reptiles, amphibians and aquatic mammals. Impaired prey and predators result in complicated lethal and sublethal effects that ripple throughout this aquatic food web.

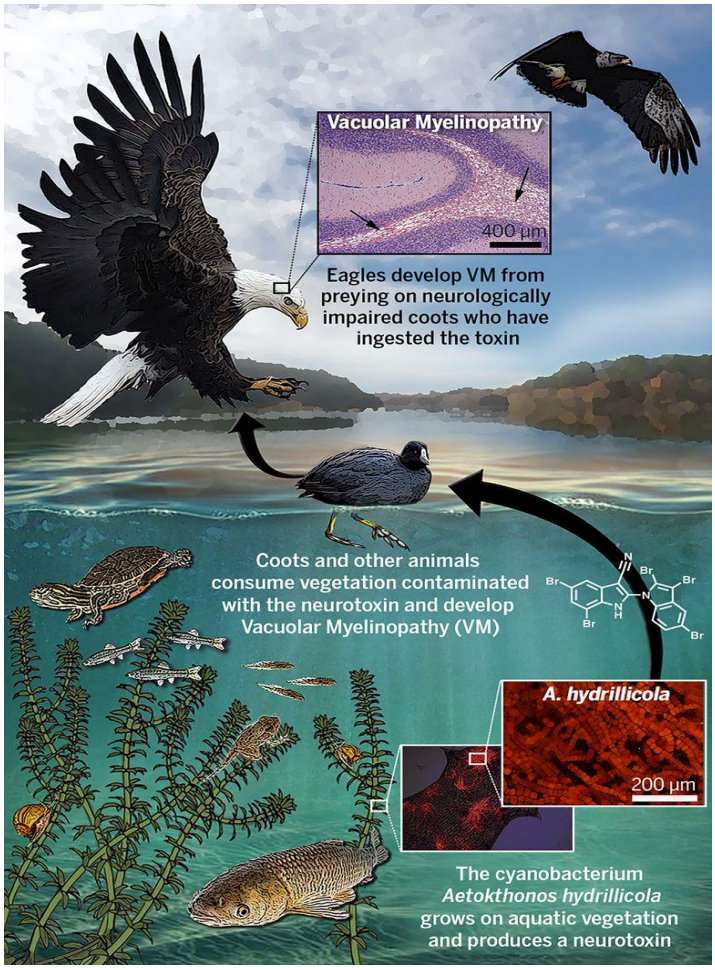

Figure 1. Investigations into Hydrilla, Aetokthonos hydrillicola, and aetokthonotoxin food chain resulting in Vacuolar Myelinopathy and wildlife mortality.

After evaluating four presence-background models for their ability to predict preferred habitats of *A. hydrillicola*. MAXENT emerged as the best predictive model, with *soil cation exchange capacity* and *percentage of land cover as needleleaf trees* as the best predictive variables. Additionally, nationwide calls for plant samples to reservoir managers and collaborators have confirmed the expanded occurrence of *A. hydrillicola* and the predictive capabilities of our Ah model. Ultimately, this study will contribute to strategies for risk reduction from AETX bioaccumulation in aquatic food webs and wildlife and potential human neuropathy.

We have documented AETX in fishes and waterfowl from herbivorous to piscivorous feeding guilds within southeastern reservoirs and trophic isotope analysis is underway.

Introduction

Cyanobacterial harmful algal blooms (cyanoHABs) are a threat to aquatic ecosystems worldwide— a trend that is expected to increase with eutrophication, the spread of non-native species, and climate change (Sukenik and Kaplan 2021). Benthic and epiphytic cyanobacteria present an emerging threat to species and community dynamics >50% are known toxin producers with potentially far-reaching effects across taxa and trophic levels within aquatic communities (Paerl et al. 2018; Bouma-Gregson, et al 2019, Haram et al. 2020, Wood, et al 2020).

Breinlinger et. al 2021 successfully described and structured a novel neurotoxin, aetokthonotoxin (AETX), which is produced by *A. hydrillicola*. AETX was confirmed as the cause of vacuolar myelinopathy via a chicken trial, in which chickens were exposed to a purified form of the toxin. The study also found that the structure of aetokthonotoxin was such that *A. hydrillicola* would require a source of bromide to produce the toxin (Figure 2) (Breinlinger *et al.* 2021).

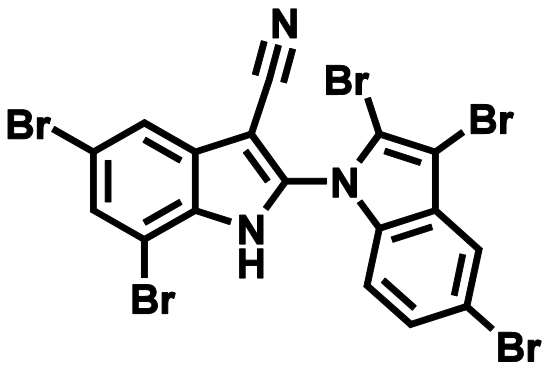

Figure 2. Structure of aetokthonotoxin described by Breinlinger et al.

Gerrin et. al (submitted) investigated environmental conditions that could trigger production of aetokthonotoxin. Using toxin concentration data from multiple years of hydrilla samples and numerous environmental variables (temperature, precipitation, lake elevation), models predicted that a decrease in maximum daily water temperature was the key environmental factor contributing to increases in toxin concentration. A species distribution model (Figure 3) was developed to further understand the distribution of the cyanobacteria and to also predict where potential suitable habitat areas are for *A. hydrillicola* colonization. This model highlighted several parameters negatively impacting the habitat suitability including increased soil cation exchange capacity, land cover dominated by hardwood trees, and urban land cover. There was one main factor positively impacting habitat suitability: land cover dominated by conifers, which in the tested areas correspond to pine species. This has vast implications since a large commodity within the southeastern U.S. is commercial loblolly pine forests.

Aquatic plant management is still the only known mitigation for reducing wildlife mortalities caused by the plant infestations supporting *A. hydrillicola* and novel neurotoxin. A key factor in determining risk for VM is estimating the potential distribution of *A. hydrillicola.* Pine forested wetlands are at highest risk for this disease invasion.

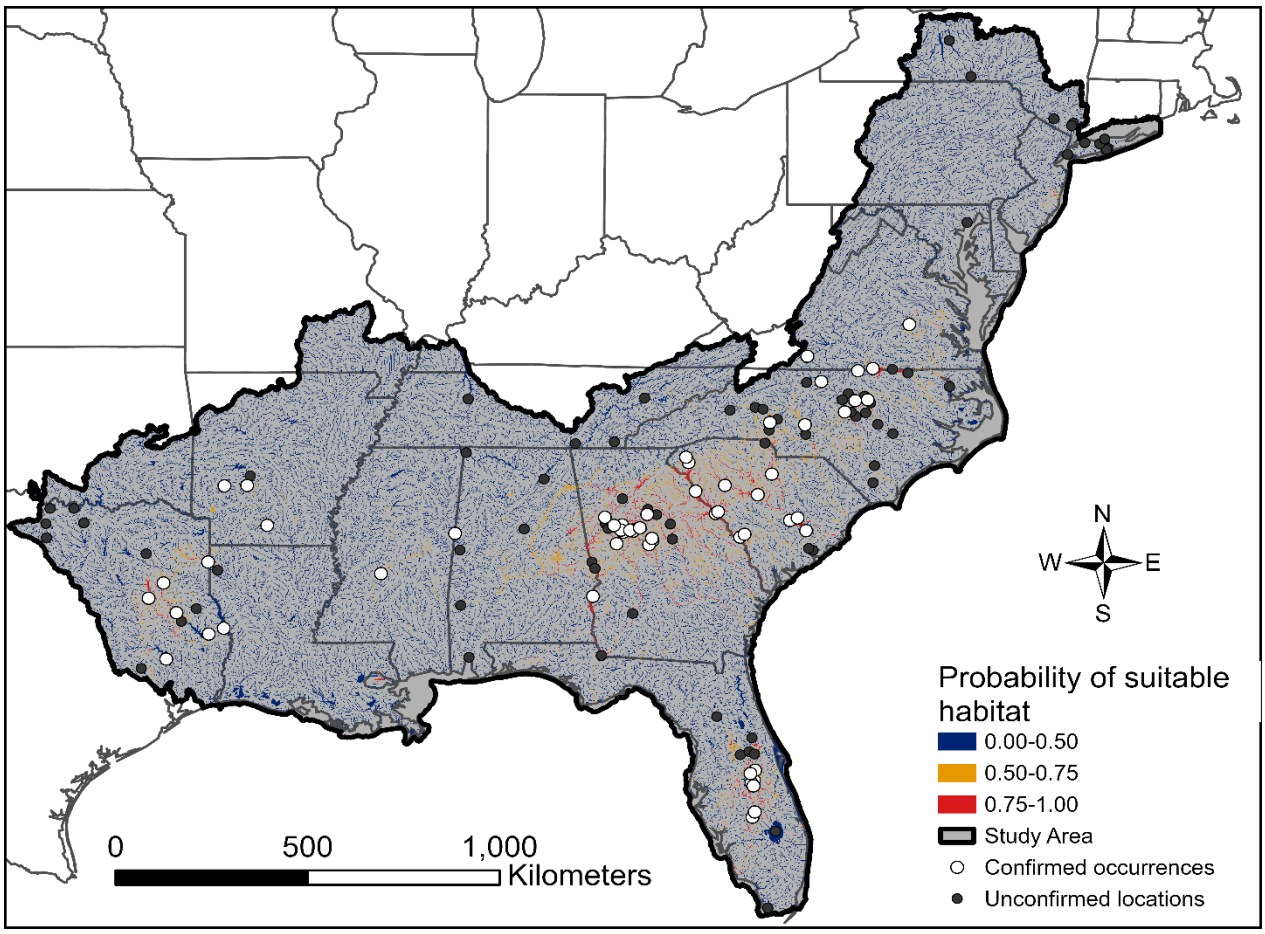

Figure 3. Species distribution model of occurrences and probability of suitable habitat for Aetokthonos hydrillicola within the model region.

We have documented *A hydrillicola* in lakes which have VM disease confirmed by the histological analysis of brain tissue from field collected fish, birds, and mammals and/or avian feeding trials. Unfortunately, we recently found AETX in Everglades apex predator, the Florida panthers. They are experiencing hind limb ataxia, have the characteristic intramyelinetic edema white matter legions.

There are 12 known lakes/reservoirs in Florida with hydrilla and A. hydrillicola and 11 are part of the Kissimmee Chain of Lakes draining via Lake Okeechobee through the Everglades into Florida Bay. We continue to investigate locations with snail kite/eagle nest failures and Feline leukomyelopathy (FLM) in panthers/bobcats.

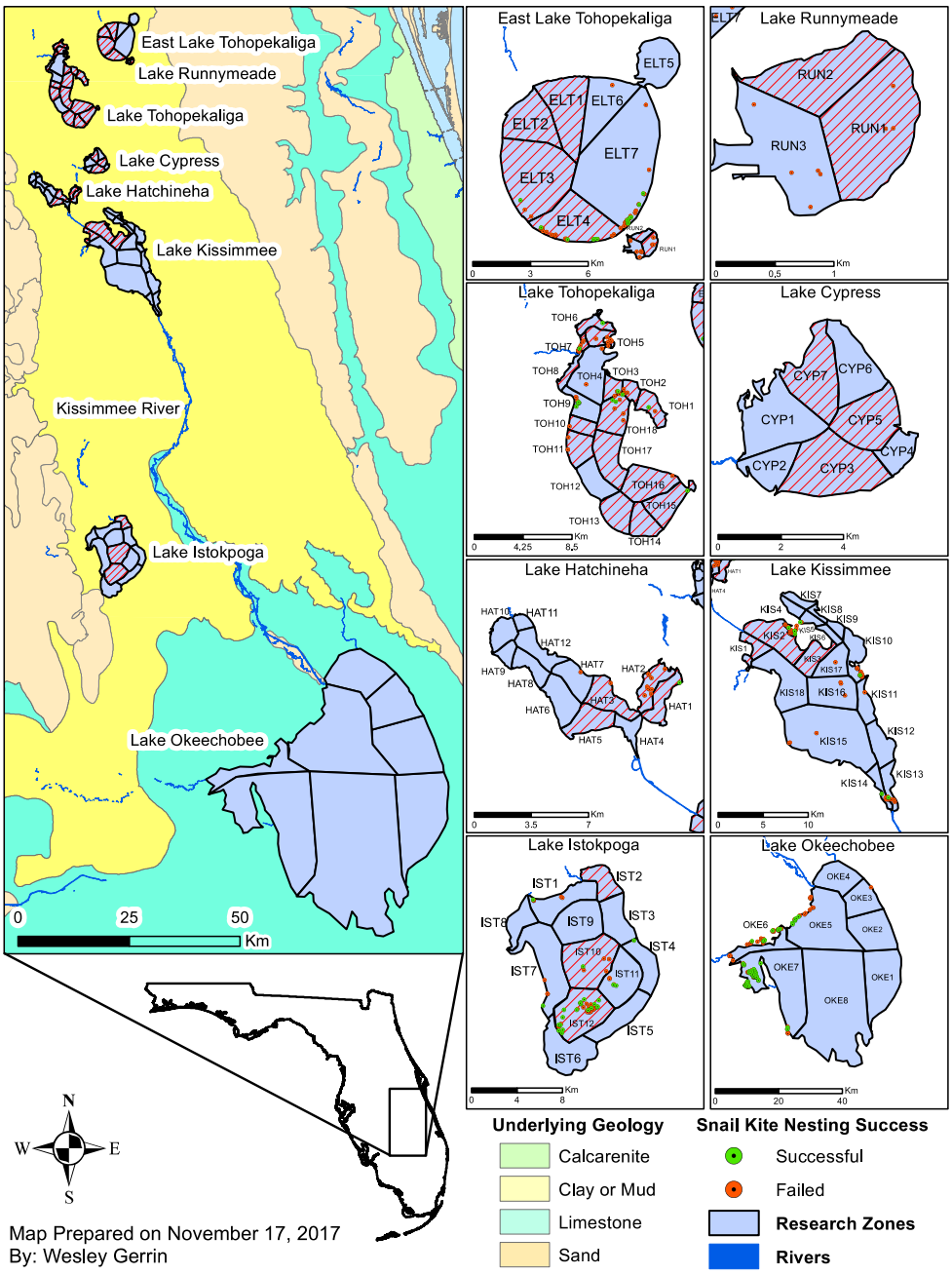

Figure 4. Snail kite nesting success in Florida lakes declined significantly in subwatershed with *Aetokthonos hydrillicola* in the Kissimmee Chain of Lakes. Subwatersheds were based on the location of inflows, and this figure indicates those documented with *A. hydrillicola* using red hatching.

Disorder Impacting Panthers and Bobcats--*The FWC is investigating a disorder detected in some Florida panthers and bobcats. Affected animals exhibit varying degrees of rear leg weaknesses that lead to difficulty in walking. The FWC takes this situation seriously and is increasing monitoring efforts to locate affected animals via the deployment of video trail camera in areas where the condition has been most frequently documented. The FWC has termed this condition feline leukomyelopathy or FLM.*

https://myfwc.com/wildlifehabitats/wildlife/panther/disorder/updates/

We will ground truth the previously created species distribution model to determine its accuracy in predicting *A. hydrillicola* risk by using LAMP to detect presence and absence of *A. hydrillicola*. We also plan to use qPCR to quantify *A. hydrillicola* present among samples from infested reservoirs. These analyses will be performed on low and high probability reservoirs predicted by the species distribution model.

The molecular detection of *A. hydrillicola* is currently limited to recently developed Polymerase Chain Reaction (PCR) assays that target the AETX biosynthetic gene cluster (Štenclová *et al.* 2023). Conventional PCR, however, is time consuming, requires very specific lab equipment, and high-quality DNA extracts (i.e., free of inhibitors). Loop-Mediated Isothermal Amplification (LAMP), on the other side, offers a valuable tool for addressing these limitations. This isothermal molecular technique allows rapid, sensitive, and highly specific detection of a target region from crude DNA extracts, thus allowing for in-field testing capability with minimal equipment (Aglietti *et al.* 2021; Hamilton *et al.* 2020; Jenkins *et al.* 2011; Notomi *et al.* 2000; Villari *et al.* 2013; Williams *et al.* 2017). Quantitative PCR (qPCR) is a form of PCR used to quantify DNA within a sample using standard concentration curves (Kralik and Ricchi 2017). Testing samples both in field with LAMP and quantitatively with qPCR will allow us to test the validity of the species distribution model to confirm testing regions that are at high probability of having suitable habitat characteristics for *A. hydrillicola.*

Previous research has been focused on the causative neurotoxin for VM, however, due to its apparent seasonality, detection of AETX and presence of *A. hydrillicola* is limited. Utilizing molecular techniques will allow for detection of the cyanobacteria regardless of the season. By partnering with USGS and additional resource managers we continue to expand monitoring and to optimize plant management strategies that are effective at controlling dense plant infestations supporting the epiphytic cyanobacteria without initiating AETX production.

Progress on FY22 Activities

- **Send invasive plant sampling instructions to reservoir managers and collaborators**

  USGS collaborator Ian Pfingsten and Tobias Haymes sent a nationwide call for plant samples to 45 reservoir managers and collaborators. Mail out includes instructions for sampling and required shipping permits, freezer packs and waterproof padded mail pouch.

- **Receive/collect plant samples and complete microscopic screening**

  A total of 780 SAV samples from 12 different states across the United States were screened for *A. hydrillicola.* New hydrilla/Ah locations were documented in Georgia, Florida, North Carolina, Texas, Louisiana, Florida, Virginia, and Kentucky.

- **Collect invasive plants, invertebrate prey, fish, and waterbirds from GA sites**

  Fish and SAV samples were collected from Tussahaw Reservoir, Georgia demonstrated food chain AETX accumulation. SAV samples collected from Longbranch, Tussahaw, and Covington reservoirs, Georgia had dense colonies of A. hydrillicola and extremely high AETX concentrations. (>2500 ppb)

- **Complete toxin extraction and analysis of plant and animal tissues**

  All 275 fish, 25 panther, 15 bobcats, and 12 wood duck eggs have been biopsied and extracted for AETX. Fish tissue AETX concentrations were varied by season and feeding guild. A total of 115 SAV samples were extracted and evaluated AETX during FY22. Analysis is ongoing.

- **Update final MAXENT distribution models using updated presence dataset**

  The final model will be generated during Fall 2023 using updated SAV/Ah locations.

Critical genetic detection supporting expanded monitoring

We are also developing an efficient protocol for detection of *A. hydrillicola* by designing a specific field-portable LAMP test and a quantitative laboratory assay obtained by adapting to use with qPCR technology an already published PCR primer set. We propose to sample *A. hydrillicola* from Florida watersheds encompassing previously confirmed positive reservoirs as well as potential *A. hydrillicola* -free ones. This protocol will be made accessible to labs throughout the U.S. to support early detection and eradication efforts. Specific steps for the achievement of this objective include:

i. Developing LAMP primers that detect specific genes responsible for producing AETX within *A. hydrillicola*.
ii. Adapting the current PCR primers for use in quantitative assays (i.e., qPCR)
iii. Assessing the specificity and sensitivity of the LAMP and qPCR assays using pure DNA extracts of *A. hydrillicola*, non-target cyanobacterial species, and plants from infested reservoirs.
iv. Determining the parameters needed for application of in-field LAMP testing.
v. Validating the versatility of the LAMP assay by using it to detect *A. hydrillicola* on different substrates (such as *Hydrilla* or other plants) in multiple reservoir locations within watersheds that are at high and low probability of colonization by *A. hydrillicola* based on the species distribution model.

vi. Evaluating the level of *A. hydrillicola* colonization on plant samples collected from infested reservoirs using qPCR.

Methods

Field Data Collection

This collaborative project with University of Georgia and USGS/EPA analytical chemists and USGS outreach professionals has facilitated further partnerships enabling expanded detection of invasive aquatic plants and toxigenic epiphytic cyanobacteria. Our partnership includes small grants, contract AETX analysis, in-kind contributions from Florida Fish and Wildlife Commission (FWC Invasive Plant Management) and University of Florida (IFAS) Research & Education Center.University of Florida / IFAS (FWC/UF Snail kites, Florida panthers). UGA graduate student, Tobias Haymes worked as an intern for USGS Nonindigenous Aquatic Species, Wetland and Aquatic Research Center. This effort expanded our sampling distribution, following a consistent field protocol. We prioritize *Hydrilla verticillata* screening as this species most commonly supports *A. hydrillicola*, however, other plant species as well as soil samples will also be tested for cyanobacterial presence to test the versatility of our LAMP assay. We have also documented *A. hydrillicola* growing densely on additional invasive species (*Najas quadalupensis*, *Hygrophila polysperma*, *Limnophila sessiflora)* as well as native SAV (*Bacopa*, *Cabomba caroliniana*, *Ceratophyllum demersum*, *Utricularia* spp.). *(Figure 5.)*

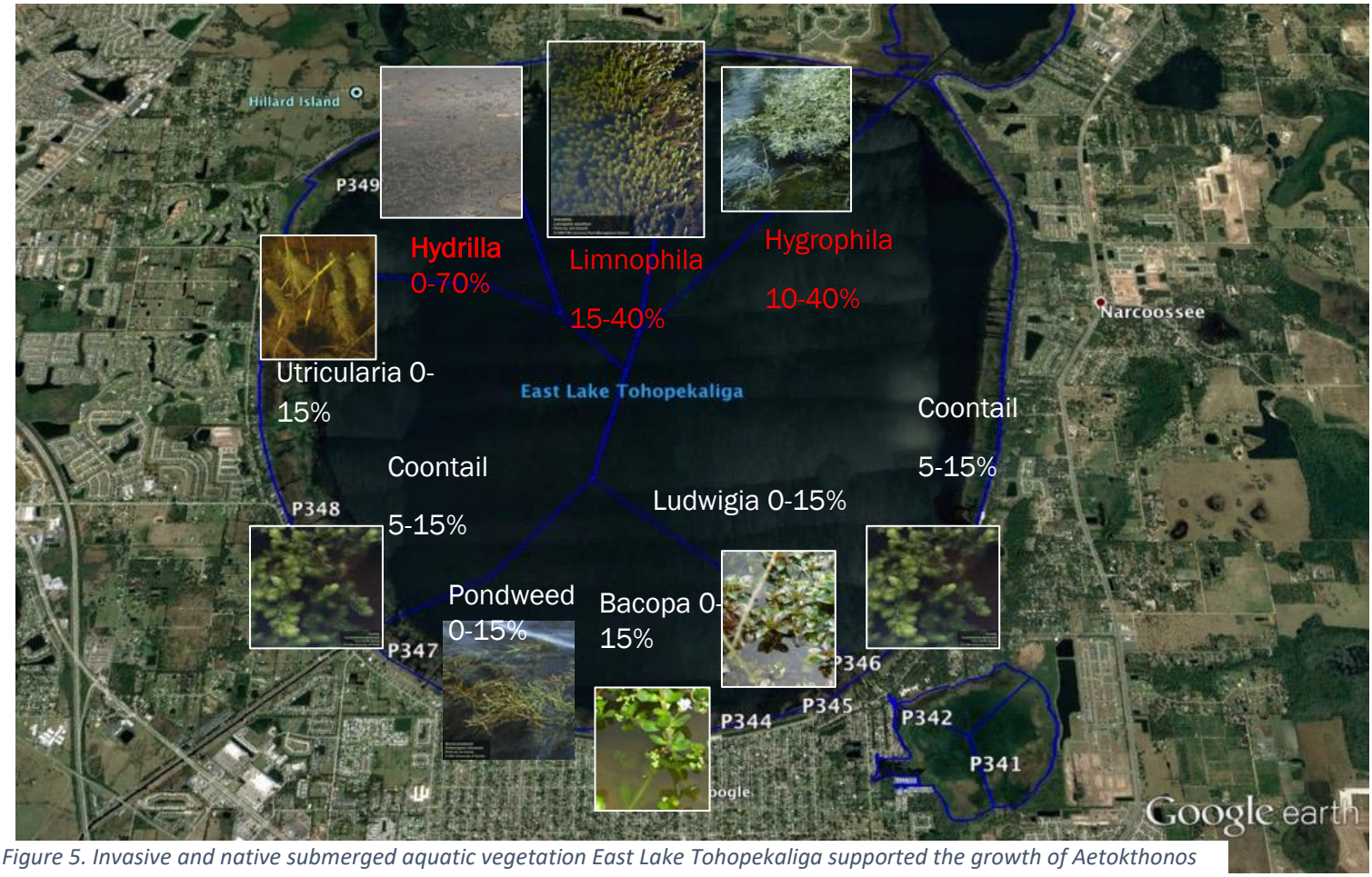

Figure 5. Invasive and native submerged aquatic vegetation East Lake Tohopekaliga supported the growth of Aetokthonos hydrillicola. Invasive plant infestations consistently have higher A. hydrillicola density and higher aetokthonotoxin levels.

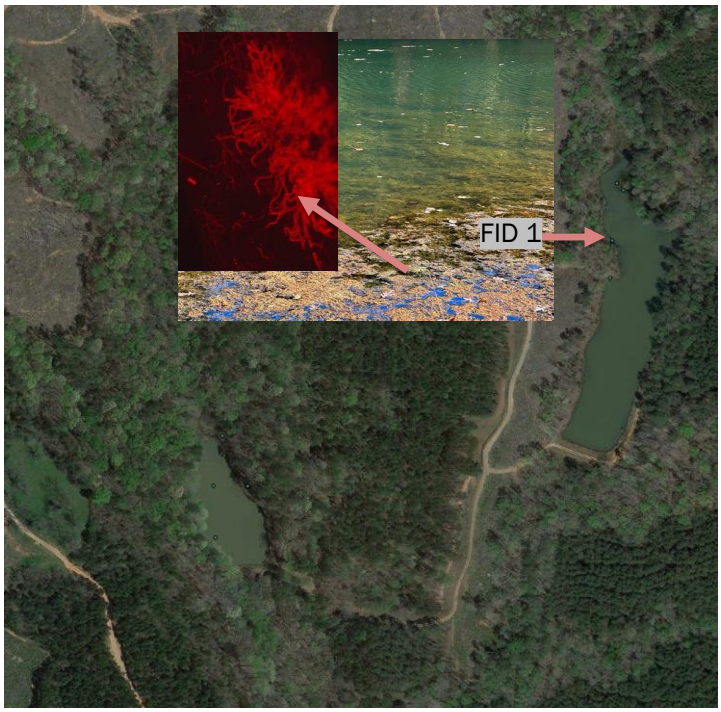

Figure 6. The BF Grant Forest, owned by UGA Warnell School of Forestry and Natural Resources, is a Georgia DNR wildlife management area. Wood duck nesting failed in boxes on constructed ponds with dense mats of invasive *Najas quadalupensis* supporting *A. hydrillicola*.

Aquatic plant sample collection protocol

IMPORTANT: Prior to collecting and shipping specimens, please contact us to obtain a copy of our APHIS permit that MUST be included with your shipment.

Plant sample collection: Collect hydrilla or other plant sample from at or below surface, squeeze excess water out, and place in a ziplock bag. A 1-quart freezer style bag is plenty for screening purposes. Please be sure to *only* include vegetation. Label the bag with site and date information. Please include with submission: The GPS location of each site, and any water quality data that you're equipped to measure in the field (DO, turbidity, ph, temp, etc).

Soil Sample Collection: At time of plant sample collection, collect additional soil sample in the same manner as plant sample collection.

Shipping: Place the sealed sample bag(s) in a cooler or waterproof packaging with the APHIS permit, a coldpack, tape the cooler/package shut, place it inside a box and mail* it to UGA Wilde Lab. Please call or email to let us know to anticipate your shipment and include the tracking number.

Submerged Aquatic Vegetation FIELD DATA COLLECTION FORM

DATE:

RESERVOIR:

Location Description:

GPS coordinates:

Water column depth:

Plant height:

Depth where plants were collected:

Temperature:

Oxygen:

pH:

Conductivity:

Alkalinity/Hardness: (any data on these parameters from your reservoirs would be valuable)

Turbidity: (please comment on water clarity, if instrumentation is not available)

Secchi depth:

Comments: (Was hydrilla actively growing, dying back? Treated? Were birds present? Any sign of impaired waterfowl?)

LAMP Design

LAMP primers will be designed utilizing the programs Geneious Prime[ã] and Primer Explorer v5[ã] (Eiken Chemical Company). The complete DNA sequences of each AETX gene cluster (*aetA*, *aetB*, *aetC*, *aetD*, *aetE*, and *aetF*) will be retrieved from the National Center for Biotechnology Information (NCBI) repository and assessed in Geneious Prime. Candidate target region sequences will then be extracted and uploaded to Primer Explorer to generate candidate LAMP primer sets. The loop-binding primers will be designed with a fluorescent probe attached for visualization during amplification. The current methods of DNA extraction for *A. hydrillicola*, NucleoSpin Soil Mini kit and CTAB buffer extractions, require clean DNA that is difficult to obtain in the field due to the requirement of lengthy and laborious procedures and several pieces of equipment (Howard and Wilde 2019; Štenclová *et al.* 2023). Using LAMP, which is less sensitive to inhibitors, there are many crude DNA extraction methods that may enable detection of *A. hydrillicola* without extensive processing (Aglietti *et al.* 2021; Hai-sheng *et al.* 2012; Hamilton *et al.* 2020; Hodgetts *et al.* 2015; Mason and Botella 2020; Nagai *et al.* 2012; Stehlíková *et al.* 2020; Zou *et al.* 2017). Our study will assess these different methods to determine which extraction technique best prepares *A. hydrillicola*-contaminated samples for amplification. Different visualization techniques will also be tested to determine which is most accurate and suitable for field testing. A dipstick extraction method and fluorescent probe-based visualization will be the first pair of extraction and visualization methods tested (Mason and Botella 2020; Meinecke *et al.* 2023)). Sensitivity and specificity testing will also be performed with several other species of bacteria, including other cyanobacteria.

qPCR Design

We will adapt a conventional PCR assay developed to detect *A. hydrillicola* AETX biosynthesis genes (Štenclová *et al.* 2023) for use in qPCR by the addition of fluorescent probes or dyes for visualization of amplification. Quantification of *A. hydrillicola* DNA will be based on comparison to standard curves, generated by amplification of known quantities of DNA from cultured freeze-dried *A. hydrillicola*. Field samples will be tested using LAMP to screen for the presence of *A. hydrillicola* and then with qPCR to quantify the amount of *A. hydrillicola* DNA present in each sample. This will allow to assess the relative level of colonization among different substrates.

DNA extraction protocol identification

Along with freeze-dried cultured *A. hydrillicola*, samples from *Hydrilla* leaves that have the cyanobacteria growing on them will be used to identify the most suitable extraction protocol for both in-field and laboratory settings. The Qiagen DNeasy Plant Kit, a dipstick extraction, boiling, Chelex, or a combination of several methods will be tested (Aglietti *et al.* 2021; Hai-sheng *et al.* 2012; Hamilton *et al.* 2020; Hodgetts *et al.* 2015; Mason and Botella 2020; Nagai *et al.* 2012; Stehlíková *et al.* 2020; Zou *et al.* 2017).

Application of LAMP and qPCR testing to ground-truth a Species Distribution Model

To test both assays' ability to detect *A. hydrillicola* from field samples and ground-truth the species distribution model, *Hydrilla* samples from 15 different sites in Florida will be collected. Each sample will first be analyzed using a portable LAMP device in the field (Hamilton *et al.* 2021). If positive, 3-5 additional samples will be collected and shipped to the lab for qPCR analysis to confirm the field-based results using pure DNA extractions. High probability watersheds from the species distribution model where *A. hydrillicola* has not yet been detected will be tested for presence of the cyanobacteria. Low probability watersheds will also be sampled to determine how accurately the model can predict the presence of *A. hydrillicola* in reservoirs. The upper Mississippi River basin shows a relatively low probability to house suitable habitat for *A. hydrillicola*, based on the model, however, the distribution of *Hydrilla* encompasses the region and reservoirs have not yet been testing for cyanobacterial presence.

Other Substrate Testing

Besides *Hydrilla*, *A. hydrillicola* has also been observed growing on leaves, stems and root hairs of invasive and native aquatic plants including; *Egeria densa*, *Myriophyllum spicatum*, *Najas quadalupensis*, *Potamogeton illinoiensis.* Interestingly, we have also found *Aetokthonos* growing on water willow root hairs and on submerged loblolly pine needles. *A. hydrillicola* found growing on American water-willow was detected using PCR assays targeting the toxin gene cluster and the internal transcribed spacer 1 (ITS1) portion of ribosomal DNA. However a primer set specific to the ITS2 region did not detect the cyanobacteria on this new substrate, suggesting there might be some variability within the species (Štenclová *et al.* 2023). Moreover, there was no toxin production, indicating that different substrates may influence AETX synthesis. This is the first indication of genetic and phenotypic diversity among colonies of *A. hydrillicola.* To better delimit the habitats of *A. hydrillicola* within an infested reservoir, we will collect samples from other substrates, such as soil, other aquatic vegetation, and submerged pine needles.

We will continue to add all A.hydrillicola & invasive submerged vegetation and confirmed VM mortalities to Warnell VM Wilde, UGA Bugwood network hosted at the University of Georgia in conjunction with the Warnell School of Forestry and Natural Resources. This site will be linked to Center for Invasive Species and Ecosystem Health and Army Corps of Engineers: Invasive Aquatic Nuisance Species Program.

References

Aglietti C, Meinecke CD, Ghelardini L, Barnes I, Nest Avd, and Villari C (2021) Rapid detection of pine pathogens lecanosticta acicola, dothistroma pini and d. Septosporum on needles by probe-based lamp assays. *Forests* **12**. doi: 10.3390/f12040479

https://www.mdpi.com/1999-4907/12/4/479.

Breinlinger S, Phillips TJ, Haram BN, Mares J, Yerena JAM, Hrouzek P, Sobotka R, Henderson WM, Schmieder P, Williams SM, Lauderdale JD, Wilde HD, Gerrin W, Kust A, Washington JW, Wagner C, Geier B, Liebeke M, Enke H, Niedermeyer THJ, and Wilde SB (2021) Hunting the eagle killer: A cyanobacterial neurotoxin causes vacuolar myelinopathy. *Science* **371**, 1335-+. doi: 10.1126/science.aax9050.

Hai-sheng X, Lin H, Sun-jian L, Qi G, and Song L (2012) Establishment of universal loop-mediated isothermal amplification method (lamp) for rapid detection of pathogenic vibrio spp. In aquatic organisms. *African Journal of Microbiology Research* **6**, 3447-3454.

Hamilton JL, Fraedrich SW, Nairn CJ, Mayfield AE, and Villari C (2021) A field-portable diagnostic approach confirms laurel wilt disease diagnosis in minutes instead of days. *Arboriculture & Urban Forestry* **47**, 98-109. doi: 10.48044/jauf.2021.010.

Hamilton JL, Workman JN, Nairn CJ, Fraedrich SW, and Villari C (2020) Rapid detection of raffaelea lauricola directly from host plant and beetle vector tissues using loop-mediated isothermal amplification. *Plant Disease* **104**, 3151-3158. doi: 10.1094/PDIS-02-20-0422-RE

https://apsjournals.apsnet.org/doi/10.1094/PDIS-02-20-0422-RE.

Hilborn ED, Beasley VR. One health and cyanobacteria in freshwater systems: animal illnesses and deaths are sentinel events for human health risks. Toxins (Basel). 2015 Apr 20;7(4):1374-95. doi: 10.3390/toxins7041374. PMID: 25903764; PMCID: PMC4417972.

Hodgetts J, Hall J, Karamura G, Grant M, Studholme DJ, Boonham N, Karamura E, and Smith JJ (2015) Rapid, specific, simple, in-field detection of xanthomonas campestris pathovar musacearum by loop-mediated isothermal amplification. *Journal of Applied Microbiology* **119**, 1651-1658. doi: https://doi.org/10.1111/jam.12959.

Howard A and Wilde S (2019) 'Genetic investigations of a novel, toxic, epiphytic cyanobacteria: Aetokthonos hydrillicola.' (ProQuest Dissertations & Theses)

Jenkins DM, Kubota R, Dong J, Li Y, and Higashiguchi D (2011) Handheld device for real-time, quantitative, lamp-based detection of salmonella enterica using assimilating probes. *Biosensors and Bioelectronics* **30**, 255-260. doi: https://doi.org/10.1016/j.bios.2011.09.020.

Kralik P and Ricchi M (2017) A basic guide to real time pcr in microbial diagnostics: Definitions, parameters, and everything. *Frontiers in microbiology* **8**, 108-108. doi: 10.3389/fmicb.2017.00108.

Mason MG and Botella JR (2020) Rapid (30-second), equipment-free purification of nucleic acids using easy-to-make dipsticks. *Nature Protocols* **15**, 3663. doi: 10.1038/s41596-020-0392-7.

Meinecke CD, De Vos L, Yilmaz N, Steenkamp ET, Wingfield MJ, Wingfield BD, and Villari C (2023) A lamp assay for rapid detection of the pitch canker pathogen fusarium circinatum. *Plant Disease* **0**, null. doi: 10.1094/pdis-04-22-0972-sr.

Nagai S, Yamamoto K, Hata N, and Itakura S (2012) Study of DNA extraction methods for use in loop-mediated isothermal amplification detection of single resting cysts in the toxic dinoflagellates alexandrium tamarense and a. Catenella. *Marine Genomics* **7**, 51-56. doi: https://doi.org/10.1016/j.margen.2012.03.002.

Notomi T, Okayama H, Masubuchi H, Yonekawa T, Watanabe K, Amino N, and Hase T (2000) Loop-mediated isothermal amplification of DNA. *Nucleic acids research* **28**, E63. doi: 10.1093/nar/28.12.e63.

Stehlíková D, Luchi N, Aglietti C, Pepori AL, Diez JJ, and Santini A (2020) Real-time loop-mediated isothermal amplification assay for rapid detection of fusarium circinatum. *BioTechniques* **69**, 11-17. doi: 10.2144/btn-2019-0168.

Štenclová L, Wilde SB, Schwark M, Cullen JL, McWhorter SA, Niedermeyer THJ, Henderson WM, and Mareš J (2023) Occurrence of aetokthonotoxin producer in natural samples – a pcr protocol for easy detection. *Harmful Algae* **125**, 102425. doi: https://doi.org/10.1016/j.hal.2023.102425.

Villari C, Tomlinson JA, Battisti A, Boonham N, Capretti P, and Faccoli M (2013) Use of loop-mediated isothermal amplification for detection of ophiostoma clavatum, the primary blue stain fungus associated with ips acuminatus. *Applied and Environmental Microbiology* **79**, 2527-2533. doi: 10.1128/AEM.03612-12

https://aem.asm.org/content/79/8/2527.abstract.

Williams MR, Stedtfeld RD, Engle C, Salach P, Fakher U, Stedtfeld T, Dreelin E, Stevenson RJ, Latimore J, and Hashsham SA (2017) Isothermal amplification of environmental DNA (edna) for direct field-based monitoring and laboratory confirmation of dreissena sp. *PLoS One* **12**, e0186462. doi: 10.1371/journal.pone.0186462.

Zou Y, Mason MG, Wang Y, Wee E, Turni C, Blackall PJ, Trau M, and Botella JR (2017) Nucleic acid purification from plants, animals and microbes in under 30 seconds. *PLoS biology* **15**, e2003916.

Paerl HW, Otten TG, and Kudela R (2018) Mitigating the expansion of harmful algal blooms across the freshwater-to-marine continuum. Environmental Science and Technology 52(10), 5519-5529. doi: 10.1021/acs.est.7b05950

Haram BN, Wilde SB, Chamberlain MJ, and Boyd KH (2020) Vacuolar myelinopathy: Waterbird risk on a southeastern impoundment co-infested with *Hydrilla verticillata* and *Aetokthonos hydrillicola*. Biological Invasions 22, 2651-2660. doi: 10.1007/s10530-020-02282-w.

Carmichael WW, and Boyer GL (2016) Health impacts from cyanobacteria harmful algae blooms: implications for the North American Great Lakes. Harmful Algae 54, 194-212. doi: 10.1016/j.hal.2016.02.002

Sukenik A, and Kaplan A (2021) Cyanobacterial harmful algal blooms in aquatic ecosystems: a comprehensive outlook on current and emerging mitigation and control approaches. Microorganisms 9(7). doi: 10.3390/microorganisms9071472